NATIONAL AND KAPODISTRIAN UNIVERSITY OF ATHENS

FACULTY OF SCIENCES

DEPARTMENT OF CHEMISTRY

Ph.D. THESIS

Properties and dynamics of Chromophoric Dissolved Organic Matter (CDOM) in Eastern Mediterranean Waters

ELLI PITTA
CHEMIST

ATHENS

JULY 2016

Ph.D. THESIS

Properties and dynamics of Chromophoric Dissolved Organic Matter (CDOM) in Eastern Mediterranean Waters

ELLI PITTA

A.M.: 001106

SUPERVISOR:

MICHAEL SCOULLOS, Professor, Dpt of Chemistry, University of Athens

SUPERVISORY COMMITTEE:

Professor Michael Scoullos, Dpt of Chemisrty, University of Athens

Dr. Christina Zeri, Senior Researcher, Hellenic Centre for Marine Research

Associate Professor Maria Tzortziou**,** Dpt of Earth and Atmospheric Sciences, City University of New York

EXAMINATION COMMITTEE

Prof. Michael Scoullos, Dpt of Chemistry, University of Athens

Dr. Christina Zeri, Senior Researcher, HCMR

Associate Prof. Maria Tzortziou, City University of New York

Prof. Manos Dassenakis, Dpt. Of Chemistry, University of Athens

Dr. George Mousdis, Senior Researcher, NHRF

Associate Prof. Evangelos Bakeas, Dpt. Of Chemistry, University of Athens

Prof. Vassilios Roussis, Dpt. Of Pharmacy, University of Athens

DATE OF EXAMINATION 29/07/2016

ABSTRACT

The purpose of this study is to investigate the optical properties of Dissolved Organic Matter (DOM) and to gain information regarding the nature and transformation processes of DOM in a large region of the Eastern Mediterranean Sea covering the Marmara Sea, the North-Central and South Aegean Sea, the Ionian Trench and Northwestern Levantine Sea as well as Sperchios River and Maliakos Gulf. A secondary purpose of this study is to get insights into autochtonous CDOM production. Chromophoric Dissolved Organic Matter (CDOM) and Fluorescent Dissolved Organic Matter (FDOM) are used for the characterization of the optical properties of DOM but they can also provide information about DOM composition and track transformation processes. CDOM is the fraction of DOM that has the ability to absorb light in the UV-visible region of the electromagnetic spectrum. FDOM is the fraction of CDOM that additionally has the ability to fluorescence upon excitation. CDOM is of significant ecological importance as is a major factor in the light attenuation in the sea impacting the primary production. In order to achieve the purposes of this study, absorption spectra in the UV-visible region and fluorescence Excitation and Emission Matrices (EEMs) were obtained while Parallel Factor Analysis (PARAFAC) was applied for the identification of the fluorescent components. Our results show the distinct optical print of rivers and that their influence in the coastal waters is better tracked through fluorescence analysis. CDOM/FDOM dynamics at the surface of Marmara Sea deviate from the observed summer pattern in open seas while Black Sea Water (BSW) outflowing the Dardanelles introduce significant amounts of CDOM, amino acid-like and humic-like substances in North Aegean Sea (NAS). The influence of BSW and the established optical properties in NAS presents seasonal variations. Photodegradation appears to be a major sink of CDOM and humic substances at the surface layer of the Aegean Sea. Contrary in mesopelagic and bathypelagic layers microbial activity seems to leed to the depletion of amino acid-like substances and the production of humic nature DOM. Overall our results suggest that CDOM and FDOM can provide important information regarding DOM composition and its dynamics (sources and sinks) in various water bodies.

SUBJECT AREA: Optical properties of Dissolved Organic Matter

KEY WORDS: CDOM/FDOM, absorption, fluorescence, PARAFAC analysis

ΠΕΡΙΛΗΨΗ

Ο σκοπός της εργασίας είναι η διερεύνηση των οπτικών ιδιοτήτων της Διαλυτής Οργανικής Ύλης, DOM, σε μια μεγάλη περιοχή της Ανατολικής Μεσογείου η οποία καλύπτει τη Θάλασσα του Μαρμαρά, το Βόρειο-Κεντρικό και Νότιο Αιγαίο, το Νότιο Ιόνιο, τη Βορειοδυτική Θάλασσα της Λεβαντίνης καθώς και το Σπερχειό Ποταμό. Δευτερεύων στόχος της διατριβής είναι να μελετήσει την αυτόχθονη παραγωγή της CDOM. Για τον χαρακτηρισμό των οπτικών ιδιοτήτων της DOM καθώς και στη διερεύνηση της χημική σύνθεσης της DOM και στον προσδιορισμό διεργασιών μετασχηματισμού χρησιμοποιούνται η Χρωμοφόρα Διαλυτή Οργανική Ύλη (CDOM) και η Φθορίζουσα Διαλυτή Οργανική Ύλη (FDOM). Η CDOM είναι το τμήμα της DOM που έχει την ικανότητα να απορροφά ακτινοβολία στο υπεριώδες και ορατό τμήμα του ηλεκτρομαγνητικού φάσματος. Η FDOM είναι το τμήμα της CDOM που επιπλέον παρουσιάζει φθορισμό. Η CDOM παρουσιάζει μεγάλη οικολογική σημασία καθώς είναι από τους κυριότερους παράγοντες που ευθύνονται για την απορρόφηση της ηλιακής ακτινοβολίας στα φυσικά ύδατα επηρεάζοντας τις φωτοσυνθετικές διεργασίες. Για το σκοπό της εργασίας λήφθηκαν φάσματα απορρόφησης καθώς και φάσματα φθορισμού Excitation Emission Matrices. Για την ταυτοποίηση των φθοριζόντων στοιχείων πραγματοποιήθηκε ανάλυση Parallel Factor Analysis, PARAFAC. Τα αποτελέσματά μας δείχνουν ότι τα ιδιαίτερα οπτικά χαρακτηριστικά των ποταμών και η επίδρασή τους στα παράκτια ύδατα μπορούν να προσδιοριστούν καλύτερα μέσω του φθορισμού. Η επιφάνεια της Θάλασσας του Μαρμαρά παρουσιάζει οπτικές ιδιότητες οι οποίες αποκλίνουν από τις παρατηρούμενες στις ανοικτές θάλασσες. Η Μαύρη Θάλασσα φαίνεται να εισάγει σημαντικές ποσότητες CDOM και FDOM πρωτεϊνικής και χουμικής φύσεως στο Βόρειο Αιγαίο επηρεάζοντας τις οπτικές ιδιότητες της περιοχής και παρουσιάζοντας ταυτόχρονα εποχιακές διακυμάνσεις. Η φωτοδιάσπαση φαίνεται να είναι καθοριστικός παράγοντας αποικοδόμησης της CDOM και της FDOM χουμικής φύσεως στην επιφάνεια του Αιγαίου. Αντίθετα σε μεσοπελαγικά και βαθυπελαγικά νερά η μικροβιακή δραστηριότητα φαίνεται να οδηγεί σε εξάντληση των φθοριζόντων ουσιών πρωτεϊνικής φύσεως και στην παραγωγή χουμικών ενώσεων. Συνολικά η παρούσα εργασία δείχνει ότι η ανάλυση της CDOM και FDOM μπορεί να παρέχει χρήσιμες πληροφορίες σχετικά με τη σύνθεση της DOM και να παρακολουθήσει χημικές διεργασίες αλλοίωσης στις οποίες υπόκειται.

ΘΕΜΑΤΙΚΗ ΠΕΡΙΟΧΗ: Οπτικές ιδιότητες διαλυτής οργανικής ύλης

ΛΕΞΕΙΣ ΚΛΕΙΔΙΑ: CDOM/FDOM, απορρόφηση, φθορισμός, ανάλυση PARAFAC

To my parents

AKNOWLEDGEMENTS

A part of this research has been co-financed by the European Union (European Social Fund – ESF) and Greek national funds through the Operational Program "Education and Lifelong Learning" of the National Strategic Reference Framework (NSRF) - Research Funding Programs at *Hellenic Centre for Marine Research*: 1.*THALES*- Investing in knowledge society through the European Social Fund. 'Technological and oceanographic cooperation Network for the Study of mechanisms fertilizing the North-East Aegean Sea –AegeanMarTech'. 2. *KRIPIS*-'Development of an integrated management system for river basin, coastal and marine zones.'

This work was also financially supported by the programs: 1. *ECODOM*, Advancing understanding of carbon cycling and coloured dissolved organic matter dynamics in European wetlands & coastal ecosystems through integration of observations and novel modelling approaches; and 2. *DeFishGear*: Derelict Fishing Gear management system in the Adriatic Region, co-funded by the European Union, Instrument for Pre-Accesion Assistance. (*Hellenic Centre for Marine Research*)

I would like to thank and express my appreciation to my academic supervisor, Professor Michael Scoullos for giving me the opportunity to have these doctoral studies and for the continuous support throughout these years. I would also like to thank and express my graditude to my supervisor at HCMR, Dr. Christina Zeri for the help, guidance, support and mentoring during the experimental work and the interpretation of the data. I sincerely thank Dr. Maria Tzortziou for the guidance, knowledge and constructive comments. I would like to thank Dr. George Mousdis for the 'hospitality' at the NHRF, the help and advices. I thank Dr. Stella Psarra for giving me the opportunity to be a part of the progam THALES-AegenMarTech and Dr. Elias Dimitriou for giving me the opportunity to participate in ECODOM and KRIPIS programs. I thank Dr. Ioanna Varkitzi, Angeliki Konstantinopoulou, Thodori Zoulia and Dr. Antonia Giannakourou for the collaboration and assistance at the laboratory experiments. I also thank Vasiliki Markogianni for all the help (field and information) regarding the work at the Sperchios River and Maliakos Gulf. I also thank George Pappas for the help and technical support. I truly thank Stelios Iliakis for the assistance at the laboratory, the productive discussions and all the support. Finally i would like to thank and express my graditude to my family and especially my parents for the huge, unwavering support throughout these years.

TABLE OF CONTENTS

LIST OF FIGURES

LIST OF TABLES

CHAPTER 1
INTRODUCTION

1.1 Purpose of the study

The optical properties of dissolved organic matter, absorption and fluorescence, have gained a lot of attention in the past decades and many studies have focused on the optical properties of Dissolved Organic Matter, DOM, in different aquatic environments. This concern is mainly due to the ecological importance of Chromophoric Dissolved Organic Matter, CDOM, as is a major factor in light attenuation in the sea and thus affecting the primary production. CDOM and Fluorescent Dissolved Organic Matter, FDOM, have proven though to give valuable information regarding the origin and composition of DOM and the transformation processes that goes through while they can also point out anthropogenic pollution in aquatic environments. Therefore during the last years the optical properties of DOM were also used in order to track water mass mixing in estuarine and coastal environments, distinguish between water masses, examine ocean circulating features as well as to track DOM transformation through various mechanisms. Despite the global interest, data regarding the absorption and fluorescence properties in Eastern Mediterranean are very scarce.

The purpose of the present study is to provide information about the optical properties of CDOM in a large region of the Eastern Mediterranean Sea. The study area covers the Marmara Sea, the Aegean Sea and the adjacent basins i.e. the South Ionian Sea and the Western Levantine Sea, as well as Sperchios river and Maliakos Gulf. The study region involves the North Aegean Sea (NAS) which is a highly dynamic area due to the outflow of Black Sea Water (BSW) and mixing with the Levantine Water (LW). The South Aegean Sea is also of great importance due to the deep water formation inside the Cretan Sea and the potential of dense water export in the adjacent basins. We furthermore investigate whether absorption and fluorescence analysis can give insights into the nature of DOM and its sources and sinks in the various

aquatic environments studied. In order to get some insights on the sources of marine autochthonous CDOM we conducted two laboratory experiments with DOM exudates from macroalgae and zooplankton.

1.2 Outline

Chapter 2 discusses the importance of DOM in aquatic environments and its optical properties. Absorption and fluorescence are discussed along with the indices that are used for the characterization of DOM. Production and removal processes of CDOM and FDOM and global distribution are also reported.

Chapter 3 focus on the Mediterranean Sea and discusses the available data on dissolved organic carbon (DOC), CDOM and FDOM.

Chapter 4 reports the methodology followed in the analysis of the samples and gives a description of PARAFAC modelling.

Chapter 5 presents the results of Marmara Sea and gives an optical characterization of BSW that enters the NAS.

Chapter 6 is focused in the NAS. It examines the influence of the BSW, the mixing with Levantine Water (LW) and the seasonal variation of CDOM.

Chapter 7 presents the results of the South, Central and North Aegean discussing both spatial as well as vertical variations and gives information about CDOM dynamics in surface, mesopelagic and bathypelagic layers.

Chapter 8 presents the results of seasonal samplings in Sperchios River and Maliakos Gulf. These results are used as an indicator of terrestrial inputs in the sea.

Chapter 9 presents some preliminary observations of experiments contacted at the laboratory focusing on the production of CDOM from i) macroalgae and ii) zooplankton.

Chapter 10 provides a synopsis of the results and the conclusions obtained from the study.

CHAPTER 2

DISSOLVED ORGANIC MATTER AND ITS OPTICAL PROPERTIES

2.1 Dissolved Organic Matter

Dissolved organic matter (DOM) is defined as the organic matter present in natural waters and passes through filters with pore size from 0.7μm (GF/F) up to 0.2μm [1]. The importance of DOM is connected to its ecological significance and its central role in the marine carbon cycle. Dissolved organic carbon (DOC) is used as a quantitative index of DOM while the structure and chemical characterization of DOM is still largely unknown. A sub-pool of simple biochemicals such as amino acids, simple sugars, vitamins, ketones, aldehydes and fatty acids has been identified as well as a sub-pool of more complex biopolymers such as proteins, polysaccharides and lignins. The majority though of DOM, is still unidentified due to the need of isolation and concentration before chemical characterization. The uncharacterized DOM is believed that consists by very complex and of high molecular weight degradation products of unknown origin the so called humic substances [1][2][3].

In aquatic environments the main mechanisms of DOM production are the extracellular release from phytoplankton during photosynthesis, grazer-mediated release and excretion, release via cell lysis (viral and bacterial), solubilisation of detrital and sinking particles and release from prokaryotes. [2]. The removal of DOM occurs through both biotic and abiotic mechanisms. Heterotrophic bacterioplankton is responsible for both the transformation of DOM to POM or more refractory forms of DOM [4][5] as well as the remineralization of DOM to its inorganic constituents [6][7]. The most important abiotic sink of DOM is photo-oxidation [8][9][10]011]. Abiotic removal mechanisms also include the sorption of DOM onto sinking particles [12][13] while under physical or chemical changes (temperature, ph) HMW DOM that is in self assembled microgel forms [14] can flocculate into dense particles that can sink.

Figure 2.1, presents DOM cycle in the sea which includes photosynthesis that release labile forms of DOC with turnover times less than few days and microbial and physicochemical processes which can release more resistant forms of DOC, refractory DOC, with turnover times up to 40000 years.

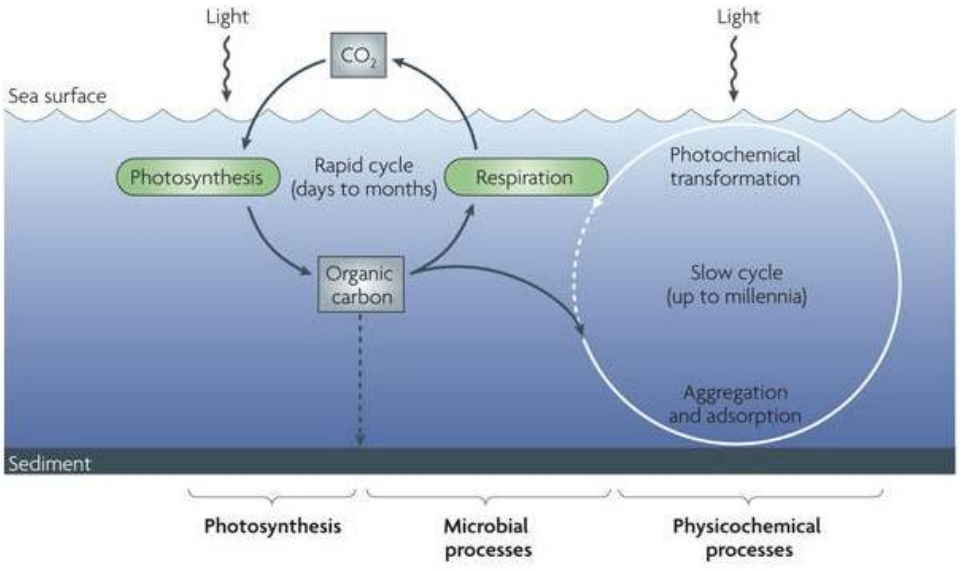

Figure 2.1: DOM cycle in the sea [5].

2.1.1 DOC fractions

Hansell [15], proposed five fraction of DOC based on their lifetime, instead of the more general groups of labile and refractory DOC.

Labile DOC, LDOC, is the fraction of DOC that experiences high turnover, supports heterotrophic microbial production but does not accumulate within the surface ocean for periods of more than hours to days. It is of great importance as it provides autochthonous support for the euphotic zone microbial loop [16][17] but it does not implicate significantly in the biological pump or carbon sequestration as its mineralization product (CO_2) remains in the upper ocean. LDOC probably include the majority of the extracellular released DOM along the photosynthetic production of particulate organic matter (POM) and also the products of food web processes in the euphotic zone. LDOC, however, is also produced within the mesopelagic and bathypelagic zones by processes such as solubilisation of sinking particles, excretion by vertical migrating zooplankton and chemoautotrophy in the deep water column, providing substrate for resident heterotrophic microbes [15].

Semi-Labile DOC, SLDOC, is the primary constituent of DOM that accumulates above the seasonal pycnocline with lifetime ~1.5 years allowing both horizontal and vertical export from the region of formation. Therefore it can provide allochthonous supplemental support for heterotrophic bacterial carbon demand within the euphotic zone as it is exported horizontally via surface currents. On the other hand, the significant vertical export (~1.5 Pg $year^{-1}$ globally) indicates the SLDOC as the most quantitatively important DOM fraction contributing to the biological pump. Due to its relatively short lifetime, SLDOC export is mostly limited to the upper mesopelagic zone (~500m) where it supports subsurface microbial production [15].

Semi-refractory DOC, SRDOC, that requires the presence of a permanent pycnocline, is of secondary importance in the biological pump but its contribution to long-term carbon sequestration is important. SRDOC as well as SLDOC are encounter mostly at the upper 1000m while the composition of SRDOC has not been distinguished from that of SLDOC [15].

Refractory DOC, RDOC, is the fraction observed directly when the SLDOC and SRDOC fractions are absent (commonly at depths >1000m and at DOC concentrations of <42μmol kg^{-1}) where deep DOC vertical profiles show minimal gradient. It is present everywhere in the ocean reaching ~630 Pg C, while it is considered to be a recalcitrant pool that is transported mostly conservatively with the ocean circulation and has a lifetime of ~16000years. Due to its refractory nature it does not seem to implicate into the biological or microbial pump [15].

Ultra-refractory DOC, URDOC is a small, globally distributed pool of DOC that has a lifetime of ~40000 years, greater than the ocean circulation. It constituted by polycyclic aromatic compounds such as thermogenic black carbon. It may have a role in controlling the inventory of atmospheric CO_2 [15].

2.1.1.1 Refractory DOC: Sources, sinks and the role of microbial pump

The molecularly uncharacterized and refractory DOM, resistant to decomposition, has been attributed mostly to abiotic, physiochemical reactions such as the polymerization of low molecular weight, LMW, DOM through condensation reactions catalyzed by light and metal complexation

[18], the binding of monomers to macromolecular DOM [19] and adsorption of labile DOM to colloids [20][21]. Photochemical reactions were also proposed as a source of refractory DOM since the photoproducts resulting from the free radical reaction between the UV light and simple compounds and/or autotrophic by-products can be resistant to biological utilization [22][23][24][25]. Furthermore, the incomplete combustion of biomass and fossil fuels produces a group of thermogenic and refractory polycyclic aromatic hydrocarbons, named as black carbon [26][27], which are leached from soils and are transported to the ocean or are supplied to surface waters via atmospheric deposition [28][29]. The biotic, microbial origin of refractory DOM has also been discussed [30][31][32] the exact mechanism of microbial production of DOM is though unclear. It was believed that the pelagic bacteria receive passively DOM leaking from the grazing food chain while more recent studies showed that bacteria also attack all organic matter through surface-bound enzymes that can cause the hydrolysis of the polymeric DOM [4]. More recently, Jiao et al., [5] proposed that microbial metabolism of labile DOM and trophic interactions within the microbial loop generate refractory DOM. Figure 2.2 presents the biotic transformation processes of DOM in the ocean.

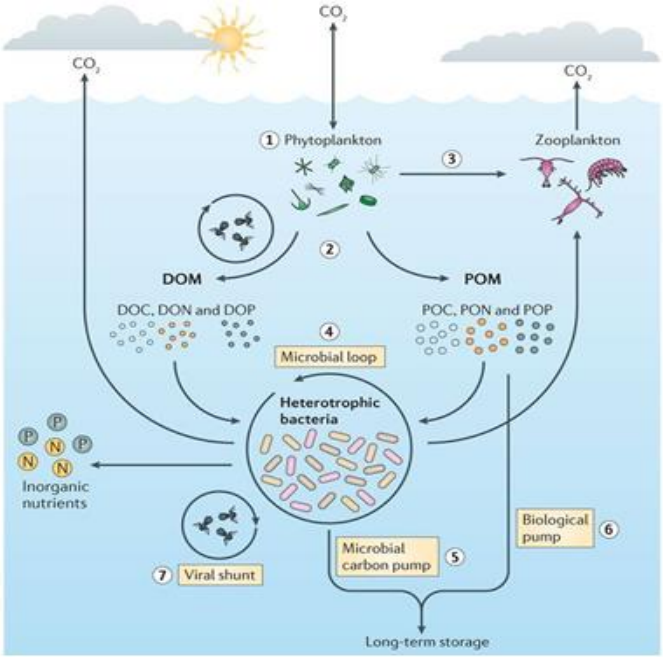

Figure 2.2: Biotic transformation processes of DOM (Buchan et al., 2014)

Microbial loop has gain a lot of attention in the past years and has been characterized as a major biological force in the ocean [33] as it is estimated that on average one half of oceanic primary production is channelled via bacteria and into the microbial loop [4][34]. In fact, in the eastern Mediterranean it has been estimated that the fraction of the primary production used by bacteria is as high as 0.85 [35]. The microbial carbon pump and the biological pump are intertwined in the ocean carbon cycle. The majority of the primary production is in the form of POM while a small portion of the fixed carbon is released as DOM in the water. The biological pump is essentially the process of the downward flux via passive sinking of particles, active transport by animals and mixing, of the organic matter that escapes decomposition and respiration, to the deep ocean and its burial to the bottom. The microbial carbon pump on the other hand, can partially transform the DOM released from primary production and DOM from other sources along the food chain, into refractory DOM. The biological pump therefore relies on vertical flux of organic matter in order to store carbon in the deep ocean while the microbial carbon pump acts independently of depth, and it is able to sequester carbon in recalcitrant forms from the surface up to the deep ocean. Specific cellular components of bacteria have been identified in marine DOM indicating microbial origin [36] while Kaiser and Benner, [37], estimated that about 25% of the DOC throughout the ocean water column is of bacterial origin. Several bioassay experiments have demonstrated that the microbial activity can rapidly transform labile substrates to semilabile and refractory forms [30][38] and produce dissolved humic substances [31] while the molecular weight distribution of the accumulated DOM was similar to that of natural marine DOM suggesting similar processes between the experiments and the ocean. Ogawa et al., [39] demonstrated that bacteria can utilize labile substrates such as glucose and glutamate to produce semilabile, chemically complex and refractory DOM within hours to days, while Kramer and Herndl [40] and Shimotori et al., [41] furthermore illustrated that refractory chromophoric DOM can also be released from bacteria upon glucose utilization. Overall, Benner and Herndl [42] estimated that the microbial pump maintains ~155Pg of RDOC and also 10Pg of the less recalcitrant fractions. Consequently, it is now believed that the microbial processing of organic

matter may generate ~25% of the global DOC inventory and ~50% of SLDOC plus SRDOC [15].

Hansell [15] suggests that the losses of SRDOC and RDOC could involve biotic processes as shown by the regression of oceanic DOC concentrations and the apparent oxygen utilization (AOU) [43][44][45] as well as abiotic mechanisms such as scavenging onto suspended or sinking particles. Furthermore, at the surface layer the RDOM may be altered via photo-oxidation and become susceptible to microbial mineralization [9][22][46]. In the deep ocean, formation of organic gel can occur [14][47] that are either adsorbed onto suspended and sinking particles or even form new particles [48][49].

2.1.2 DOC in the oceans

DOC exists in the ocean at extremely low concentrations (~34 to >80 μmol kg^{-1}). Higher concentrations, 65-80 μmol kg^{-1}, are encountered at warm tropical and subtropical systems (40˚N to 40˚S) where the vertical stratification of the upper column allow the accumulation of DOC. Contrary, subpolar areas and the circumpolar Southern Ocean (>50˚S), present lower concentrations, ~40-50 μmol kg^{-1}, due to the deeper vertical mixing that dilutes surface accumulated fractions with low DOC concentrations from depth [15]. DOC that has accumulated in the subtropical gyres is either exporter of surface waters through the ventilation of the main thermocline and transport to depths of a few hundred meters or is curried by the surface currents from low to high latitudes and is exported to greater depth with ventilation of the deep ocean interior [45][50][51]. Export of DOC to greater depth is also observed in other locations where deep water formation occurs, such as in the Mediterranean Sea [52]. Through this mechanism, waters ventilating the intermediate and deep portions of the ocean effectively sequester the carbon for years to centuries [15].

2.1.3 DOC in coastal waters

Rivers, wetlands, upland ecosystems as well as coastal vegetation and anthropogenic pollution are the main sources of DOM in the coastal environments, each one contributing DOM in different amounts and quality.

Overall, the coastal environments are characterized by high concentrations of lignin phenol which is a constituent of terrestrial vascular plants as well as dissolved black carbon that originates from combustion sources such as wildfires and fossil fuel burning [53].

The total riverine DOC flux to the ocean is estimated to be ~ 260Tg C per year. In general, riverine organic matter pools are made up of complex mixtures of compounds of varying ages [53]. Relatively undisturbed small watersheds show a tendency of young DOM [54] mostly during high flow as at higher discharge, riverine DOM takes on a more terrestrial character due to a shift in sources (greater leaching of organic rich soil horizons and surface litter layers) while older DOC can be found both during lower flow as the DOM shifts to a less terrestrial nature due to the increased residence time and therefore greater potential for microbial mineralization [55][56] as well as in rivers that are rapidly eroding old soil profiles [57]. DOC has been found to behave conservatively in the estuaries [58][59] while non conservative behaviour was also observed. The nonconservative behaviour has been attributed to the removal of specific components of the DOM pool [60][61] but also to concurrent inputs of DOM from anthropogenic pollution, phytoplankton productivity, salt marshes, tributaries and desorption from sediments and flushing of porewaters [60][62][63]. Furthermore, there are contradictory findings whether the marine bacteria are more capable in consuming terrestrial DOM than the riverine bacteria contributing to the nonconservative behaviour of DOC [64][65][66].

Wetland can export significant amounts of DOM [67][68] which can be characterized as more fresh [63] that is though less microbially available than the phytoplankton exudates and other DOM sources [69][70] but highly photo-reactive [71]. The export of DOM from upland systems is more significant during precipitation events. Salt marshes, seagrasses and mangroves export large amounts of DOC per unit area due to the consistently flooded root systems and direct contact between plants, their detritus and water, resulting to ~10-100$gCm^{-2}year^{-1}$ [53][72]. Furthermore, a large proportion of exported detrital material from these areas is transformed to DOM in coastal waters [73], resulting to even higher DOC inputs.

Less than 75% of the DOM exported from land reach the ocean [74][75] while more than 25% is lost during the transport. DOM undergoes various biogeochemical reactions such as flocculation, adsorption onto suspended sediments and microbial and photochemical degradation in the river plumes, estuaries and at the land-ocean interface that determine both the concentration of DOC as well as the composition of DOM that reach the ocean [61][71][76]. Photochemical degradation of DOM is typically minimal in rivers [77][78]; in plumes and coastal waters however DOM becomes highly susceptible [79]. Lignin phenols and black carbon are among the most sensitive to photodegradation substances [61][80][81]. Black carbon molecules are particularly resistant to biodegradation [82] comprising ~10% of the global riverine flux of DOC to the oceans [29]. Thus photochemistry holds a unique role as it preferentially removes biorefractory fractions of terrestrial DOM.

2.2. Optical properties of DOM in aquatic environments

A fraction of the DOM has the ability to absorb light in the UV and visible region of the electromagnetic spectrum and is called Chromophoric Dissolved Organic Matter (CDOM). Due to the yellow or brown color resulting from high concentrations of CDOM, it was firstly termed as ‘yellow substance’ or ‘gelbstoff’ (in german) [83]. CDOM was estimated to made up between 20 and 70% of the total DOC [84]. The fraction of CDOM that additionally has the ability to fluorescence is called Fluorescence Dissolved Organic Matter (FDOM). CDOM plays a very important role in cycling carbon, trace elements and trace gases of importance to biological activity and global climate [85]. CDOM in aquatic environments is one of the major factors regulating the ultraviolet and visible light attenuation due to the strong absorbing ability at the UV-Visible region of the solar spectrum [86]. It has been shown that CDOM can play a significant role in light attenuation even in clear, open ocean waters [87][88]. Therefore is of great importance regarding the primary production as it can limit the available light for photosynthesis, while on the other hand it can act as a protective shield for the plankton populations absorbing the harmfull UV radiation [89]. In addition, the interaction of CDOM with UV radiation can lead to reactants such as hydroxyl radicals that could be

harmfull to live organisms [9][90][91] while it can also mediate redox reactions of some trace metals and influences air-sea exchange of trace gases [9][92]. On the other hand the photoreactivity of CDOM can act as a fuel for the microbial growth forming bio-available compounds [10][46]. Moreover, CDOM implicates with the remote sensing applications [93][94] and should be taken under consideration in the estimations of chlorophyll concentrations from space [95]. Therefore CDOM was primarily used for the quantitative estimation of the absorption fraction of DOM and also in order to derive information about the origin, quality, structure and diagenetic state of DOM. CDOM has also proven to be a useful tool in other applications such as the investigation of the mixing processes in coastal and estuarine waters [96][97], distinguishing between water masses of different origin [98][99], tracking distribution of river-borne pollutants [100], verifying exchange of ballast water in ocean-going vessels and the investigation of ocean circulation features such as upwelling and eddies [101][102][103] .

Natural waters can be distinguished in two cases regarding the origin of the absorbing material. Systems that are unaffected by external sources and the optical properties of waters are determined by the functioning of the local marine ecosystem (photosynthetic, metabolic and decay processes) are named as ‘Case 1 waters’ [104]. Contrary, systems in which allochthonous substances play a significant part in the interaction with light are referred as ‘Case 2 waters’[104]. ‘Case 1 waters’ represent mainly open oceans while ‘Case 2 waters; include coastal and estuarine environments.

2.2.1 Absorption of UV-visible light

Absorption of visible and UV radiation occurs through the interaction of photons with the valence electrons of a molecule. When the energy of a photon equals the energy distance between the ground state and an excited state, then the photon can be absorbed by a valence electron for the transition to the excited energy state. The absorption at the visible and UV region of the spectrum is attributed to π-electrons that are characteristic of unsaturated bonds and to n-electrons which are nonbonding electrons and are typical of molecules containing atoms of elements such as oxygen, nitrogen and

sulphur [105][106]. The part of the organic compound capable of absorbing light is called a chromophore. The light absorption bands of the transitions of n electron to σ orbital and π electron to π orbital are in the mid-UV region of the spectrum while those of n electrons to π orbital require less energy and therefore are in the near-UV and visible regions [105]. These electronic transitions characterize the nature of the light absorption while the intensity is determined by the molar absorptivity (ε) and concentration (c) of the chromophore according to the Beer-Lambert law:

$A=\varepsilon cl$

where A is the absorbance measured by spectrophotometer, a unitless ration of spectral radiant power transmitter through the sample across the pathlength, l (i.e. the width of the cuvette used in the measurements):

$A=\log_{10}(I_0/I)$ where I_0= incident intensity, I= transmitted intensity

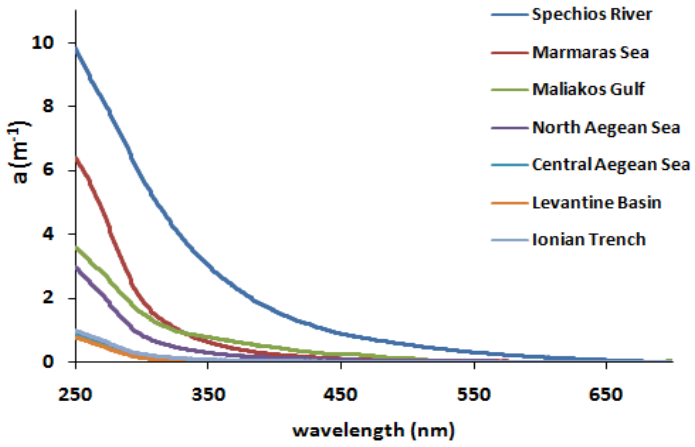

Figure 2.3: Absorption spectra in surface water of different regions.

Figure 2.3 illustrates typical absorption spectra of CDOM in different aquatic environments. It is characterized by an exponential decrease from the UV region, (250nm) towards the visible and IR regions (700nm) with no discernible peaks. This feature is due to the fact that CDOM is a complex mixture of compounds that have overlapping absorption spectra with no single compound dominating [85]. High conjugated molecules and aromatic rings increase both absorption wavelength as well as molar absorptivity. Therefore simple aromatic compounds exhibit absorption at wavelengths <300nm while more complex, conjugated substances present broader spectra shifted to

greater wavelengths. Especially at long wavelengths, >350nm, absorption is a result from a continuum of coupled states which are connected through intramolecular charge-transfer interaction between electron donors and acceptors formed through the partial oxidation of lignin and other hydroxyl- or polyhydroxy- aromatic substances, rather than from the summation of multiple individual compound absorption spectra [107][108][109]. Species that are capable of these interactions are considered of terrestrial origin due to the lignin and phenolic content [107].

Because absorbance is depended on the length of the light path, comparisons based on absorbance are difficult and therefore the napierian absorption coefficient α(λ) with units of m^{-1} and normalizated to the light pathlength is used:

$$\alpha(\lambda)=2.303*A(\lambda)/l$$

The absorption spectrum provides quantitative information on CDOM through the intensity of the absorption coefficients as well as qualitative information through the shape of the spectrum expressed by the spectral slope with units of nm^{-1}. The spectral slope is defined by the following equation [110]:

$$\alpha(\lambda)=\alpha(\lambda_0)e^{-S(\lambda-\lambda_0)}$$

where $\alpha(\lambda_0)$ is the absorption coefficient at reference wavelength.

The slope is better estimated by using a non linear regression routine and it is mostly dependent by the lower bounds of the wavelength range across which the model is fitted [111]. The spectral slope has been proposed to be indicative of CDOM origin with generally lower slopes in freshwater and coastal environments and higher in open oceans [112]. This is also evident in figure 2.3 presenting the absorption spectra in surface samples of various marine and riverine waters. Slope is also an indicator of CDOM quality and diagenetic state. Photobleaching has been shown to cause an increase in slope values [113] while slope was also negatively correlated to the weighted average molecular weight of DOM and therefore can be used as a proxy for average molecular weight [114][115]. Bacteria activity has also been shown to have a decreasing effect on spectral slope [116][117].

The comparison though of spectral slope S between studies is rather limited due to its dependence on the wavelength interval over which it was calculated and the method used for the calculation (linear or non linear regression fitting). Therefore, the slope at the short wavelength range of 275-295nm, $S_{275-295}$, was proposed by Helms et al., [118] as an alternative to S. $S_{275-295}$ can also serve as an indicator of shifts in MW and CDOM sources as Helms et al., (2008) showed that it is inversely related to molecular weight while small values of $S_{275-295}$ indicate fresh, terrestrial CDOM. It was furthermore shown that photobleaching cause an increase in $S_{275-295}$ [118][119] making this index also useful to track the photo-transformation of CDOM. $S_{275-295}$ was also found to be inversely related to microbial activity [118]. Helms et al., [118] also proposed the dimensionless parameter S_R which is the ratio of $S_{275-295}$ to the slope at a longer wavelength region of 350-400nm as an additional index that could truck changes in CDOM origin, molecular weight and microbial and photo-transformations of CDOM. Like $S_{275-295}$, low S_R values indicate CDOM of terrestrial origin while it is also inversely related to MW and microbial activity but positively related to photodegradation.

Another index derived from the absorption spectra has been used in order to give more qualitative characteristics of CDOM; the carbon specific absorption coefficient, a*(λ) with units of $m^2g^{-1}C$. This index is the ratio between the value of the absorption coefficient at a certain wavelength and DOC concentration of the sample. Carbon specific absorption coefficient is an indicator of the color indensity of CDOM and is positively correlated to the MW and aromaticity [120].

2.2.2 Fluorescence of UV-visible light

Fluorescence generally occurs when an excited electron due to the absorption of light relax to the ground state giving up its excess energy as photons. Fluorescence occurs almost always from the lowest-lying excited electronic state to the ground state. Fluorescence though is not always observed upon excitation of an electron as in some cases the relaxation occurs through internal conversion. Internal conversion involves the transfer of the excess energy of species in the lowest vibrational level of an excited electronic state to solvent molecules and conversion to the excited species to a lower or the

ground state without emitting light [106]. Figure 2.4 shows the excitation of an electron caused by absorption of incident radiation and the relaxation through both internal conversion and fluorescence emission.

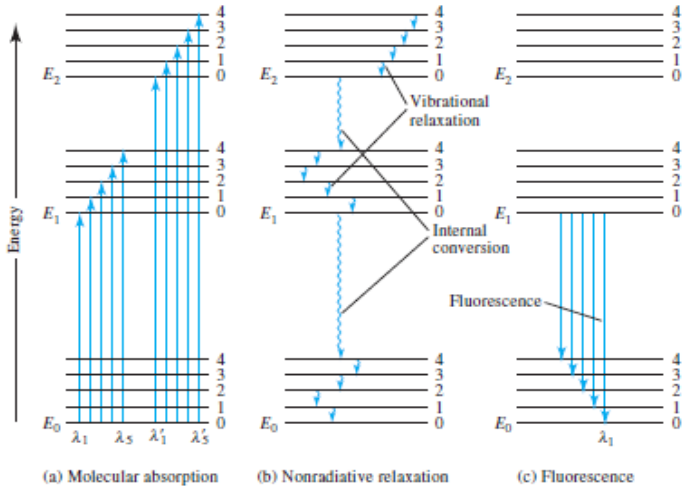

Figure 2.4: a) absorption of radiation, b) internal conversion, c) fluorescence [106].

Aromatic compounds have fewer vibration degrees due to their rigid structures and therefore often exhibit fluorescence. Contrary aliphatic compounds usually relax without fluorescence. In addition, as the MW, the conjugation of aromatic compounds and oxidized forms increase, the energy difference between ground and excited states decreases resulting in a longer wavelength fluorescence, a process termed as red shift [111][119][121].

The fluorescence properties of seawater were recognized as early as 1949 and were attributed to the presence of CDOM [123]. Fluorescence techniques are more sensitive than absorption spectroscopy and both excitation and emission spectra show greater detail and provide more information regarding the chemical composition than do absorbance spectra [85]. A relatively new technique that collects hyperspectral fluorescence data, the excitation-emission matrix spectroscopy (EMMs) involves collection of multiple emission spectra at a range of excitations which are concatenated into a matrix [124]. The fluorescence properties of FDOM are largely limited to excitation wavelengths 240-500nm and emission wavelengths 300-600nm. Emission at excitation wavelengths below 240nm is not obtained due to the low excitation intensity in standard fluorometers while inner filter effects in standard cuvettes

are very high due to the high absorbance by CDOM resulting to a very low fluorescence signal with substantially low signal to noise ratio [111].

EEMs matrices provide information that allows the discrimination of CDOM sources based on which fluorophores are present and their relative concentrations. EEMs also provide information on changes in CDOM resulting from mixing, biological production and degradation, and photobleaching [85]. Many fluorescence peaks have been identified in natural waters and categorized in distinct groups [66][125]. Two groups distinguish as they are widely observed; the humic-like that exhibit fluorescence at the visible region therefore its signal is referred to as 'humic-fluorescence' or 'visible-fluorescence' and the amino acid-like group that exhibit fluorescence at the UVA region and is referred to as 'amino acid-fluorescence' or 'protein-like fluorescence' or 'UVA-fluorescence'.

Huguet et al. [126], furthermore proposed the humification index, HIX and biological index BIX, for studying the complex DOC dynamics in estuarine environments and later on many studies included these indices in the investigation of CDOM in various marine environments [127][128][129]. High HIX values indicate the presence of high molecular weight complex aromatic substances, while increase of the BIX index indicates an increase in the fluorescence characteristics of autochthonous CDOM, released from biological activity.

2.2.2.1 Amino acid-fluorescence

The amino acids that are capable of absorbing and emitting light at the UV region are only those containing aromatic rings, i.e. tyrosine, tryptophan and phenylalanine. Tyrosine and tryptophan both absorb strongly at 275nm and emit at 300nm and 350nm respectively. Phenylalanine though reveals excitation (255nm) and emission maxima (<300nm) shifted to shorter wavelength and gives a weaker signal compared to the other amino acids due to the fact that the relevant transition is spin forbidden [105]. Therefore phenylalanine is difficult to be identified in aquatic environments. In aquatic environments, amino acid-fluorescence is likely derived from a mixture of dissolved amino acids and other organic materials with similar fluorescence

characteristics rather than pure dissolved amino acids [130][131[132]. Peaks with excitation and emission wavelength close to those of tyrosine were named by Coble et al., [124][125] as peaks B and were attributed to substances with similar structure to tyrosine amino acid while peaks similar to that of tryptophan were named as peaks T and attributed to substances that resemble the tryptophan amino acid (Table 2.1). Substances responsible for both peaks T and B are considered to be products of biological activity representing freshly produced DOM [133] and they have been found to be strongly correlated to measured concentrations of the corresponding amino acids in the waters as well as with the total hydrolysable amino acids [130]. Peak T is considered to be indicative of the presence of intact proteins or less degraded peptide material while Peak B is considered to be representative of more degraded peptide material [66]. Tryptophan fluorescence shifts to shorter wavelengths (blue shift) when bound in proteins due to shielding from water [134][135]. Tyrosine on the other hand, when bound in proteins is difficult to detect due to energy transfer to tryptophan and quenching by neighbouring groups [135].

Few other peaks presenting spectral characteristics resembling the tryptophan and tyrosine fluorescence have been reported. One of the most common is peak N (Ex/Em= 280/370nm) which is considered to be very labile and it was associated with freshly produced DOM and increased phytoplankton activity [66,125].

Table 2.1: Commonly observed natural fluorescence peaks in aquatic environments.

Peak Name	***Excitation and Emission maxima***	***Nature***
B	270-275nm / 304-312nm	Tyrosine-like
T	270-280nm / 330-368nm	Tryptophan-like
A	<260nm / 448-480nm	HMW and aromatic humic-like
M	290-325nm / 370-430nm	LMW Humic-like
C	320-360nm / 420-460nm	HMW humic-like

2.2.2.2 Humic-fluorescence

The humic-fluorescence is characterized by broad emission spectra around 400-600nm. The fluorescence of these substances in the visible region is due

to the presence of large number of aromatic rings and the high conjugation of the molecules that allow the absorption of low energy radiation and the emission at a broad band. It was called humic-like due to the fact that similar fluorescence was reported originally in soil organic matter and XAD extracts. Marine humic substances have been linked to the humic and fulvic acids found in soils and transported via rivers to the oceans as aquatic humic substances. Terrestrial humic materials display excitation and emission maxima at longer wavelengths than do marine humic-like materials due to the more aromatic chemical nature and higher molecular weight as they contain lignin, phenols and other plant degradation products [85]. Marine humics on the other hand are less aromatic, have lower C/N ratios and contain more carboxylic groups and sugars than the terrestrial humics [136][137]. This is probably the cause of the blue shifted fluorescence of the marine humics compared to the terrestrial.

Three primary peaks of humic character were identified in natural waters [124][125] named as A, C and M. The excitation and emission wavelengths of the peaks are given in Table 2.1. Peaks A and C exhibiting broad emission bands over 400nm represent the higher molecular weight fraction of the DOM and are considered to have a strong terrestrial character while substances representing peak A are considered to be of higher aromatic character than peak C [66][125]. Both peaks are widespread but are particularly high in wetlands and forested environments [66]. Peak M on the other hand exhibit emission at shorter wavelengths and is thought to be less aromatic and of lower molecular weight than peaks A and C. It is common in marine environments associated with biological activity but it can be also found in wastewater, wetland and agricultural environments [66][138][139]. Catala et al., [140] estimated the turnover time of peak M in the global ocean at 610±55years while a component with two emission maxima representing both peaks A and C was estimated to have a turnover time of 435±41years. Both turnover times exceed the turnover time of the bulk DOC, 370 years [141] as well as the turnover time of the terrestrial DOC in the open sea, <100 years [61] indicating the refractory nature of these humic substances. A variety of other peaks presenting spectral properties characteristic of humic

fluorescence were reported in literature which were attributed to degradation products of terrestrial material [131] [142] or anthropogenic pollution [129][139].

2.2.3 CDOM sources

CDOM in the sea can be of either autochthonous or allochthonous/terrestrial origin. Autochthonous CDOM is more pronounced in the open ocean [88] [143] while at coastal areas the terrestrially derived CDOM dominates [112][144]. Riverine discharges are the main supplier of the sea with allochthonous CDOM which is mostly synthesized by degradation products of terrestrial plants or substances leached by soils and can be modified along the route to the coastal waters [111] (see also section 2.1.3). Due to the large variety of compounds that compose the riverine inputs, including complex and humic substances, CDOM presents high absorption coefficients and low slope values. Allochthonous CDOM can also result from anthropogenic runoffs, sewage disgorge and other effluents [85]. Autochthonous CDOM on the other hand is produced within the system via various mechanisms. Direct release of CDOM by phytoplankton has been supported by many studies either through culture experiments or field observations where CDOM was found to covary with chlorophyll [116][125][145][146][147]. Contrary, other studies suggested that microbial processes are responsible for the majority of the autochthonous CDOM production [148][149][150]. CDOM maximum lagging behind algal blooms by about 1-2 months has been recorded in field studies [88][151] while at the same time it was at the depth of bacterial abundance maximum and was therefore attributed to bacterial processes. Other studies though [146][152] suggest that the post-bloom production is rather attributed to bacterial activities coupled to plantkonic food web interactions rather than only bacterial activity. In addition, in coastal and estuarine environments CDOM release from marshes and tidal flats has also been observed [68][153]. Abiotic processes can also contribute to the oceanic CDOM. Photoreactions have been shown to produce CDOM in some cases such as the photooxidation of fatty acids and triglycerides while also the interaction of tryptophan with natural DOM under solar radiation [154][155]. CDOM can be also released from sediments especially in coastal waters and shelf seas where sediment

resuspension and hypoxia events occur [62][156][157]. CDOM was also found in pore waters representing refractory low molecular weight material generated during diagenesis of sediment organic matter [158][159]. Release of this organic matter from sediment pore waters seems to appear under anoxic conditions, while under oxic conditions the organic matter retains in sediments by association with iron oxides [156].

2.2.3.1 Sources of amino acid-fluorescence

Some studies claim that substances responsible for the amino acid-like fluorescence can be directly release by phytoplankton. Romera-Castillio et al., [147] demonstrated the production of peak T at axenic cultures of four common phytoplankton species. Likewise, Chari et al., [160] showed the production of peak T in bacterial free cultures of three microalgal species, while Fukuzaki et al., [161] demonstrated the production of both peaks T and B at axenic cultures of eight species of bloom-forming marine phytoplankton. Contrary other studies claim that the protein-like fluorescent substances are products of the bacterial activity utilizing the products of primary production or other simple compounds [150][162][163]. Substances responsible for the presence of peaks B and T were considered to be biolabile and have been used as a tracer of the dynamics of labile DOM [130][164][165] while they were found to be also correlated with the bioavailable fraction of DOC [166]. On the other hand, a concurrent production of both labile and refractory protein-like fluorescent substances along the microbial activity has been reported [150][166], while Catala et al., [167] estimated the turnover time of tyrosine-like component in the dark ocean (>200m) at 379 ±103 years. This long turn-over time was assumed to be attributed to a minor fraction of more refractory tyrosine-like substances among the bulk labile pool.

2.2.3.2 Sources of humic-fluorescence

The appearance of humic substances in marine environments was attributed to terrestrial as well as autochthonous origin, both abiotic and biotic. Polymerization of simple molecules such as sugars, amino acids and other small molecules under the influence of UV radiation has been suggested to result in the formation of humic substances [168]. The main source though of

marine humics was thought to be the allochthonous input of terrestrial humic material. Thurman, [169] suggested that marine humics are products of degradation processes acting on terrestrial humics, mostly comprised by major plant biochemicals. Murphy et al., [139] examining waters across the Atlantic and Pacific oceans reported that terrestrial humic-like CDOM components can be traced to the open ocean at levels up to ~1.5% of riverine signal, suggesting a significant contribution of modified terrestrial CDOM to the open oceans. Hernes and Benner, [170] reported that 10-16% of annual fluxes of terrigenous DOM from Arctic rivers could be entrained during North Atlantic deep water formation while they estimated that the terrigenous DOC accounts for 1-2% of the DOC in surface and deep waters of the North Atlantic. Moreover, Andrew et al., [171] through the investigation and comparison of the absorption and fluorescence properties of marine and terrestrial humics and their response to the reduction of carbonyl-containing moieties, concluded that dissolved humic material in the Equatorial Atlantic is possibly of terrestrial origin. On the other hand autochthonously produced visible FDOM through microbial activity has been widely reported. Rochelle-Newall and Fisher, [148] proposed the production of FDOM with signal at Ex/Em=355/450nm during the bacterial processing of non chromophoric organic matter released by a small selection of marine and estuarine algal species. Likewise, Kramer and Herndl, [40] recorded that bacterioplantkon utilizing glucose produce FDOM with similar signal (Ex/Em=350/450nm). Nieto-Cid et al., [165] reported the production of peak M in incubated unaltered natural marine samples that was positively correlated to the consumption of dissolved oxygen. Stedmon and Markager, [164] demonstrated the production of a variety of humic components similar to peaks A, M and C during the microbial processing of algae-derived DOM. Romera-Castillio et al., [163] furthermore indicated that bacteria growing on phytoplankton exudates utilize both protein-like substances as well as humic-like substances fluorescing at the region of peak M while they mainly produce more complex humic substances representative of peak C. Jorgensen et al., [172] also demonstrated the long term (13months) production of recalcitrant substances with fluorescence maxima at 438nm which is more pronounced during microbial turnover of semilabile DOM rather than labile DOM. Many

other studies also manifest the bacterial production of humic nature FDOM [41][150][166][173], indicating that even complex molecules resembling the fluorescence properties of traditional terrestrial humics can be microbialy produced in the oceans. This microbially produced humic fluorescence is furthermore considered to be recalcitrant as it accumulates over time when not exposed to UV light [40][148][172].

2.2.4 CDOM removal processes

The most significant removal mechanism of CDOM in the ocean is photodegradation [79][90][174]. Direct mineralization of organic matter can occur through the interaction of CDOM with UV radiation [175] or indirect by the production of compounds that are more labile to microbial degradation [165]. Photoreactions result in the reduction of the extent of π-electron system of humics, the elimination of functional groups and the reduction of molecular weight. The overall effect of photodegradation on CDOM properties is the decrease of absorption coefficient, increase of the spectral slope [176][177][178][179] and the blue shift in fluorescence maxima [85][179]. Swan et al., [178] furthermore demonstrated that diversity on CDOM composition has a significant effect on photobleaching while they also showed the appearance in the surface ocean of low values of photobleached CDOM that is resistant to further photodegradation. Microbial decomposition has also been proposed as CDOM removal pathway [79][180] it has been shown though to be of less importance than photodegradation [177] and restricts mostly to very labile compounds that are freshly produced by phytoplankton [149] [116]. Overall, terrestrial CDOM has been found to be more susceptible to photodegradation than biodegradation while CDOM released by phytoplankton is characterized by a more bio-labile character [181]. It was though shown the existence of semilabile or even refractory CDOM that escapes both microbial degradation and photobleaching and is transported to deeper layers [149] [155].

2.2.5 CDOM global distribution

2.2.5.1 Geographical distribution

The highest CDOM concentrations are encountered in estuaries, coastal regions, continental shelf and restricted seas due to the terrestrial inputs, [111][143]. The spectral shape of these regions is closest to exponential compared to the open ocean [143].The distribution of CDOM in estuaries has been generally observed to be conservative, with decreasing CDOM concentrations as salinity increases. This reflects the dominance of riverine CDOM in the system that often carry high concentrations of CDOM due to the leaching of organic matter from soils. Exceptions were attributed to in situ production, local production in saltmarshes and mud flats that fringe the estuary [85]. Terrestrial CDOM has been found though to decline rapidly across the continental shelves due to precipitation, mixing and photodegradation [85][112][145]. Therefore terrestrial CDOM does not appear to influence open ocean surface waters on an annual timescale, but it may be present as a persistent background [61][88][143]. Overall, in the open ocean CDOM reveals generally lower concentrations, somehow elevated though values can be found at high latitudes and in upwelling areas reflecting the contribution of both productivity and CDOM-rich deep waters. The highest overall CDOM in the ocean is recorded in the subarctic North Atlantic and Pacific while intermediate values are found in the equatorial upwelling regions and the Southern Ocean. Contrary, the lowest CDOM concentrations are found in the subtropical gyres due to the low productivity, high stratification that leads to long residence time of surface water above the mixed layer and prolonged exposure to sunlight. Extremely low values are found in the subtropical South Pacific [85][143][182][183].

2.2.5.2 Vertical distribution

CDOM abundance in surface waters is controlled by a balance between production, photodegradation and mixed-layer dynamics [143]. The ocean surface waters usually reveal low absorption coefficient values and high and variable slope values due to photo-oxidation while below the surface CDOM concentrations generally increase [85]. Visible fluorescence also reveals

depletion in the surface waters [128][167][182][184] as it was shown to be more sensitive to photodegradation compared to UV fluorescence [138][165][179]. Exceptions though with high humic fluorescence near the surface were observed in the North Atlantic and upwelling regions such as the Equatorial and South Atlantic and Eastern South Pacific [184] and were attributed to both nutrient fertilization by deep waters that results in net production of humic fluorescence [162] as well as the upward flux of humic substances from deep layers [162][185]. Contrary, open ocean surface waters at the subtropical oliogotrophic gyres of the central North Pacific and Indian Oceans showed total removal of the C humic-like peak [125][167]. On the other hand, the surface oceanic fluorescence has characteristically enhanced UVA fluorescence signal [128][184]. It was shown that UVA fluorescence at the global ocean scale is strongly related to salinity indicating that the spatial variations of the UVA fluorescence are controlled by physical processes such as changes in evaporation-precipitation regime [167].

Below the surface there are often local CDOM maxima associated with or just below the deep chlorophyll maxima in the lower photic zone [128][146][186]. CDOM maxima observed in some areas like Pacific Ocean [187][188], Indian Ocean and Sargasso Sea [88] were attributed to remineralization processes of sinking organic matter and the extreme length of time since ventilation of the deep water masses of the Pacific and Indian Ocean basins [143][183]. Also upwelling of deeper waters has been found to contribute in subsurface CDOM maxima [125]. Visible fluorescence also increases with increasing depth while the opposite is observed for UVA fluorescence. The decreasing trend of UVA fluorescence was attributed to its biolabile character leading to rapid consumption by bacteria as shown in incubation experiments as well as in field observations were negative correlation was found between UVA fluorescence and AOU [138][165][166][184]. Waters of the aphotic ocean present enhanced visible fluorescence signal. This fluorescence probably represents material that is produced by heterotrophic bacteria acting on DOM or biogenic sinking particles as strong correlations have been found with AOU and nutrient mineralization [140][165][184][187][189]. Peaks C and M appear to be a ubiquitous oceanic humic-signal as they were both identified with

almost identical spectral characteristics in studies involving different regions of the global oceans [184][190]. Murphy et al., [139] though reported the presence of two humic components representing terrestrial material in the Atlantic and Pacific open ocean, beside the autochthonously produced humic components. Likewise, Jorgensen et al. [184] reported the presence of a fluorescing component in the North Atlantic that was attributed to terrestrial lignin-like material while Catala et al., [140] reported high terrestrial humic signal in the North Atlantic Deep Water that was attributed to the high load of terrestrial fluorescent material transported by the Arctic rivers. Finally, both humic-like and protein-like fluorophores have been detected in sediment porewaters [99] (Coble, 1996, Komada et al., 2002, 2004; Burdige et al., 2004). Diffusion, bio-irrigation and resuspension from organic-rich sediments may serve as a locally important source of CDOM/FDOM in the deep ocean [159][191].

2.2.6 CDOM-DOC relationships

Correlation between DOC and CDOM has been reported almost only in coastal environments under the influence of significant terrestrial inputs, mixing and limited degradation processes [113][192][193][194]. Contrary there is a complete lack of relationship between CDOM abundance and DOC concentrations in the ocean [88][143]. This lack of association in the open sea was attributed to the various processes occurring in the sea e.g. photochemical oxidation and degradation that have been shown to have different impacts on DOC and CDOM resulting to the decoupling or nonlinear relationships between the two pools [107][143]. These relationships indicate that CDOM is a small part of the oceans total DOC pool but is enhanced in coastal environments under the freshwater influence [87][88][143][183].

CHAPTER 3
MEDITERRANEAN SEA

3.1 General Characteristics of the Mediterranean Sea

The Mediterranean Sea is an elongated and semi-enclosed basin, with an anti-estuarine circulation pattern forced by the negative hydrological balance and the density gradient with the Atlantic Ocean [195]. It covers about 2.5 million km^2 with an average water depth of about 1.5 km [196]. The drainage basin of the Mediterranean Sea is roughly 1.5 million km^2 with an average land to sea area ration of 0.55 (0.79 for the Western and 0.43 for the Eastern Basin) [197]. The Mediterranean Sea is characterized by the limited water exchange with the Atlantic ocean through the Gibraltar strait where Atlantic water inflows in the surface layer and the Levantine Intermediate Water (LIW) outflow at mid-depth. Mediterranean Sea is divided in two sub-basins linked via the Sicilian strait, the Western and Eastern Mediterranean basins. Water mass circulation of the Eastern Mediterranean Basin will be further discussed in chapter 7. An exceptional feature of the Mediterranean Sea is the formation of specific deep waters during the winter. In the West Mediterranean the most active convection and deep water formation occurs in the gulf of Lions while in the Eastern Mediterranean deep water formation occurs mainly in the North Aegean and Adriatic Seas. Intermediate water of Levantine origin is also formed in the vicinity of Rhodes gyre.

The Mediterranean Sea carries low nutrient concentrations. The oligotrophic character of Mediterranean Sea increases from west to east. The low nutrients content has been attributed to the export of the rich in nutrients deep waters to the Atlantic Ocean caused by the prevailing water circulation [198] resulting to a definitive lose of these nutrients for the basin internal primary production [197]. Therefore rivers seem to play a significant role in sustaining the marine productivity of the Mediterranean Sea since zones with high productivity are mainly restricted to the coastal waters in the vicinity of freshwater inputs [199]. The two largest rivers of the Mediterranean Sea are the Rhone and Po and account for about the one third of the freshwater input,

while there is a great number of small rivers due to strong relief favouring the formation of small watersheds. Estimates of the riverine freshwater inputs in the Mediterranean Sea range from 400-450 km^3yr^{-1}, the accurate though estimation is difficult due to the presence of many small rivers that are not monitored and the major changes in the discharge of Nile river due to infiltration in swamps, river evaporation and anthropogenic water use [197]. Ludwig et al., [197] estimated that there was at least a 20% decrease in freshwater discharge to the Mediterranean Sea over the 1960-2000 period due to both the climate change but also the dam construction that reduce discharge even further. Also they reported an important increase in the inorganic nitrogen flux while they also confirm the phosphorus limited character of the Mediterranean Sea.

3.2 DOC in the Mediterranean Sea

3.2.1 DOC distribution

The total DOC stock in Mediterranean Sea is $1980x10^{12}$gC, from which the 1309 $x10^{12}$gC are encountered in the East Mediterranean and 671 $x10^{12}$gC in the West Mediterranean. Around 7.7-9.7 $x10^{12}$gC per year are imported from the Atlantic Ocean through the Gibraltar Strait while only 4.6-7.3 $x10^{12}gCyear^{-1}$ enter the Eastern Mediterranean through the Sicily Strait [200]. There is also an import of about 1.32-1.44 $x10^{12}$g DOC per year from the Black Sea through the Dardanelles Straits; its influence though is restricted to the Aegean Sea [201]. Terrestrial inputs in the Mediterranean Sea are considered to be significant due to the extensive coastline, the human population density and the modest dimensions of the basin. The total river inputs in the Mediterranean Sea are estimated at 0.644-0.712 $x10^{12}$gC per year, of which 0.235-0.303 $x10^{12}gCyear^{-1}$ are in the West Mediterranean and 0.409 $x10^{12}gC\ year^{-1}$ in the East Mediterranean [200].

Overall, DOC concentrations in the Mediterranean Sea range between 31 to 128 μM and are similar to values observed in the open ocean [200]. An eastward increase in DOC is observed with values greater than 65μM in the easternmost part of the basin [202][203] due to the influence of the newly formed Levantine waters. The largest variability in the DOC concentrations

ranging between 57 and 101 μM is observed at the surface layer (0-100m) under the influence of terrestrial inputs, mesoscale activity and stratification/destratification pattern. The highest DOC values are encountered in the riverine plumes, in the mixed layer of high stratified waters and in the core of anticyclonic eddies [204][205]. Contrary the lowest surface values are found at areas where the water column is completely mixed due to winter convection or to the occurrence of cyclonic eddies [204][205]. Below the surface layer in the Mediterranean Sea, the Levantine waters originating from the Levantine Basin dominate presenting higher DOC concentrations (64-67μM) in the eastern Mediterranean and decreasing towards the west Mediterranean reaching at a minimum of 41-45μM. The good relationship between DOC and AOU suggests that the removal of DOC could be due to microbial mineralization. In the deep layers of the Mediterranean Sea the lowest observed in the ocean DOC concentrations are recorded ranging between 34 and 44 μM, in both the East and West Mediterranean. This organic matter is considered to be refractory with lifetime ~16000 years [15][200]. A tendency though of higher concentrations near the bottom is observed with highly variable concentrations in the areas where deep water formation occurs. The bottom water presents DOC concentrations between 35 and 60 μM with the highest values in the southern Adriatic Sea, the Ligurian Sea and Gulf of Lions, while the lowest are found in the Tyrrhenian and Ionian Seas [200].

3.2.2 DOC fractions in the Mediterranean Sea

The fractions of DOC encountered in the different basins of the Mediterranean Sea are mostly governed by the stratification and mixing in each area. In general, SLDOC is responsible for the seasonal variations and can be exported in other areas by horizontal advection and to depths >1000m by deep water formation. SLDOC in deep waters has a lifetime lower than 1 year and represents a significant source of energy for deep metabolism. This great depth of export is the biggest difference in DOC dynamics between the Mediterranean Sea and the open oceans [200]. SRDOC and RDOC are found at deep waters circulating along the water column according to the winter vertical mixing and deep water formation. It seems though that some RDOC

removal mechanisms are more efficient in the Mediterranean Sea than in the open ocean [200][206].

3.3 CDOM and FDOM in the Mediterranean Sea

Little is known about CDOM and FDOM spatial and vertical distribution in the Mediterranean Sea. The available data regarding the absorption and fluorescence properties recorded in Mediterranean Sea are summarized in Table 3.1. Data on the fluorescence properties are really scarce and restricted to the estuaries of major rivers (Rhone, Evros and Arno) and to the Northeastern Aegean Sea at the mixing zone of the incoming Black Sea Water with the Levantine Water. In these studies the common humic and amino acid components were identified along with an unknown peak in the Evros coastal waters which was attributed to anthropogenic pollution [129]. Comparison of CDOM among studies is rather difficult as absorption coefficients are reported at different wavelengths. Furthermore, most studies are restricted to narrow regions especially in estuaries and coastal waters while data from long term monitoring of the absorption properties covering both the Western and Eastern basins are limited [152][207]. Therefore the characterization of CDOM status in Mediterranean Sea is inadequate. A distinct though feature of the optical properties of Mediterranean Sea has been recognized. That is its unusually high yellow substances content presenting at least two times greater absorption coefficient values than the nearby oceanic waters with similar trophic conditions. A gradient inside the Mediterranean Sea is also observed as the Western basin was found to hold higher concentrations of yellow substances than the Eastern Mediterranean [207]. A possible explanation that was given for these high concentrations is the vertical transport of deep yellow substances during convection episodes (Nelson and Siegel, 2002) which are more enhanced in the Western basin where the vertical mixing process is more active than in the Eastern basin (Morel and Gentili, 2009).

General characteristics of CDOM in Mediterranean Sea can be derived by the studies that provide long term data from extended regions [152][207][208]. A seasonal cycle of surface CDOM in the Mediterranean Sea was reported by Morel and Genitli, [207] using remote sensed data. In the Western

Mediterranean a broad winter surface maximum started in October and extended up to May while in the Eastern Mediterranean the winter surface maximum was sharper and coincided with the Levantine algal bloom in February. Both basins presented minimum values during summer due to the strong stratification and the photobleaching. In all seasons the recorded absorption coefficients of the western basin exceeded those of the eastern basin by about 50%. This seasonal cycle is consistent with the water characterization by Lee and Hu, [209]. They found the Mediterranean water to be constant to the 'Case-1' status during summer probably due to photobleaching of CDOM while during winter it was characterized as 'non-Case 1'. During spring and autumn, only the Western basin was found to departure from the 'Case-1' status as it presents higher absorption coefficients. This surface seasonal cycle was later confirmed by two Bio-Argo floats (profiling floats equipped with bio-optical and biogeochemical sensors) deployed in the Northwestern Mediterranean and in the Eastern Mediterranean Sea (Levantine Sea) in 2008 [152] while a build up of a CDOM subsurface maximum was also reported. This study [152] suggested that the subsurface CDOM is biologically driven by a strong coupling to phytoplankton and to lesser extent by bacterial processes while at the surface CDOM is physically driven by photobleaching. The same seasonal trend in both surface and subsurface CDOM was reported by Organelli et al. [151] in the NW Mediterranean. They however attributed the subsurface CDOM production to heterotrophic bacteria rather than the direct release from the phytoplankton. Subsurface (40-100m) CDOM (a_{300}) maximum coincident with the deep chlorophyll maximum was also reported by Bracchini et al. [208] in the Central – Eastern Mediterranean basin (southwest of Sicily - southern Ionian Sea) along with the lowest slope values. This study further provides data according CDOM in deeper layers and its nature. Positive correlation was observed between a_{300} and chlorophyll-a concentrations but the overall highest positive correlation was established between chlorophyll-a and absorption between 260 and 280nm which was attributed to the presence of algal derived proteins and polysaccharides species. Based on these observations, they concluded that the semi-labile or even refractory CDOM was most likely attributed to production in the deep chlorophyll maximum with a possible concurrent

bacterial transformation rather than upwelling of deep waters or downwelling form the surface. They further reported relatively low slope values and increased a_{300} values near the bottom indicating the presence of higher molecular weight CDOM compared to intermediate depths that was attributed to release from seabed sediments.

Table 3.1: Optical properties in Mediterranean regions

Study Area	*a (m^{-1})*	*S (nm^{-1})*	*Fl. Peaks*	*Source*
Western Mediterranean				
Northward 38˚	a_{443}=0.02-0.078			[207]
Ligurian Sea	a_{440}= 0.015-0.048	S=0.015-0.021		[151]
Banyulsur Sea (FR)	a_{350}=0.46			[210]
Buy of Marseilles	a_{350}=0.06-0.33	S=0.014-0.026	T, M, C, B	[211]
Gulf of Lions	a_{443}=0.008-0.28	S=0.0114-0.0251		[212]
	a_{350}=0.05-1.71	S=0.013-0.028		[213]
Tyrrhenian Sea	a_{280}=0.95-2.3 a_{355}=0.86-1.89	S=0.012-0.029		[214]
	a_{280}=1.26 a_{355}=0.3	$S_{275-295}$=0.025	A, M, C, T	[215]
Blanes Buy (Spain)	a_{254}=1.59±0.02			[216]
Eastern Mediterranean				
Southward 38˚	a_{443}=0.013-0.05			[207]
Sicily – South Ionian	a_{300}=0.25-0.49	S=0.026-0.042		[208]
North	a_{443}=0.014-0.32	S=0.0161-0.0240		[212]

Adriatic Sea	a_{280}=2.2±0.9 a_{355}=0.5±0.3	S=0.0207±0.005		[217]
	a_{365}=0.124± 0.05			[218]
Cyprus Gyre	a_{300}=0.29±0.06			[219]
North Aegean Sea			A-C, B, N	[220]
North Aegean – Evros Coastal	a_{300}=0.85-11.73	S=0.0165-0.0301	A, B, T1, T2, P6, C	[129]

CHAPTER 4
MATERIALS AND METHODS

4.1 Physical Parameters

Salinity, temperature, water density, and chlorophyll a, were recorded by sensors (Seabirds electronics) during CTD deployment. Apparent oxygen utilization, AOU, is defined as the difference between the saturation oxygen concentration at certain temperature and salinity and the measured oxygen. AOU is widely estimated to infer respiration in the oceans by assuming that surface oxygen concentration is close to saturation with the overlying atmosphere.

4.2 Dissolved Organic Carbon, DOC

Dissolved Organic Carbon concentrations were determined using a Shimadzu TOC 5000A organic carbon analyzer and following the high temperature catalytic oxidation (HTCO) method as described by Sugimura and Suzuki [221] and Cauwet [222]. The system was standardized prior to analysis using a potassium hydrogen phthalate standard solution series. Each sample was injected 3 to 5 times and DOC concentration was calculated by the average value of three replicates that yielded standard deviation <2%. Analytical precision and accuracy were tested against Deep Atlantic Seawater Reference Material provided by the DOC-CRM program (University of Miami – D.A. Hansell); measured value: 40 ± 2 μmol L^{-1} (n=5), certified value: 42 ± 1 μmol L^{-1}. Drift correction of the DOC results according to the reference sample was applied when needed.

4.3 Absorption analysis

Absorption spectra were obtained between 250 and 700nm at 1nm increments using a dual beam UV-visible spectrophotometer (Perkin Elmer, Lambda 25) equipped with 5cm quartz cells and referenced to Milli-Q water. The average absorbance between 680-700nm was subtracted from each sample in order to correct for the residual scattering by fine particle fractions, micro-air bubbles or colloidal material present in the sample, or refractive index differences between the sample and the reference [216]. A blank scan

(Milli-Q water) was measured every 5 samples to check for the stability of the instrument while it was also subtracted from each spectrum for baseline correction. Absorption units were converted to absorption coefficients using the relationship:

$$\alpha(\lambda) = 2.303*A(\lambda)/ l$$

where, $\alpha(\lambda)$ is the absorption coefficient (m^{-1}), $A(\lambda)$ is the absorbance at wavelength λ, and l is the cell's light path length in meters. The detection limit was calculated as three times the standard deviation of 10 repeated scans of Milli-Q water following the same measurement routine. The limit of detection at 300nm was 0.0372m^{-1}.

The mass-specific CDOM absorption at 300nm (a^*_{300}) was calculated by dividing the absorption coefficient at 300nm by the concentration of DOC. Spectral slope (nm^{-1}) at 300-650nm was calculated by fitting the absorption spectra to an exponential decay function by nonlinear regression [103] using Matlab, according to the following equation:

$$\alpha(\lambda) = \alpha(\lambda_0)*e^{-S(\lambda-\lambda_0)}$$

where λ_0 = reference wavelength (400nm) and S=spectrum slope.

Spectral slope of the narrow regions $S_{275-295}$ and $S_{350-400}$ were calculated using linear regression of the log – transformed spectra of the absorption coefficients, while the slope ratio S_R was determined by the ratio of the slope $S_{275-295}$ to the slope $S_{350-400}$ [118].

4.4 Fluorescence analysis

4.4.1 Spectra acquisition

CDOM fluorescence was measured using a Fluorolog 3-21 (Jobin-Yvon) spectrofluorometer equipped with a 450W Xe lamp and using a 1cm path length quartz cuvette and a Grating: Density 1200. Excitation Emission Matrices (EEMs) were obtained over a range of wavelength between 250-450nm (5nm intervals) for excitation and 262-600nm (2nm intervals) for emission spectra. Bandwidths were set to 5nm for both excitation and emission. The fluorescence emission signal (S_C), was measured by a photomultiplier and was corrected for the different response of the detector,

gratings and other instrument components to different wavelengths. This signal was divided by the Rc (that is the signal measured by the referenced semiconductor photodetector after the excitation monochromator) to correct the fluctuations in the lamp output according to the manufacturer. The spectra obtained from the spectrofluorometer where processed using MATLAB R2010a. A blank spectra (MilliQ water) was measured daily and subtracted from each sample spectra in order to correct for Raman scattering. Rayleigh scatter effects were removed from the data set by not including any emission measurements made at wavelengths ≤ excitation wavelength +20nm. Correction for inner filter effect was not applied as the absorption values obtained by the absorption analysis were low.

4.4.2 Raman calibration

The fluorescence intensities obtained from the analysis are expressed in arbitrary units (A.U.) which are instrument dependent (Lawaetz and Stedmon, 2009) and thus cannot be used in comparisons between different studies. We chose to calibrate our data using the Raman scatter peak of water following Lawaetz and Stedmon, [223] as it has been widely reported in other studies and also yields lower risk of errors due to the lack of need of standard solution use and preparation.

The wavelength dependent Raman cross-section of water is a fixed property of water and the integral of the measured Raman peak is directly proportional to it. The integral of the Raman peak is therefore suitable to be used to calibrate measurements made on different instruments or using different instrumental settings as the peak height and width will vary accordingly. The Raman scatter emission peak of a MilliQ water sample excited at 350nm measured daily was used. In order to calculate the integral of the Raman peak, the wavelength band over which to integrate must be defined. The signal on either side of the peak should be very low and within instrumental noise. In our case the band ranged between 375-426nm and 379-428nm. The integration was performed using the Origin Pro 8 software and the calibration of each sample was performed by normalizing the fluorescence at each wavelength with the integral of the daily Raman peak. The resulting units are Raman Units (R.U.)

4.4.3 Parallel Factor Analysis, PARAFAC

The EEMs spectra were farther analysed using Parallel Factor Analysis, PARAFAC, as described by Bro [224], Stedmon et al, 2003 and Stedmon and Bro, [225]. The analysis was performed in MATLAB R2010a using the "Nway toolbox" and "DOMFluor toolbox" for MATLAB [225][226].

4.4.3.1 Description of PARAFAC analysis

EEMs spectra provide three-way data as the fluorescence of a sample varies depending on the wavelength of light absorbed and the wavelength at which fluorescence is observed. The measured fluorescence is the sum of the contribution from each component. PARAFAC provides both a quantitative and qualitative model of the data and separates the complex signal into its individual underlying fluorescent phenomena with specific excitation and emission spectra. The identified fluorescent phenomena may be individual fluorophores but may also be approximations of the effects of other local processes occurring such as quenching or intra molecular charge transfer.

PARAFAC decomposes the data matrix into a set of trilinear terms and a residual array, while the model is fitted by minimising the sum of squared residuals with an alternating least squares algorithm:

$$\chi_{ijk} = \sum_{f=1}^{F} a_{if} b_{jf} c_{kf} + \varepsilon_{ijk}, \qquad i = 1,...,I,\ j=1,...,J;\ k = 1,...,K$$

In the case of EEMs modelling, PARAFAC decomposes the complex mixture of fluorophores without any assumptions regarding their spectral shape and number. In this case, χ_{ijk} is the intensity of fluorescence for the ith sample at emission wavelength j and excitation wavelength k. a_{if} is directly proportional to the concentration of the fth analyte in sample i, while b_{jf} is linearly related to the fluorescence quantum efficiency of the fth analyte at emission wavelength j. c_{kf} is linearly proportional to the specific absorption coefficient at excitation wavelength k. F describes the number of components in the model and a residual matrix ε_{ijk} represents the variability not accounted in the model [224][227].

The initial stage of the PARAFAC analysis consists of fitting a series of models to the data using an increasing number of components until a reasonable fit is explained. Depending on the data, a reasonable fit for EEM

data is normally above 99% variance explained. At this stage identification of outliers also occurs through the inspection of the leverage for each sample. The next stage is the validation of the model through four approaches. First the residuals are tested in order to verify that they are characterized by instrument noise and contain little structure. Second we examine the spectral properties of each component. The spectra should be smooth while a component can have one or more excitation maxima but only one emission maxima. Third comes the split half analysis were the data are split into two halves and each half is modelled independently. Then the spectral properties derived from each half are compared and if found to be identical (mathematic comparison of excitation and emission loadings using Tucker Congruence Coefficients) then the model is considered robust. Last step is random initialization where a series of models are fitted using random numbers as the initial estimates. Then the PARAFAC model provides the scores which represent only the relative intensities of the fitted components. The intensity of each component in every sample is estimated as the fluorescence intensity at the peak excitation and emission maximum of the certain component using the following equation:

$$I_n = Score_n * Ex_n(\lambda_{max}) * Em_n(\lambda_{max})$$

where $Score_n$ is the relative intensity of the nth component, $Ex_n(\lambda_{max})$ is the maximum excitation loading of the nth component and $Em_n(\lambda_{max})$ is the maximum emission loading of the nth component derived from the model [225].

4.4.3.2 PARAFAC results

Initially, PARAFAC modelling was carried out separately for each sampling identifying different number (2 up to 4) of components. The analysis of the residuals however from the fitted models showed systematic deviations rather than instrument noise indicating the inadequateness of the model suggesting an inappropriate number of fitted components. This could resulted from the relatively small number of samples in each analysis (n<50). Therefore the model was run again including the spectra of all samplings (n=242) with exception the samples from Spercios River and Maliakos Gulf (Chapter 8), resulting to residuals more indicative of instrument noise and with absence of

clear structure. Split half analysis and random initialization confirmed the robustness of the model acquired from the analysis of the sum of the samples (figure 4.1b). Since the PARAFAC model was run once including the samples obtained in the different study areas the identified components will be presented here.

PARAFAC analysis identified four components: two humic-like of terrestrial origin, one humic-like of marine origin and one protein-like component (Figure 4.1a, Table 4.1). Excitation and emission maxima of component 1 (C_1, λex/λem 255/448nm) fall in the range of peak A established by Coble [124] and has been attributed to HMW and highly conjugated humic substances that are derived primarily from vascular plant sources. Component 2 (C_2) exhibits a peak at 300nm excitation and 402nm emission equal to peak M defined by Coble [125] representing low molecular weight humic substances, common in marine environments [66]. Previous researches have characterized this component as marine humics, resulting either from microbial processes [164] or produced directly from marine phytoplankton [125][147]. Contrary, Stedmon and Markeger [138] suggested the export of this component from agricultural subcatchments while Murphy et al. [139] argued that peak-M can be produced microbially in terrestrial as well as marine environments. Component 3 (C_3) has two excitation peaks, a primary at 280nm and a secondary at 370nm with a single emission at 480nm. The broad excitation and emission bands coupled with the long emission wavelength indicate terrestrial humics of higher molecular weight and a more aromatic character compared to C_1, as suggested by McKnight [228]. The secondary peak (λex/λem 370/480nm) resembles Coble's [125] peak C (λex/λem 320-360/420-460), shifted slightly to longer wavelengths (both for excitation and emission), while the major peak (λex/λem 280/480nm) has excitation maxima shifted also to longer wavelength compared to peak A. The high excitation and emission wavelengths of peak C indicate (beside the HMW and conjugated substances) the presence of oxidized polyhydroxyl-aromatic factions that act as electron acceptors and provoke intramolecular charge-transfer interactions with the non oxidized fractions that act as electron donors [107].

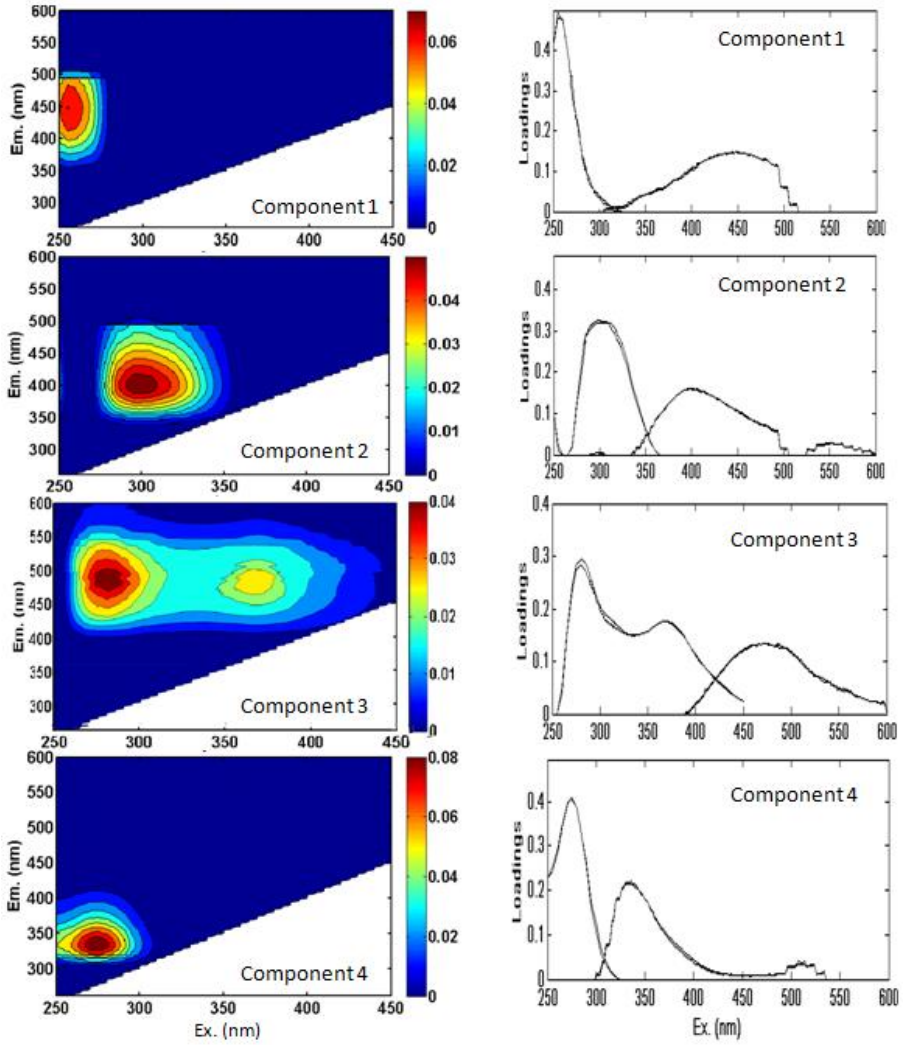

Figure 4.1: a) Fluorescent components identified by PARAFAC, b) split half validation.

Similar components to ours C_3 have been previously reported in many studies mostly in estuarine and coastal waters [129][138][142][229]. Component 4 (C_4) has spectral characteristics (λex/λem 275/336nm) close to tryptophan corresponding to peak T [99] and is attributed to microbial processing. Earlier studies in marine environments that are not directly affected by terrestrial inputs showed that protein-like components dominate over the other components [139][128]. Specifically for tryptophan –like fluorescence it has been associated with algal blooms and eutrophic environments [134][164][211]. Based on their emission spectra components C_1, C_2, C_3 contribute to visible fluorescence and component C_4 to UVA fluorescence.

Tyrosine-like peak B was not identified through the PARAFAC analysis (marine samples) but was contrary identified by the 'peak-picking' method in the samples of the Maliakos Gulf (Chapter 8). Peak B presents excitation at

~270-280 nm and emission at ~300nm which is close to the primary Rayleigh scatter. Even though water blank is subtracted from each sample in order to reduce the Rayleigh scatter band, traces usually remain. The remaining scatter signal is then removed by replacing the affected area of the spectra with missing values. In the samples of the Maliakos Gulf the water blank subtraction had more successfully removed the Rayleigh scatter than in the marine samples and therefore a narrower area of the spectra was replaced by missing data. We speculate that the need of replacing a more extended area with missing values in the marine samples could prevent the identification of peak B.

Table 4.1: Excitation and emission wavelengths of the PARAFAC identified components.

	Peak (1990-8)	*Excitation (nm)*	*Emission (nm)*
Component 1	A	255	448
Component 2	M	300	402
Component 3	C	280, 370	480
Component 4	T	275	336

4.4.4 Fluorescence indices

Humification index HIX and biological index BIX were calculated using the EEMs spectra obtained from the fluorescence analysis. HIX is the ratio of the emission spectrum areas between 300-345nm and 435-480nm at 254nm excitation wavelength. BIX is the ratio of fluorescence intensity at 380nm to the fluorescence intensity at 430nm, at excitation wavelength 310nm.

4.5 Statistical Analysis

Statistical analysis was performed using IBM SPSS Statistics, MatLab and R software. Before proceeding to the statistical analysis, all of the data were tested to check the normal distribution of each parameter and the homogeneity of variance between the groups using Shapiro-Wilk and Levene test respectively. Since the results showed that our data do not follow normal distribution and in most cases we did not find homogeneity of the variances between groups, non-parametric tests were chosen. For the purpose of examining the differences between a pair of groups Mann-Whitney U test was

used, while for more than two groups Kruskal-Wallis test – post hoc pairwise analysis was applied. Simple regression (relationships with salinity) and model II regression (relationships between DOC, absorption and fluorescence) were applied to define the coefficient of determination between variables.

Figure 4.2: a) Sampling on board R/V Pelagia, b) filtration of samples in an ultraclean container on board R/V Pelagia, c) sampling on board R/V Aegeao. Details for samplings on each cruise are given in the respective chapters.

CHAPTER 5

ALTERATION PROCESSES OF CHROMOPHORIC DISSOLVED ORGANIC MATTER (CDOM) IN THE MARMARA SEA

5.1 Introduction

The Marmara Sea is the area that connects the Black and the Mediterranean Seas. Low salinity and rich in terrigenous and marine DOM waters, originating from the Black Sea (BSW), mix with the saline (S >38) oligotrophic waters of the Aegean Sea (AgW). A two –layer counterflow and a permanently stratified system is therefore established. Marmara Sea is also of significant importance for the Eastern Mediterranean Sea as the Black Sea water inputs in the Mediterranean Sea through the Turkish straits, i.e. the Bosphorus Straits, Marmara Sea and Dardanelles Straits, have been reported to be comparable with the water inputs of riverine and atmospheric origins [230][231]. The net Black Sea Waters (BSW) outflow from the Dardanelles Straits to the North Aegean Sea has been estimated to be 300 km^3y^{-1} (~1,300 km^3y^{-1} surface outflow of BSW, ~1,000km^3y^{-1} subsurface inflow of AgW) [295][300], while it has been shown to be enriched in dissolved organic carbon and nitrogen [201][220]. Despite the recognition that significant DOM enters the Marmara and North Aegean Seas through the BSW current, little is known about the nature and composition of this organic matter. In this study we investigate possible DOM alterations occurring in this buffering zone based on CDOM properties. In particular we focus on the nature of CDOM that is transported to the Aegean Sea.

5.2 Material and Methods

5.2.1 Study Area

The Marmara Sea (figure 5.1) is a small basin located between Europe and Asia continents characterized by three depressions with bottom depths over 1000m at the northern region separated by deep sills while the southern half is shallow with average depth of 100m [232]. The Marmara Sea receives waters from the Mediterranean and Black seas though the Dardanelles and Bosphorus Straits respectively.

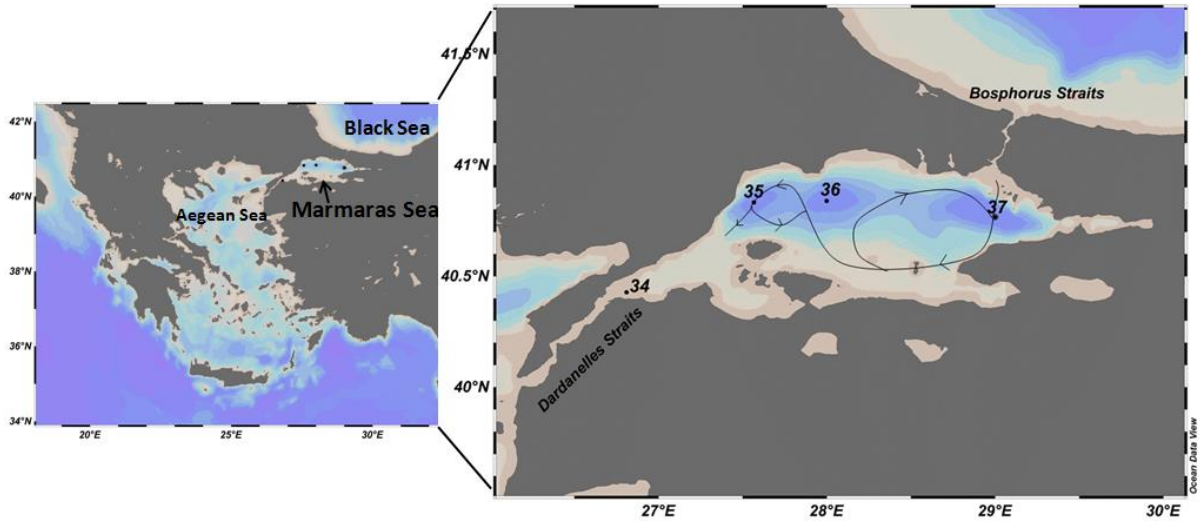

Figure 5.1: Sampling site and circulation in Marmara Sea.

Due to the different physical characteristics of the two water masses a two layer stratified system is created where a sharp pycnocline at approximately 25m depth inhibits the mixing between the layers [232][233]. The low salinity Black Sea water (BSW) (S= 22.0 – 29.6) enter the Marmara Sea through the Bosphorus Straits and buoy over the denser and more saline Aegean waters (AgW) (S=38.8-38.9); approximately after 4 months BSW reach the Dardanelles Straits and outflow in the Aegean Sea [233]. These incoming waters are rich in inorganic nutrients and organic matter due to the discharge in the Black Sea of a large number of rivers while it receives also a significant amount of industrial and agriculture wastes [231][234]. On the other hand, the more saline and well oxygenated oligotrophic Aegean Waters (AgW) enter the Marmara Sea through the Dardanelles Straits and plunge below the surface layer moving eastwards and filling the three depressions of the Marmara Sea [232]. The intermediate and deep waters become depleted in oxygen (D.O. <20 $\mu molL^{-1}$) due to the long residence time of the Aegean waters in the Marmara Sea, around 6-7 years [233], and the significant oxygen consumption resulting from the continuous supply of particulate organic matter from the upper layer [235]. The Marmara Sea also receives major wastewater discharges from land – based sources along the coast line, including the Istanbul metropolitan area [236].

5.2.2 Sampling

Sampling was conducted onboard NIOZ RV *Pelagia* on a cruise during June 2013. Four stations were sampled located in the Dardanelles Straits and in the three depressions of the Marmara Sea (figure 5.1). Station 34 is shallow station (40 m depth) situated in the Dardanelles Straits, while stations 35, 36 and 37 were located in the west (1110 m), central (1242 m) and east (1225 m) depressions respectively. All stations were sampled from the surface ~10m up to the bottom using Niskin PVDF plastic bottles (UltraClean CTD,UCC) deployed by a CTD rosette (Seabird electronics). Samples for DOC and CDOM analysis were directly filtered from the UCC sample bottles under nitrogen pressure using 0.2μm Sartobran 300 catridges (Sartorius) in an ultraclean container and collected in precombusted (480°C, 12h) amber glass bottles and stored in the dark at ~-20°C.

5.2.3 Methodology

Dissolved organic carbon, absorption and fluorescence were analyzed as described in Chapter 4, while the spectra from the fluorescence analysis were included in the PARAFAC modeling and the identified components are described in Chapter 4. The qualitative indices of CDOM absorption, carbon specific CDOM absorption coefficient a^*_{300} and spectral slope $S_{275\text{-}295}$ as well as fluorescence humification index HIX were estimated as described in Chapter 4.

5.3 Results

The results recorded in the two major water masses are summarized in Table 5.1.

5.3.1 Water Column Structure

During the time of our sampling, in early summer, any mixing between the upper and the underlying layer is expected to be limited due to both the increased brackish BSW inflow and the high surface temperatures that intensify the pycnocline. In figure 5.2a the vertical distribution of salinity is presented and the two stratified layers in the Marmara Sea are apparent. The buoyant BSW layer is expanding up to 25m depth with salinity values between 21.6 and 31.7 while below the 25m the high and uniform salinity values, 38.7

Table 5.1: Physicochemical and optical properties in the BSW and AgW water masses

	BSW	***AgW***
Salinity	21.60-31.68	38.68-38.87
Temperature (˚C)	11.20-20.09	14.37-18.41
AOU	-90.6 – 72	-17.1 – 239.6
DOC (μmol/L)	114-181	50-65
a_{300} (m^{-1})	1.97-2.92	0.46-0.80
a^*_{300} (m^{-1})	0.97-1.50	0.58-1.16
$S_{275-295}$	0.0280-0.0307	0.0241-0.0376
I_1 **(R.U.)**	0.067-0.101	0.019-0.060
I_2 **(R.U.)**	0.048-0.070	0.013-0.040
I_3 **(R.U.)**	0.034-0.055	0.009-0.040
I_4 **(R.U.)**	0.054-0.077	0.006-0.016
HIX	1.4-2.7	2.3-12.4

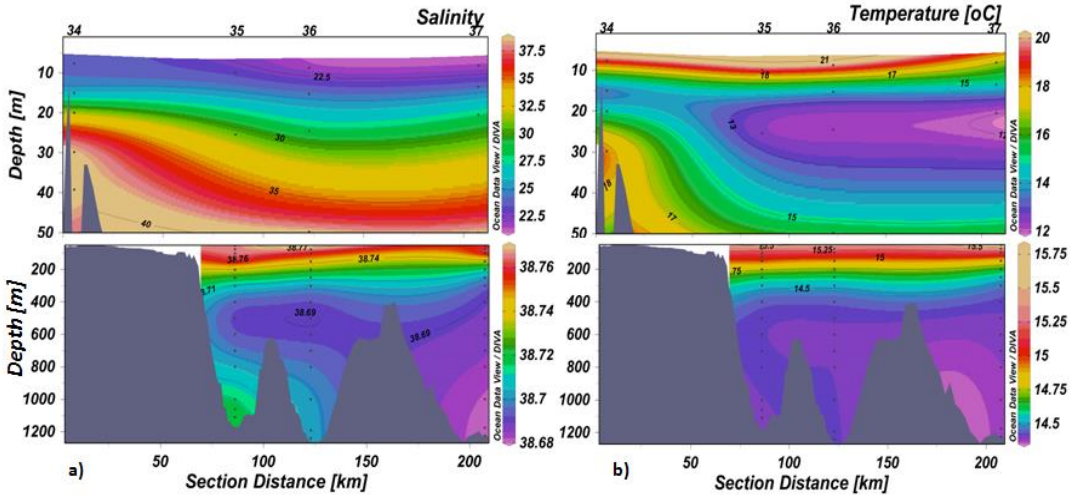

Figure 5.2: Vertical distribution of a) salinity and b) temperature (˚C) along the sampled transect. The upper panel shows the surface 50m and the lower panel from 50m up to the bottom.

– 38.9, indicate the presence of Aegean waters (AgW). The temperature at BSW fluctuated between 11.2 and 20.1˚C, with lower values recorded at the eastern part of the sampled transect while the highest were recorded at station 34 in the Dardanelles Straits (figure 5.2b). A zone of minimum temperatures (~12˚C) was identified between 20-30m, more intense at the eastern region (st.37) of the Marmara Sea. This zone represents the Cold

Intermediate Layer (CIL) which results from advection through the Bosphorus Straits of the CIL formed in the Black Sea as well as local winter cooling in Marmara Sea [237]. The CIL persists through most of the year with highest contrast with surface temperatures in the spring and summer [238].The underlying Aegean waters showed overall lower and less variable temperature values with a range of 14.4-18.4˚C. The highest temperatures were recorded at the shallow area of the Dardanelles Straits and at the lowest sampled depths (up to 150m) of the rest stations. The lowest AOU values were recorded at the BSW layer, while in the subsurface waters AOU increased and reached its maxima in the easternmost station 37 (figure 5.3).

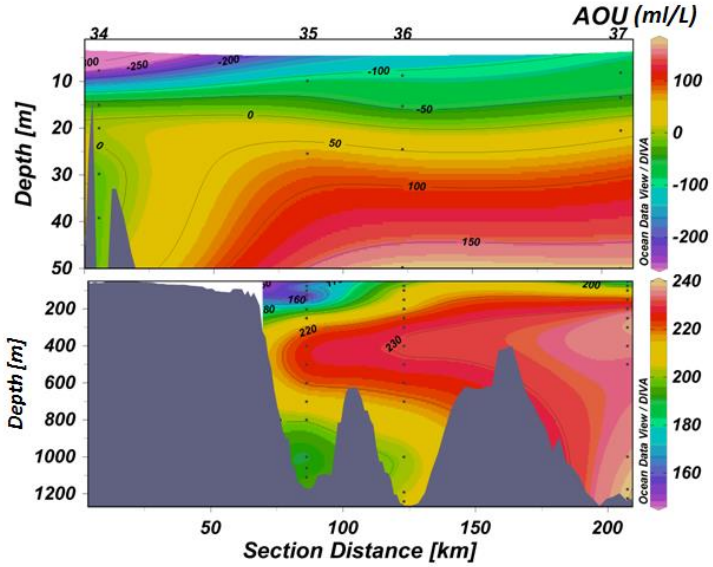

Figure 5.3: Vertical distribution of AOU along the sampled transect.

In subsurface waters up to 300m depth, station 35 presented overall lower AOU values than stations 36 and 37, marking the more direct influence of the well oxygenated new incoming Aegean waters (‘new’ AgW). At the deepest layers of the Marmara Sea (800m -1200m), both stations 35 and 36 presented low AOU values while station 37 of the eastern depression presented overall the highest values. The deep waters of the Marmara Sea are renewed entirely by the intrusion of the dense Aegean waters through the Dardanelles Strait resulting in the enrichment in dissolved oxygen. This is more pronounced in the western and central basins while it fades along the eastern route due to the mixing with the existing older waters (‘old’ AgW).

5.3.2 Dissolved Organic Carbon and absorption properties

At the BSW layer DOC ranged between 114 and 181 μmol/L (mean 151 μmol/L) revealing highest concentrations at stations 36 and 37 (figure 5.4a). At the AgW layer DOC decreased significantly (Mann-Whitney Test, P=0.000), presenting a narrow range of 50 to 65 μmol/L (mean 55 μmol/L). Variation though between the stations was observed, as the highest values were recorded at the easternmost station 37 occupied by 'old' AgW waters.

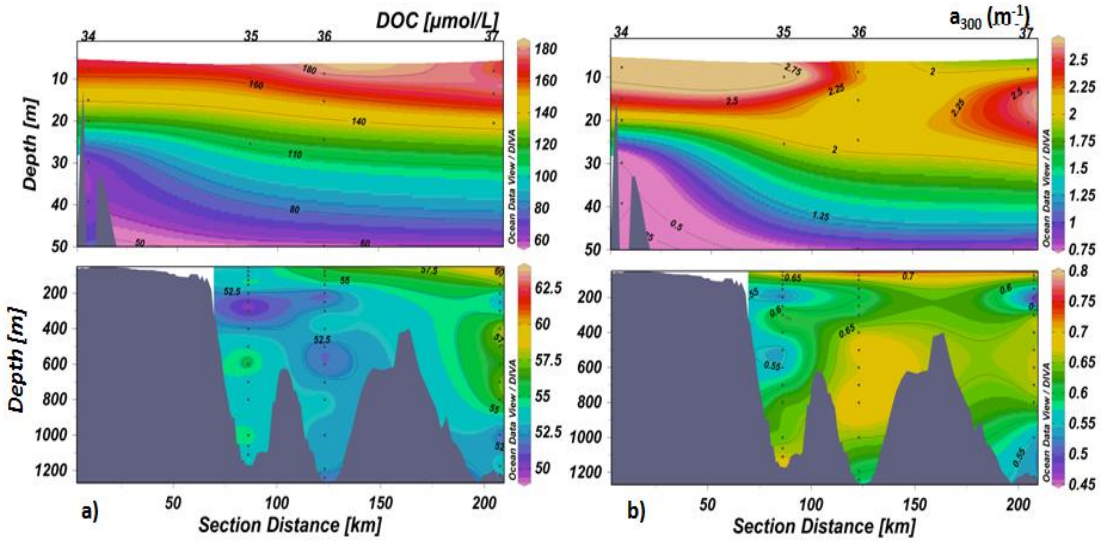

Figure 5.4: Vertical distributions of a) DOC (μmol/L) and b) a_{300} (m^{-1}) along the sampled transect.

At the BSW layer, absorption coefficients at 300nm a_{300} (m^{-1}), ranged between 1.97 and 2.92 m^{-1} (mean 2.32 m^{-1}) and were significantly higher (Mann-Whitney Test, P=0.000) than those recorded in the underlying AgW waters with a range of 0.46-0.80 m^{-1} and a mean of 0.62 m^{-1} (figure 5.4b). The maxima in a_{300} were recorded at depths 10-15m at stations 34 and 35 but deepened to 15 and 25m depth at the eastern station 37. At the AgW layer, a zone of increased a_{300} coefficients can be observed from 800m to1000m of station 35, shallowing to 300m - 800m towards the eastern station 37. Carbon specific absorption coefficient, a^*_{300}, presented elevated values at the BSW layer (figure 5.5a) and especially at the western stations 34 and 35 than the eastern ones. At the AgW layer a similar distribution to a_{300} is observed with a patch of somewhat elevated a^*_{300} coefficients at intermediate and deep water depths. The lowest values were found at station 34 while station 36 presented

the highest a^*_{300} values, significantly higher than station 37 (Kruskal Wallis P=0.034, pairwise post hoc P=0.03 in stations 36 and 37).

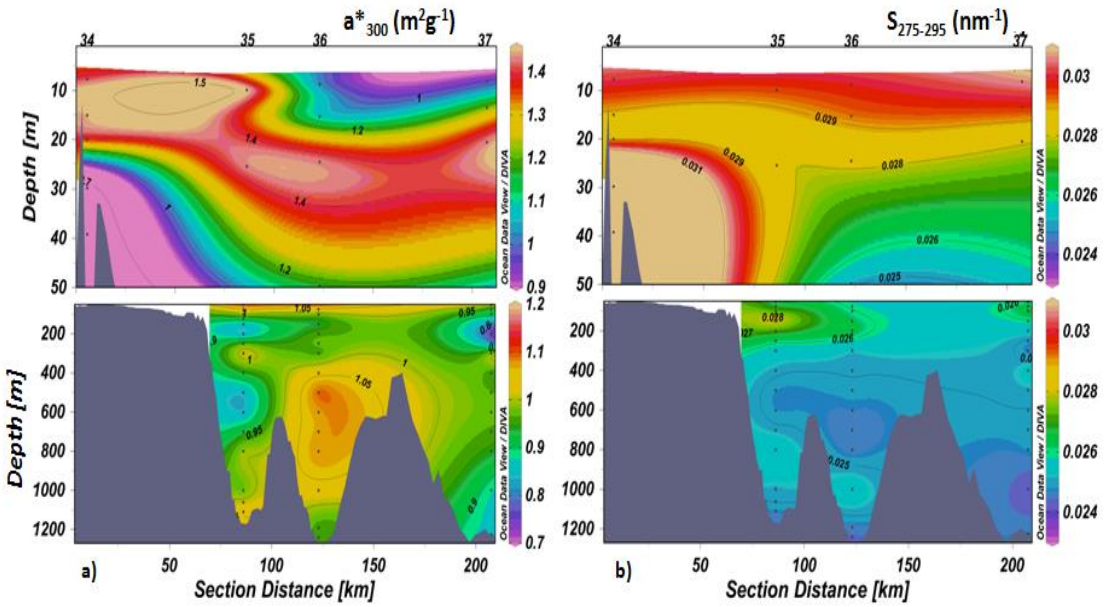

Figure 5.5: Vertical distributions of a) a*300 (m^2 g^{-1}) and b) $S_{275-295}$ (nm^{-1}) along the sampled transect.

Absorption spectral slopes $S_{275-295}$ presented higher average (0.0292 ± 0.0008 nm^{-1}) values in the BSW than the AgW (0.0260 ± 0.0026 nm^{-1}) (figure 7.5b). Nevertheless, the maxima in $S_{275-295}$ were recorded at the subducted Aegean waters ('new' AgW) of the western station 34 coincident with the lowest a_{300} and a^*_{300}. The minima in $S_{275-295}$ were observed at the deepest layers of the western stations 36, 37 where the highest a_{300} were found.

5.3.3 Fluorescence properties

All the PARAFAC fluorescent components presented significantly higher values (Mann-Whitney, P=0.000) at the BSW compared to the AgW (figure 5.6 a) – d)). In addition, all fluorescence intensities follow the a_{300} distribution with subsurface maxima at ~25m at the eastern stations and at ~15m at the western ones. In the BSW, the primary terrestrial humic – like component C_1 (peak A) presented the highest intensities (I_1) in all stations and depths denoting the strong terrestrial character of this water mass.

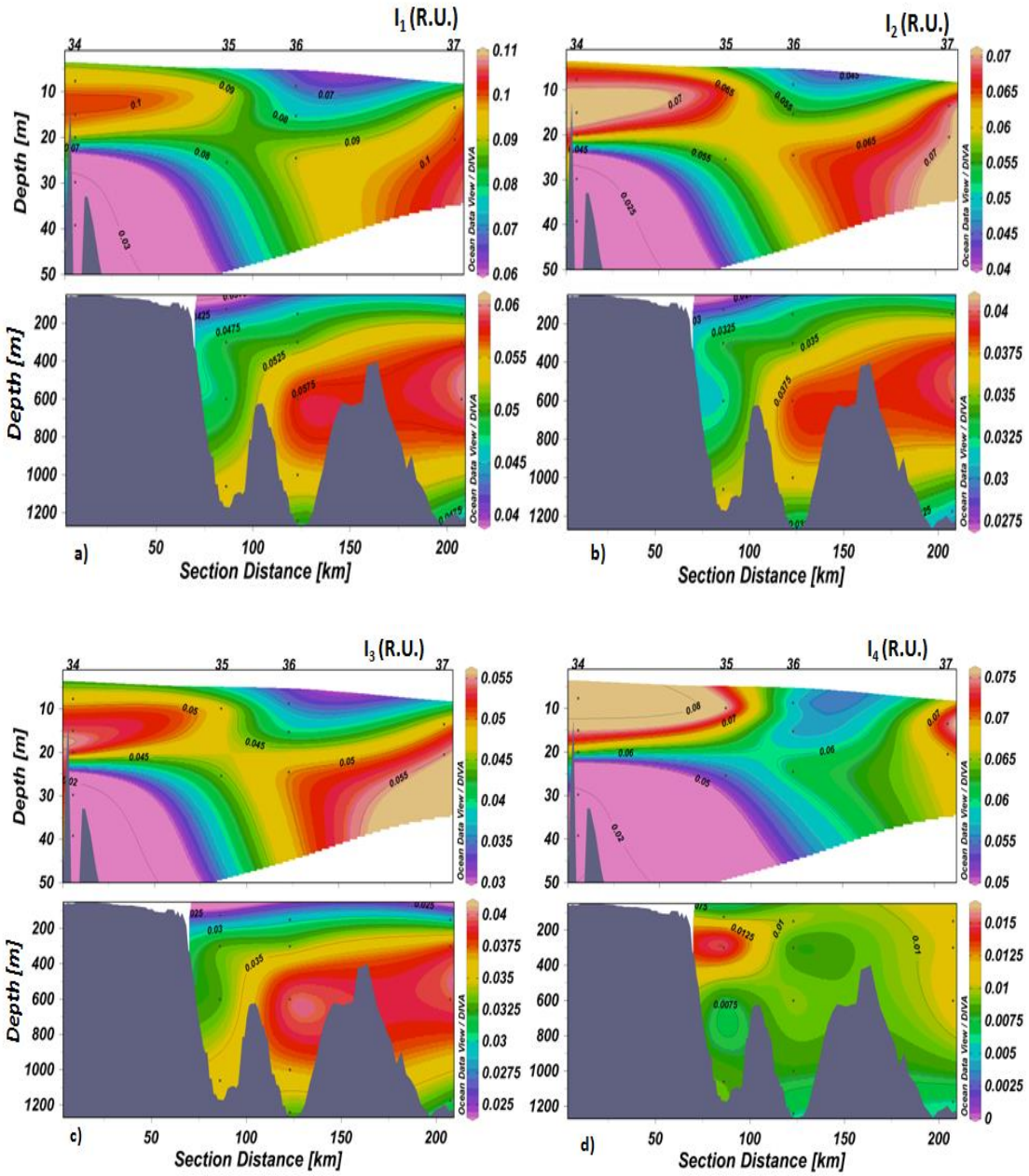

Figure 5.6: Vertical distributions of the fluorescence intensities (I_i) in Raman units (R.U.) of the 4 PARAFAC components, a) I_1 (C_1) b) I_2 (C_2), c) I_3 (C_3) and d) I_4 (C_4), along the sampled transect.

In the top 20m, the protein – like component C_4 (peak T) showed the second highest intensities (I_4) followed by the marine humic – like component C_2 (I_2) (peak M), while at the lower part of the BSW layer (20-30m), I_2 presented higher values than I_4. The secondary humic-like component C_3 (peak C) showed constantly the lowest intensities (I_3) among the fluorescence components. At the AgW layer, C_1 preserved the highest intensities (I_1) throughout the water column. At the shallow area of the Dardanelles straits (< 75m) (st.34), the second highest intensity I_4 corresponded to the protein- like

component C_4 following the order $I_1>I_4>I_2>I_3$. Contrary within the Marmara Sea (stns 35,36,37) the protein-like component presented constantly lower intensities than the humic-like ones suggesting humification processes and/or parallel consumption of the labile amino –acid substances ($I_1>I_2>I_3>I_4$). All humic – like components presented maximum values at intermediate depths of stations 36 and 37. The humification index HIX, was lowest (2.2-2.7) in the BSW while at the AgW was significantly increased (6.9-12.4) (figure 5.7). This is due to the higher amino acid – like content of the BSW compared to the underlying AgW, as expected for this productive water layer. Elevated HIX values were observed at depths >600 m at the western basin of the Marmara Sea (stnn 35) while at eastern basins (stns 36 and 37) high HIX values start to appear from shallower waters (>200m).

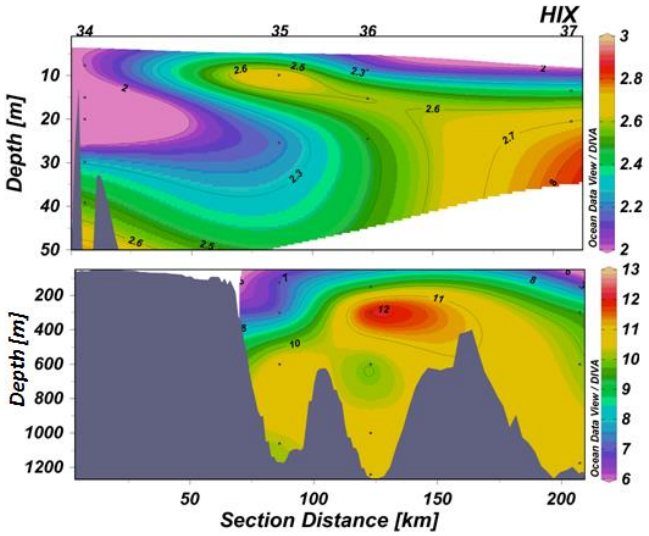

Figure 5.7: Vertical distribution of humification index HIX, along the sampled transect.

5.4 Discussion

5.4.1 Black Sea Water

The surface layer of the Marmara Sea is exclusively occupied by the BSW and the lengthwide salinity gradient has been attributed to the exchange between the layers caused by turbulent entrainment processes [233][238]. Hence, mixing and circulation are expected to be two major factors regulating the distributions of the DOM pools in this water mass. During summer, a meandering jet flow prevails the surface circulation in the Marmara Sea. BSW entering through the Bosphorus Straits flows initially to the south where it

deflects to the west and northwest circulating around an anticyclonic circulation attached to the Thracian coast. When the flow reaches the Thracian coast, the main branch turns southwest and towards the Dardanelles Straits following a cyclonic circulation (figure 5.1). The circulation mode described, may explain the distribution of CDOM optical parameters in the BSW layer and the position of maxima at different depths (figure 5.4b, 5.6). At stn 37, affected by the anticyclone, the maxima in a_{300} and I_i are found at ~25 m depth while at stn 35 affected by the cyclone, they are uplifted at ~15m depth. Stn 36 does not seem to be under the direct influence of the meandering jet. The negative linear relationship of DOC *vs* salinity (R^2=0.889, P<0.005) (figure 5.8) indicates conservative mixing and suggests that significant amounts of organic matter of both terrestrial and autochthonous origin originating from the Black Sea [239] become diluted along their transport towards the Dardanelles Strait due to mixing with high salinity waters.

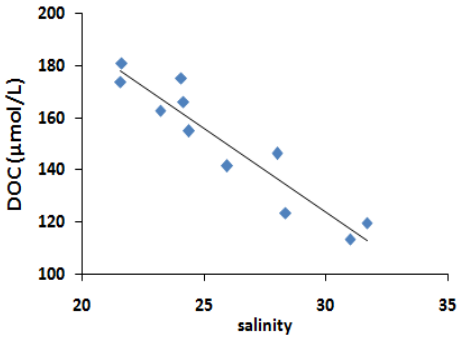

Figure 5.8: Relationship of DOC *vs* salinity in the BSW

In figure 5.9a and 5.9b the relationships of a_{300} and I_4 vs salinity are shown. It becomes clear that a_{300} and I_4 follow the DOC trend with decreasing values in high salinities, but these relationships are not significant, since negative deviations from the mixing line are observed in both parameters in low salinity waters. The negative deviations from linearity correspond to samples from station 36. It seems that in these waters (st.36), not directly affected by the incoming jet, CDOM degradation processes become apparent. Furthermore, the strong correlation of the absorption coefficient a_{300} with the protein-like UVA intensity I_4 (R^2=0.787, P<0.05, figure 5.9c), indicate that the two sub-pools of CDOM-FDOM are associated.

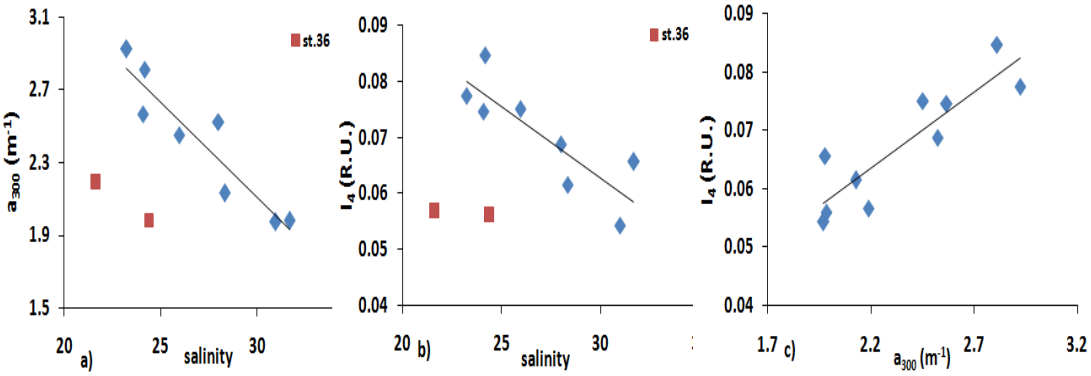

Figure 5.9: Relationships of a) a_{300} *vs* salinity, b) I_4 *vs* salinity, c) I_4 *vs* a_{300} at the BSW.

To further investigate photodegradation and mixing acting on CDOM we have examined the relationships between slope $S_{275-295}$ and both absorption coefficient a_{300} and salinity. Photodegradation has been shown to have an increasing effect on $S_{275-295}$ [118] and therefore a negative relationship (linear or exponential) is expected between a_{300} and $S_{275-295}$ when photodegradation is dominant. In our case no relationship was observed between a_{300} and $S_{275-295}$ (figure 5.10a) indicating that other factors beside photodegradation have significant impact on CDOM.

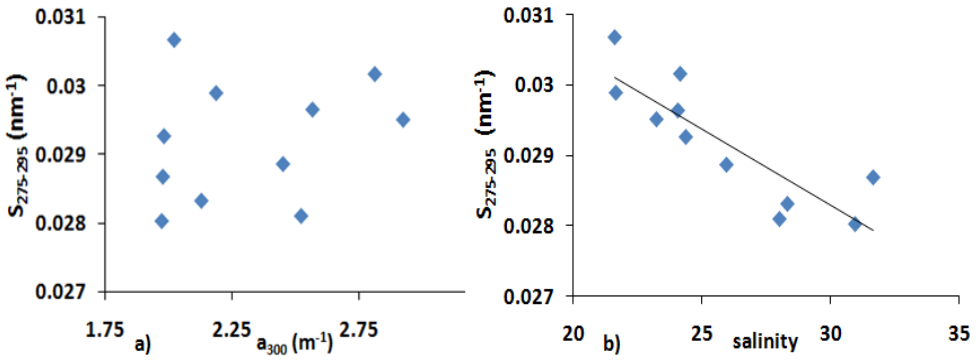

Figure 5.10: Relationships of $S_{275-295}$ vs a) salinity and b) a_{300}, at the BSW.

The lack of correlation between $S_{275-295}$ and a_{300} further implies that neither mixing is the determinant factor as Stedmon and Markager [240] showed that during mixing of water masses with different optical characteristics slope presents an exponential decreasing trend along a_{300} gradient. Furthermore, they demonstrated that $S_{275-295}$ exhibits an exponential increase along salinity gradient during the aforementioned mixing. Contrary our results showed a strong negative correlation of $S_{275-295}$ and salinity (figure 5.10b, R^2=0.734, $P<0.05$) indicating the decrease of slope from Bosphorus Straits towards the Dardanelles. Decreasing slope values were shown to be related with microbial

transformations [118] indicating that at the surface parallel to the mixing and the possible photodegradation of CDOM which is expected during the time of our sampling (June), microbial transformation processes take place and seem to have the greater impact on CDOM and control its dynamics.

The relationships of all humic-like components ($I_{1\text{-}3}$) with salinity are not significant ($P>0.05$) (not shown). In this case too, the samples from stn 36 present the lowest intensities. For the rest of the samples no clear mixing line can be identified and humic fluorescence intensities remain more or less stable. It is expected that processes such as mixing with Aegean waters of low humic content and exposure of surface waters to photodegradation would have resulted in decreasing humic content. The fact that the humic content in the BSW remains unchanged implies that humic production is taking place in the Marmara Sea.

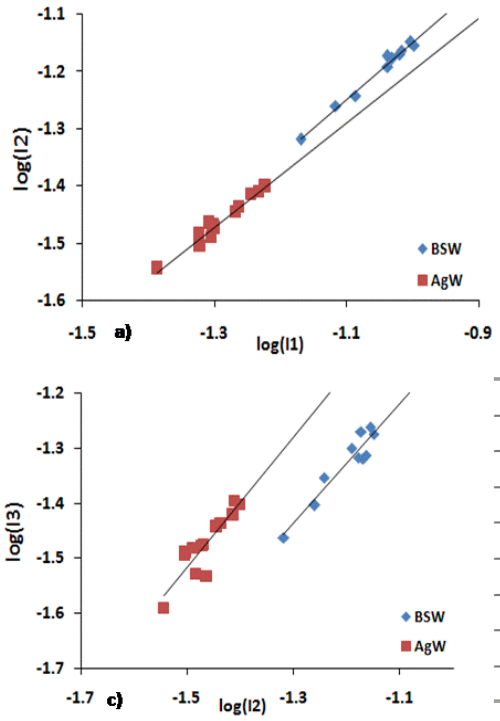

	Equation	R^2
BSW		
$\log(I_1)$ vs $\log(I_2)$	y=0.996x-0.151	0.985
$\log(I_1)$ vs $\log(I_3)$	y=1.089x-0.181	0.897
$\log(I_2)$ vs $\log(I_3)$	y=1.088x-0.021	0.902
AgW		
$\log(I_1)$ vs $\log(I_2)$	y=0.912x-0.284	0.956
$\log(I_1)$ vs $\log(I_3)$	y=1.189x-0.0.62	0.919
$\log(I_2)$ vs $\log(I_3)$	y=1.185x-0.261	0.795

Figure 5.11: Correlations among the components

The humic – like components were strongly correlated with each other (figure 5.11) while in all cases the slopes of the regression equations of the log transformed fluorescence intensities ($\log(I_{1\text{-}3})$) were close to 1 (slope = 1±0.1), indicating that all humic-like components are subjected to similar processes at the BSW layer.

Despite the high humic – like intensities, BSW exhibited very low HIX values (figure 5.7). This is a result of the high protein – like content of this water mass rather than the low aromatic character of the DOM. This is possibly due to the enhanced primary production in these waters [241] resulting from the high nutrients concentrations entering the Black Sea through the riverine discharges. Polat and Tugrul [242] estimated that DON comprises about 75% of the total nitrogen inflow from the Black Sea while Zeri et al. [220] reported the percentage of DON to total nitrogen pool at the surface layer of the Marmara Sea to be over 90%. These findings suggest that the CDOM and FDOM pools in the surface BSW layer are decoupled from the DOC pool. The strong relationship of DOC *vs* salinity observed throughout the sampled transect indicate that the DOC pool is affected mainly by mixing. Nevertheless, alteration processes not observable in the bulk DOC concentrations are discernible in the CDOM and FDOM pools, indicating not loss but rather transformation of dissolved organic matter. Overall CDOM transformation processes taking place at the surface BSW layer deviate from what has been described for surface CDOM during summer in open oceanic waters [85][143][182][184] attributed to photodegradation processes. In the case of Marmara Sea the alteration observed for surface CDOM are largely attributed to microbial processes.

Coble et al. [124] investigating the fluorescence properties of the Black Sea during July 1988, reported the identification of peaks A, C and T. The excitation and emission maxima of peaks A and T we report here, deviates just slightly from the excitation and emission maxima of these peaks while peak C appears to be red shifted in Marmara Sea. The PARAFAC analysis allowed us to resolve an additional peak, peak M. Due to the relatively high proximity of the excitation and emission maxima of peak M to those of peaks A and T that are very intense in areas affected by freshwater inputs, peak M is difficult to resolve by using the traditional peak picking method in these areas. Our data, consistent with the reported fluorescent components from the Black Sea, indicate that the fluorescent properties of the Black Sea persist in the Marmara Sea and up to the Dardanelles. Especially the almost absolute coincidence of peaks A and T denotes a more persisent character of these

substances while the red shift of peak C suggests more extensive chemical alteration. On the other hand, in a more recent study of Zeri et al., [220] reporting the fluorescence properties of the Marmara Sea during the late August of 2008, three different peaks were identified. An unresolved pair of peaks A and C, where peak A is in a good agreement with both Coble's and our results and two amino acid – like peaks, B and N. The inconsistency in the amino acid – like components of the later study may be a result of the different sampling times (late August in Zeri et al. [220], July in Coble et al. [124], early June in this study) indicating a greater variety in the labile substances associated with both phytoplankton and bacterial activity. Peak M was once more not resolved which could be due to the difference among the number and the nature of the included samples in the PARAFAC analysis.

5.4.2 Aegean Water

In deep stagnant waters such as the deep layer of the Marmara Sea, dissolved organic matter decomposition is expected to be concurrent with oxygen consumption by bacteria. In the underlying Aegean waters (AgW) however, an accumulation of DOC in the eastern part of the basin (st.37) is apparent (Kruskal Wallis Test, post hoc $P=0.015$ and $P=0.037$ for sts 35-37 and sts 36-37 respectively) coincident with the highest AOU values (>230). A similar spatial gradient was observed for I_4 as well. The elevated I_4 values at station 37 suggest that the elevated DOC in this region is rich in amino acid – like substances. It should be noted here that the range of I_4 intensities found in the AgW water mass are overall lower than those recorded at the source of this water mass in the N. Aegean Sea (LIW) (0.0158-0.0418 R.U. during July 2014) (see chapter 6).The overall lack of correlation between DOC vs AOU and I_4 vs AOU in these deep waters and the coincidence of high DOC and I_4 values with high AOU suggest that bacteria rely on other carbon sources most probably POM. Moreover, we hypothesize that POM sinking and mineralization acts as a source of DOM. However, this is apparent only at the easternmost station 37 and not at stns 35, 36. Ergin et al., [243], reported higher primary production at the northeastern region of the Marmara Sea compared to the north and central Marmara Sea which was attributed to the organic rich surface inflow from the Black Sea at the northeastern part and the

absence of major rivers at the northern region. Lagaria et al. [241] also reported the highest particulate primary production at the easternmost region of the Marmara Sea, decreasing towards the Aegean Sea. Sinking of organic particles could be therefore assumed to be higher in the northeastern part of the Marmara Sea, which is in accordance with the higher measured AOU values. This POM, which is mostly phytoplanktonic cells and detritus can be enzymatically solubilised by bacteria resulting to the release of DOM [4] which is expected to be reach in amino acid substances. Therefore the elevated I_4 intensities at station 37 could be a result of the higher particulate primary production and POM solubilisation at the northeastern Marmara Sea. Another factor that could result in the concentration of organic material (POM and DOM) only at the eastern part of the Marmara Sea is the dilution of the residing waters by the incoming 'new' AgW waters which are poor in both DOM and POM.

The similar distribution of the absorption indices (a_{300}, a^*_{300} and $S_{275-295}$), the humic – like intensities (I_1-I_3) and fluorescence index HIX indicate the presence of high aromatic DOM of HMW almost throughout the entire water column (200m up to the bottom) of the central and eastern basins, while at the western basin high aromatic DOM is evident only in deeper layers (>600m). The low optical signature of the intermediate waters (50-600m) of the western basin, denote the presence of 'new' AgW waters there; indeed the I_{1-3} intensities for the Aegean waters (>30 m depth) are low (0.0032-0.0263 R.U) (see chapter 6). Thus, humification processes seem to take place in the 'old' AgW. In this case too, particle sinking and dilution processes hinder any strong relationship between DOM and AOU. The pairs of log transformed fluorescence intensities log(I_1) *vs* log(I_2) and log(I_1) *vs* log(I_3) retained the strong correlation found in the BSW (R^2=0.956 and 0.919 respectively), while log(I_2) *vs* log(I_3) showed a weaker correlation (R^2=0.795) (figure 5.11). The slope of the regression equation between I_1 and I_2 did not deviate significantly from 1 (0.912). The deviation on the other hand of the slopes found for the relationships log(I_1) *vs* log (I_3) and log(I_2)*vs* log(I_3) was greater (1.189 and 1.185) indicating an overall faster accumulation of C_3 during the humification processes over both C_1 and C_2. These inter-relationships indicate the

favourable production of the secondary humic-like component (peak C) during humification in the deep Marmara Sea waters. The differences in UVA-fluorescence between the central and eastern basin (lowest at st.36 and elevated at st.37) indicate that the DOM occurring in the central basin is comprised mostly of humic substances and probably is a result of humification while the DOM in the eastern basin has also a protein – like character related to the dissolution of biogenic particles.

5.5 Conclusion

Chemical and optical measurements showed that BSW in the surface layer of the Marmara Sea is of distinct properties, very rich in carbon, strongly absorbing and strongly fluorescence in both the UV and visible spectral regions. The lenghtwide distributions of the measured parameters along the route from the Bosphorus to the Dardanelles Strait indicate different behaviour of DOC over CDOM and FDOM. CDOM and FDOM presented unique characteristics that deviate from typical summertime patterns. Absorption coefficients did decrease along the Marmara Sea which could be a result from mixing and photodegradation. However, the concurrent decreasing slope values along the Marmaras Sea do not support photodegradation as the dominant transformation process of CDOM but rather indicate microbial transformations. The humic intensities preserved similar values throughout the Marmaras Sea surface waters indicating humification processes. In the underlying AgW humification processes seem to be further enhanced, covering almost the whole water column of the central and eastern basins, while they are also evident at the deepest layer of the western basin. The protein – like substances at the AgW are diminished, falling at concentrations lower than the adjacent Aegean Sea. The high AOU values could indicate bacterial consumption, however the lack of correlation between I_4 and AOU appears to be inconclusive. Most likely, the relative accumulation of protein – like substances in the eastern basin was due to the higher primary production in the eastern basin resulting in increased POM and DOM derived from POM mineralization.

CHAPTER 6

SEASONAL VARIATIONS IN DISSOLVED ORGANIC MATTER COMPOSITION USING ABSORBANCE AND FLUORESCENCE SPECTROSCOPY IN THE DARDANELLES STRAITS-NORTH AEGEAN SEA MIXING ZONE

6.1 Introduction

The North Aegean Sea is a highly dynamic coastal area of the eastern Mediterranean Sea, where the low salinity, rich in dissolved organic matter Black Sea Waters (BSW) mix with the highly saline and poor in DOM oligotrophic Levantine Waters (LW) [220][242]. Previous studies in the area have suggested that the inflowing BSW waters may have a direct or an indirect effect on the relatively higher productivity of the North Aegean compared to other eastern Mediterranean regimes [244][245][246]. The study of CDOM in this environment is of particular importance since it represents the area where highly eutrophic continental waters are transferred to the oligotrophic Mediterranean Sea. A first work on CDOM fluorescence in this area has been reported by Zeri et al. [220], as part of the investigation of the dynamics of DOM in the Marmara Sea-Dardanelles Straits-North Aegean Sea during August 2008 and showed that DOM exported from the Dardanelles Strait is highly fluorescent. Furthermore the previous chapter (Chapter 5) showed that BSW reaching the Dardanelles is rich in both CDOM and FDOM. Nevertheless, due to the increased seasonal variability observed in both the water flux and the dispersion pattern of the outflowing BSW [247], it is essential to examine more precisely the modulations of CDOM in this area.

In the present study we focus on CDOM seasonal dynamics in the Dardanelles Straits – North Aegean mixing zone based on both absorbance and fluorescence properties. The aims of our work are: (i) to assess the seasonal variability of CDOM absorption and of modeled fluorescence using PARAFAC analysis; (ii) to relate CDOM optical properties with water mass mixing in the area; (iii) to deduce compositional changes of CDOM in the transition zone from the Dardanelles Straits to the Aegean Sea.

6.2 Materials and Methods

6.2.1 Study Area

The study area corresponds to the frontal area of the Dardanelles outflow in the N. Aegean Sea from 39.6 ºS to 40. 3 ºN and from 25.4 ºW to 25.7 ºE (Figure 6.1).

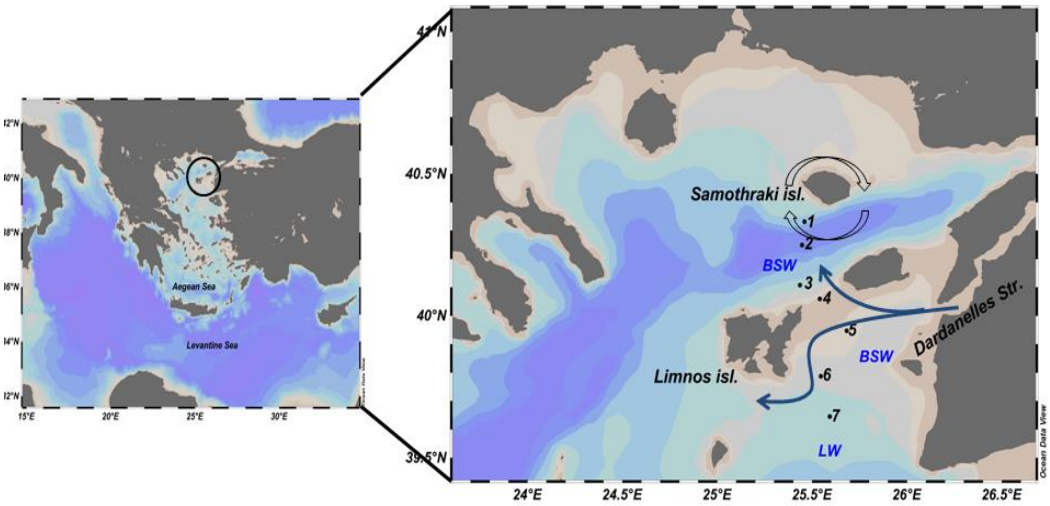

Figure 6.1: Study area and the sampled stations. The solid arrows represent the Dardanelles BSW current while the black open arrows the Samothraki anticyclone. Areas affected by BSW and LW are also marked.

The topography of this region includes the Limnos plateau, a shallow area (<100m) located east of Limnos isl., as well as the Limnos deep basin (~1600m) located between Limnos and Samothraki islands. It is the area where low salinity (S~29) waters originating from the Black and Marmara Seas (BSW) enter into the Mediterranean and mix with the highly saline (S>38) Levantine waters (LW) originating from the southeastern Aegean Sea. The highest outflow of the BSW takes place in the summer caused by the increased river discharges into the Black Sea during spring [248][249]. The less saline BSW outflowing the Dardanelles Straits occupies the surface layer (down to 20-30m) and follows a northwestward route where it is trapped into the Samothaki anticyclone, a permanent feature in the area which results in high residence time of BSW there [249][250]. In summer under the effect of the NE winds (Etesians) the surface circulation alters, and a second branch appears in the BSW route which bifurcates towards the south – southwest direction [250[251]. The average flux of the incoming BSW is estimated to 1160 km^3per year [233][238]. The Aegean Sea also receives freshwater

inputs from many rivers of the Greek and Turkish coastlines. The contribution of the riverine freshwater that reach the N. Aegean is considered minor, compared to the inflow of the BSW, as the total volume of the riverine inputs (Greek and Turkish) are estimated ~ 20 km^3 per year [249].

6.2.2 Samplings

Three cruises in the North Aegean Sea were conducted onboard the R/V Aegaeo in October 2013 (10/10-11/10), March 2014 (22/03-24/03) and July 2014 (16/07-17/07). Samples were collected along a transect of 7 stations, covering the region south of Samothraki isl. and expanding to the east and southeast of Limnos isl. (Figure 6.1). Station 2 is the deepest station (900m) located at the Limnos basin while stations 3, 4, 5 and 6 are situated at the Limnos plateau with depths less than 100m. An additional station where only CTD cast was performed, T1, located at the northern extremity of our sampled transect is also presented here in order to give a more complete picture of the hydrography of the area. All stations were sampled from the surface 2m to 100m depth (or to the bottom in the case of the shallow stations) using Niskin bottles deployed by a CTD rosette (Seabird electronics).

Water samples for DOC and CDOM analysis were filtered through 0.22μm polycarbonate filter immediately after sampling. The filters were flushed with ~200ml MilliQ water prior the filtration and the first milliliters of the filtrate were discarded to avoid any contamination. Samples for DOC analysis were collected in precombusted glass ampoules (480°C, 12h), acidified with 2N HCl to ph~2, flame sealed on board and kept at +4°C until analysis. Samples for CDOM analysis were transferred into acid (HCL 10%, 12h) cleaned amber glass bottles and kept in the dark at +4°C if the analysis was performed within the next few days otherwise they were stored in the dark at ~-20°C.

6.2.3 Methodology

Dissolved organic carbon, absorption and fluorescence were analyzed as described in Chapter 4, while the spectra from the fluorescence analysis were included in the PARAFAC modeling and the identified components are described in Chapter 4. The qualitative indices of absorption, carbon specific absorption coefficient a^*_{300} and spectral slope $S_{275-295}$ as well as fluorescence

indices, humification index HIX and biological index BIX were estimated as described in Chapter 4.

6.3 Results

6.3.1 Hydrography and water column structure

Temperature reached the highest values in July (15.6 – 24.6 °C) and the lowest in March (12.3 – 15.4°C). In October temperature fluctuated between 16.4 and 21.1 °C. The lowest salinity values recorded in October 2014 (31.4 – 39.1) consistent with the period of highest water outflow from the Dardanelles Straits. In March and July salinity values ranged between 32.5 – 39.0 and 32.6 – 39.1 respectively. A strong stratification of the water column (upper 30-40m) throughout the study area, caused by the increased outflow rates of brackish BSW and the higher surface temperatures is evident in October 2013 and July 2014 (Figure 6.2).

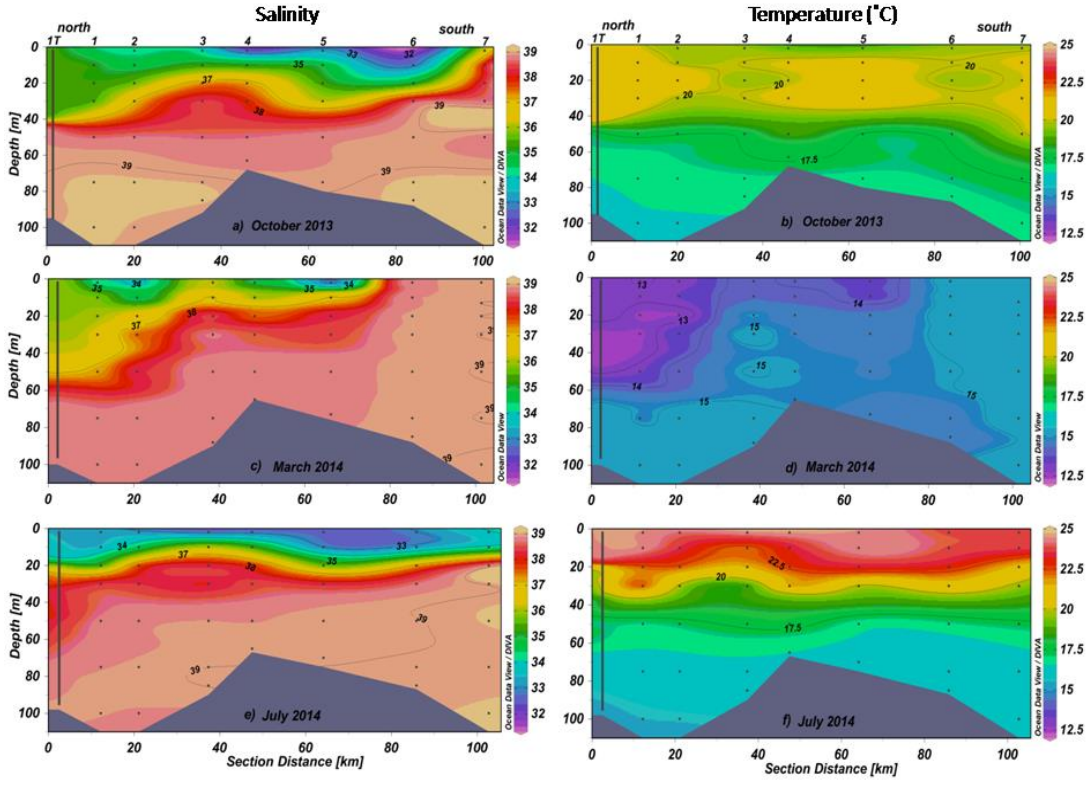

Figure 6.2: Vertical distribution of salinity and temperature (˚C) along the sampled transect during each campaign: (a, b) October 2013; (c, d) March 2014; (e, f) July 2014.

In addition, during these months, the prevailing strong NE winds (*Etesians*) spread the surface brackish layer towards the south. In March 2014 (Figure

6.2 (c), (d)), BSW waters were confined to the north part of the section and a less pronounced stratification was observed, favored by the lower surface temperatures and the limited Dardanelles outflow during winter. The frontal zone is distinguished between stations 5 and 6. The northern part of the sampled section is clearly affected by the presence of the Samothraki anticyclone, as it can be inferred by the deepening of the salinity isolines. In figure 6.2(d) it is also distinguishable a lens of cooler waters residing at depths 20-45m of stations T1, 1, 2 which corresponds to winter – older BSW. These features seem to fade progressively during the July and October samplings due to the presence of the strong thermocline which is expected to attenuate the anticyclone. Based on previous investigations in the area [247][251] we may describe that the major flux of BSW travels towards the northeast, where it is trapped in the permanent anticyclone and mix with 'older' BSW while a second branch formed during October 2013 and July 2014, bifurcates towards the south and mixes with 'new' LW. Thus two mixing modes can be distinguished between winter-spring and summer-autumn months.

6.3.2 DOC and CDOM spatio -temporal variability

The vertical distribution of DOC during the three sampling periods is given in Figure 6.3 (a, c, e) and shows that surface brackish layer is systematically enriched in DOC. Highest concentrations of DOC were found in October 2013 ranging from 65-126 μmol/L with a mean value of 92 μmol/L.

Table 6.1: Averages and range of values for DOC (μmol L^{-1}), the absorption coefficients a_{254}, a_{300} (m^{-1}), the spectral slope $S_{275-295}$ (m^{-1}) and the absorption indices SUVA, a^*_{300} (m^2 g^{-1}), in the two water masses present during the three samplings .

		BSW	LW
DOC (μmol L^{-1})	October 2013	109 76-126	79 65-98
	March 2014	83 68-98	62 55-72
	July 2014	96 72-115	64 53-79
a_{254} (m^{-1})	October 2013	2.14 1.04-2.88	1.36 0.89-1.86

	March 2014	2.31 1.51-3.10	1.39 1.31-1.60
	July 2014	2.01 1.13-3.35	1.24 0.75-1.97
a_{300} (m^{-1})	October 2013	0.54 0.32-0.73	0.39 0.23-0.57
	March 2014	0.67 0.41-0.94	0.37 0.30-0.49
	July 2014	0.51 0.29-0.90	0.34 0.18-0.53
$S_{275-295}$ (nm^{-1})	October 2013	0.036 0.031-0.039	0.033 0.030-0.038
	March 2014	0.033 0.032-0.035	0.035 0.031-0.039
	July 2014	0.037 0.033-0.039	0.035 0.031-0.039
SUVA (m^2 g^{-1})	October 2013	1.62 1.14-1.93	1.47 0.93-1.96
	March 2014	2.31 1.72-2.64	1.89 1.53-2.19
	July 2014	1.74 1.09-2.51	1.62 0.92-2.26
a^*_{300} (m^2 g^{-1})	October 2013	0.41 0.32-0.52	0.42 0.24-0.62
	March 2014	0.67 0.46-0.80	0.50 0.40-0.67
	July 2014	0.44 0.30-0.67	0.44 0.22-0.63

During March, the lowest concentrations were recorded with a range of 55-103 μmol/L and average value 69 μmol/L, while in July, DOC values ranged

from 53 to 115 μmol/L with a mean of 74 μmol/L (Table 6.1). During October 2013 and July 2014 the presence of the thermocline affects DOC vertical distribution, restricting higher values at the upper ~30m. Contrary in March 2014, it is evident that DOC concentrations at the northern part of the transect (stns 1, 2, 3) follow the anticyclonic circulation of the BSW water mass (Figure 6.3c).

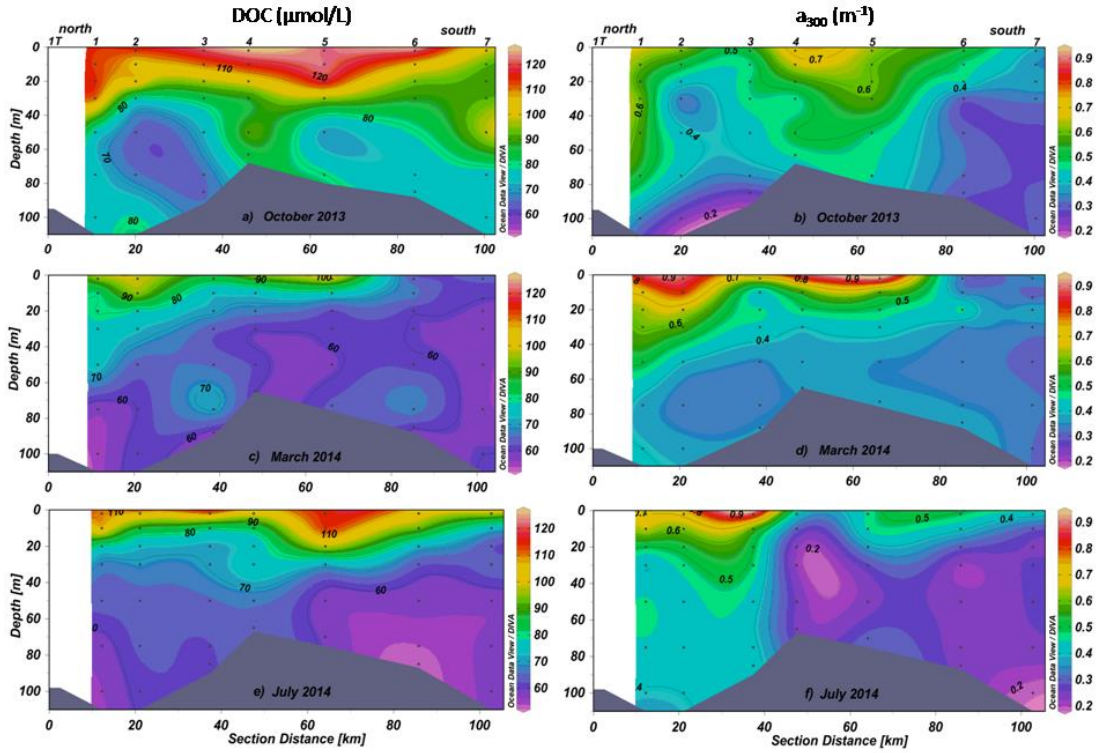

Figure 6.3: Vertical distribution of DOC (μmol/L) and a_{300} (m^{-1}) along the sampled transect for (a, b) October 2013; (c, d) March 2014; (e, f) July 2014.

Overall in our study system, DOC showed strong negative correlation with salinity (Figure 6.4a) indicating that mixing of BSW with LW regulates DOC distribution in the N. Aegean Sea, and explains 75% of DOC variability in October (R^2 = 0.751, p<0.001) and 87% in March and July (R^2 = 0.874 and 0.875 respectively, p<0.001). In figure 6.4a the theoretical mixing line of the high salinity- low DOC Levantine waters with the low salinity- high DOC Black Sea waters is drawn (based on salinities from the present data set). Most samples from the October 2013 cruise fall above the mixing line indicating DOC accumulation during autumn leading to significantly maximum concentrations in October (Kruskal-Wallis test: P=0.000, post-hoc pairwise:

October-March P=0.000, October-July P=0.000, March-July P=0.372). DOC accumulation in coastal regions during autumn is a feature characteristic for this parameter that has been attributed to low biodegradation rates due to limited nutrient availability to bacteria [252].

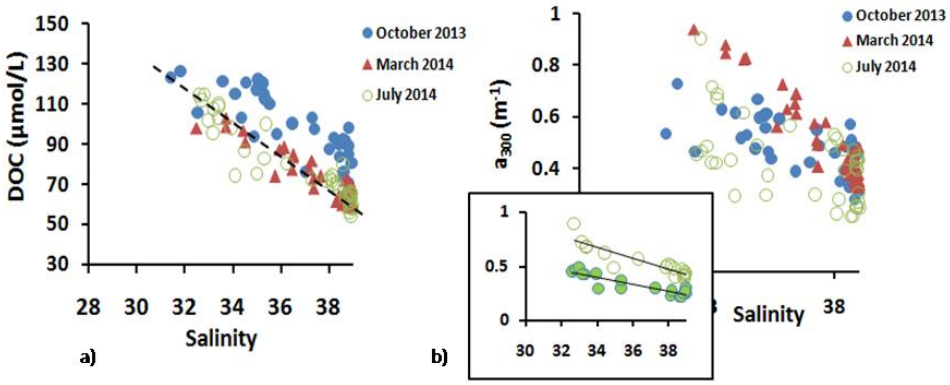

Figure 6.4: Relationships of salinity with: (a) DOC (µmol/L); (b) absorption coefficient a_{300} (m^{-1}), during the three samplings. The inset in 5(b) shows the two different mixing lines established between the northern part (stns 1,2,3) and the southern part (stns 4,5,6,7) of the sampled transect in July 2014.

CDOM during October 2013 showed a_{300} coefficients ranging from 0.23 to 0.73 m^{-1} (average 0.46 m^{-1}). During March 2014, a_{300} values were highest, in the range of 0.30 to 0.94 m^{-1} (average 0.47 m^{-1}) while in July 2014 were found lowest ranging from 0.18 to 0.90 m^{-1} (average 0.40 m^{-1}) (Table 6.1, Figure 6.3 (b, d, f)). CDOM absorptiom coefficient at 300nm showed strong negative correlation with salinity only during March 2014 (R^2=0.920, p<0.001) while during October 2013 and July 2014 the relationship fainted (R^2=0.484; R^2=0.364 p<0.001) as a_{300} coefficients dropped at salinity range 32-37 (Figure 6.4b). Specifically for the July 2014 samples, two separate mixing lines are formed for the a_{300} *vs* S distribution (figure 6.4b, inset figure): one for stations 1, 2, 3 at the northern part of the section with elevated a_{300} coefficients (0.394 – 0.900 m^{-1}) and R^2=0.84 (p<0.001) and a second one for stations 4, 5, 6, 7 at the southern part of the section with lower a_{300} coefficients (0.184 - 0.487 m^{-1}) and R^2=0.84 (p<0.001). The elevated a_{300} coefficients at the northern part of the section, where mixing of 'new' BSW with 'old' BSW takes place, clearly show that CDOM retains its BSW character there. At the southern part of the section 'new' BSW mix with LW which are poor in CDOM resulting in the overall lower a_{300} coefficients. The differences observed between DOC and

CDOM distribution show that these two pools are decoupled at the sampled transect of the North Aegean Sea. CDOM presented high absorption coefficients and a strong conservative character only during March and clearly differentiates from DOC seasonal distribution; which retains some conservative character during all samplings and exhibits accumulation in October 2013.

6.3.3 Fluorescence properties

During all of our samplings the protein – like component C_4 exhibited the highest fluorescence intensity followed by the terrestrial humic – like C_1. The marine humic – like C_2 ranked third while the secondary terrestrial humic – like component C_3 showed the lowest intensity (Table 6.2). This order was consistent not only among seasons but also between the two water masses (BSW and LW). The terrestrial humic components are expected to be found in the low salinity waters of our study area and are related to the source of these waters, i.e. the Black Sea. All four peaks identified in North Aegean Sea during our samplings (2013-2014) were also found in Marmaras Sea during May 2013 as discussed in Chapter 5. Peaks A, C and T similar to our components C_1, C_3 and C_4 have been identified in the Black Sea by Coble et al. (1990). In a previous study [220] in the area of the Marmara – N. Aegean Seas, peaks A and C were present but peak (T) was not detectable; instead a quinine –like component resembling peak N and the tyrosine-like component (peak B) were present as discussed in Chapter 5. Nevertheless, during the present campaigns the fluorescent protein-like component C_4 is detected in high levels in the N. Aegean. The eutrophic environment of the Marmara Sea, with elevated rates of both primary and bacterial production [220][242] compared to the N. Aegean Sea must be responsible for the release of component C_4.

Consistent with the DOC and absorption (a_{300}) results, increased fluorescence intensities of all components (I_i) were recorded at the surface brackish waters. The highest fluorescence intensities (I_1, I_2, I_3, I_4) were observed in October 2013. Fluorescence intensities of the four Parafac components were well correlated with salinity only during March 2014 (I_i *vs* S R^2>0.705, P<0.001) (Figure 6.5), similar to the results of CDOM absorption.

Table 6.2: Averages and range of values for the fluorescence intensities (I_i) (R.U.) of the four Parafac components and of the indices HIX and BIX, in the two water masses present during the three samplings.

		BSW	LW
I_1 Ex/Em= 255/448nm	October 2013	0.0267 0.0189-0.0373	0.0229 0.0175-0.0307
	March 2014	0.0246 0.0175-0.0327	0.1465 0.0105-0.0174
	July 2014	0.0263 0.0145-0.0374	0.0163 0.0116-0.0263
I_2 Ex/Em= 300/402nm	October 2013	0.0197 0.0147-0.0341	0.0166 0.0126-0.0219
	March 2014	0.0174 0.0128-0.0240	0.0104 0.0072-0.0131
	July 2014	0.0195 0.0135-0.0300	0.0128 0.0093-0.0183
I_3 Ex/Em= 280/496, 370/496nm	October 2013	0.0117 0.0084-0.0186	0.0106 0.0085-0.0128
	March 2014	0.0114 0.0083-0.0147	0.0068 0.0048-0.0082
	July 2014	0.0107 0.0051-0.0154	0.0068 0.0032-0.0132
I_4 Ex/Em= 275/336nm	October 2013	0.0354 0.0175-0.0733	0.0273 0.0139-0.0494
	March 2014	0.0354 0.0255-0.0486	0.0196 0.0135-0.0337
	July 2014	0.0446 0.0299-0.0684	0.0224 0.0158-0.0418
	October 2013	1.29	1.53

		0.92-1.92	0.91-2.65
HIX	March 2014	1.34 1.20-1.65	1.41 0.66-1.88
	July 2014	1.14 0.98-1.26	1.61 0.85-2.91
BIX	October 2013	0.98 0.84-1.20	0.95 0.83-1.10
	March 2014	0.96 0.61-1.11	1.00 0.88-1.22
	July 2014	1.14 0.98-1.60	1.16 0.98-1.50

The two mixing lines observed in the a_{300} *vs* S distribution in July 2014, however, were not apparent for any of the four fluorescence components. At intermediate salinities negative deviations of the mixing line are observed for C_1 and C_3 in July 2014 and for C_4 in October 2013. Finally, an excess in fluorescence of all components was recorded sporadically in surface waters during October 2013 (Figure 6.5).

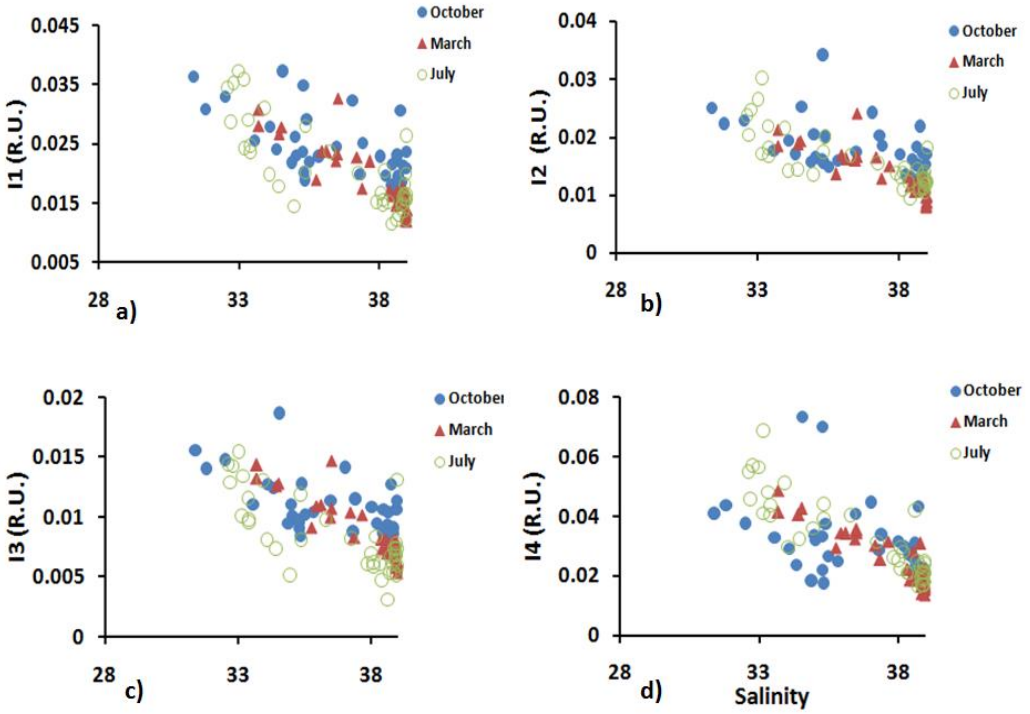

Figure 6.5: Components relationship to salinity during the three samplings.

6.3.4 CDOM-FDOM qualitative indices

The range of values obtained for the optical indices used in this work ($S_{275-295}$, SUVA, a^*_{300}, HIX, BIX) is presented in Tables 6.1 and 6.2. The carbon specific absorption coefficients a^*_{300} and SUVA showed significant negative correlation with salinity only during March (R^2 =0.686 and 0.753 respectively, P<0.001), evidencing conservative mixing only in early spring, as observed also for a_{300}.

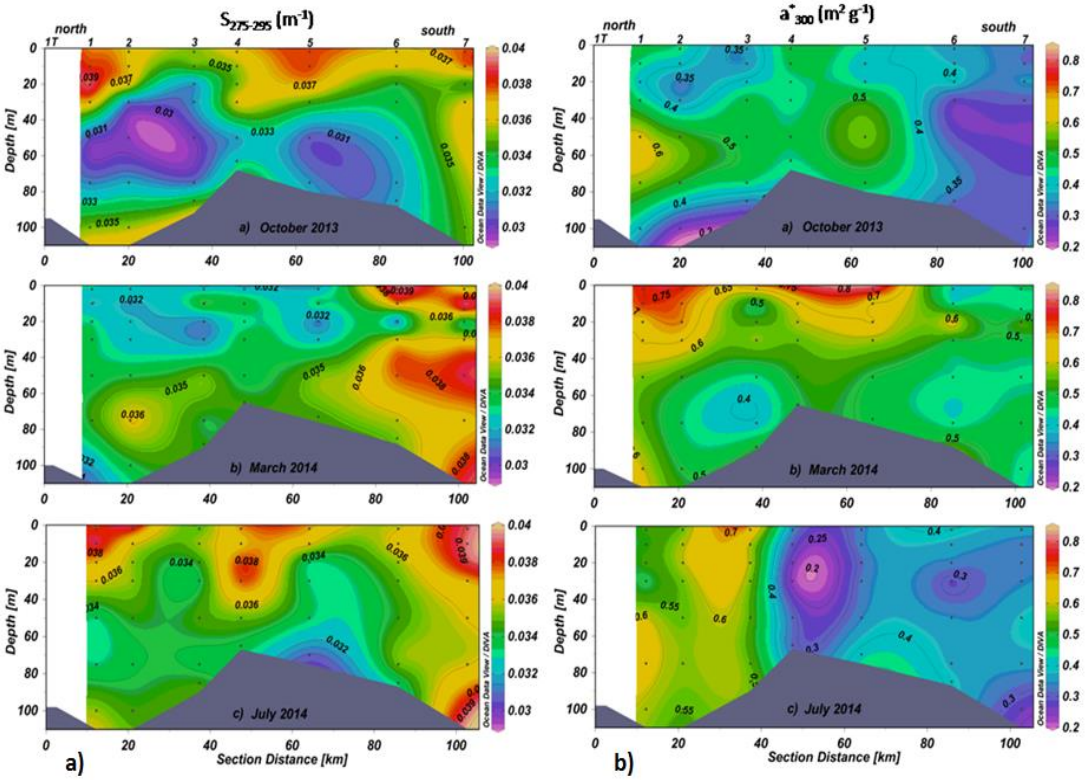

Figure 6.6: Vertical distribution of (a) absorption slope $S_{275-295}$ (nm^{-1}) and (b) coefficient a^*_{300} ($m^2g^{-1}C$) during the three samplings.

At the BSW layer (S<38), the recorded $S_{275-295}$ values in March 2014 were significantly lower than those in October 2013 and July 2014 (Figure 6.6(a)) (Kruskall-Wallis test: P=0.000, post hoc Pairwise: P≤0.001 between March-October and March-July). At the same time, carbon specific absorption coefficients a^*_{300} and SUVA revealed significantly higher values during March in BSW (S<38) (Kruskall-Wallis test: P=0.000, post hoc Pairwise: P≤0.001 between March-October and March-July) (Table 6.1, Figure 6.7, (SUVA not shown)). The lower $S_{275-295}$ values coupled with the higher a^*_{300} and SUVA values indicate the occurrence of terrestrial aromatic material in BSW during

early spring. On the other hand, the distribution of $S_{275-295}$ and a^*_{300} for October 2013 and July 2014 in the surface brackish layer (S <38, BSW) (Figures 6.6(a) and (b)), shows a shift toward higher and lower values respectively, implying an increase of low molecular weight compounds and an overall loss of CDOM contribution to the bulk DOM during these months. In LW waters (S>38), the southern stations (sts 6 and 7) retain highest $S_{275-295}$ during all samplings. At the stations over the Limnos plateau and basin (sts 1 to 5) and at depths 30m to 80m, the lowest $S_{275-295}$ values were recorded especially in October 2013 (Figure 6.6(a)) when also increased a^*_{300} values were observed, indicating the presence of higher molecular weight chromophoric material there, not consistent with the optical properties of this water mass (LW) (high $S_{275-295}$, low a_{300}).

HIX values are considered low with small variation range, from 0.6 to 2.9 (Figure 6.7).

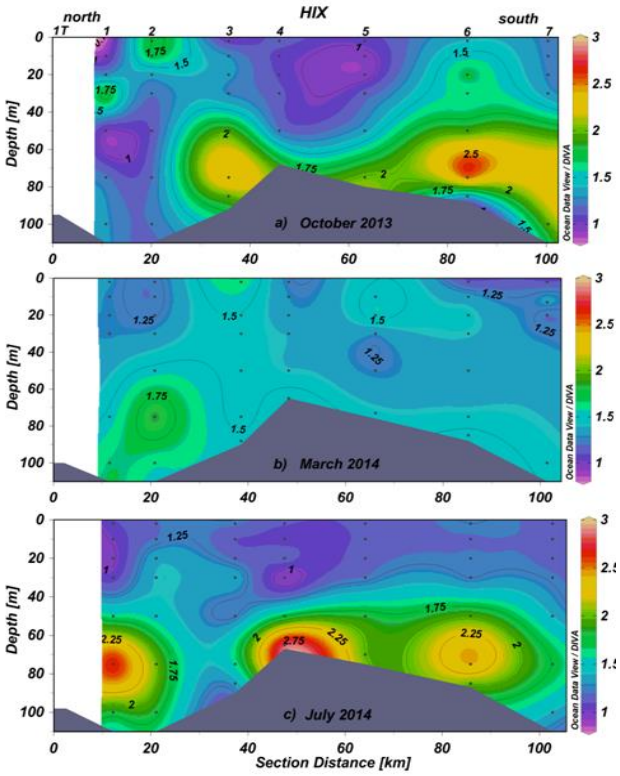

Figure 6.7: Vertical distribution of the humification index HIX in: (a) October 2013, (b) March 2014, and (c) July 2014.

Low HIX values (<4) are attributed to organic material of autochthonous origin [126] and in our study system the low HIX observed reflect the dominance of

the UVA fluorescent component C_4 transported from the Marmara Sea.The maxima (2-2.2) observed in the HIX index at the bottom samples of the Limnos plateau (in October 2013 and July 2014) reflect small increases in visible fluorescence independent of the UVA fluorescence and therefore a different source of FDOM.

The variation range of BIX index (0.8 - 1.6) indicates autochthonous organic material of biological origin [126]. The significantly higher BIX values for the July 2014 samples (Kruskall-Wallis test: P=0.000, post hoc Pairwise: P=0.000 between July-October and March-July, P=0.006 for October - March) indicate that FDOM has been subjected to intense microbial modification during this month (Figure 6.8).

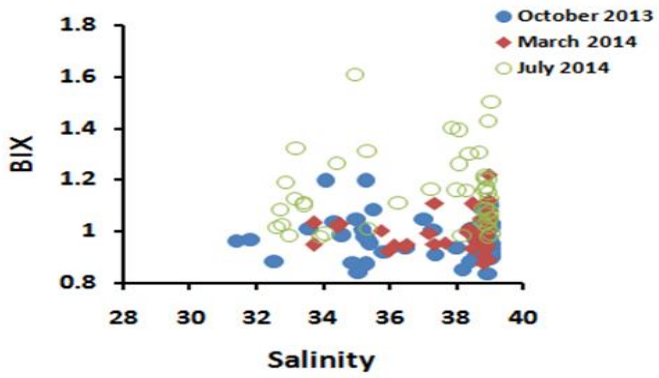

Figure 6.8: BIX distribution along the salinity gradient during the three samplings.

6.4 Discussion

6.4.1 Alterations in CDOM and FDOM pools

The observation of higher SUVA and a^*_{300} values in March (Table 6.1) indicate the presence of more aromatic DOM and of higher molecular weight in early spring. The decrease in the carbon specific CDOM absorption at 300nm observed for the surface layer during summer and autumn and the parallel increase in the spectral slope $S_{275-295}$ is indicative of photodegradation processes caused by the increased solar radiation in the preceding period (late spring and summer). Especially in Eastern Mediterranean waters the photochemical degradation is expected to be an important process because of the low cloudiness during the summer that results in strong exposure to light and also because the oligotrophic waters lead in low light attenuation in the water column. Previous studies demonstrated that CDOM exposure to

sunlight in natural waters causes the increase of spectral slope and the decrease of absorption coefficients [79][113][176][253]. Bricaud et al. [110], showed that in similarly low absorbing open ocean waters, the effect of UV radiation can reduce a_{300} values more than 75%, while Nelson et al. [88], demonstrated maximum summertime surface CDOM depression in the Sargasso Sea coincident with the seasonal maxima in surface irradiance and mixed layer shallowing. It appears that in our study area, highly aromatic and conjugated moieties comprise a significant fraction of DOM only in early spring, and are more pronounced in the low salinity surface waters. Summer photodegradation processes have a profound impact on CDOM *in situ* transformations resulting in a CDOM optical signature indicative of lower molecular weight and less aromatic chromophoric compounds in the surface brackish waters (0-30m).

The observed changes in CDOM absorption signature were consistent with changes in the relative contribution of CDOM fluorescence components. Following Murphy et al. [139], we examined the correlation between different fluorescent components, with conservative mixing expected to result in a linear relationship between the log transformed intensities with slope equal to 1 (Figure 6.9).The correlation of the secondary terrestrial humic component I_3 against the primary one I_1 suggests conservative behavior of the two components in March 2014 and July 2014 (slope= 1.015; slope=1.062 respectively) and some consumption of C_3 relatively to C_1 during October 2013 (slope=0.773) (Table 6.3, Figure 6.9 (c)). The decoupling of the two components is suggested also by the ratio of intensities I_1/I_3 drawn against I_3 in figure 6.9 (d), where it is shown that the ratio variability is independent of the variation in C_3. Fluorophore groups similar to the visible humic-like peak C_3 observed here (widely characterized as Peak C in the literature) are characterized as the most labile to photodegradation [139] and therefore C_3 consumption would be expected during summer. It is possible that the highest irradiation during the spring –summer period reduces the fluorescence ability of both fluorophores C_1 and C_3, so that C_3 loss relatively to C_1 is distinguishable only later in autumn. Nevertheless, the ratio I_3/I_1 acquires the lowest values in July and the highest in March, clearly showing a greater loss

of fluorescence of component C_3 relatively to C_1 during July 2014. The picture described here explains the negative deviations of the $I_{1,3}$ *vs* S relationship observed for these two components during summer and autumn (section 6.3.3; Figure 6.5(c)).

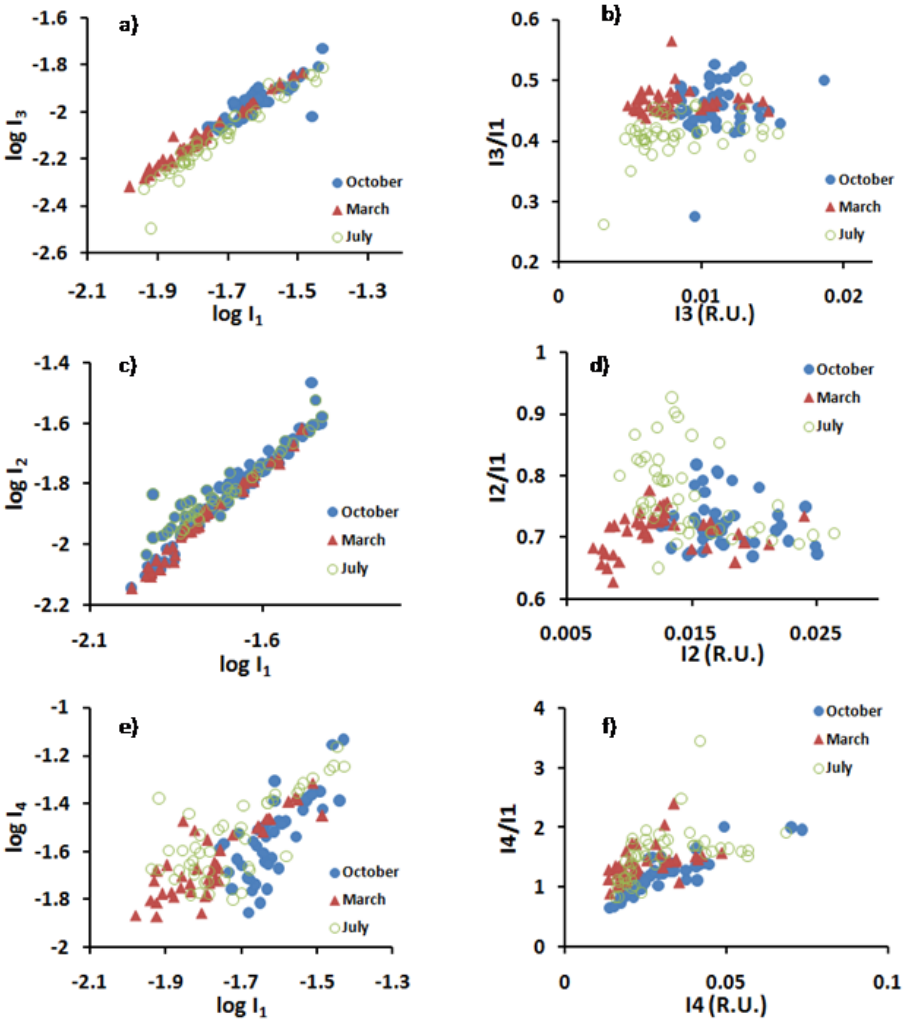

Figure 6.9: Relationships of the log-transformed fluorescence intensities of the components C2, C3, C4 against the log-transformed intensity of C1: (a); (c) $logI_2$:$logI_1$; (e) $logI_4$:$logI_1$. Distributions of the ratio I_i:I_1 ($_i$=2,3,4) as a function of I_i (b, d, f).

Changes in the relative contributions of fluorescence components C_2 (marine humic- like) and C_1 (UV humic- like) were indicative of impacts of biological processes on CDOM dynamics. Fluorescence intensities I_1 and I_2 were linearly correlated in all our samplings (Figure 6.9 (a)). During October 2013 and March 2014 the slope of linear approximation of $LogI_1$ *vs* $LogI_2$ was 0.961 and 1.024 respectively, indicating that conservative mixing is controlling the concentrations of the two components (Table 6.3). In July 2014 the slope

decreased to 0.800, and linearity deviates at low I_1 fluorescence towards higher I_2, implying a faster removal of C_1 relatively to C_2 in summer (Figure 6.9 (a)). At the same time the hyperbolic distribution of the ratio of the intensities I_2/I_1 as a function of the intensity of C_2 for the July samples (Figure 6.9 (b)) shows a simultaneous constant production of the marine humic like component C_2. Production of C_2 during summer can be supported by the higher rates of bacterial production found in our study area in July 2014 (0.29 ± 0.09 mg C $m^{-3}d^{-1}$), compared to March 2014 (0.22 ± 0.1 mg C $m^{-3}d^{-1}$) and October 2013 (0.22 ± 0.05 mg C $m^{-3}d^{-1}$) [254] and is consistent with the increased BIX values during summer, while the removal of C_1 may be driven by the intense photodegradation during summer [112][255].

Table 6.3: Regression between the log-transformed intensity of component 1 (I_1) and the log-transformed intensities of the other components ($I_{2,3,4}$).

October 2013	R^2	P
$\log(I_2) = 0.962*\log(I_1) -0.199$	0.871	<0.001
$\log(I_3) = 0.773*\log(I_1) -0.709$	0.711	<0.001
$\log(I_4) = 1.492*\log(I_1) +0.869$	0.566	<0.001
March 2014		
$\log(I_2) = 1.024*\log(I_1) -0.107$	0.977	<0.001
$\log(I_3) = 0.990*\log(I_1) -0.351$	0.979	<0.001
$\log(I_4) = 1.015*\log(I_1) +0.159$	0.711	<0.001
July 2014		
$\log(I_2) = 0.800*\log(I_1) -0.455$	0.892	<0.001
$\log(I_3) = 1.062*\log(I_1) -0.279$	0.932	<0.001
$\log(I_4) = 0.928*\log(I1) +0.045$	0.529	<0.001

Fluorescence component C_4 (protein like peak) was dominant in our study system. The negative relationship of this component with salinity (section 6.3.3; Figure 6.5(c)) suggests that it is transported to the N. Aegean Sea

through the Dardanelles Straits, along with the visible fluorescent components (C_1, C_2, C_3), rather than being produced *in situ*. The increased scattering however, in the correlation of Log(I_4) *vs* Log(I_1) (Figure 6.9 (e)) implies that the two components are not strongly related to each other. Especially for the October 2013 sampling, the rise in the slope of the regression equation to 1.4 suggests a decoupling of C_4 relatively to C_1.This might be explained by C_4 consumption, as it is also inferred by the loss of its fluorescence intensity observed in the I_4 *vs* S distribution (described in section 6.3.3). Given that the amino-acid tryptophan – like fluorophores have been reported as biological labile [130][184] and photoresistant [256], the observed distribution implies biodegradation processes.

Microbial transformations of FDOM during summer and autumn are therefore traceable in our study system through the production of the visible fluorescent component C_2 and the consumption of the UVA component C_4. FDOM is also affected by solar radiation in the upper water layer during these months, since both humic-components C_3 and C_1 decreased during the summer, with the most photoreactive C_3 showing a relatively stronger decrease than C_1 after prolonged exposure.

6.4.2 Dynamics of DOC, CDOM, FDOM

During our campaigns two contrasting hydrographic situations were encountered in the mixing zone of BSW and LW in the N. Aegean Sea. Winter-spring conditions, when BSW flows towards the northwest and mixes with ‘old’ BSW under the effect of the anticyclone, and summer –autumn conditions, when a second branch of the BSW flow is formed which travels south and mixes with LW waters. In addition, during summer-autumn a strong pycnocline covers the whole study region. This spatiotemporal variability in the hydrography was depicted in the DOC and CDOM distribution. Highest DOC and CDOM were always associated with low salinity waters as observed previously by Zeri et al. [220]. Nevertheless the three campaigns conducted during the present study allowed us to trace several *in situ* transformations of DOM taking place in the Dardanelles Straits - North Aegean Sea mixing zone. The strong conservative character and coupling of DOC and CDOM -FDOM

was established only during winter (March 2014) (Table 6.4). CDOM was found to explain 86% of DOC variability and FDOM 72-79% (Table 6.4).

Table 6.4: Relationships between DOC (μmolL^{-1}) and the optical parameters a300 (m^{-1}), I_i (R.U.) during the three samplings (Model II Regression).

	R^2	P
October 2013		
DOC = 112.41*a_{300} + 41.66	0.514	<0.001
March 2014		
DOC = 64.892*a_{300} + 37.79	0.863	<0.001
DOC= 1857.83*I_1 + 35.19	0.789	<0.001
DOC= 2495.71*I_2 + 36.74	0.724	<0.001
DOC= 4028.89*I_3 + 34.99	0.789	<0.001
DOC =1090.47*I_4 + 41.44	0.720	<0.001
a_{300} = 27.515*I_1 -0.020	0.845	<0.001
a_{300} = 37.373*I_2 – 0.003	0.793	0.006
a_{300} = 60.034*I_3 – 0.026	0.855	<0.001
a_{300} = 16.199*I_4 + 0.071	0.776	<0.001
July 2014		
DOC = 78.393*a_{300} + 44.14	0.418	<0.001
DOC = 2054.64*I_1 + 34.38	0.558	<0.001
DOC = 31.3537*I_2 + 27.62	0.572	<0.001
DOC = 4237.06*I_3 + 40.37	0.442	<0.001
DOC = 1247.54*I_4 + 37.41	0.762	<0.001

The inflowing waters are rich in DOC and CDOM-FDOM compounds of high molecular weight and of aromatic character and mix with Levantine waters poor in DOC and CDOM-FDOM compounds of low molecular weight. Due to

the distinct optical properties of the two water masses we checked the possibility to describe water mass mixing in our study area based on the optical properties alone. Following the mixing scenarios reported by Stedmon and Markager [240], we used the slope of the short wavelength range $S_{275-295}$ and the absorption coefficient at 300 nm. The distributions we came up with during March 2014 are plotted in figure 8.10 and approximate the scenario of the conservative mixing of two completely different pools. It becomes clear that all BSW samples fall to the high a_{300} –low $S_{275-295}$ terrestrial pool, and all LW samples to the low a_{300} – high $S_{275-295}$ marine pool. The distributions of the two other samplings did not show any clear trend.

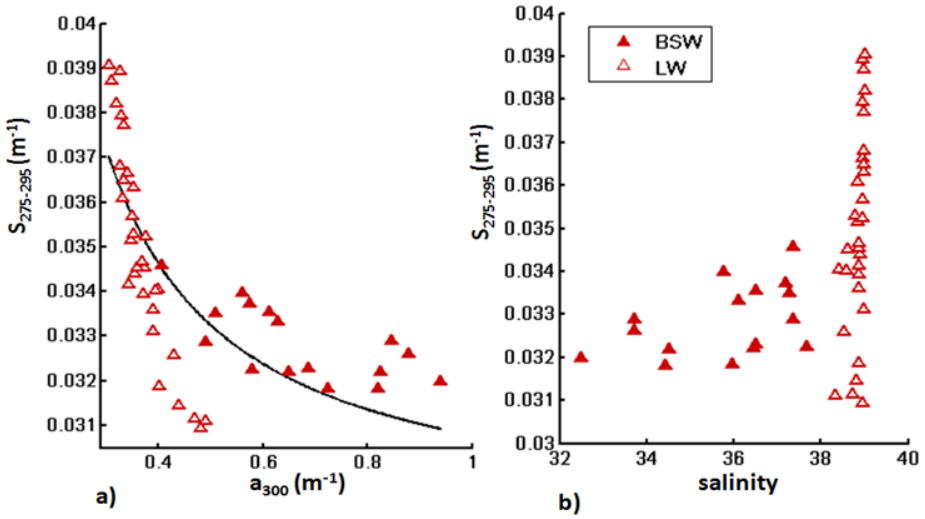

Figure 6.10: a) Relationship between the spectral slope $S_{275-295}$ (nm^{-1}) and the absorption coefficient a_{300} (m^{-1}) during March, b) distribution of the spectral slope $S_{275-295}$ (m^{-1}) as a function of salinity during March.

During the summer months, CDOM in surface waters is expected to be strongly affected by photochemical processes, especially in the mostly cloud-free Eastern Mediterranean oligotrophic waters, consistent with the changes we observed in CDOM optical signature in the upper layer (0-30m). During summer (July 2014), at the northern part of our sampled section the continuous flux of BSW, assign a 'BSW character' to CDOM occurring there, i.e. relatively more aromatic. At the southern section, BSW waters mix with the already photobleached LW. After the summer months (October 2013) the effect of photodegradation processes on CDOM becomes evident throughout the surface waters of the study area. It is understood that the non-

conservative behaviour of CDOM and the decoupling between DOC and CDOM (Table 6.4) during summer-autumn months is due largely to photodegradation processes affecting the surface water layer. During these months the contribution of CDOM to DOC pool drops and CDOM explains only 40-50% of DOC variability (Table 6.4). The observed variation in CDOM is not followed by FDOM in the same manner. During summer, FDOM components C_1, C_2, C_3 explain only 44-57% of DOC variability (Table 6.4), but the photoresistant UVA fluorescent component C4 still holds a strong coupling to bulk DOC (76%). Later in autumn (October 2013) FDOM is totally decoupled from both DOC and CDOM. The interrelationships of the PARAFAC components showed that photodegradation reduces the visible fluorescence of components C_3 and partly of C_1. Moreover, *in situ* microbial processes have a traceable effect on FDOM through the production of the visible fluorescent component C_2 observed during summer. The dominance of the UVA fluorescent component C_4 (tryptophan –like) and its consumption during autumn revealed that the CDOM transported to the N. Aegean from the Dardanelles may serve as bacterial substrate especially under nutrient limitation conditions. Nevertheless, photo- and bio- degradation processes acting upon CDOM -FDOM during autumn have only minor effect on the bulk DOC mineralization which was found to accumulate in the N. Aegean Sea during October 2013.

Under the strong pycnocline conditions and the limited exchange between the two water layers during summer and autumn, it is expected that the subsurface LW waters (S>38) retain their optical properties i.e. low a_{300}, high $S_{275\text{-}295}$. Instead, our results showed low a_{300}, low a^*_{300} but also low $S_{275\text{-}295}$ values. This could be due to impacts of microbial processes [118], but it could also be due to the influence of particles and sedimentary processes which should be taken under consideration when studying DOM dynamics in coastal areas and shallow waters. Under stratified conditions, the Samothraki anticyclone is expected to be attenuated and particle export becomes less intense. We suspect that macromolecular compounds that otherwise will tend to flocculate and adsorb onto particles now remain in solution and may explain the decrease in $S_{275\text{-}295}$ values. Another feature, which differentiates bottom

waters under stratified conditions, is the existence of a different source of FDOM at the Limnos plateau, as inferred by the relatively high HIX values, i.e. relatively increased visible fluorescence. Resuspension of sediments has been recorded for the October 2013 and July 2014 samplings at the Limnos plateau exactly at the same sites were HIX was found elevated [257]. As LW waters travel northward, they are subducted under the pycnocline during these months and are forced to pass through a shallow ~40m water layer over the Limnos plateau, so that their velocity is expected to increase resulting in sediment resuspension events. Moreover, the generation and release of visible fluorescent FDOM from sediments has been reported by Skoog et al. [156] and provides strong evidence that the site specific increases observed in the visible fluorescent FDOM are linked to sedimentary organic material. We therefore suggest that the modulation of CDOM-FDOM characteristics in the subsurface layer is related to changes in the particle regime under stratified conditions.

6.5 Conclusion

This study provides insights on the composition, transformation and seasonal dynamics of both CDOM and FDOM in the Dardanelles Straits - North Aegean Sea mixing zone. Conservative mixing determines optical properties distribution only in winter- spring when CDOM is an important fraction of DOM showing the same behavior with the bulk DOC. Contrary DOC holds strong relation to salinity during all the sampled periods. Therefore the use of the optical properties to describe the mixing of the two water masses (BSW and LW) can be applied only during winter-spring months when the conservative character is retained. The optical indices related to CDOM absorbance properties ($S_{275-295}$, a* and SUVA) demonstrated for the first time for the study region, that CDOM experiences important transformations in the surface brackish waters as a result of photodegradation rather than during water mass mixing. Changes in CDOM and FDOM spectral signature consistently suggested decrease in molecular weight and aromaticity (increase in $S_{275-295}$, decrease in SUVA and a^*_{300}, decrease in C_1, C_3 and C_3:C_1) during exposure in later summer. We have demonstrated that the changes in surface circulation and water mass mixing during summer months, although not

obvious in the bulk DOC distribution can be traced by CDOM absorbance. Furthermore, we suggest that CDOM dynamics are affected by the seasonal changes in the particle regime, and that DOM with lower $S_{275\text{-}295}$ and visible-humic like fluorescence is introduced from particle and sedimentary sources. Bacterial transformation of DOM was traceable in the N. Aegean waters by contributing to the humic-like components and diminishing the amino acid-like ones. The latter was particularly evident during autumn and provides evidence that although DOM accumulates under low inorganic nutrient conditions, dissolved organic nitrogenous compounds can be used as bacterial substrate. From the results presented in this work, it appears that photodegradation, particle and sedimentary processes as well as biological transformations modify the composition and reactivity of DOM, but only photodegradation acts as a driver for the removal of terrestrial DOM from the surface waters of the N. Aegean Sea.

CHAPTER 7

CHROMOPHORIC DISSOLVED ORGANIC MATTER NATURE AND DYNAMICS FROM PELAGIC TO BATHYPELAGIC WATERS: AEGEAN SEA, SOUTH IONIAN AND NORTHWESTERN LEVANTINE BASIN.

7.1 Introduction

7.1.1 Geomorphology and Water Masses

The Eastern Mediterranean Sea is comprised by the Adriatic, Ionian, Aegean and Levantine Seas. Our sampling stations cover Aegean, South Ionian and North-western Levantine Seas (figure 7.1). The South Aegean Sea, Cretan Sea, communicates with the Levantine and the Ionian Seas through the eastern and western Cretan Straits, namely the Cretan Arc. The eastern Cretan Straits are comprised by the Cassos Strait, the Karpathos Strait and the Rhodes Straits while the western Cretan straits consist of the Elafonisos, the Antikithira Straits, and the Kithira Straits. The Cretan Sea has been characterized as an ultra-oligotrophic basin with low nutrients and high oxygen content due to the regulated water exchanges through the straits of the Cretan Arc and the intense convective mixing of the water columumn [258]. The water masses that are encountered in the Cretan Arc are: a) The Modified Atlantic Water (MAW) that enters the Cretan Sea as a surface water body through the western straits and is traceable by its sub-surface salinity minimum of 38.5-38.9 up to 100m depth. b) Traces of low salinity waters (<38.9) originating from the Black Sea (BSW) can be found at the surface layer especially at the north-western extremity of the Cretan Sea. c) The Levantine Surface Water (LSW) of high salinity, ~39.5 [259] entering from the eastern Cretan Straits. d) The Levantine Intermediate Water (LIW) that forms in the Levantine basin during winter [260] and expands up to 300m throughout the study area with salinity ~38.9-39.1 [261]. e) In the Cretan Sea intermediate masses are formed, namely the Cretan Intermediate Water (CIW) characterized by slightly lower temperature, higher salinity and density

compared to the LIW and expanding up to ~700m [259][261]. These waters eventually exit the Cretan Sea through

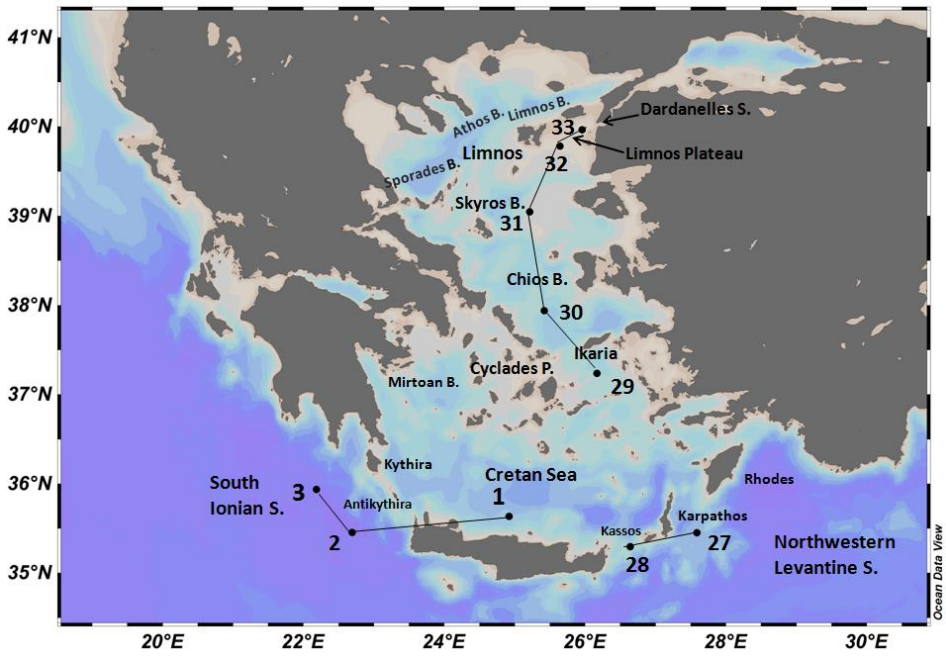

Figure 7.1: Study area.

the Cretan Straits and settle at various depths in the Levantine and Ionian basins according to their density. f) Dense intermediate masses that exit the Cretan Straits with densities between 29.1 and 29.2 kg/m^3, greater than those of the LIW but lower than those of the Eastern Mediterranean Deep waters (EMDW), comprise a discrete water mass named dense-CIW (dCIW) [259]. g) The Cretan Dense Water (CDW) formed also in the Cretan Sea and residing at depths >700m with salinity <38.95 and σ_θ up to 29.2 kg/m^3 [259][261]. h) In the South Ionian and Levantine Basins a largely homogenous water mass with salinity ~ 38.7, is encountered below the LIW layer and up to 1600m, namely Transitional Mediterranean Water (TMW), while it is occasionally detected in the Cretan Sea [262][263]. This water mass is considered to be the oldest water mass in the Eastern Mediterranean formed by the mixing of intermediate (LIW) and deep water masses (EMDW). Due to its old character the TMW is depleted in oxygen but enriched in inorganic nutrients compared to the surrounding water masses [264]. i) The Eastern Mediterranean Deep Water mass (EMDW) presenting very constant characteristics, T~13.3˚C, S~38.65 and σ_θ~29.2kg/m^3 [265], occupy the deepest layer of the Ionian and the Levantine Seas (>2000 m) but is not

traceable in the Cretan Sea. This mass is produced in the Ionian Sea by the mixing of the transformed LIW with the deep, cold and dense Adriatic water [265].

The Central Aegean consists of the northern shelf of the Cyclades islands and the Skyros, Chios and Ikaria Basins with maximum depth of 1100m while in the North Aegean four deep basins isolated from each other exist: the Athos, the Limnos, the North Sporades and Saros basins with maximum depths up to 1500m. Four main water masses prevail in the Central and North Aegean: a) High salinity ≤39.5 Levantine Surface Waters (LSW) that flow from the south Aegean along the eastern coasts. b) Low salinity waters (S~29) of Black Sea origin (BSW) outflow in the North Aegean through the Dardanelles Straits and form a distinct surface brackish water layer (0-30m) which follows a south south-western route. c) Levantine Intermediate Water (LIW) of increased salinities (38.9-39.1) which occupies a layer from ~30m to 400m depth. Due to the higher density of the LIW a thermohaline front is created where LIW are subducted under BSW layer and flow towards the North Aegean and up to the Samothraki Plateau [261] (see chapter 6). d) The deep isolated basins of the North Aegean Sea (Athos, Limnos, Skyros, Chios) with depths >400m are filled with dense North Aegean waters (NAgDW), presenting slightly different characteristics in each basin and of overall higher density (~29.40) than the deep waters of the Cretan Sea (~29.20) [266].

7.1.2 Dense Water Formation in Aegean Sea

Dense water formation (DWF) in the North and Central Aegean is mostly observed during winter (November - February). In the deep basins of the North Aegean Sea, DWF is a rare feature because it requires both limited BSW outflow and extreme cold winters [266]. On the other hand, dense waters formed at intermediate depths (up to 400m) are more frequent in the Central Aegean (Skyros and Chios basins) during winter [267]. The intrusion of the more saline LIW in Central-North Aegean is a major factor triggering DWF in the south areas [267]. Thus DWF occurs mostly in the Central Aegean (Skyros and Chios basins) while in the northern part (Athos - Limnos basin) the formation is inhibited due to the greater influence of the brackish

BSW and the limited influence of the LIW. The buoyancy loss in Central Aegean is enhanced by the trapping of water in the permanent and semi-permanent cyclonic features over the Chios and Skyros deep basins [251][268]. In Chios basin, the dense water masses formed were observed to be spreading isopycnally at 400m while an outflowing of these waters in the South Aegean through the Myconos-Ikaria strait was also reported [268].

Inside the Cretan Sea under strong winter conditions convective processes occur resulting to the formation of CIW and CDW that occupy the intermediate and deep layers below LIW [260][[262]. More recently it was suggested [266] that CDW originate from the Cyclades Plateau, and shelf areas of Asia minor and the Greek penninsula with a possible contribution from north Aegean deep waters during periods of episodic massive dense water formation in the north Aegean (e.g. during 1987 and 1992-1993).

7.1.3 The role of the Cretan Sea in providing dense waters to the Eastern Mediterranean Sea.

The main source of dense deep waters in the Eastern Mediterranean up to 1987 it was believed to be the Adriatic Sea [263]. During 1987-1995 though, an extreme rise of the density of the deep waters (>1000m) in the Cretan Sea reaching ~29.4, resulted in the outflow of denser, more saline CDW from the Cretan Straits that reached the bottom of eastern Mediterranean sections uplifting the existing EMDW to lower depth layers; an event called the Eastern Mediterranean Transient, EMT, [269]. The increase of the densities of CDW causing the EMT was attributed to the extreme winter of 1987 leading to convective episodes and dense water formation inside the Cretan Sea [269] while Zervakis et al., [266] suggested that the EMT was initiated by the dense water formation in the north Aegean during the winters of 1986/1987 and 1992/1993 and the southward flow of these dense waters towards the Cretan Sea. The newly formed EMDW, being warmer and more saline, is considered of Aegean origin rather than Adriatic origin. During the EMT, a ‘nutrient rich-oxygen poor’ water mass (namely Transitional Mediterranean Water - TMW) [264] has entered the Cretan Sea from the adjacent Levantine Basin from depths 700-1600m [262][263] in order to compensate the CDW outflow and

settled between the LIW and the CDW giving a signal of a local salinity minimum [268][270]. This signal though has been diminished in the next years as the CDW outflow relaxed causing the limitation of the TMW inflow in the Cretan Sea. In addition, the previously intruded TMW was no longer traceable in the Cretan Sea due to the mixing with the LIW and CDW and the ventilation that reached below the TMW horizon [266][270]. Very recently, Velaoras et al., [259] argued that the export of CDW that either reach the bottom (EMT-event) or of lower density dCIW that settle at lower depths (the so called EMT-like event) is a recurrent phenomenon that appears at a quasi regular, almost decadal time intervals. The last EMT-like event was observed in the 2000s decade as during 2007-2009 dCIW exited the Cretan Sea through both the western and eastern straits and settled at depths below LIW horizons and up to about 1000 m [259][271]. The EMT events were firstly attributed to atmospheric forcing [272] while more recent studies argued that internal mechanisms is the dominant factor in creating favourable dense water formation conditions through salinity preconditioning [259][273]. Furthermore, Krokos et al. [273] suggested an alternating activation of the two dense water sources, the Adriatic and the Aegean Sea, in a decadal time interval that results from the oscillation in the thermohaline properties of the upper and intermediate water masses in both the Ionian and the Levantine/Aegean Seas. They reported dense water (dCIW) export from the Aegean Sea to the Levantine during 2007-2011 and a gradual decrease of salinity in the Levantine basin from 2010 onwards with a simultaneous increase of the salinity in the Ionian Sea. The time of our sampling, May-July 2013, is long after the dCIW export period and according to Krokos et al., [273] we expect to be at the phase of the salinity relaxation in the Aegean Sea and the increase in the Adriatic Sea.

7.1.4 Water Circulation

The circulation in the Eastern Mediterranean is regulated by various cyclonic and anticyclonic gyres (figure 7.2).

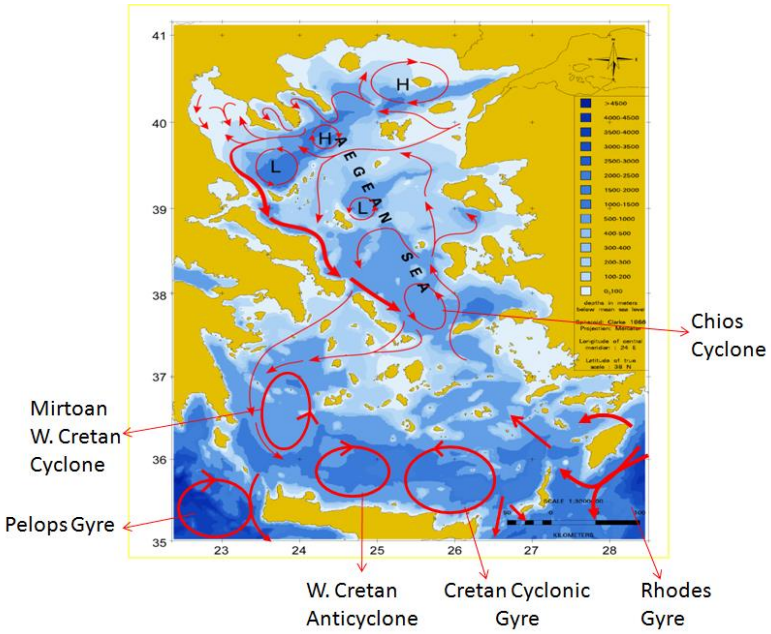

Figure 7.2: Water circulation in the studied area (adapted from Theocharis et al., 1999; Olson et al., 2007).

In the northwest Levantine Sea the most predominant feature is the sub-basin multicentered cyclonic Rhodes gyre [261] that causes the upwelling of deeper waters while under favourable conditions the vertical mixing of the water column can reach as deep as 900m [274]. In the eastern Ionian Sea a strong anticyclone, Pelops gyre dominates the region to the south and southeast of Peloponissos presenting spatial variations, while it can be detected up to 2000m causing the transportation of LIW to deeper layers. In the western Cretan Sea a cyclone, Cretan gyre [261][271] is located to the northwestern part of the Cretan Passage affecting the water mass exchange between the Cretan and the Ionian Seas. In the Central Cretan Sea on the other hand, the presence of an anticyclonic eddy [262] traps and stirs down to greater depths the warm and saline Levantine waters. In Central Aegean two cyclonic features prevail the water circulation over the Chios and Skyros deep basins.

7.1.5 Purpose of the study

The Eastern Mediterranean Sea has gained a lot of attention within the scientific community mostly due to the very oligotrophic character of this region and the dense water formation taking place in both the Adriatic and Cretan Sea resulting to the export of dense waters to the Ionian and Levantine Basins. Despite the many studies that were conducted in the past

decades investigating the formation and circulation within the Cretan Arc [259][261][262][273], the nutrients status and particulate organic matter of the Cretan Sea and the adjacent basins as well as the optical properties of the particulate organic matter [275][276], in our knowledge no studies have been conducted regarding the dynamics of dissolved organic matter and in particular of its chromophoric sub-pool. The North and Central Aegean were also been extensively studied mostly in regards of the BSW outflow and the established circulation [250][251] as well as for the impact on the productivity of these parts of the Aegean Sea [244][246][264]. Only one study is available regarding the fluorescence properties of the North Aegean seawater [220] while no data exist for the optical properties of DOM in the Central Aegean Sea.

In this study we aim a) to investigate for the first time CDOM and FDOM dynamics in the aforementioned geographical regions and b) to track the transformation processes (sources and sinks) that CDOM undergoes in the formed water masses.

7.2 Materials and Methods

7.2.1 Samplings

Samplings were conducted onboard NIOZ RV Pelagia during two cruises (figure 7.1). The first cruise took place during 02-13/06/2016 and 7 stations were sampled: sts 27, 28, 29, 30, 31, 32, 33. The second cruise was conducted during 27-28/07/2013 and stations 1, 2, 3, were sampled. All stations were sampled from ~10m up to the bottom using Niskin PVDF plastic bottles (UltraCelan Ctd,UCC) deployed by a CTD rosette (Seabird electronics). Samples for DOC and CDOM analysis were directly filtered from the UCC sample bottles under nitrogen pressure using 0.2μm Sartobran 300 catridges (Sartorius) in an ultraclean container and collected in precombusted (480°C, 12h) amber glass bottles and stored in the dark at ~-20°C.

Stations 27, 28, 1, 2 and 3 are located in the Cretan Sea and the adjacent Basins. Station 27 with bottom depth of 1150m is located east of Karpathos island in the northwestern extremity of the Levantine Basin and falls in the periphery of the permanent Rhodes cyclonic gyre. Station 28 with bottom

depth of 1084m is located at the Kassos Strait (between Crete and Kassos islands) and it is expected to be mainly influenced by the LSW/LIW that carries saline Levantine Water into the South Aegean while at a lesser extend it may also receive fresh water by the MAW current [261]. Station 1 is located at the south of the Cretan Sea with bottom depth of 936m which is the average depth of the Cretan Sea. Station 1 is expected to be influence by the Cretan anticyclone. Stations 2 and 3 are situated In the Ionian Trench reaching depths of 4088m and 3911m respectively. Stations 2 and 3 are in the area affected by the Pelops anticyclone located southwest of Peloponnisos while station 2 is expected to be more influenced by the MAW current than the rest stations.

In the Central and North Aegean five stations were sampled, sts 29, 30, 31, 32, 33. The southernmost station, station 29 is located south of the Ikaria Island and east of the Cyclades Plateau with bottom depth 535m. Station 30 is located at the southern extremity of the Chios Basin with bottom depth 522m, while the maximum depth inside the Chios Basin is 1100m. Station 31 is situated east of the Skyros Basin with bottom depth 294m. The northernmost sampled stations, stations 32 and 33 are located at the Limnos plateau presenting bottom depths of 77m and 66m respectively. Surface waters of stations 29 to 31, central and east region of the Central Aegean, are expected to be dominated by the LSW rather than the BSW. At the area of stations 32 and 33, northeastern Aegean, the influence by the outflowing BSW is dependent mostly from the winds that prevail each season. BSW exiting the Dardanelles flow mainly towards the north of Limnos Island and may not affect the sampled stations. In the presence though of strong northerly winds (Etesians), BSW is directed to the south of Limnos Island and is more possible to influence the sampled stations.

7.2.2 Methodology

Dissolved organic carbon, absorption and fluorescence were analyzed as described in Chapter 4, while the results from the fluorescence were included in the PARAFAC modeling and the identified components are described in Chapter 4. The qualitative indices of absorption, carbon specific absorption

coefficient a^*_{300} and spectral slope $S_{275-295}$ were estimated as described in Chapter 4. All the relationships reported hereafter are statistically significant ($P<0.05$).

7.3 Results

7.3.1 Hydrography and Water Column Structure

Based on the salinity, temperature, density and dissolved oxygen values recorded during the samplings, most of the water masses discussed at section 9.1.1 were discernible. The physicochemical data for each water mass are given in Table 7.1 for the Cretan Sea and adjacent basins and in Table 7.2 for the Central and North Aegean.

In the Cretan Arc (stns 1, 28), Levantine Basin (st. 27) and Ionian Trench (stns 2, 3), salinity (figure 9.2) and temperature showed a decreasing vertical trend (Table 7.1). At the shallower sampled depths (~10-30m), stations 27 and 28 presented lower temperature values than the Cretan Sea (st. 1) and the Ionian Trench (sts 2,3) which is probably due to the samplings taking place in the early summer and middle summer respectively. In the pelagic waters (10-100m) of stations 27 and 28, salinity fluctuated between 39.1 and 39.2 and temperature between 17.1 and 21.6 ˚C. At stations 1, 2 and 3 the salinity in the pelagic waters ranged between 39.0 and 39.2 and temperature between 16.0 and 25.9 ˚C.

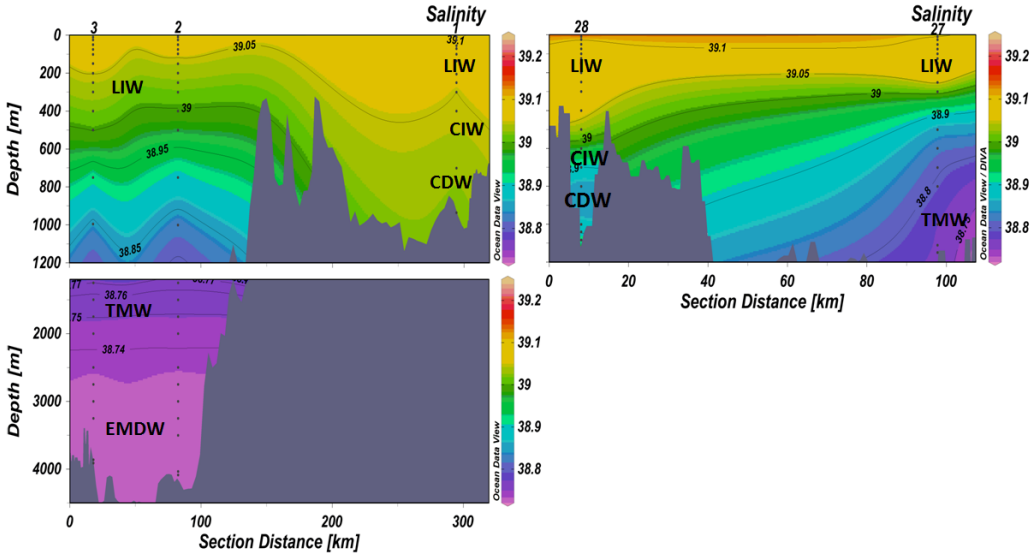

Figure 7.3: Salinity distribution in Cretan Sea and adjacent basins. The upper panel shows results up to 1200m while the lower panel shows results from 1200m - 4500m.

Table 7.1: Physicochemical and optical results in Cretan Sea and adjacent basins.

	Pelagic (10-100 m)	***LIW***	***CIW***	***TMW***	***CDW***	***EMDW***
Salinity	39.1 39.0-39.2	39.1 39.0-39.1	39.0 38.8-39.1	38.8 38.7-39.0	38.9 38.9-39.0	38.7
Temp. (˚C)	19.9 16.3-25.9	16.0 15.0-17.6	14.6 13.9-15.2	14.0 13.6-14.9	14.2 14.0-14.5	14.0 13.9-14.1
AOU (ml/L)	-14 -33 – 8	12 -17 – 42	25 5-44	60 44-71	38 32-47	63 62-63
DOC (μmol/L)	68 55-82	56 48-67	52 45-55	39 33-47	44 42-48	39 36-43
a_{300} (m^{-1})	0.38 0.27-0.53	0.32 0.23-0.46	0.31 0.24-0.34	0.23 0.18-0.32	0.28 0.25-0.32	0.21 0.18-0.23
a^*_{300} (m^2g^{-1})	0.48 0.30-0.74	0.47 0.36-0.62	0.49 0.44-0.52	0.48 0.39-0.67	0.53 0.49-0.64	0.45 0.40-0.53
$S_{275-295}$ (nm^{-1})	0.0407 0.0347-0.0488	0.0399 0.0345-0.0424	0.0373 0.0324-0.0390	0.0365 0.0277-0.0404	0.0359 0.0340-0.0369	0.0368 0.0352-0.0395
I_1 **(R.U.)**	0.0114 0.0066-0.0173	0.0152 0.0136-0.0171	0.0176 0.0163-0.0183	0.0159 0.0134-0.0181	0.0183 0.0180-0.0186	0.0171 0.0161-0.0185
I_2 **(R.U.)**	0.0082 0.0038-0.0117	0.0110 0.0099-0.0130	0.0136 0.0122-0.0143	0.0112 0.0094-0.0125	0.0140 0.0139-0.0141	0.0121 0.0115-0.0130
I_3 **(R.U.)**	0.0050 0.0025-0.0077	0.0069 0.0061-0.0085	0.0087 0.0085-0.0089	0.0089 0.0079-0.0096	0.0100 0.0098-0.0104	0.0097 0.0091-0.0104
I_4 **(R.U.)**	0.0130 0.0084-0.0254	0.0129 0.0066-0.0176	0.0092 0.0076-0.0109	0.0059 0.0032-0.0186	0.0068 0.0065-0.0073	0.0052 0.0036-0.0101

The high salinity values recorded at the surface of all the sampled stations indicate that the MAW current carrying low salinity waters (<39.0) was not traceable as a distinct water mass at the time of our sampling. LIW was found underlying the surface layer of all stations at intermediate depths up to 400m

(figure 7.3). The Cretan Sea (st1) and the adjacent eastern region (sts 27, 28) presented uniform salinity values in the LIW layer with an average value of 39.1 in all stations. Temperature at the same stations showed also similar values ranging between 15.0 and 17.6 ˚C. As observed for the surface layer, stations 2 and 3 exhibited slightly lower salinity values than stations 1, 27 and 28 with a mean value of 39.0. In the Cretan Sea (st.1) and the eastern straits (st.28) below the LIW, the CIW mass was detected forming a distinct layer of slightly colder and denser (σ_θ= 29.06-29.18) waters than the LIW (σ_θ= 28.51-29.04); expanding up to 800m. The salinity values in this layer fluctuated between 38.8 and 39.1 and the temperature between 13.9 – 15.2˚C. The bottom layers of station 1 (1200m) and 28 are occupied by the even denser CDW (σ_θ= 29.19-29.21) with salinity values between 38.9 and 39.0 (figure 7.2) and temperature between 14˚C and 14.5˚C. The lowest AOU values (5.5-46.7 ml/L in CIW and CDW) were recorded in the Cretan Sea (st. 1) and the eastern Straits (st. 28) indicating higher vertical mixing (figure 7.4). Winter convective mixing driven by favourable weather and hydrographic conditions occurs frequently in the Cretan Sea, leading to the ventilation of the intermediate and deep layers [258].

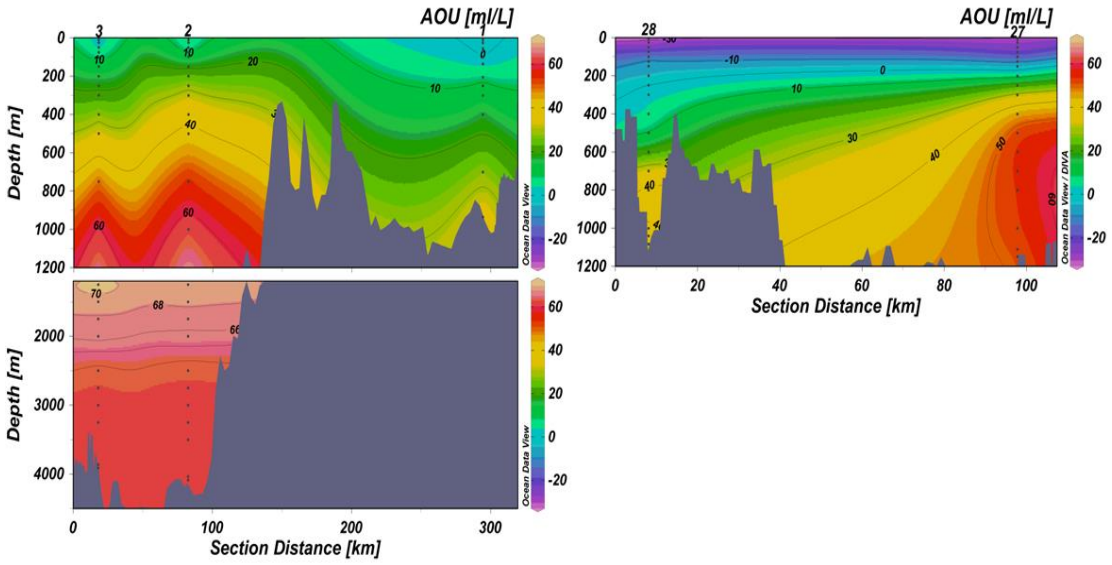

Figure 7.4: AOU distribution in the Cretan Sea and adjacent basins.

At station 27, located in the northwestern Levantine Basin the intermediate and deep layers, below LIW and up to the bottom (400-1150 m) are occupied by the TMW (σ_θ=29.15-29.18), characterised by increased AOU values (46.8-54.9 ml/L), salinity (38.8 – 38.9, mean 38.9) and temperature values (13.6 –

14.3˚C) than both the CIW and CDW. The TMW mass was also tracked in the Ionian Trench (sts 2, 3) residing below the LIW and up to 2000m depth (σ_θ=29.11-29.19). At these stations TMW reached maximum AOU values (43.7-71.4 ml/L). The salinity and temperature were uniform at the two stations of the Ionian Trench with a range of 38.7 – 39.0 for salinity and 13.8 – 14.9˚C for temperature.

The EMDW mass was identified only at the deepest layers (> 2400m) of stations 2 and 3 in the Ionian Trench. EMDW presented uniform physical characteristics. The overall lowest salinity (constant at 38.7) and temperature (13.9-14.1˚C) were recorded while the density of this mass was constant at 29.19, equal to the highest density found in the overlying TMW but lower than the density in the CDW (σ_θ=29.19-29.21). AOU also presented uniform values (62.2-63.8 ml/L).

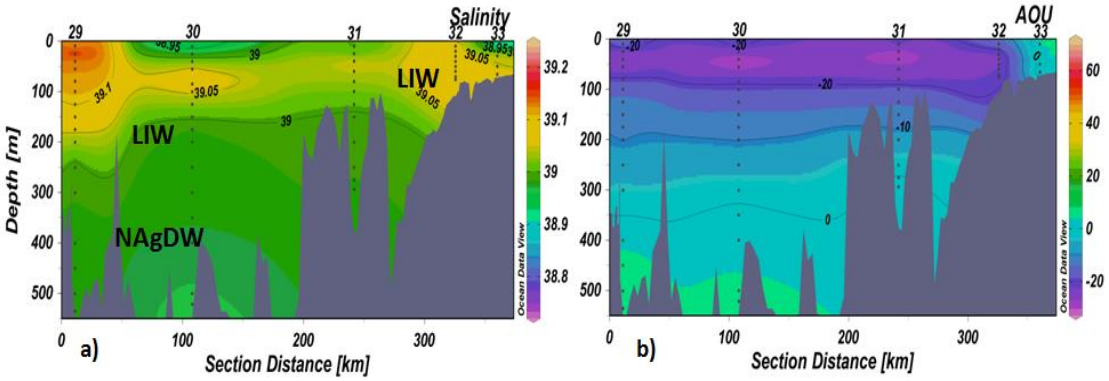

.Figure 7.5: Distribution of a) Salinity, b) AOU in the Central and North Aegean Sea.

In the pelagic waters of the Central and North Aegean (sts 29-33) temperature fluctuated between 17.2 and 20.8˚C with no significant variation between the stations. High salinity values ranging between 38.8 and 39.2 (figure 7.5a), were recorded throughout the surface of the sampled transect indicating that the BSW current was not tracked at our sampled region, not even at the northernmost station 33 located close to the Dardanelles Straits. At the time of our sampling, early summer, the Etesians winds may have not been intensified yet, thus the BSW outflowing the Dardanelles follows a northward route, north of station 33. Nevertheless, the lowest salinity values were recorded at the northernmost station 33, while the highest at station 29.

Table 7.2: Physicochemical and optical results in Central and North Aegean Sea.

	Pelagic (10-100m)	***LIW***	***NAgDW***
Salinity	39.0 38.8-39.2	39.0 39.0-39.1	39.0
Temp. (˚C)	19.4 17.2-20.8	15.9 14.2-17.9	14.2 14.1-14.5
AOU (ml/L)	-17 -32 – 16	-14 -31 – 16	5 3-8
DOC (μmol/L)	66 62-68	60 53-67	51 49-53
a_{300} (m^{-1})	0.36 0.29-0.45	0.38 0.30-0.53	0.38 0.33-0.49
a^*_{300} (m^2g^{-1})	0.46 0.35-0.57	0.53 0.40-0.69	0.56 0.48-0.73
$S_{275-295}$ (nm^{-1})	0.0420 0.0369-0.0459	0.0388 0.0354-0.0427	0.0361 0.0300-0.0371
I_1 (R.U.)	0.0108 0.0090-0.0133	0.0154 0.0138-0.0172	0.0195 0.0167-0.0207
I_2 (R.U.)	0.0073 0.0057-0.0098	0.0108 0.0093-0.0128	0.0146 0.0129-0.0155
I_3 (R.U.)	0.0047 0.0041-0.0057	0.0070 0.0063-0.0084	0.0095 0.0084-0.0103
I_4 (R.U.)	0.0125 0.0096-0.0154	0.0145 0.0105-0.0228	0.0149 0.0084-0.0248

The LIW layer presented less variable salinities throughout the sampled transect, ranging between 39.0 and 39.1. At the deeper and southernmost stations, 30 and 29, the water mass residing at depths >350m for 30 and >400m for 29 presented higher densities than the overlying LIW marking the presence of North Aegean Deep Waters (NAgDW). The NAgDW revealed uniform temperature values fluctuating between 14.1 and 14.5˚C and constant salinity values (39.0). In the NAgDW the highest densities (σ_θ= 29.15-29.24) were recorded during our sampling, clearly showing the potential of these waters to overflow towards the Cretan Sea. In addition this water mass presented very low AOU values (2.7-7.7 ml/L, figure 7.5b) indicating a much

younger age of these waters relatively to the dense water masses of the Cretan Sea.

7.3.2 DOC, CDOM absorption and chlorophyll-a

The Ionian Trench (sts 2,3) and eastern Cretan straits (st.28) presented uniform vertical chl-a distributions as clear deep chlorophyll maximum (DCM) was encountered at 100m (figure 7.6). Station 2 presented the highest peak (0.2171 a.u.) while station 28 presented the lowest (0.1674 a.u.). In the Cretan Sea (st1) the chl-a increased from the surface and down to 135m where a peak was encountered (0.1144 a.u.), deeper than the peaks at the straits.

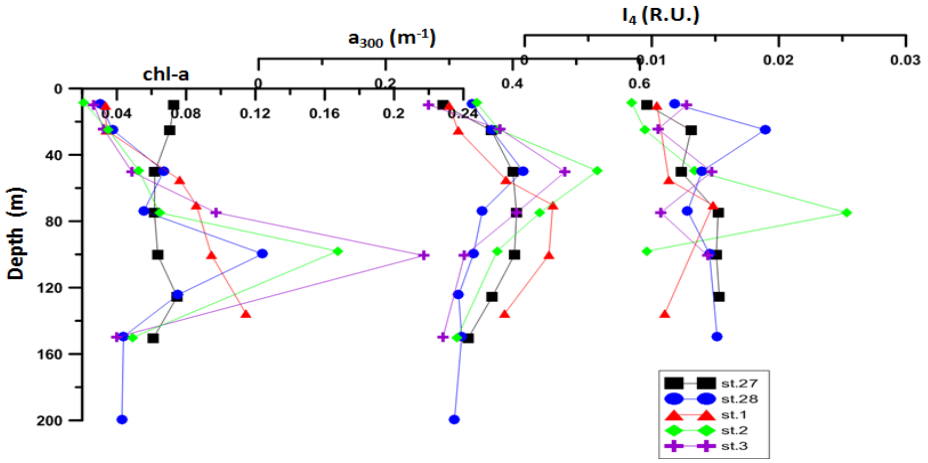

Figure 7.6: Vertical distributions of chl-a, a_{300} and I_4 in Cretan Sea and adjacent basins.

Station 27 on the other hand presented uniform chl-a concentrations from the surface and up to 200m. The values though at the first 25m were considerably higher (0.0706-0.0729) than the other stations (0.0208-0.0325).

DOC concentrations fluctuated between 33 and 82 μmol/L (figure 7.7). Higher values (55-82 μmol/L) were recorded at the surface decreasing with depth as expected for this parameter. At the surface of station 27, located in the northwestern Levantine Basin, maximum DOC values (74-82 μmol/L) were recorded, while the lowest (55-71 μmol/L) were found at the southernmost station of the south Ionian Sea (st2). The Cretan Sea and eastern straits (sts 1 and 28) appeared to hold the highest DOC concentrations below the surface (>100m) and up to the bottom. The lowest DOC values were recorded at the TMW (33-47 μmol/L) and EMDW (36-43 μmol/L) water masses.

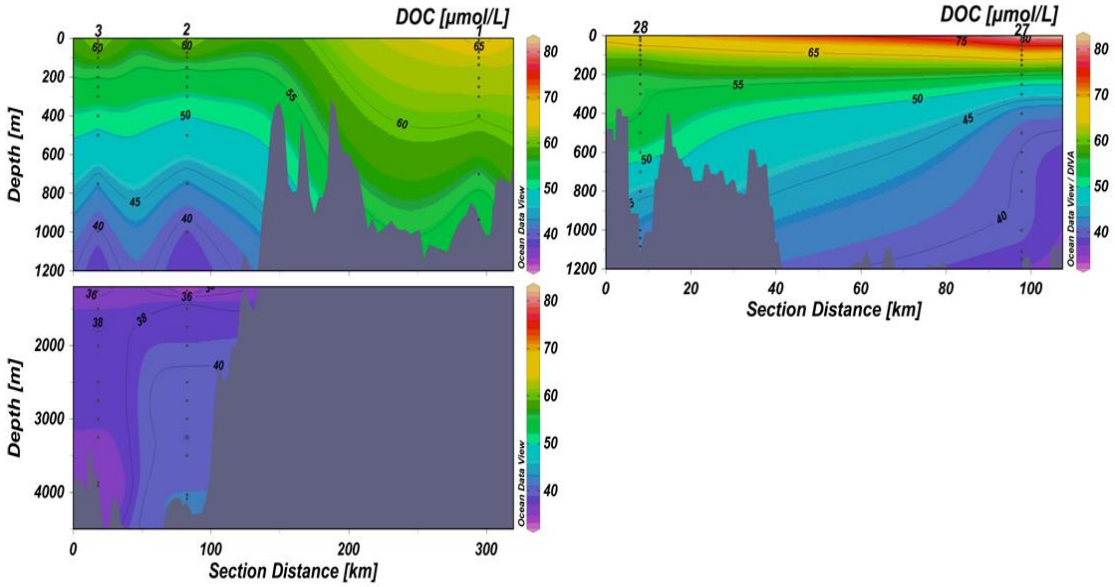

Figure 7.7: DOC distribution in Cretan Sea and adjacent basins.

The low range in the DOC values of the TMW and EMDW is expected as it has been shown that in old water masses, such as TMW, or at great depths exceeding 1000m, such as EMDW, only the more resistant to microbial degradation organic substances are encountered (refractory and semi-refractory DOC) [15].

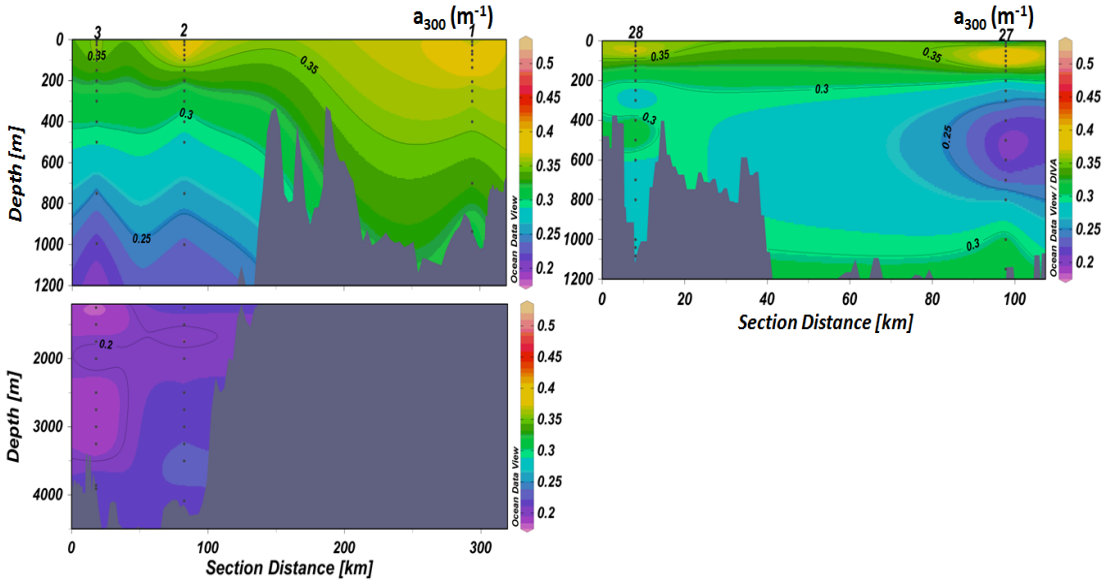

Figure 7.8: Absorption coefficient a_{300} distribution in Cretan Sea and adjacent basins.

The absorption coefficient at 300nm, a_{300}, ranged from 0.18 to 0.53 m^{-1} (figure 7.8). In contrast to DOC distribution, a_{300} coefficients presented very clear subsurface maxima at ~40 – 80 m depth and shallower than the DCM (figure 7.6). Within the first 30m very low absorption coefficients were recorded (0.27-

0.38 m^{-1}). The highest a_{300} values in pelagic waters (<100m) were observed at station 2 (0.34-0.53 m^{-1}) located in the Ionian Trench. The Cretan Sea (st1) and the eastern straits (st 28) preserved elevated a_{300} values in the underlying layers and up to the bottom, while the lowest a_{300} values were recorded in the TMW and EMDW water masses (0.18-0.23 m^{-1}). As an exception to this distribution, in the deepest layers of station 27 (1000 – 1200 m), elevated absorption coefficients were recorded.

Specific absorption coefficient a^*_{300} (0.30-0.74 m^2g^{-1}), followed the a_{300} distribution and overall exhibited low values at the surface layer (<30m) and subsurface maxima (figure 7.9).

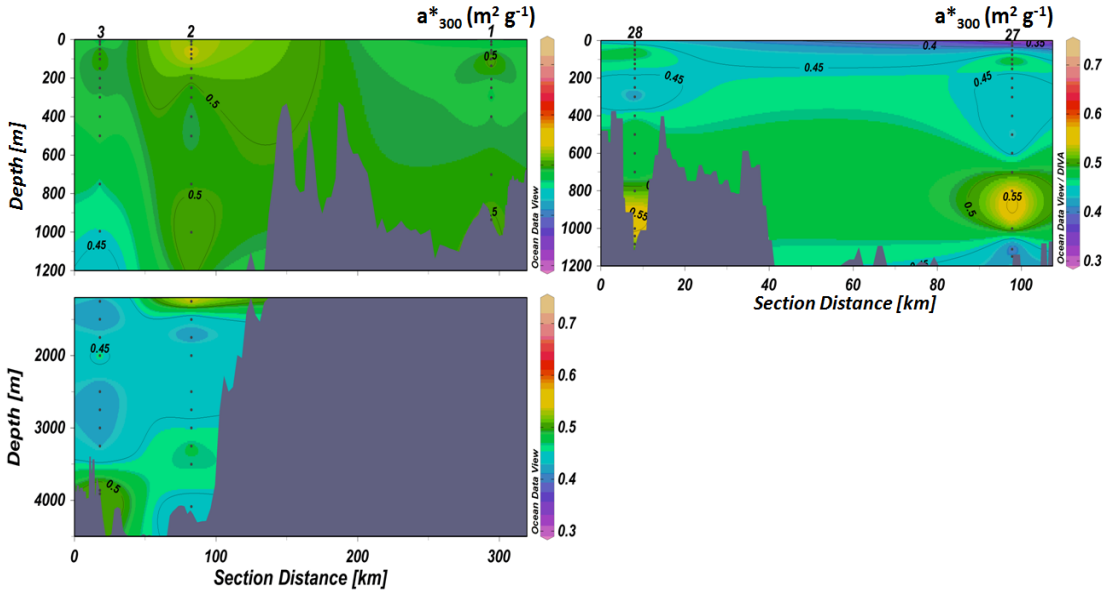

Figure 7.9: Specific absorption coefficient distribution in Cretan Sea and adjacent basins.

The highest a^*_{300} values in pelagic waters were found at stations 2 and 3 (0.32-0.74 m^2g^{-1}) situated in the Ionian Trench, in agreement with the recorded highest absorption coefficients. In the LIW layer, a^*_{300} was clearly higher in the Cretan and Ionian Sea rather than the eastern straits and Levantine Basin. The highest overall values were observed at the deepest layers (TMW) of station 27 (0.60-0.67 m^2g^{-1}) followed by the CDW in the eastern straits (0.51-0.64 m^2g^{-1}) (st 28). Station 2 preserved high values up to 1300m while at station 3 the a^*_{300} values were reduced below 700m depth (figure 7.9 upper panel). EMDW revealed in general low values, but with a more patchy distribution (figure 7.9 lower panel). Absorption spectral slope

$S_{275-295}$ ranged between 0.028 and 0.049 nm^{-1} (figure 7.10). Overall $S_{275-295}$ was found increased at the surface (10-30m) of all stations (0.035-0.049 nm^{-1}), where also the minimum of the a_{300} values were recorded. Below the surface layer, slope gradually decreased and reached minima at the deepest waters (1000m-1200m) of station 27 (0.028-0.029 nm^{-1}), concurrent with the highest carbon specific coefficients a^*_{300}. Low spectral slopes (0.033-0.037 nm^{-1}) were also recorded at CDW in the eastern straits (stn 28). In the Ionian Trench station 3 presented elevated spectral slopes $S_{275-295}$ throughout the water column.

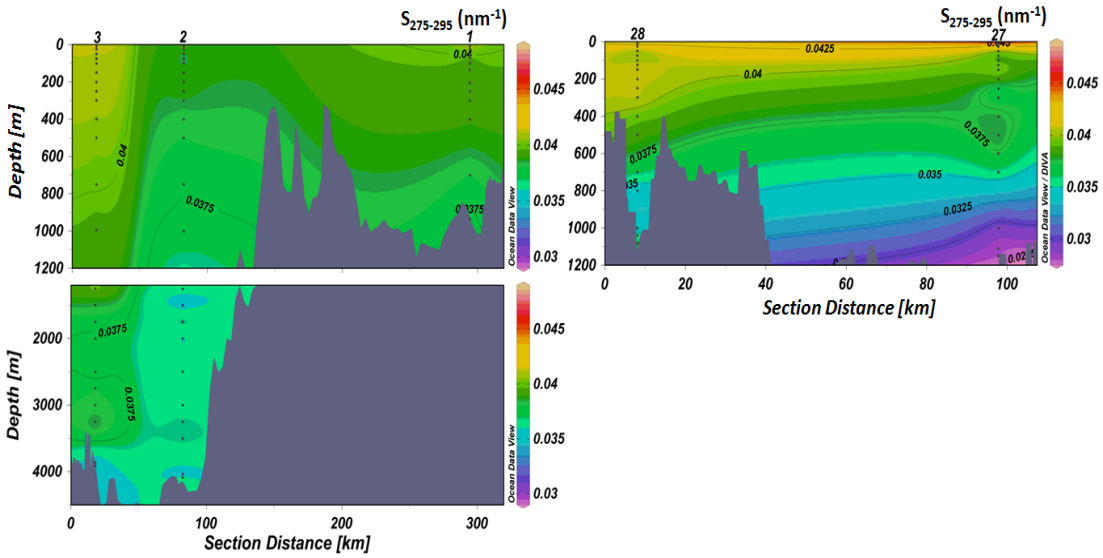

Figure 7.10: Absorption spectral slope distribution in Cretan Sea and adjacent basins.

In the Central and North Aegean, the highest peaks in chl-a values were observed at the southernmost station 29 and at the shallow station 32, both at 76m depth (figure 7.11).

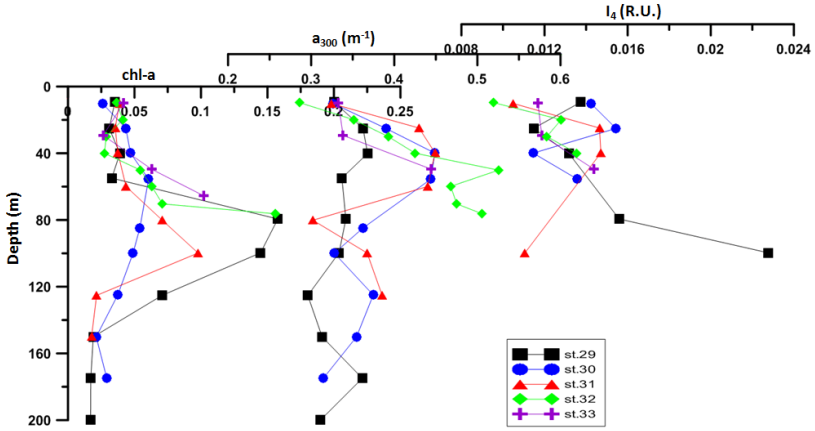

Figure 7.11: Distributions of chl-a, a_{300} and I_4 in Central and North Aegean.

Stations 33 and 31 followed, presenting maximum chl-a values at 65 and 100m respectively. Station 30 presented the lowest chl-a values with a peak at 55m.

DOC presented highest values in pelagic waters, ranging from 62 to 68 μmol/L while no horizontal gradient was observed along the sampled transect (figure 7.12a). Below the surface DOC gradually decreased reaching the lowest values at the NAgDW (49-53 μmol/L).

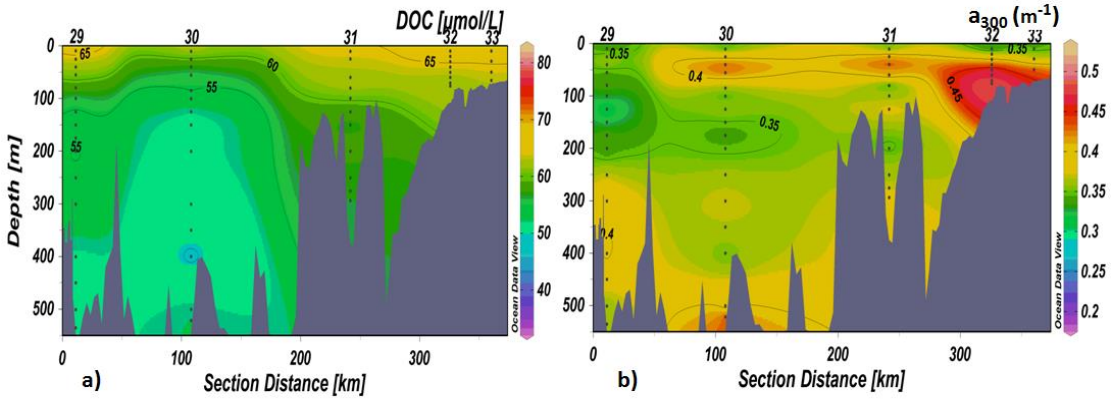

Figure 7.12: Distribution of a) DOC, b) a_{300} in Central and North Aegean.

North Aegean (sts 31-33) preserved higher DOC values at intermediate depths (up to 300m) compared to the southern stations 29 and 30. The observed DOC values in the Central-North Aegean (mean 60±5 μmol/L) were similar to DOC values found at the same depths (up to 550m) of the South Aegean (mean 59±9 μmol). Absorption coefficient a_{300}, showed minima at the surface layer (<30m) with a range of 0.29-0.45 m^{-1}, presenting the lowest values at the northern part (figures 7.11, 7.12b). The subsurface maxima of a_{300} were observed in the LIW layer were coefficients ranged from 0.30 to 0.53 m^{-1} with a decreasing north – south trend. In the NAgDW, a_{300} showed overall comparable values with the overlying LIW fluctuating between 0.33 and 0.49 m^{-1}. Some increases in a_{300} coefficient are traceable in the bottom samples of stations 30 and 31 along the slope. Also station 29 presented somewhat elevated a_{300} coefficients at ~ 450m depth. Overall in the Central and North Aegean Sea slightly elevated a_{300} values (mean 0.38±0.06 m^{-1}) were recorded compared to the same depths (up to 550m) of south Aegean Sea (mean 0.34 ± 0.07m^{-1}).

Following a_{300}, absorption coefficient a^*_{300} (figure 7.13a) presented the lowest values in pelagic waters (0.037-0.046 m^2g^{-1}), increasing in the LIW (0.035-0.043 m^2g^{-1}) and NAgDW (0.30 -0.39 m^2g^{-1}). The higher a^*_{300} values were recorded at the areas where the highest a_{300} were observed, i.e. subsurface waters of st 31, the deepest layers of stations 32, 33 and 30 and the upper limit of NAgDW at station 29. The distribution of spectral slope $S_{275-295}$ (figure 7.13b) is the exact opposite of the distributions of a_{300} and a^*_{300}.

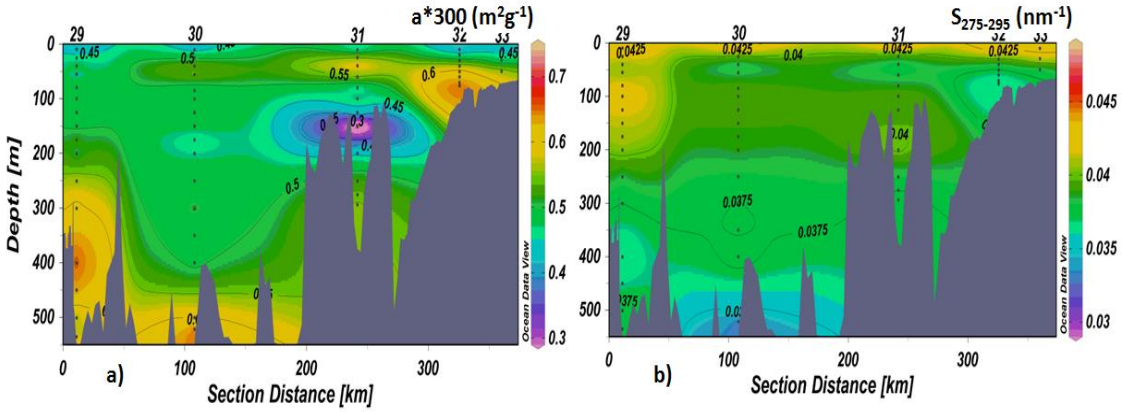

Figure 7.13: Distribution of a) a^*_{300}, b) $S_{275-295}$ in the Central-North Aegean Sea.

7.3.3 Fluorescence characteristics

The vertical distributions of the four identified components are given in figures 7.14 to 7.17. All humic-like components display a vertical distribution of fluorescence intensities (I_{1-3}) with minima in the very surface layer (0-30m) and increasing trend with depth (figures 7.14-7.16). On the other hand, the protein-like component (C_4) (figures 7.11, 7.17), showed maxima in pelagic and meso-pelagic waters with a smooth diminishing gradient with depth. In pelagic waters, C_4 presented higher intensities than all the humic – like components. In the LIW on the other hand, the primary terrestrial humic-like component C_1 showed the highest intensities followed by C_4 while below the LIW all the humic – like components dominated over the protein – like. Among the humic – like components C_1 presented the highest intensities followed by C_2, and C_3. This order was consistent in all deep water masses.

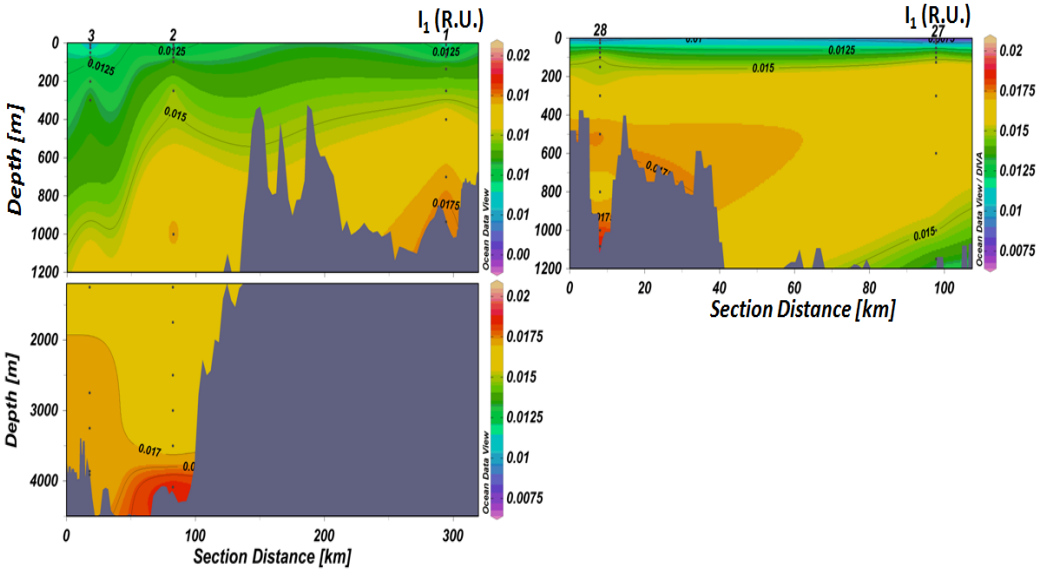

Figure 7.14: Distribution of the modelled fluorescence intensity (I_1 R.U.) of the primary terrestrial humic-like component (C_1) in the Cretan Sea and adjacent basins.

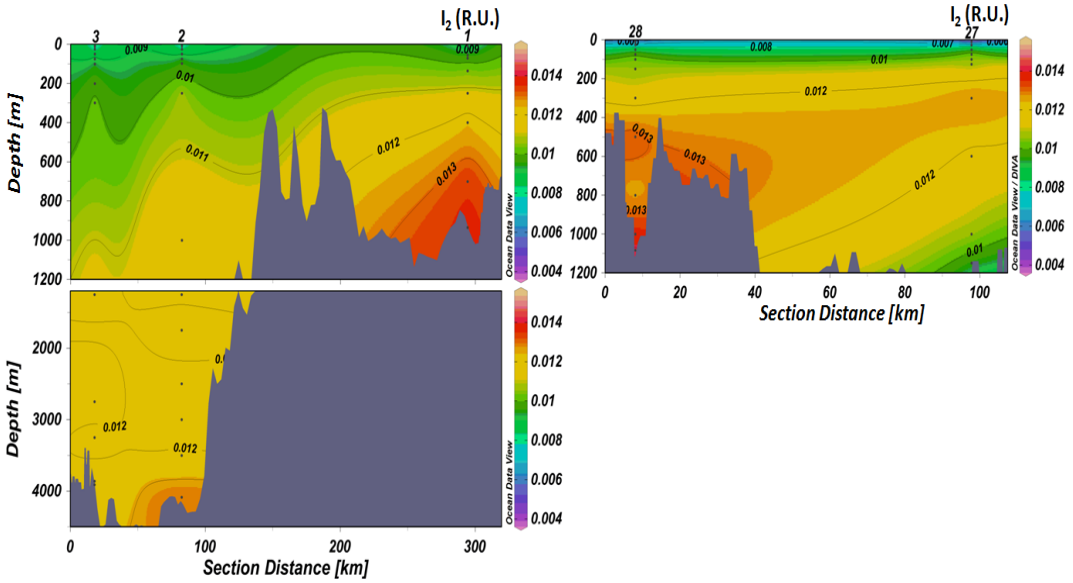

Figure 7.15: Distribution of the modelled fluorescence intensity (I_2 R.U.) of the humic-like component (C_2) in the Cretan Sea and adjacent basins.

In the pelagic waters and the LIW layer, higher intensities of the humic – like components were found at station 2 situated in the Ionian Trench. Below the LIW and up to 1200m, the Cretan Sea (st1) and the eastern straits (st28) (CIW, CDW) appear to hold the highest intensities of the humic like components C_1, C_2. Secondary humic-like component C_3 (figure 7.16) presented overall more uniform geographical distribution among the stations sampled with an increasing trend with depth presenting high uniform intensities in CDW, TMW and EMDW.

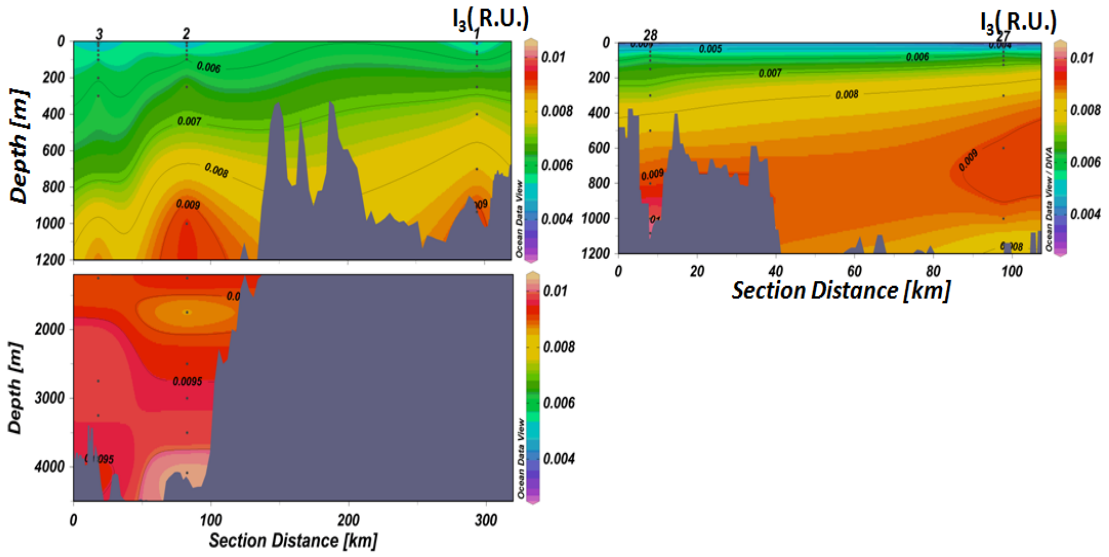

Figure 7.16: Distribution of the modelled fluorescence intensity (I_3 R.U.) of the secondary terrestrial humic-like component (C3) in Cretan Sea and adjacent basins.

In pelagic waters the highest intensities of C_4 were recorded at station 28 and the lowest at station 1 and 3, while in the LIW layer C_4 showed the highest intensities at station 3 and the lowest at station 2 (figure 7.17). Below the LIW the protein – like fluorescence decreased significantly. The CIW and CDW (sts 1and 28) retained though higher C_4 intensities than the adjacent TMW. TMW presented overall the lowest C_4 values, lower than those of the EMDW, especially at station 27.

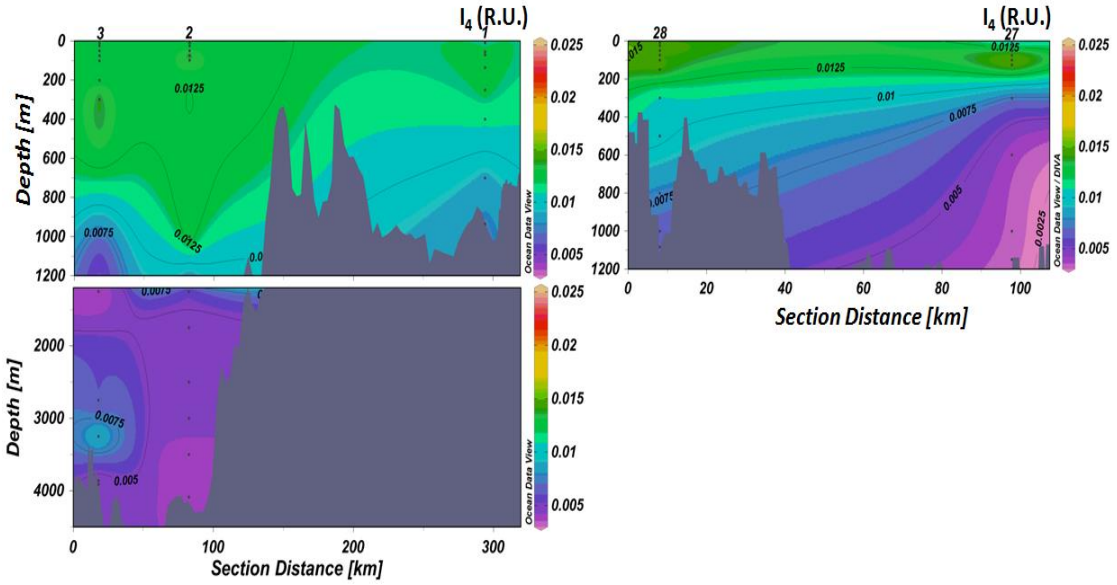

Figure 7.17: Distribution of the fluorescence intensity (I_4 R.U.) of the protein-like component (C4) in the Cretan Sea and adjacent basins.

Figure 7.18 illustrates the vertical distributions of the four fluorescent components in the Central-North Aegean. In the pelagic waters the protein – like component showed the highest fluorescence intensity (I_4) of all other components, following the order: $I_4>I_1>I_2>I_3$. The humic – like components revealed the lowest intensities (I_{1-3}) at the surface layer, increasing with depth and reaching highest values near bottom samples (st.31-32) and especially at the NAgDW of station 29. In the LIW, the intensity of component C_1 becomes dominant and the order of components changes to $I_1>I_4>I_2>I_3$. At the deepest NAgDW the order of fluorescent intensities changes to $I_1>I_2>I_3=I_4$. The protein – like component C_4 overall decreased from surface towards the bottom with exception the southernmost station 29 which retained elevated values at depths over 100m.

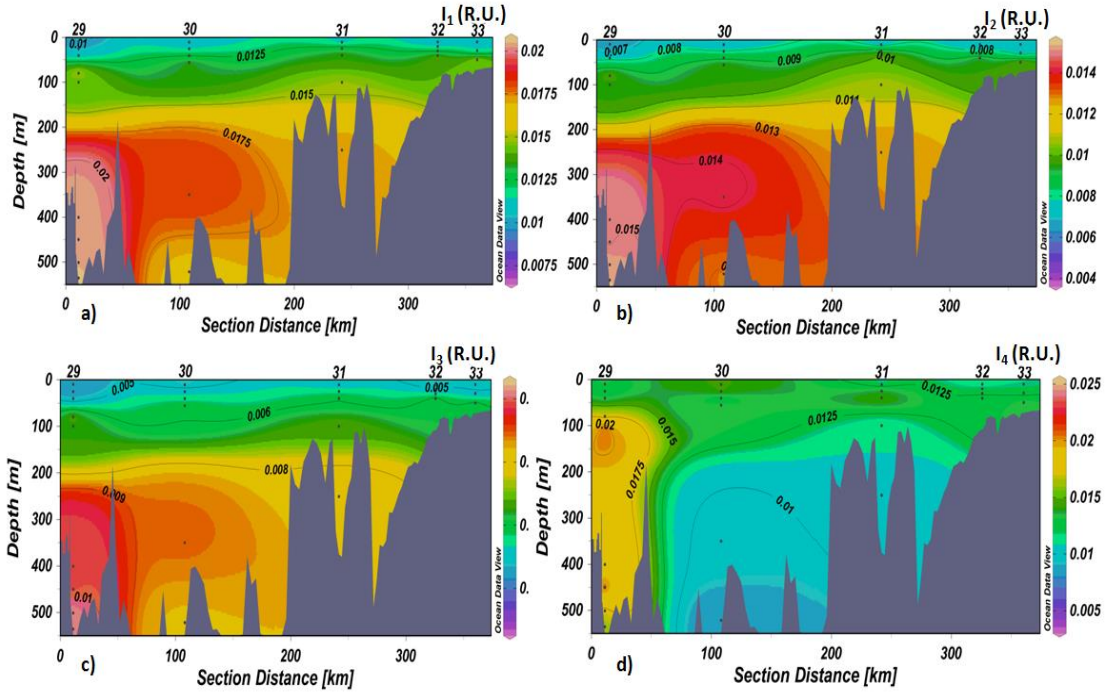

Figure 7.18: Distribution of the fluorescence intensities (I_{1-4}) of the four PARAFAC components in the Central-North Aegean.

7.4 Discussion

7.4.1 Pelagic waters (10 - 100m)

7.4.1.1 DOC and CDOM sources

The easternmost part of the Mediterranean Basin presents the highest DOC values at the surface and LIW layer gradually decreasing towards the west

Mediterranean [52][202][203]. The Eastern Mediterranean Basin is characterized by higher nitrogrn to phosphorous, N/P, ratio than the Western Mediterranean Sea, as an eastward increase in phosphorus limitation was observed [277]. Thingdstad and Rassoulzadegan [278], claimed that at P-limited systems the bacterial degradation of DOC is more restricted than in systems characterized by N-limitation, leading to an accumulation of DOC. The higher DOC values of the Eastern Mediterranean could be therefore attributed to the more P-limited character of this region [203]. In accordance, our results showed the area of the northwestern Levantine Basin (st27) more enriched in dissolved organic carbon at the surface layer, while the lowest DOC values were recorded at the southernmost Ionian Sea (st 2). The surface layer of the central and north Aegean presented uniform DOC values which could be indicative of the presence of the same water mass throughout the sampled transect i.e. LSW. These DOC values were lower (62-68 μmol/L) than the values found at station 27 (74-82 μmol/L) but comparable to DOC concentrations (55-71 μmol/L) of the Cretan and Ionian Seas. Station 27 presenting the maximum DOC concentrations is located at the periphery of the Rhodes cyclonic gyre where the LIW is being formed [260][279] indicating a source of DOC there. The upwelling of deep waters rich in inorganic nutrients at the Rhodes gyre has been shown to lead to enhanced primary production within the body of the cyclone which contrast with the surrounding oligotrophic eastern Mediterranean [280][281]. Napolitano et al., [280] reported the primary productivity of the Rhodes basin as comparable to the northwestern Mediterranean while the productivity of the south Ionian accounts only 10% of the Rhode's gyre productivity. This could propose the primary production as the source of the increased DOC in the periphery of the Rhodes gyre. Our sampling conducted in post bloom period when release of DOM is expected. The less oligotrophic character of Rhode's gyre is supported by the chl-a distribution at station 27 where chl-a retains the high and uniform values from the surface down to 100m without clear DCM due to the mixing and upwelling under the effect of the gyre. Although the upwelled deep waters are rich in nutrients and result in the aforementioned trophic situation, during summer a strong thermocline is established preventing vertical mixing and resulting to an extremely poor in nutrients mixed layer

[280]. Therefore a limited microbial degradation of organic matter is expected that results to the higher DOC concentrations observed. LIW after being formed in the Levantine Basin enter the Cretan Sea from the eastern straits at both surface and intermediate depths [261], follow a westward route and exit the Cretan Sea through the western straits where it occupies the subsurface layer of the south Ionian region. The results from the DOC analysis (figure 7.7) indicate that the DOC content of LSW/LIW decreases along its route from the eastern to the western limits of our study area. The removal of DOC in the core of LIW during its route from the Levantine Basin to the west Mediterranean has been shown to be a combined effect of both mixing and microbial mineralization [52][203].

No significant correlation was established between chl-a and a_{300} in our study area, and the maximum of CDOM in South Aegean was consistently established above the chl-a maximum (with exception of st.27) (figure 7.6). At stations 2, 3 and 28 the maximum of a_{300} was encountered at 50m, while the chl-a maximum was recorded at 100m. At station 27 were uniform chl-a values were found from surface down to 200m, no clear peak of a_{300} was observed, elevated values though were recorded between 50 and 100m.Both the maximum of chl-a and a_{300} at station 1 were found deeper, at 135m and 70m respectively. This could be due to the presence of the anticyclone in the Cretan Sea that stirs down the surface water, transferring both the chl-a and a_{300} maximum to deeper layers. Subsurface CDOM maxima during summer have been previously reported in the Mediterranean Sea. Xing et al., [152] and Bracchini et al., [208] found the subsurface summer CDOM maxima within the DCM. Bracchini et al., [208] reported positive correlation between chl-a and CDOM during November while Xing et al., [152] reported positive correlation between chl-a and CDOM in spring during the algal growth and negative correlation in summer-autumn along the algal decay. They both attributed the release of CDOM to direct release from phytoplankton with a possible contribution from microbial activity. Contrary Organelli et al., [151], reported the subsurface CDOM maxima above the DCM but coincident with higher bacterial abundance. Moreover multiple regression among CDOM, chl-a and bacterial abundance revealed that the microbes were primarily

responsible for CDOM production. These findings are in good agreement with what has been previously reported in the Sargasso Sea [88] where the CDOM maxima was found shallower than the DCM but concurrent with the highest bacterial biomass. Consequently our results presenting the CDOM subsurface maxima above the DCM and the lack of correlation between CDOM and chl-a could suggest that microbial activity is the major source of CDOM during summer in South Aegean Sea. Contrary to a_{300}, the spatial and vertical distributions of C_4 deviated significantly from those of chl-a (figure 7.6). Only stations 28 and 2 presented a peak of I_4 at 25m and 75m respectively that could follow the peak of chl-a at 100m. Catala et al., [167] in a study including samples from the Atlantic, Pacific and Indian oceans reported the maximum of peak T at the depth of the DCM; nevertheless their data showed that salinity and AOU dominated over chl-a in the explanation of peak T distribution. Our results in the oligotrophic Mediterranean waters indicate a decoupling between C_4 and chl-a and probably show that other factors such as the microbial activity may implicate in the production of UV-FDOM [147][164] or that the bio-labile character of the protein – like substances inhibit the establishment of a relationship between chl-a and C_4. Humic components at the surface revealed the highest intensities at the southwest station 2 while the lowest humic intensities were recorded at both stations 1 and 3. This pattern was consistent within the LIW layer too. The lowest intensities at stations 1 and 3 could be linked to the presence of the Pelops and Cretan anticyclones respectively that inhibit the upward flux of deeper water and the enrichment of the surface layer with unbleached humic substances. Lower humic-like intensities have been reported in subtropical oligotrophic anticyclonic gyres and were attributed to the prevailing downwelling circulation [167]. On the other hand, higher yellow substances content of the West Mediterranean Sea compared to the East Mediterranean has been reported [207][282] and attributed to the more frequent vertical mixing in the West Mediterranean resulting to greater transportation of unbleached yellow substances to upper layers at the sites of deep waters formation [207]. Therefore, the highest humic –like intensities recorded at station 2, could be related to the greater influence of this station by waters originating from the

Western Mediterranean. The fact though that the MAW current was not detected during our samplings does not support this assumption.

7.4.1.2 CDOM and FDOM sinks: Photodegradation

At the first 30m of the surface layer throughout the studied area the observed a_{300} coefficients were considerably lower (0.27-0.38 m^{-1}) than those found between 50-100m (0.34-0.53 m^{-1}). These results coupled with the highest observed spectral slopes (0.0347-0.0488 nm^{-1}) point to photodegradation of CDOM [113][176][253] which is expected to be important in the cloud free Eastern Mediterranean region. Photodegradation is also evident from the distribution of $S_{275-295}$ along the a_{300} gradient found at the surface layer (figure 7.19), which was approximated by an exponential function (R^2=0.951).

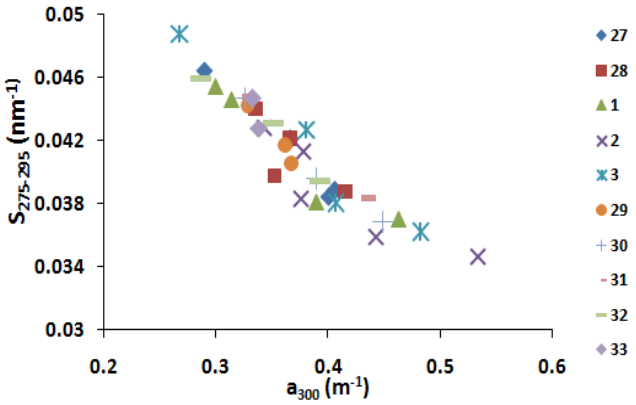

Figure 7.19: Distribution of $S_{275-295}$ along the a_{300} gradient at the first 30m.

Moreover, the lowest a^*_{300} values observed at depths down to 30m coupled with the high spectral slopes (figures 7.10, 7.13b) indicate a loss of the aromatic character of the DOM during the photobleaching processes [118][120]. This is in accordance with the lowest intensities of the humic – like components recorded at the surface layer and evidence the photo-labile character of the fluorescent humic substances [256]. Consequently, photodegradation appears to be an important sink of both CDOM and visible-FDOM (humic substances) at the surface layer of the studied area but does not seem to affect the UV-FDOM (protein fluorescence). The protein-like components have been characterized as more refractory to photodegradation than the humic-like components [256]. The relationships established at the surface layer among DOC, CDOM and FDOM (figure 7.20) seem to be determined by the effect of photodegradation. DOC presented negative linear

correlations with the humic – like components indicating the impact of photodegradation on the humic substances and the decoupling of the FDOM pool from the bulk DOM (figure 7.20 a,b,c). The values of station 27 were excluded since they deviate from the rest stations due to the excess DOC concentrations. Stronger negative correlations were found between DOC and both I_1 and I_3 (R^2=0.672 and 0.692 respectively) than with I_2 (R^2=0.573). On the other hand no relationship was established between DOC and absorption coefficient a_{300} or I_4.

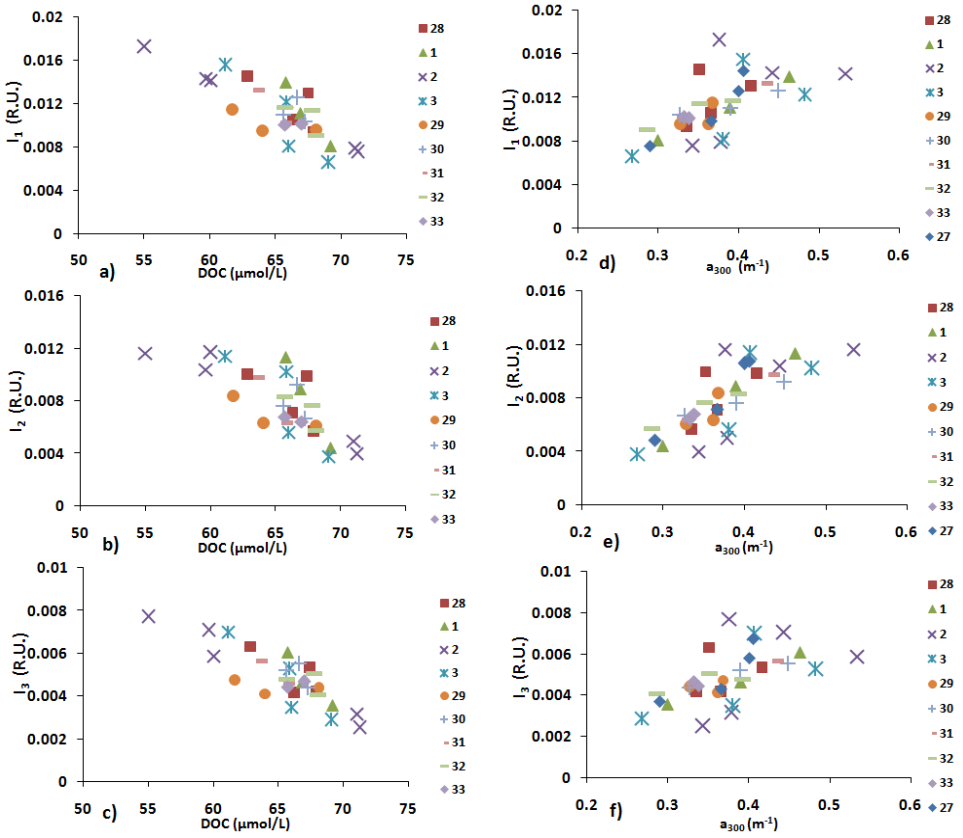

Figure 7.20: Relationships of the intensities of the humic components with DOC (a,b,c) and a_{300} (d,e,f) in the top 30m.

Absorption coefficient a_{300} showed weak positive association with the humic – like components (figure 7.20 d,e,f), indicate the same influence of photodegradation on CDOM and visible-FDOM while no relationship was established between a_{300} and I_4. The strongest positive correlation was established between a_{300} and marine humic-like component I_2 (R^2=0.623) while the correlations with I_1 and I_3 were very weak (R^2=0.443 and 0.449 respectively). The log-transformed intensities of the humic-like components were strongly correlated with each other (Table 7.3) illustrating the same

behaviour at the surface layer, while the protein-like component showed no relationship with any of the humic like components. For the relationships of log(I_1) *vs* log(I_2) and log(I_3) *vs* log(I_2) the slopes of the regression equations were higher than 1, indicating a faster removal of C_1 and C_3 over C_2 which reflects the more photoresistant character of the marine humic-like component C_2 as suggested by Murphy et al., [139].

Table 7.3: Relationships between the humic-like components in pelagic waters.

	Equation	***R^2***
$logI_1$ vs $logI_2$	y=1.340x+0.506	0.938
$logI_1$ vs $logI_3$	y=1.057x-0.247	0.929
$logI_3$ vs $logI_2$	y=1.182x+0.623	0.879

7.4.2 Mesopelagic Waters – LIW/CIW, TMW (100-2000m)

The presence of the anticyclonic gyre in the Cretan Sea that traps and stirs down to greater depths the incoming LSW [262] seems to cause the enrichment of the intermediate layers of the Cretan Sea in both DOC and CDOM. These feature results in the highest DOC concentrations in the LIW layer recorded in Cretan Sea and also in increased a_{300} and carbon specific a^*_{300} coefficients. Contrary the rest stations revealed low a_{300} values with small variation among them. However, an overall increase in the humic-like components was observed in the LIW layer relatively to the pelagic waters, as a result of photodegradation processes taking place in surface waters. The increasing trend of humic substances below the surface has been widely reported in studies all over the word [125][128][158][173]. Station 2 still holds the highest intensities of the humic – like components, while station 3 presented the lowest. Overall, stations 2 and 3 presented variations in both CDOM and FDOM which could be attributed to the presence of the Pelops anticyclone in accordance to what has been stated in section 9.4.1.1.The influence also of LIW at the two stations is possible to vary as it depends on the prevailing circulation features at the western straits [261].

In the Central and North Aegean Sea, the LIW layer presented lower DOC but an overall increase of the absorption coefficients and humic components

compared to pelagic waters. The northern region (sts 31-33) appeared to hold relatively higher concentrations of DOC and CDOM (higher a_{300}). The vertical distribution of a_{300} (figure 7.11), presenting peaks above the chl-a maximum (except st.29) coupled with the lack of correlation between a_{300} and chl-a indicate a possible bacterial source of CDOM during summer in the Central and North Aegean Sea, as discussed in section 7.4.1.1. I_4 presented no clear vertical trend (figure 7.11), the highest intensity was though encountered at station 29 where the maximum of chl-a was also found. Contrary, the lowest a_{300} values with no clear peak were recorded at this station indicating an overall accumulation of UV- and visible-FDOM over CDOM in the southernmost region of the Central Aegean.

CIW that underlies the LIW in the Cretan Sea (sts 1, 28) showed decreased values of DOC, a_{300}, $S_{275-295}$ and I_4 but increased a^*_{300} and fluorescence of the humic – like components (I_1,I_2,I_3) compared to LIW. The observed differences between the two water masses indicate that there is an overall loss in DOC, CDOM and UV-FDOM from the LIW towards the CIW in parallel with an increase in AOU, but at the same time an increase in the aromatic and humic character of the organic matter. This vertical distribution is expected and related to the bacterial degradation of the semi-labile and semi-refractory DOM and CDOM compounds with depth. The lateral distribution shows that in the CIW water mass, DOC, a_{300} and the fluorescence intensities I_1 and I_2 reached their maxima compared to the TMW that occupies the adjacent Levantine and Ionian Seas. The excess, in C_1 and C_2 observed in the CIW relatively to the adjacent TMW (at same depths) cannot be explained by enhanced *in situ* bacterial reworking-humification of CDOM in the CIW layer since this water mass is well oxygenated (AOU=5-44 ml/L). CIW is formed locally in the Cretan Sea from adjacent coastal shelf waters and this might explain the excess terrestrial character of DOM retained in the CIW. This indicates that the Cretan Sea can act as a significant source of both CDOM and FDOM to the Eastern Mediterranean during the export of the dense CIW that takes place in a decadal basis [259]. The export of the bio-labile CDOM and protein-like fluorescent organic material is expected to enhance the microbial loop in the old TMW. The highest AOU values (68-71 ml/L) were

found in the core of the TMW (750-1500m) indicating the old character of this water mass while at the upper and lower limits AOU fluctuated between 44 and 66 ml/L probably due to the mixing with the overlying and underlying LIW and EMDW water masses. The lower DOC, absorption coefficients and intensities of the protein-like component C_4 found in the TMW compared to LIW and CIW indicate the consumption of DOM in this old water mass. Indeed the negative correlations found between DOC, a_{300}, I_4 and AOU (R^2=0.815, 0.622, 0.637 respectively) (figure 7.21) indicate bacterial mineralization of DOC in the mesopelagic waters which is more intense in the TMW and includes consumption of both absorbing dissolved organic matter as well as fluorescent substances of amino acid nature. Component C_4 (figure 7.21c) presented uniform extremely low intensities (I_4) at the highest AOU values found at the TMW indicating the depletion of protein-like substances in this water mass.

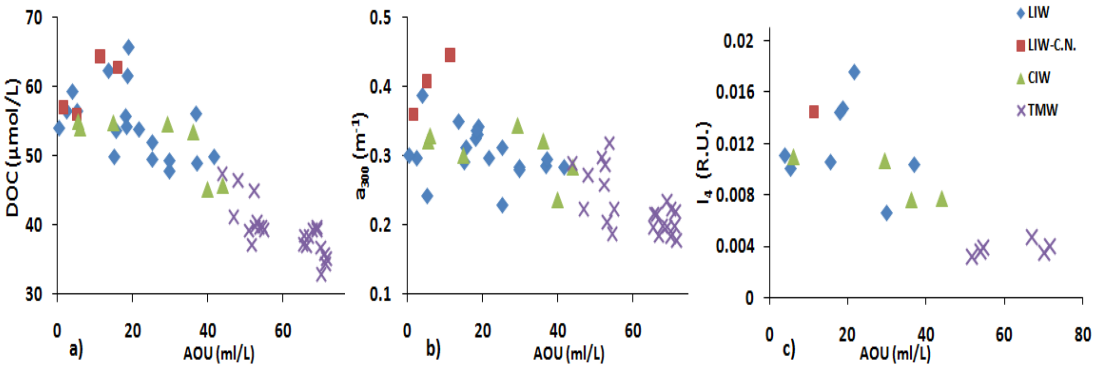

Figure 7.21: Relationships of AOU with a) DOC, b) a_{300}, c) I_4 in mesopelagic water.

On the other hand, the intensities of the humic – like components in the TMW point to a preferential production/accumulation of C_3, as C_3 was the only component presenting higher values in the TMW than both the LIW and CIW. Contrary C_1 and C_2 revealed comparable intensities with LIW but clearly lower than the CIW. This is clear in the relationships between the intensities of the humic-like components (I_{1-3}) and AOU (figure 7.22) in the mesopelagic waters (LIW, CIW, TMW) since only I_3 showed a weak positive correlation with AOU (R^2=0.530, figure 7.22c). These results indicate that this old water mass with the high AOU values favours the accumulation of C_3. This component which is a combination of peaks A and C, has been linked to the prokaryotic microbial processing in both terrestrial and oceanic regions [147] while it was also

proposed that bacteria can utilize humic substances representative of peak M and produce more complex humic substances corresponding to peak C [163].

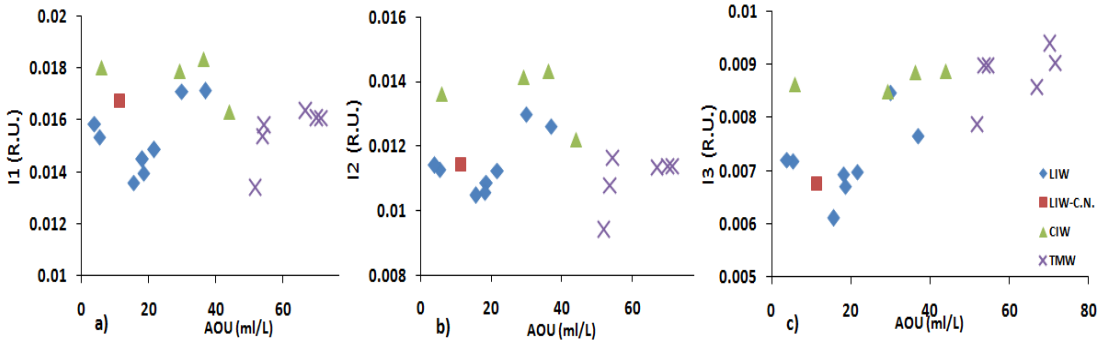

Figure 7.22: Relationships between AOU and the intensities of a) C_1, b) C_2, c) C_3 in mesopelagic water.

Catala et al., [140] identified two humic-like components in the global ocean similar to ours C_2 (peak M) and C_3 (peak A/C) and reported a higher production rate of C_3 per unit of consumed oxygen over C_2 that was attributed to different mechanisms of production [184] linked to the phylogenetic nature of producers (bacteria, archaea, eukarya) [163] and/or the sensitivity to environmental oxygen concentration. Nevertheless, the ratios of the fluorescent intensities of the components to the DOC concentrations (I_i/DOC, I^*_i) that express the fraction of FDOM to the bulk DOC were strongly positively correlated to AOU (figure 7.23, R^2=0.894, 0.860, 0.913). This indicates that despite the fact that microbial activity in the mesopelagic water of the study region may not directly lead to increased intensities of components C_1 and C_2, it clearly results in increased participation of FDOM to DOC. This is probably due to the consumption of non humic substances present in the bulk DOM.

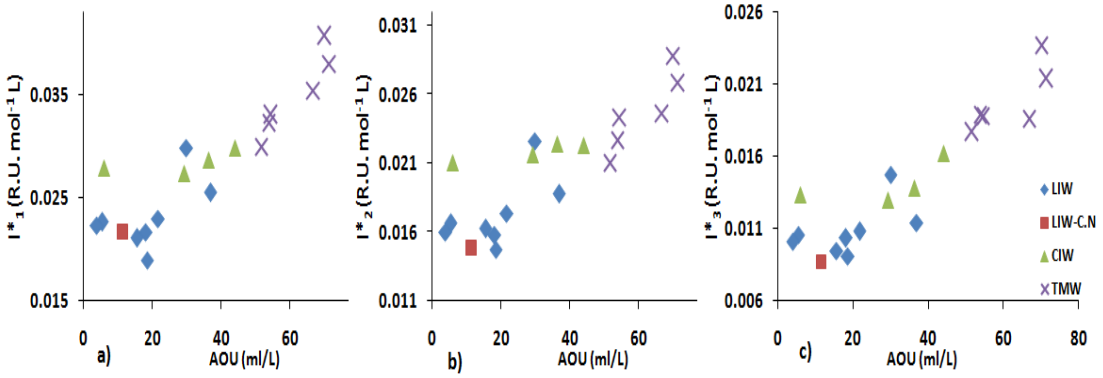

Figure 7.23: Relationships between AOU and a) I^*_1, b) I^*_2, c) I^*_3 in mesopelagic water.

Absorption coefficient, a_{300} and I_4 were positively correlated with DOC presenting an exponential trend (R^2=0.793 and 0.852 respectively) at the LIW layer of the Central and North Aegean Sea (figure 7.24). This indicates that in the LIW branch that flows towards the N. Aegean, DOM becomes enriched in CDOM. Most probably this relates to the influence of BSW on the top 30m and some vertical diffusion processes that take place. I_1 and I_2 were not correlated to DOC while a weak negative correlation (R^2=0.540, not shown) was found between I_3 and DOC, indicating the opposite trends of the two parameters (increasing for I_3, decreasing for DOC) with increasing depth in the studied region.

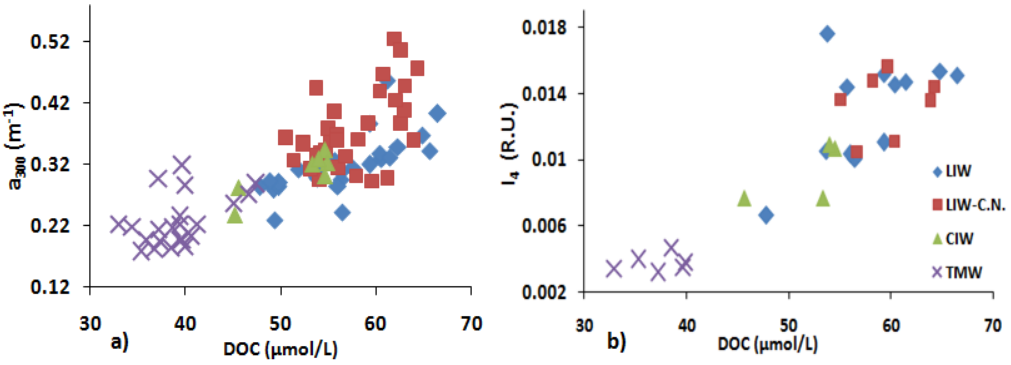

Figure 7.24: Relationships between DOC and a) a_{300}, b) I_4. (Red symbols correspond to LIW samples in the Central and North Aegean Sea).

Absorption coefficients and fluorescence intensities on the other hand, showed no correlation indicating that these two sub-pools of DOC are decoupled in the mesopelagic waters throughout our studied stations. As expected from the vertical distribution of the components and their relationship with AOU, I_1 and I_2 were strongly correlated with each other while they were both poorly correlated to I_3 (Table 7.4). I_3 though, was weakly negatively correlated to I_4 illustrating the parallel consumption of I_4 and accumulation of I_3 in the mesopelagic water. No relationship was found between I_4 and I_1 or I_2.

Table 7.4: Relationships between the humic-like components in mesopelagic water.

	Equation	***R^2***
$logI_1$ vs $logI_2$	y=1.071x-0.004	0.842
$logI_1$ vs $logI_3$	y=0.802x-0.657	0.321
$logI_2$ vs $logI_3$	y=0.524x-1.088	0.186
$logI_3$ vs $logI_4$	y=-3.136x-8.699	0.532

Station 27 presented distinct absorption characteristics as the absorption coefficient a_{300} presented elevated values at the deepest layers, ~1000m, resulting to high a^*_{300} and low $S_{275-295}$ values, indicative of high aromatic CDOM. This increase though in the aromatic character of CDOM was not followed by an increase in the intensities of the humic-like components indicating a source of only absorbing aromatic material. This could be the result of sediment resuspension [156] induced by turbulent currents in this area but the present data are not adequate to provide interpretations.

7.4.3 Bathypelagic and Dense waters - CDW, EMDW, NAgDW

CDW in the deepest layers of the Cretan Sea presented AOU values (32-47 ml/L) lower than the EMDW (62-64 ml/L) in the Ionian Trench indicating a younger age of this water mass. CDW presented also higher DOC, absorption coefficients, carbon specific absorption coefficients a^*_{300} and intensities of the humic components C_1 and C_2 compared to EMDW, but similar intensities of the C_3 component (Table 7.1). At the same time spectral slope $S_{275-295}$ values were found somewhat lower in the CDW. As already stated for the CIW water mass, in the CDW water mass, the excess I_1 and I_2 intensities were coupled with notable lower AOU values (32-47 ml/L) compared to EMDW (62-64 ml/L), indicating that these substances are transported to the Cretan Sea, rather than being produced *in situ* through microbial reworking – humification of DOM. CDW is formed in the Cretan Sea and similarly to CIW, it receives dense coastal shelf waters from the adjoining land (Cyclades plateau, Asia Minor, Eastern Peloponnese). Our observations clearly show an accumulation of DOM and CDOM in the CDW which is characterized by high MW and aromatic substances. Contrary, the lower values of DOC, CDOM and fluorescence intensities in the Adriatic origin EMDW illustrate a more extensive degradation of the dissolved organic material in the deepest layers of the eastern Mediterranean, in accordance with the elevated AOU values found there. This outcome suggests that the contribution of the Cretan Sea to the DOM, CDOM and FDOM pool in the Eastern Mediterranean during the dense water export can be more significant than the organic load that is

transferred by the Adriatic deep water. As discussed in section 7.4.2, regarding the CIW, this input of semi-labile, semi-refractory DOM can fuel the microbial loop. Component 3 on the other hand differentiated from C_1 and C_2, as similar values were found in CDW and EMDW (figure 7.25).

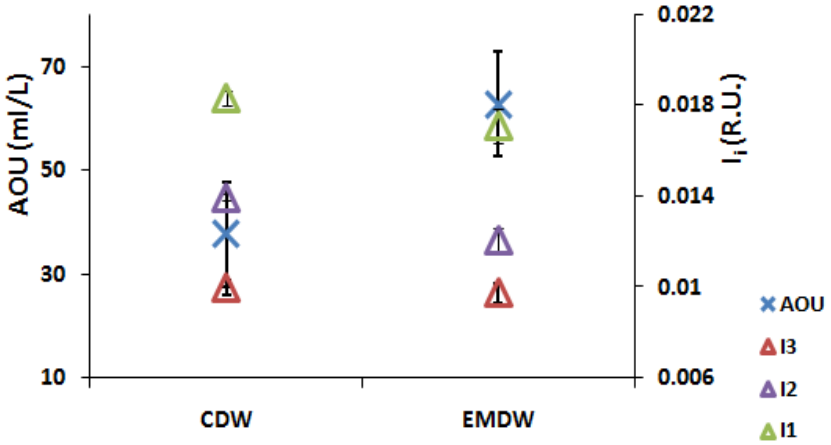

Figure 7.25: AOU and intensities of I_1, I_2 and I_3 in CDW and EMDW.

This indicates that in the abyssal EMDW water mass there is a favourable production of C_3, a feature also observed in the highest AOU TMW water mass. Moreover in abyssal EMDW a strong positive correlation (R^2=0.892) was found between DOC and a_{300} indicating that at the deepest layers of the Ionian Trench CDOM becomes an important fraction of DOC (figure 7.26). The non absorbing fraction of DOC is estimated at only 14 μmol/L.

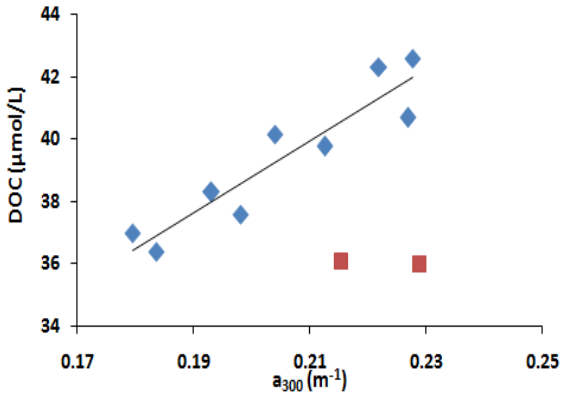

Figure 7.26: Relationship between DOC and a300 in the EMDW. (Red symbols correspond to the deepest samples of stn 3).

The two points that deviate from the correlation showing elevated a_{300} values at low DOC concentrations represent the deepest samples of station 3 (3800-3900m). Similarly to what has been stated for st. 27 (section 7.4.3.), the

increased absorption coefficients at the bottom of station 3 could be designated to sedimentary processes, but our data cannot support any relevant hypothesis. No significant correlations were found between the fluorescent components and DOC or a_{300} in the EMDW. Once again, the log-transformed intensities of C_1 and C_2 were strongly correlated to each other (Table 7.5).

Table 7.5: Relationships among the components in EMDW.

	Equation	***R^2***
$logI_1$ vs $logI_2$	y=0.950x-0.239	0.901
$logI_1$ vs $logI_3$	y=0.829x-0.546	0.710
$logI_2$ vs $logI_3$	y=0.848x-0.384	0.743

Contrary though to mesopelagic waters where C_3 was found to be decoupled from C_1 and C_2, in the 'newer' than TMW EMDW the relationship among the components is re-established. The association however of C_3 with both C_1 and C_2 was lower than the association between C_1 and C_2 (Table 7.5) while no correlation was found between C_4 and any of the humic-like components. Due to the small number of samples (n=4) in the CDW no relations among DOC and CDOM/FDOM could be investigated.

The denser NAgDW were encountered in the Central Aegean (sts 29, 30) at shallower depths (<550m) compared to CDW and EMDW presenting very low AOU values (3-8 ml/L) indicative of a newly formed water mass. NAgDW presented also clearly higher DOC concentrations and absorption coefficients than CDW and EMDW; no significant correlations were found however, between DOC and CDOM or FDOM. In the Central Aegean and especially in the Chios basin, the topography favours the renewal of deep water masses by a thermohaline circulation cell [268] which is probably the cause of the low AOU values and higher DOC and CDOM loads found in the NAgDW of the Central Aegean. The intensities of C_1 and C_2 in NAgDW were also higher than the intensities in the CDW and EMDW while C_3 presented comparable intensities among the three water masses. Due to the short renewal time of NAgDW in the Central Aegean and the low AOU values of this water mass, the high intensities of humic components is more possible to be a result of

transportation rather than *in situ* production. As discussed in section 9.1.2 vertical mixing and deep water formation is favoured in the Central Aegean and therefore terrestrial origin FDOM that was not photodegraded at the surface layer could be vertically transported to the deepest layers.

7.5 Conclusions

This study provides information according the DOC and the optical properties of dissolved organic matter in the highly dynamic area of the Cretan Arc and the adjacent basins (southeastern Ionian Sea and northwestern Levantine Basin), the North and Central Aegean Sea; in most cases for the first time. Our results indicate comparable DOC content in the surface Levantine waters (LSW), with the exception of the northwestern Levantine basin that appeared to hold higher DOC concentrations. This enrichment in DOC is attributed to the enhanced primary production in the periphery of Rhodes gyre and the accumulation of DOM due to inhibited microbial activity driven by the higher P-limitation character of this region. On the other hand, CDOM in the pelagic waters during summer is probably being produced by bacteria rather than directly released from phytoplankton. The main sink of CDOM and visible-FDOM (humic components C_1 and C_3) at the surface layer has been shown to be photodegradation. The differences in sources and sinks show an uncoupling of the bulk DOM pool from the CDOM/FDOM pool.

In the mesopelagic waters (LIW/CIW/TMW) DOM mineralization was followed by CDOM and UV-FDOM (C_4) mineralization. Humification processes through bacterial reworking of DOM are apparent by the increase in the vis-FDOM and specifically of component C_3 in parallel with the increase in AOU in the old TMW mass, while the C_1, C_2 components remain unaltered. In addition, the concurrent consumption of non-CDOM compounds results in a more humified nature of the remaining (refractory) DOM. In the Cretan Sea, the formed CIW appears to hold higher amounts of both CDOM and FDOM compared to the adjacent TMW, a feature attributed to the source of CIW. Overall a coupling of DOM, CDOM was apparent in the mesopelagic layer while vidible-FDOM follows different dynamics and is uncoupled.

The mechanisms described for the mesopelagic waters and in particular for the deeper CIW and TMW water masses continue to take place in the bathypelagic waters. DOM and CDOM were found coupled in the deepest EMDW while the accumulation of visible-FDOM compounds in deep waters resulted in the uncoupling of the FDOM pool. CDW was found to be more enriched in CDOM and FDOM compared to the abyssal EMDW. The higher DOC, CDOM and FDOM content of both CIW and CDW compared to TMW and EMDW suggest that Cretan Sea is a potential source of organic material to the Eastern Mediterranean. This export can trigger the microbial activity in the Eastern Mediterranean as it provides the mesopelagic waters with semi-labile, semi-refractory DOM. The NAgDW showed slightly higher humic content than the CDW but the very low AOU values probably suggest that this aromatic DOM was transferred at this region. Overall the uncoupling of FDOM from the DOM and CDOM pools in deep waters or under high AOU values is due to the stimulated production of C_3 while the accumulation of C_1 and C_2 is more likely a result of transportation.

CHAPTER 8

CHROMOPHORIC DISSOLVED ORGANIC MATTER DYNAMICS IN AN EASTERN MEDITERRANEAN RIVER (SPERCHIOS RIVER), A STUDY CASE OF TERRESTRIAL CDOM INPUTS TO COASTAL WATERS.

8.1 Introduction

Rivers are responsible for the input of significant quantities of terrigenous DOM in the coastal environments [283], which is a major source of reduced carbon [284]. The quantity and the nature of the DOM that enters the rivers is mostly governed by soil properties, vegetation, hydrological conditions, biotic factors and land use of the catchment [285]. The terrestrial plant-derived DOM is of high humic character as it contains high concentrations of phenolic compounds such as tannin polymers [286]. The conversion of forests to agricultural land has been shown to alter both quantitatively and qualitatively the DOM [287]. Increased human activity i.e. agricultural land and high population density has been shown to result in higher DOC [288], DON and DOP concentrations [285], and CDOM with distinctive absorption and fluorescence properties [129]. Moreover, Wilson [289] demonstrated that increased cropland leads to a more microbially derived DOM character possibly due to either the increased availability of nitrogen to the microbial community or the less complex structure of the exported DOM from agricultural land. DOM upon entering the river and along its route towards the estuary can be subjected to multiple bio-and physicochemical processes, at degrees that are mostly dependent by the chemical composition of the DOM. It can be altered or even removed from the water through photochemical degradation [61], microbial activity [290] and physicochemical transformations [291].

The principal aims of the present study are: 1) to trace the qualitative differences between the riverine and marine DOM through absorption and fluorescence analysis and b) to examine the influence of the Sperchios outflow in the optical properties and quality of DOM in the Maliakos Gulf. In spite the ecological importance of Sperchios River and Maliakos Gulf, very

few studies have focused on the bio-chemical properties of the river and the gulf [292][293] while, to our knowledge no published data are available on the optical properties of CDOM in the river or adjacent coastal waters.

8.2 Materials and Methods

8.2.1 Study Area

The Sperchios River originating from the Tymfristos mountain flows in an E-W direction covering approximately 60-80 km in length and discharges at the Maliakos Gulf forming a 'birdfoot' delta (Fig 8.1). The Sperchios River drainage area is 1780 km^2 and receives fluxes from more than twenty major tributaries. The mean annual water discharge of Sperchios River is approximately 62 m^3s^{-1} varying between 110 m^3s^{-1} in winter and 22 m^3s^{-1} in summer [294] while floods occur commonly due to both intense precipitation events typically in this region and the snowmelt during spring [295]. The highest precipitation in the Sperchios River occurs during November and December (107 mm and 123 mm respectively during 2014 and 2015) while the lower during summer (approximately 21-22 mm) [296]. The intensification of industrial activities and anthropogenic intervention in the river basin, particularly after the 50's, has led to increasing pollution [295]. Approximately 32% of the Sperchios basin is used for agricultural activities while only 1.2% can be characterized as urban zone [296]. Large amounts of agricultural and stock-farming waste end up in the Sperchios River while two wastewater treatment facilities serving a number of small towns discharge in the river along with the sewage of several small industrial units and olive refineries that remain untreated or partly treated [296][297]. In addition extensive irrigation for agricultural purposes is common resulting to the drastic decrease of the river flow in the past years [296][297]. The main part though of Sperchios basin (65.3%) is occupied by forests and vegetation [296] while is one of the very few rivers in Greece that are characterized as free flowing with no significant fragmentation altering the flow of the river. However, the lower part of the river was straightened and embanked and riparian vegetation has been removed [297].

Sperchios delta (22˚32΄, 38˚51΄) covering an area of 196 km^2 is of high ecological importance and it has been designated a Natura 2000 site. In the

Maliakos Gulf several deltaic prolongations are apparent due to the shifts in the river's main channel caused by hydrological changes or tectonic deformation [298]. Fast dispersion of the discharging Sperchios waters occurs in the Maliakos Gulf possibly due the anticlockwise circulation in the gulf [292]. Maliakos Gulf is a shallow semi-enclosed embayment with depth less than 30 m while its east to west length is approximately 11 km and its north to south width 9 km. Maliakos Gulf connects to the Aegean Sea to the northeast through the Orei Channel and to the Euboic Gulf to southeast through Knimida Channel. The Maliakos Gulf volume has been estimated to approximately $500x10^6$ m^3 while the annual freshwater inflow from Sperchios around $176.6x10^6$ m^3 amounting to about 1/3 of the gulf volume [293]. Therefore, the effect of the river in the Maliakos Gulf is expected to be of great importance.

8.2.2 Samplings

Four samplings were conducted in the Sperchios River and Maliakos Gulf. Two of these samplings took place during spring of 2014 (April) and 2015 (March) (wet season). The other two samplings were conducted during the dry season (July) and post dry season (November) of 2014. Surface water samples were collected from 7 stations in the river extending from a freshwater end-member located approximately 50 km upstream, station 1, to the delta, station 7 (figure 8.1). Station 6 situated 4 km upstream from the delta is closed to the discharge point of Lamia wastewater treatment plant. Contrary the upstream stations 1-5 are considered to be pristine stations. Samples were also collected in the Maliakos Gulf (stations 8 - 13) in transects extending up to approximately 14 km offshore (figure 8.1). Water samples for DOC and CDOM analysis were filtered through 0.22 μm polycarbonate filter. The filters were flushed with ~200ml MilliQ water prior the filtration and the first milliliters of the filtrate were discarded to avoid any contamination. Samples for DOC analysis were collected in precombusted glass ampoules (480°C, 12h), acidified with 2N HCl to ph~2, flame sealed and kept at +4°C until analysis. Samples for CDOM analysis were transferred into acid (HCl 10%, 12h) cleaned amber glass bottles and kept in the dark at +4°C if the

analysis was performed within the next few days otherwise they were stored in the dark at ~-20°C.

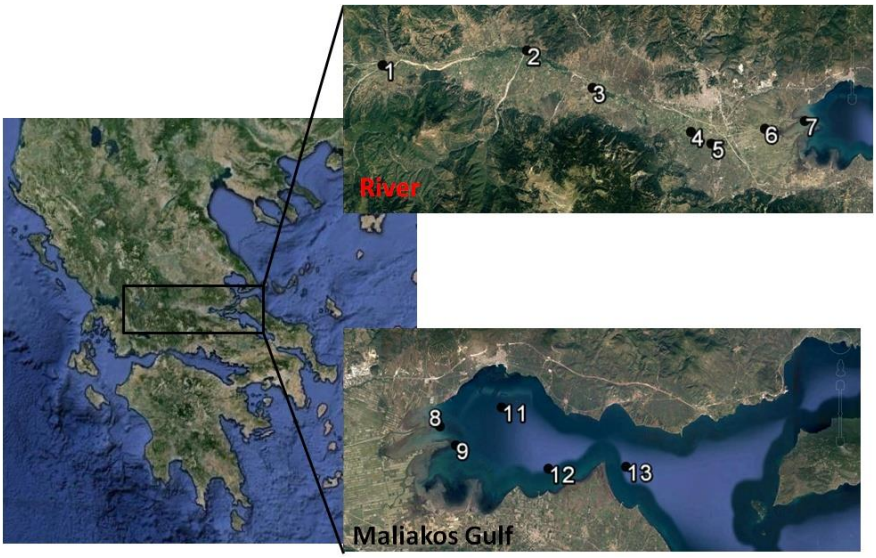

Figure 8.1: Study Area

8.2.3 Methodology

Dissolved organic carbon, absorption and fluorescence were analyzed as described in Chapter 4. The fluorescent components were identified by the traditional 'peak-picking' method. The qualitative indices of absorption, carbon specific absorption coefficient a^*_{300} and spectral slope $S_{275\text{-}295}$ as well as the fluorescence humification index HIX were estimated as described in Chapter 4.

Salinity, temperature and dissolved oxygen were measured *in situ* using a portable Aquaread AP-2000 multiparameter meter in the Sperchios River and an SBE 19plus V2 CTD in the Maliakos Gulf, both calibrated before use as required by the international scientific protocol. Sperchios River discharge (D) was measured at the uppermost stations, sts 1-3, during the samplings of April 2014 and November 2014 while in July 2014 the discharge was estimated only at stations 2 and 3. Unfortunately, no discharge data are available for March 2015. Daily precipitation measurements (P) are available at the Makrakomi station located closed to the upstream station 1 and the Lamia station close to station 4. The data from Makrakomi station were used as a proxy of the precipitation of the upper part of the river (sts 1-3) while the data from Lamia station were used to estimate the precipitation downstream of station 4. For each sampling the sum of the precipitation of the month

preceding the sampling was taken into account along with the precipitation of the current month up to the sampling date.

8.3 Results

8.3.1 Hydrological Measurements

River discharge and precipitation at Sperchios catchment are given in Table 8.1.

Table 8.1: Discharge and precipitation in Sperchios River during samplings.

	April 2014	***July 2014***	***Nov.2014***	***March 2015***
$D_{S1}(m^3\ s^{-1})$	2.07		0.91	
$D_{S2}(m^3\ s^{-1})$	4.48	0.50	0.92	
$D_{S3}(m^3\ s^{-1})$	6.30	0.39	1.81	
P_M (mm)	143	53	120	160
P_L (mm)	94	23	97	125

The precipitation in both stations was clearly lower in July 2014 (dry season) while the highest precipitation was observed in March 2015 (wet season). During April and November 2014 the precipitation was significantly higher than July 2014 but remained lower than March 2015. July 2014, along with the lowest precipitation, presented also the minimum river discharge that did not outreached 0.50 $m^3\ s^{-1}$. The discharge recorded at stations 1 to 3 during April 2014 fluctuated between 2.07-6.30 $m^3\ s^{-1}$ while during November the discharge at these stations was much lower, 0.91-1.81 $m^3\ s^{-1}$. Unfortunately no data of discharge during March 2015 are available, the highest though precipitation values of this month may imply higher discharge than April 2014 while a gradual increase of river flow from November until March has been previously reported [293].

8.3.2 Physicochemical characteristics

The physical characteristics (temperature, salinity and dissolved oxygen saturation) of Sperchios River and Maliakos Gulf are given in Table 8.2. As expected, temperature presented higher values in July 2014 and lower in March 2015 in both Sperchios River (sts1-7) and Maliakos Gulf (sts 8-13). Sperchios River, presented slightly lower temperatures in November 2014

Table 8.2: Temperature, salinity and D.O.% measured in the Sperchios River and Maliakos Gulf, MG=Maliakos Gulf

		Temperature (˚C)	***Salinity***	***D.O. (%)***
April 2014	Upstream	15.0-16.4	0.10-0.13	47-108
	St.6	17.3	0.15	87
	St.7	17.7	1.70	74
	MG (sts 8-9)	18.2-18.3	31.90-33.20	116-120
	MG (sts 11-13)	17.0-18.1	27.7-30.2	112-114
July 2014	Upstream	20.7-32.3	0.13-0.24	98-138
	St.6	27.5	0.36	88
	St.7	27.0	3.75	82
	MG (sts 8-9)	25.67	36.67	97
	MG (sts 11-13)	24.3-25.6	36.71-36.75	99-105
November 2014	Upstream	14.6-16.0	0.13-0.14	83-114
	St.6	15.0	0.21	96
	St.7	16.5	5.12	66
	MG (sts 8-9)	17.9-18.0	34.37-35.46	96-110
	MG (sts 11-13)	17.9-18.4	36.12-36.62	72-100
March 2015	Upstream	9.1-11.8	0.10-0.23	99-102
	St.6	11.4	0.13	101
	St.7	11.4	0.34	80
	MG (sts 8-9)	12.6-12.7		
	MG (sts 11-13)	12.2-12.5		

than April 2014 while in the Maliakos Gulf temperatures were comparable between the two months. During March 2015 noticeable lower temperatures than April 2014 were recorded. The distribution of salinity is given in figure 8.2a. The salinity values (Table 8.2) recorded during all samplings at stations situated in the Sperchios basin (sts 1-6) were constantly lower than 1. On the other hand station 7 situated at the Sperchios delta presented variable salinity values among the samplings. Higher salinity was recorded during November 2014 (5.1) followed by July 2014 (3.75), while samplings that took place in spring presented the lowest values (0.3 in March 2015, 1.7 in April 2014). The higher salinity values in November 2014 and July 2014 are probably due to the lower discharge of Sperchios River during summer and autumn, allowing

the intrusion of saline water in the delta. The lower salinity value of March 2015 over April 2014 may be a result of the higher precipitation and/or discharge during March. The stations located in the Maliakos Gulf (sts 8 -13) presented lower salinities during spring (April 2014, no data are available for March 2015) ranging between 27.7 and 33.2 while highest and invariable values were observed in July 2014, 36.7-36.8. Despite the increased precipitation during November 2014, salinity at these stations retained high values 34.4-36.6, probably due to the still limited river discharge during this month.

In the Sperchios River, the uppermost stations (sts 1-3) presented the highest oxygen saturation levels (98-138%) during all seasons while the delta (st7) presented the lowest ranging between 66-82% (Table 8.2, figure 8.2b). A sharp drop in D.O.% levels (47%) was observed at station 5 in April 2014. In the Maliakos Gulf, all stations were found to be well oxygenated (96-120%) during all samplings with exception station 11 (72%) during November 2014. The highest oxygen saturation levels were recorded in April 2014 most likely due to the spring phytoplanktonic bloom.

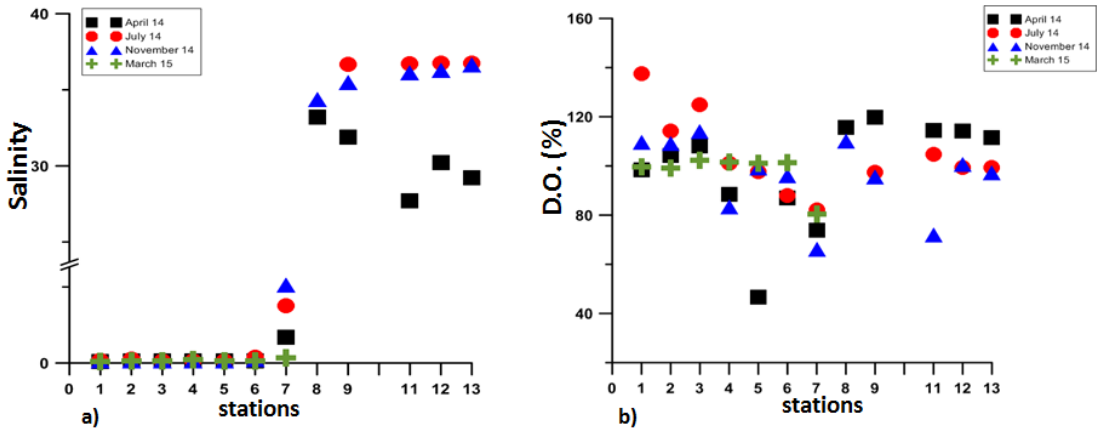

Figure 8.2: a) Salinity and b) dissolved oxygen saturation during samplings.

8.3.3 DOC and CDOM indices.

The results of DOC and CDOM analysis are given in Table 6.3. DOC revealed low concentrations (<100μmol/L) in Sperchios River upstream of station 6 during all seasons (figure 8.3a). Statistical analysis (Kruskal-Wallis post-hoc pairwise) showed that significant variation in the DOC concentrations in Sperchios River (upstream station 6) occurs only between April 2014 and

Table 8.3: DOC concentrations and absorption indices estimated in Sperchios River and Maliakos Gulf, MG=Maliakos Gulf

		DOC (μmol/L)	***a_{300} (m^{-1})***	***$S_{275-295}$ (nm^{-1})***	***a^*_{300} (m^2g^{-1})***
April 2014	Upstream	36-51	0.58-1.18	0.0141-0.0216	1.32-2.10
	St.6	118	2.88	0.018	2.04
	St.7	79			
	MG (sts 8-9)	93-101	0.82-0.86	0.0272-0.0291	0.68-0.77
	MG (sts 11-13)	94-105	0.74-1.37	0.0258-0.0313	0.64-1.08
July 2014	Upstream	40-87	1.65-3.08	0.0104-0.0156	2.22-3.77
	St.6	483	18.74	0.0154	3.23
	St.7	227	7.79	0.0155	2.86
	MG (sts 8-9)	121-123	1.47-1.52	0.0149-0.0254	1.01-1.03
	MG (sts 11-13)	113-134	0.85-1.32	0.0255-0.0310	0.53-0.93
November 2014	Upstream	24-151	1.00-4.39	0.0135-0.0168	2.35-3.45
	St.6	192	9.04	0.0145	3.92
	St.7	199	5.05	0.0144	2.12
	MG (sts 8-9)	104-108	1.34-1.45	0.0240-0.0248	1.03-1.17
	MG (sts 11-13)	99-106	0.77-0.89	0.0295-0.0315	0.64-0.70
March 2015	Upstream	59-97	1.78-5.75	0.0123-0.0164	2.25-4.93
	St.6	127	9.39	0.0120	6.14
	St.7	153	6.55	0.0149	3.57
	MG (sts 8-9)	102	1.52	0.0215	1.24
	MG (sts 11-13)	87-91	0.85-0.95	0.0282-0.0300	0.77-0.90

March 2015 (P<0.05). This indicates that during the studied period (April 2014 – March 2015) Sperchios River presents significant year to year variations but no seasonal variations. In November 2014 an increase was observed at stations 4 and 5 reaching 151 and 102 μmol/L respectively indicating a source of organic matter. The overall range of DOC upstream of station 6 (pristine stations) was 24 – 97 μmol/L (with exception sts 4and 5 in November 2014) which is in a good agreement with previous measurements taking place during 2009 and 2010, 34 – 80 μmol/L [299]. During all samplings however at the stations 6 (closed to the wastewater treatment plant and in a short distance from the delta) and 7 (delta) increased DOC values were observed which peaked in July 2014 at 483 μmol/L. The Maliakos Gulf (sts 8-13) presented during all samplings significantly higher (Mann-Whitney, P=0.000) DOC values than the upstream – pristine part of Sperchios River (sts 1-5). DOC concentrations in Maliakos Gulf range between 87-134 μmol/L presenting no significant seasonal variations.

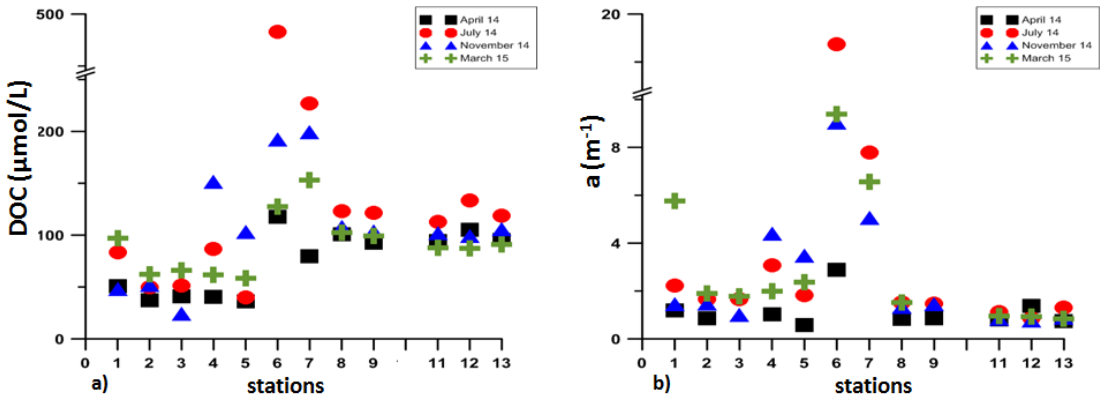

Figure 8.3: Distribution of a) DOC and b) a_{300} along Sperchios R. and Maliakos G.

The distribution of absorption coefficient a_{300} along the sampled transect is given in figure 8.3b. The distribution of a_{300} along Sperchios River and delta (sts 1-7) resembles DOC distribution showing a sharp increase in a_{300} values at stations 6 and 7 during all samples and a more moderate increase at stations 4 and 5 during November 2014. A notable though high absorption coefficient is also observed at the uppermost station 1 during March 2015 that clearly deviates from the other a_{300} values recorded upstream of st.6. Absorption coefficient a_{300} ranged between 0.58-5.75 m^{-1} in the upstream

region presenting no significant variation among samplings. Contrary though to DOC, in the Maliakos Gulf absorption coefficients fell to slightly lower values than those found in the river, with the exception of the sampling of April 2014 where a_{300} presented comparable values between riverine and marine samples. The overall range of a_{300} in the Maliakos Gulf was 0.74-1.52 m^{-1}.

The distribution of carbon specific absorption coefficients a^*_{300} ranging from 1.32 to 6.14 m^2g^{-1} (figure 8.4a) shows clearly that the riverine samples (sts 1-7) are characterized by significantly elevated a^*_{300}values than the marine ones (Mann-Whitney Test, P=0.000). The highest values of a^*_{300} were observed during March at station 6 and at the uppermost station 1, located near the springs. In the Maliakos Gulf, a^*_{300} presented overall more uniform values compared to the river with a range of 0.53-1.24 m^2g^{-1}. The distribution of $S_{275-295}$ (figure 8.4b) is the exact opposite of a^*_{300} distribution. Beside the minor differences in the a_{300} values between Spechios River and Maliakos Gulf, spectral slope presented significantly lower values in the river compared to the gulf (Mann-Whitney Test, P=0.000). The recorded slope values in Sperchios River were constantly lower than 0.02 nm^{-1}fluctuating between 0.0104-0.0183 nm^{-1} with exception station 5 during April reaching S=0.0215 nm^{-1}. $S_{275-295}$ values in the Maliakos Gulf ranged between 0.0215-0.0315 nm^{-1}.

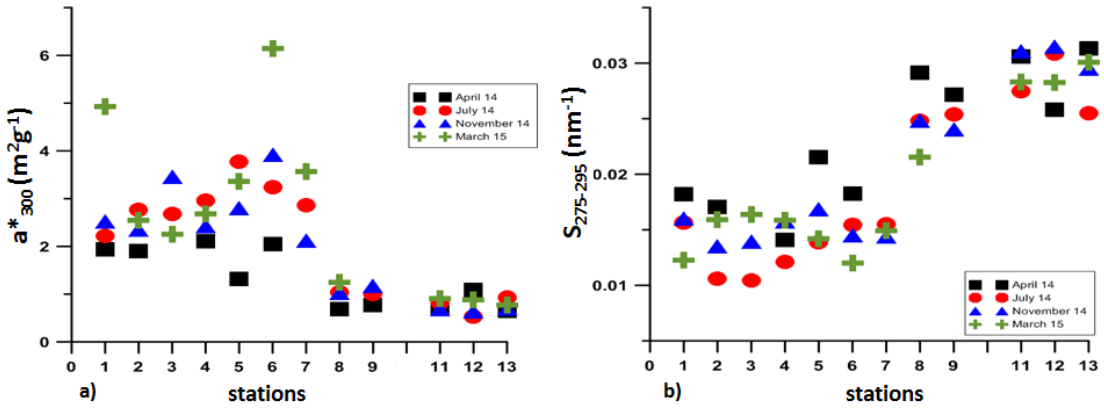

Figure 8.4: Distribution of a) a^*_{300} and b) $S_{275-295}$ along Sperchios R. and Maliakos G.

6.3.4 Fluorescence characteristics during April 2014

Six fluorescence peaks were identified in the Sperchios River and Maliakos Gulf during April 2014 (Table 8.4). Three peaks presented excitation and emission maxima that correspond to the humic – like peaks A, M and C

established by Coble [124][125]. Two peaks presented emission maxima at lower wavelengths resembling the protein – like peaks T and B [124][125]. The sixth peak exhibited excitation and emission maxima that fall between the humic – like peak M and the protein – like peak T and could be characterized as a blue shifted peak M, named hereafter as peak M´.

Table 8.4: Fluorescent peaks. First line excitation wavelength, second line emission wavelength, third line intensity. U.S.= upper Sperchios, sts 1-5. MG=Maliakos Gulf.

	Peak A	***Peak M***	***Peak C***	***Peak M´***	***Peak T***	***Peak B***
U.S.	260 448 0.071- 0.084	315-325 418-426 0.040- 0.048	335-355 436-446 0.036- 0.039	295 348 0.053- 0.054	275-280 330-348 0.025- 0.044	
St.6	260 450 0.306	325 426 0.208	350 446 0.185		280 350 0.203	
St.7	260 452 0.190	320 426 0.107	345 444 0.091		280 346 0.068	
MG 8-9	255-260 446 0.046- 0.047	300-305 426 0.022	340 444-448 0.017- 0.018		275-280 334-348 0.031- 0.035	275 310-312 0.028- 0.031
MG 11-13	255-260 446-452 0.037- 0.043	295-305 418-420 0.020- 0.025	320-340 430-444 0.015- 0.020		275-280 332-344 0.031- 0.036	275 310-312 0.026- 0.035

Figure 8.5 presents the EEMs of the samples of the Sperchios River (sts 1-5) and the delta (sts 6-7) as well as a sample representative of the Maliakos Gulf (st.13). At station 1 the humic-like peaks A, M and C were identified presenting the highest intensities among the pristine samples (sts 1-5). The protein-like peak T was also apparent presenting though lower intensity than the humic-like peaks. At stations 2 and 4 (figure 8.5 b,c) a strong signal of peak M´ appeared, ranging second after peak A, that somehow masks peak T. Nevertheless peak T at stations 2 and 4 holds a stronger signal than at

station 1. At station 5 (figure 8.5d) peak M´disappears and a more clear print of peak T is evident.

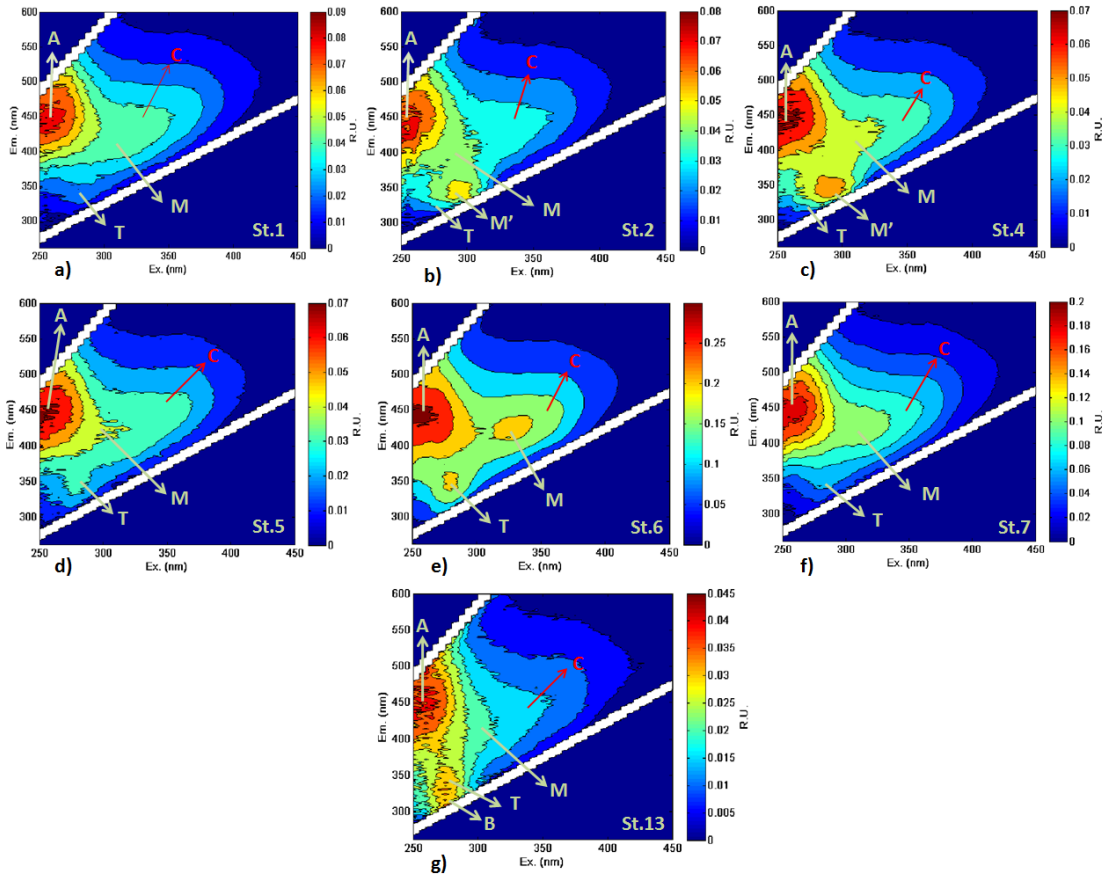

Figure 8.5: EEMs obtained in Sperchios River (a,b,c,d), delta (e) and Maliakos Gulf (f).

At station 6 located near the wastewater treatment plant the same peaks with stations 1 and 5 (A, C, M, T) were found presenting however remarkably increased intensities. At Sperchios delta, station 7 (figure 8.5e), revealed also the same peaks with intensities lower than those of station 6 but remaining higher than the intensities of the pristine stations (sts 1-5). In the Maliakos Gulf peaks A, C, M and T were identified in all samples along with an additional protein-like peak, peak B (figure 6.5f). All the marine samples revealed the same order of intensities: A>T>B>M>C.

Figure 8.6 presents the overall distribution of the humic-like components (figure 8.6a) and the protein-like components (figure 8.6b) along the Sperchios River, delta and Maliakos Gulf. It is apparent that the upstream part of the river (sts 1-5) exhibits higher intensities of all the humic-like components compared to the Maliakos Gulf. Contrary peak T presented

similar values at the riverine (sts 1-5) and marine samples (sts 8-13) with exception the uppermost station 1 where it showed the overall lowest intensity.

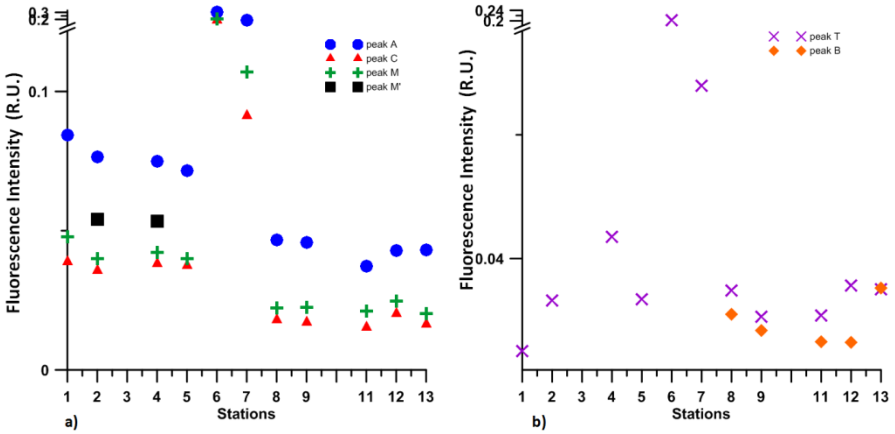

Figure 8.6: Fluorescent components distribution along Sperchios R and Maliakos G.

Figure 8.7 illustrates the HIX distribution along Sperchios River and Maliakos Gulf. The overall highest HIX value was observed at the delta station 7. Excluding station 7, HIX reveals a gradual decrease from the uppermost station 1 towards the most distant station of the Maliakos Gulf (st.13)

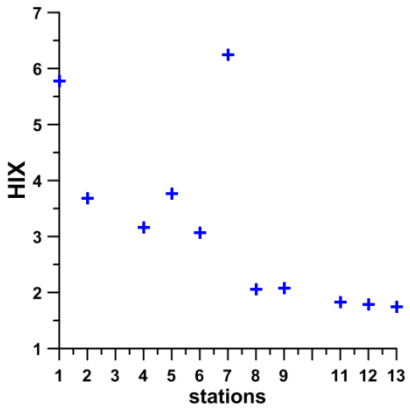

Figure 8.7: HIX distribution along Sperchios R. and Maliakos G.

8.4 Discussion

In the pristine region of the river basin (upstream from station 6) DOC and absorption coefficients a_{300} were strongly positively correlated (Figure 8.8) exhibiting a regression coefficient of R^2=0.884 (P<0.001). This strong relationship indicates that CDOM is a major fraction of DOC in Sperchios

River while the equation of the relationship (a_{300}=0.031*DOC+0.09) reveals that approximately the entire DOC pool consists of absorbing material.

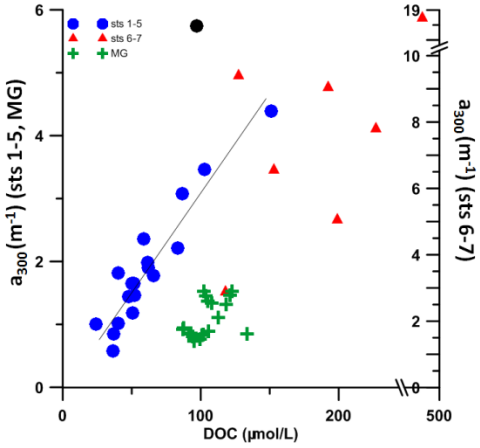

Figure 8.8: Relationship between DOC and CDOM in Sperchios R. and Maliakos G (blue dots=sts 1-5, red triangle=sts 6-7, green cross=MG).

One point (black dot) shows a positive deviation from the linearity presenting an excess in CDOM. This point represents the uppermost station 1 during March 2015 indicating that CDOM holds the greatest fraction of DOM in spring of 2015 near the springs possibly due to terrestrial inputs through snowmelt. The relationship between DOC and a_{300} at stations 6 and 7 (located closed to the delta) is more scattered indicating that CDOM is decoupled from the bulk DOM at the delta. This decoupling as well as the overall higher DOC and a_{300} values recorded at stations 6 and 7 during all samplings compared to the upstream stations could be the result of the different hydrological conditions at the delta which result in an accumulation of CDOM and DOC and/or of the influence of the waste water treatment plant at station 6. In figure 8.7 it is clear that at this group of samples (sts 6, 7) a point deviates greatly from the rest samples reaching DOC concentration of 483 µmol/L and absorption coefficient of 18.7 m^{-1}. These high values encountered during July 2014 are more likely a consequence of the influence of the wastewater treatment plant. This could be due either to a more significant wastewater discharge in July 2014 or to the limited river flow during summer resulting to insufficient dilution of wastewater. Contrary, the more moderate increases recorded at the delta during the other samplings could be also explained by the accumulation of CDOM in the delta resulting from both the transportation from upstream river as well as the enhanced primary production in the more stagnant waters of

the delta. The samples from Maliakos Gulf presented the lowest variability in both DOC and CDOM, probably due to the fast dispersion of the riverine water [292] but no relationship is apparent between these two pools. DOC concentrations in the Maliakos Gulf were higher than those of the upstream river but (sts 1-5) lower than the delta values. This reveals that the high DOC concentrations of the delta do not persist in the Maliakos Gulf probably due to mixing with the water of the gulf but still remain higher than the values found in the river. In contrast, the absorption coefficients found in Maliakos Gulf were slightly lower than the river. Consequently, an accumulation of DOC seems to occur in the Maliakos Gulf that is though of lower CDOM content.

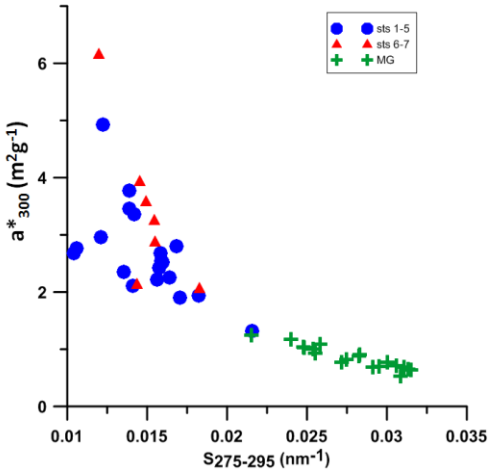

Figure 8.9: Relationship between spectral slope and carbon specific absorption coefficient in Sperchios R. and Maliakos G.

Figure 8.9 illustrates the distribution of carbon specific absorption coefficient a^*_{300} along the spectral slope gradient in the river, delta and Maliakos Gulf. It is apparent that there is an overall exponential decrease of a^*_{300} with increasing spectral slope. In this case, the samples of stations 6 and 7 do not deviate from the upstream samples as they fall in the same group presenting high a^*_{300} values and low spectral slopes, both indicative of HMW and aromatic DOM [118][120]. However the significant increase of a^*_{300} observed from station 1 up to station 6 (except during April 2014) (figure 8.4a) indicates an increase in CDOM content in the bulk DOC along the river and also possible increase of the aromatic character of CDOM. Futhermore the fluctuation of spectral slope in these stations (figure 8.4b), presenting no consistent trend, evidence continuous changes in CDOM quality indicating

transformation processes and/or different sources and sinks along the river. Contrary the samples of the Maliakos Gulf form a distinct group presenting lower carbon specific absorption coefficients and higher spectral slopes. These optical characteristics illustrate that beside the almost equal a_{300} values in Sperchios River and Maliakos Gulf, the nature of CDOM is clearly different. In the Maliakos Gulf the a^*_{300} and spectral slope values are indicative of marine CDOM characterized by lower MW and less aromatic substances while the high spectral slopes also indicate more photodegrated CDOM. Nevertheless, the continuum between the river-delta samples and the samples from the Maliakos Gulf evident at figure 8.8 suggests that CDOM in the Maliakos Gulf is at least partly attributed to the mixing with the receiving riverine water.

The results of the fluorescence analysis during April 2014 provide additional information about the nature of DOM along the Sperchios River, delta and Maliakos Gulf. The highest humic – like intensities found at the uppermost station 1 coupled with the very low intensity of peak T are indicative of the dominance of terrestrial DOM near the springs. Contrary the strong signal of peak M´ found at stations 2 and 4, where also peak T presented increased intensities, and the persistence of peak T at station 5, illustrate the presence of a combination of substances of either protein – like nature or associated to biological activity at the downward route of the river. Peak M has been linked to biological activity while it was also reported in wastewaters, wetland and agricultural environments [66]. Parlanti et al., [300] reported a blue shift in the fluorescence of peak M during spring in freshwater and coastal environments with the concurrent presence of protein-like peaks. The presence of these peaks was attributed to biological activity while they argued the possibility of peak T being the precursor of the substances responsible for the blue shift of peak M. Blue shift generally occurs when a molecule is less aromatic and contains more carboxylic groups and sugars [137] and therefore the release of less complex compounds through biological activity and the interaction between them is expected to cause a blue shift in the marine humics fluorescence. Peaks A, M, C and T have been reported in Sperchios River during July 2008 (301) along with peak B, in both the freshwater end-member

and closed to the delta. In the same study (301) a sampling site influenced by runoff from a paper factory was included which demonstrated significantly different fluorescence signal presenting two intense peaks with excitation and emission maxima of 280/430nm and 330/430nm. These two peaks are characteristics of Fluorescent Whitening Agents (FWA), compounds added during paper manufacturing. In our study however, the area influenced by the runoff from the paper factory was not included in the sampled transect. Moreover the downstream part of the river basin has been characterized as a zone of potentially high pollution pressures due to the agricultural and industrial activities [301]. Fluorescence analysis in our study did not identify any fluorescence peaks related to industrial activity and anthropogenic pollution at the downstream part of Sperchios River, such as peaks found in Sperchios River during 2008 (301) or Evros River during 2008-2010 (peak P ex/em 300/460nm, Tzortziou et al., [129]). Station 6 located closed to the discharge of the wastewater treatment plant presented natural fluorescence peaks of aquatic DOM which coincide with those found in the upstream stations, with significantly though higher intensities (Figure 8.6). Figure 8.10 shows the ratios of both the protein-like peak T and the LMW humic-like peak M with the HMW humic-like peak A along the river and the gulf.

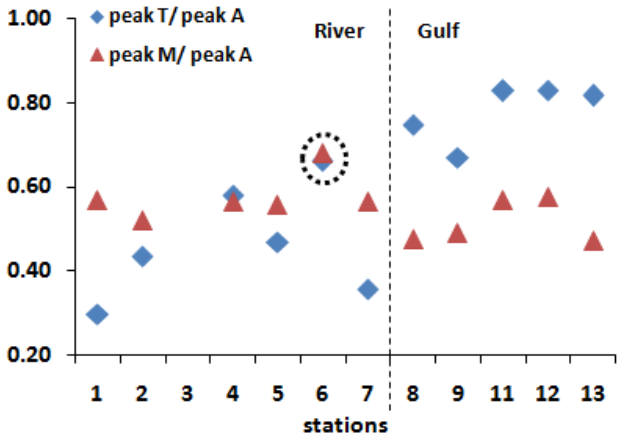

Figure 8.10: Distribution of ratio of the intensities between peaks T, M and peak A along Sperchios R. and the Maliakos G.

Station 6 presents the highest ratio of both pairs in the riverine and delta samples (sts 1-7) indicating a more significant increase of the intensities of peaks T and M relative to peak A at this station. Peak M has been identified in wastewaters [66] while increased intensities of peak T have been previously

reported at areas influenced by sewage [129][303] and have been attributed to the presence of microbially derived DOM in the sewage. The results from fluorescence analysis could therefore indicate that the runoff from the wastewater treatment plant introduce in the river a more significant load of protein-like and low MW humic substances shifting the composition and character of the riverine CDOM to a less aromatic and of lower MW.

In the Maliakos Gulf (sts 8-13) the presence of peak B reveals the occurrence of more degraded peptide material in contrast to peak T that is more representative of intact proteins [133]. It seems that in the river basin the input or release of fresh protein material possibly of biological production [66][98][142] dominates while in the Maliakos Gulf the concurrent presence of peaks T and B suggest the occurrence of notable degradation processes of protein substances. Increase of tyrosine – like peak (peak B) in the estuaries has been observed in previous studies [284]. On the other hand, peak B beside representative of degraded peptides is also a good indicator of low molecular weight polyphenolic structures [214][[304] originating from the soils, forested watershed and litterfall and was reported in many rivers and coastal areas [129][211][305]. Furthermore, peak T in Maliakos Gulf revealed overall comparable intensities with the river while the humic – like components showed lower intensities resulting to increased ratios of peak T/ peak A in the Maliakos Gulf (figure 8.10). This divergence in the distributions of the humic and the protein – like substances illustrate the terrestrial character of the humic like fluorescence in the river and the dilution of these compounds in the estuary that contrasts to the more autochthonous character of the protein – like substances. The higher intensities of the humic-like components in the river are in agreement with the higher a^*_{300} values and lower spectral slope indicative of HMW and aromatic DOM. Likewise, the decreasing distribution of HIX index along the sampled transect (with exception station 7) evidences the highest terrestrial character of the upper part of the river (st1) that gradually decreases reaching the lowest value at station 13 in the Maliakos Gulf. The overall highest HIX value recorded in the delta (st.7) indicates a faster degradation of the biolabile protein material and/or a more significant input of humic substances in the rivers delta. What is interesting in the Maliakos Gulf

is the higher intensities of peak A over the protein-like components even at station 13 located ~14km of the delta. Contrary, dominance of the peaks T and B has been reported in other Mediterranean coastal regions as in Evros coastal area [129] and the Gulf of Lion [211]. The predominance of the intensities of peak A could be due to the limited water exchange of Maliakos Gulf with the Aegean Sea and the Euboic Gulf resulting to the preservation of more terrestrial character compared to open coastal areas.

Data on the absorption and fluorescence properties of CDOM from Mediterranean rivers are available only for Evros River (Greece) [129], Rhone River (France) [211] and Arno River (Italy) [215] (Table 8.5). The DOC and a_{300} values in the Sperchios River (upstream station 6) were considerably lower than the values found in those rivers. The carbon specific absorption coefficients and slope values of Sperchios River were however comparable indicating that qualitative the DOM of Sperchios river do not deviate significantly from the recorded data of the Mediterranean rivers. In the Maliakos Gulf on the other hand both DOC and absorption coefficients were comparable with the values found in other European estuaries and coastal waters (Table 8.5). The absorption indices, specific absorption coefficient and absorption spectra slope, fell also in the range of the other estuaries and coastal waters indicating that contrary to DOM in the Sperchios River, DOM in the Maliakos Gulf is similar both quantitatively as well as qualitatively to CDOM in other coastal regions.

Table 8.5: Salinity, DOC and absorption properties in Mediterranean rivers.

Study Area		***Salinity***	***DOC (μmol/L)***	***a (m^{-1})***	***a* (m^2g^{-1})***	***S (nm^{-1})***	***Source***
North Aegean Sea	Evros River Upstream	<1	188-309	a_{300} 5.49-9.88	a^*_{300} 2.24-3.77	S 0.0160-0.0186	[129]
	Coastal Water	4.7-37.9	127-294	a_{300} 0.85-11.73	a^*_{300} 0.53-3.78	S 0.0165-0.0301	[129]
Gulf of	Rhone	Fresh-	136 ±38	a_{350}		S	[211]

Lions	River	Water		2.42 ±1.05		0.0170 ±0.001	
	Rhone Estuary	37.7-37.9	74-78	a_{350} 0.25-0.33		S 0.017-0.019	[211]
North Tyrrhenian Sea	Arno River	9	322				[305]
	Arno River	1.5	365 ±0.6	a_{280} 24.18 a_{355} 7.02		$S_{275-295}$ 0.014	[215]
	Arno coastal	38.5	67 ±1	a_{280} 1.26 a_{355} 0.3		$S_{275-295}$ 0.025	[215]
	Arno River Estuary	4.9-10.9	279-402	a_{280} 16.80-21.60 a_{355} 4.10-5.18	a^*_{280} 4.48-5.02 a^*_{355} 1.07-1.22	S 0.0166-0.0169	[214]
	Coastal Water	35.2-36	85-99	a_{280} 1.28-2.46 a_{355} 0.19-0.57	a^*_{280} 1.20-2.26 a^*_{355} 0.17-0.47	S 0.0114-0.0256	[214]
This study	Sperchios Sts 1-5	<1	24-151	a_{280} 0.92-7.44 a_{300} 0.58-5.75 a_{350} <D.L.-3.0	a^*_{280} 2.11-6.38 a^*_{300} 1.32-4.93 a^*_{350} 0.56-2.58	S 0.0121-0.0229 $S_{275-295}$ 0.0104-0.0216	

			a_{355} <D.L.-2.82	a^*_{355} 0.46-2.42	
Maliakos Gulf	27.7-36.75	87-134	a_{280} 1.41-2.51 a_{300} 0.74-1.52 a_{350} 0.21-0.77 a_{355} 0.21-0.74	a^*_{280} 0.98-2.05 a^*_{300} 0.53-1.24 a^*_{350} 0.18-0.63 a^*_{355} 0.18-0.60	S 0.0135-0.0236 $S_{275-295}$ 0.0149-0.0315

8.5 Conclusions

Our results indicate that the information gained from the analysis of both CDOM (a_{300}, a^*_{300}, spectral slope) and FDOM (fluorescence intensities, HIX) can clearly distinguish riverine from marine waters and give qualitative insights into the nature of the optically active DOM. DOC and CDOM were strongly correlated in the Sperchios River (upstream st.6) with an almost 0 intercept on the liner regression, suggesting that almost all of the DOC in the upper part of the river is colored. The fluorescence analysis revealed the high humic character of the DOM in the upper part of the river (st1) that declines towards the river delta. The protein-like signal was very low near the springs (st1) but at the middle part of the river a strong signal of protein-like and microbialy derived substances was apparent indicating release of fresh material and microbial transformations. The lower part of the river and the delta (sts 6-7) appears to hold the overall highest DOC concentrations and CDOM and FDOM content. Contrary to the freshwater segment of the river, DOC and CDOM are decoupled in the delta. This indicates different inputs

and alteration processes acting on DOC and CDOM in the more stagnant waters of the delta as well as the possible influence of the discharge of the wastewater treatment plant located at station 6. No fluorescence peaks characteristic of industrial or anthropogenic pollution were identified in the downstream section of Sperchios River, the highest though ratios of peak T/ peak A and peak M/ peak A at station 6 indicate an increase of the protein-like and LMW humic-like fluorescence relative to the HMW humic-like fluorescence which could be associated to the sewage discharge. An accumulation of DOC in the Maliakos Gulf compared to the river was observed but the absorption indices (a_{300}, a^*_{300}, slope) revealed that this DOM holds lower content in CDOM and is of lower MW and less aromatic. Fluorescence analysis revealed the presence of an additional protein-like peak (peak B) in the Maliakos Gulf representative of more altered protein-like substances, indicating a greater effect of degradation of protein material in the Maliakos Gulf. The humic-like components were overall decreased compared to the river and delta illustrating a less terrestrial character. Peak A retained however the highest intensities showing the significant influence of rivers in the FDOM pool of regions with limited water exchange with open sea such the Maliakos Gulf.

CHAPTER 9
EXPERIMENTAL OBSERVATION

9.1 Objective of the study

In the literature there is a lot of discussion regarding the optical properties of dissolved organic substances produced through biotic processes in the marine environments. As discussed in Chapter 2 there is a debate whether CDOM can be directly released through phytoplanktonic organisms or if the bacterial intervention is responsible for the production of CDOM. Here, we present two experiments conducted with macroalgae and zooplankton in an attempt to investigate autochthonous CDOM production.

9.2 Macroalgae Experiment

9.2.1 Experimental procedure

Macroalgae, red algae (jania, figure 9.1) were collected from the sub-littoral environment of Mavro Lithari coast at Anavyssos, Greece, and carried at the laboratory stored in seawater.

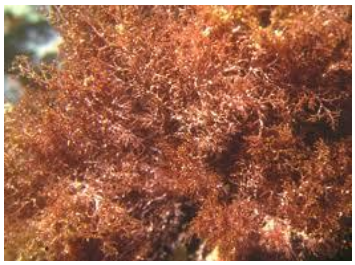

Figure 9.1: Reg macroalgae, jania.

At the laboratory macroalgae (48.6 g) were rinsed well with 0.22μm filtered seawater. Then they were added in transluscent Nalgene bottles filled with 2L of 0.22 μm filtered seawater and incubated for 24 hours at T=18˚C (sea temperature during sampling) under a 12h/12h photo cycle. The purpose of the incubation was the release of CDOM from the macroalgae. By the end of the incubation period, the water from the Nalgene bottles (2L) was filtered through 0.22 μm and the filtrate was added in a 10L Nalgene bottle along with 3L of seawater filtered through 0.8μm, in order to provide a bacterial inoculum

and filled up with 5L of 0.22 μm filtered seawater. A control sample was also prepared by mixing 3L of 0.8μm filtered seawater and 7L of 0.22 μm filtered seawater. Then each sample (macroalgae and control) was split in five bottles. The first bottle was filtered within the first hour and samples were taken for dissolved oxygen concentration (D.O.), DOC and CDOM analysis. The rest of the bottles were incubated in the dark and were filtered and sampled in specific time intervals. DOC and CDOM analysis were performed as described in Chapter 4 while D.O. was estimated using the Winkler method [306]. The sampling time intervals are given in Table 9.1.

Table 9.1: Sampling times and measured values of D.O., DOC and absorption indices in macroalgae samples (MS) and control samples (CS).

Time	*Sample*	*D.O. (ml/L)*	*DOC (μmol/L)*	α_{300} (m^{-1})	$S_{275-295}$ (nm^{-1})	α^*_{300} $(m^2\ g^{-1})$
1h	MS	5.10	104	1.30	0.0187	1.05
	CS	5.36	85	0.56	0.0281	0.54
15h	MS	5.05	98	1.13	0.0199	0.96
	CS	5.32	84	0.47	0.0285	0.46
21h	MS	4.90	98	1.11	0.0204	0.95
	CS	5.32	82	0.54	0.0258	0.55
3days	MS	4.91	92	1.06	0.0217	0.97
	CS	5.13	82	0.59	0.0269	0.60
5days	MS	4.72	99	1.01	0.0215	0.85
	CS	5.15	91	0.50	0.0263	0.46

9.2.2 Results

The results of DOC and absorption analysis are given in Table 9.1. Figure 9.1 illustrates the distribution of D.O., DOC, a_{300}, $S_{275-295}$, and a^*_{300} during the experiment in both control (CS) and macroalgae samples (MS). The MS presented lower D.O oxygen levels compared to CS with a clear decreasing trend indicating higher microbial activity. DOC presented notable higher concentrations at the beginning of the experiment in the MS (104 μmol/L) compared to CS (85 μmol/L) indicating the release of DOM during the incubation of the macroalgae (19 μmol/L excess DOC) which corresponds to

approximately 0.4 μmol/L DOC per 1g of macroalgae. A clear decreasing trend of DOC was observed in the MS up to day 3 while during the last day, day 5, an increase was observed. The CS presented a less pronounced decrease from the beginning of the experiment up to day 3, while an increase was also observed during day 5. This could indicate a contamination during the filtration and collection of DOC samples during day 5.

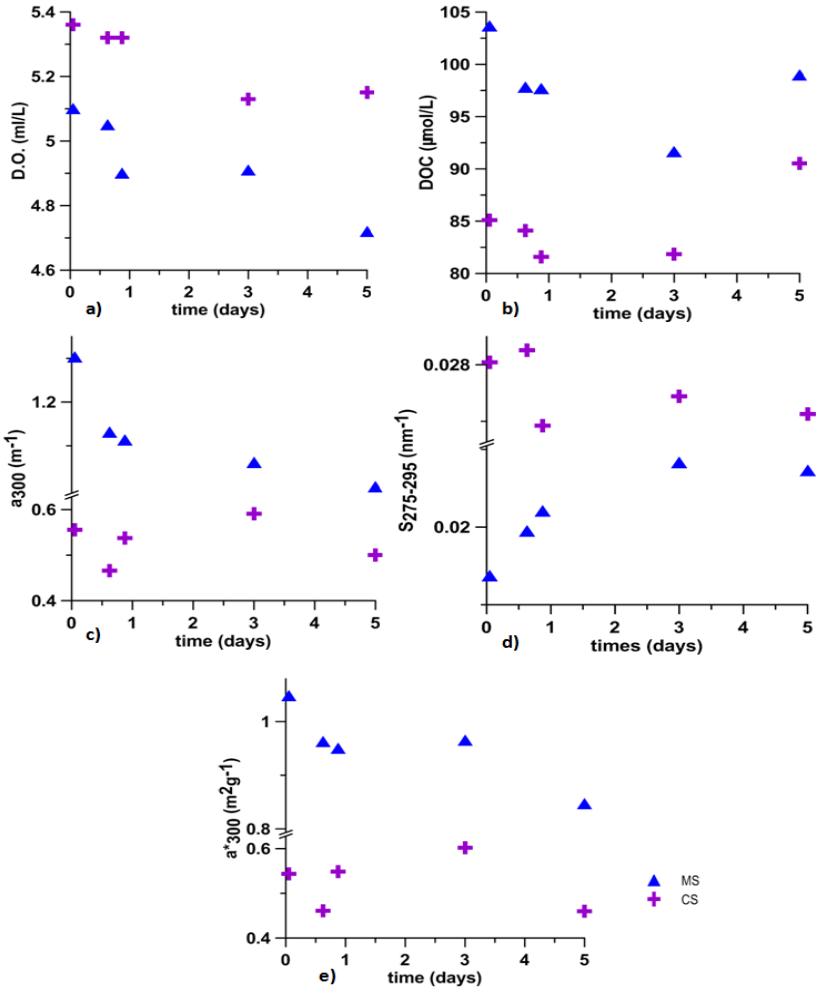

Figure 9.2 : a) D.O. (ml/L), b) DOC (μmol/L), c) a_{300} (m^{-1}), d) $S_{275-295}$ (nm^{-1}) and e) a^*_{300} (m^2g^{-1}) distribution during the experiment.

The absorption coefficient a_{300} also presented significantly higher values at the beginning in the MS (1.30 m^{-1}) compared to the CS (0.56 m^{-1}) indicating that a fraction of the released DOM (~20 μmo/L DOC) is optically active. Moreover there is an obvious divergence of the a_{300} distribution in the MS and CS as the MS presented a clear decreasing trend throughout the experiment while in the CS a_{300} coefficients were found uniform. This indicates that CDOM released from macroalgae is more susceptible to microbial

mineralization than CDOM present in the CS. It is also apparent that the more significant decrease in the a_{300} in the MS was during the first hours of the experiment indicating a very labile character of a fraction of the released CDOM. The spectral slope $S_{275-295}$, at the beginning of the experiment presented lower values in the MS (0.0187 nm^{-1}) compared to the CS (0.0281 nm^{-1}) indicating CDOM of different nature in the two samples. The lower $S_{275-295}$ values in the MS are indicative of fresh CDOM [118]. During the experiment the slope increased in the MS in the three first days and remained constant up to day 5. Contrary in the CS slope presented lower values after day 1 remaining though clearly higher than the MS sample. The increase of absorption slope in the MS indicates transformation processes acting on CDOM. Finally the carbon specific absorption coefficient a^*_{300} presented significantly higher values in the MS (0.85-1.05 m^2g^{-1}) compared to the CS (0.46-0.60 m^2g^{-1}) indicating high contribution of CDOM in the released DOM from the macroalgae. In the MS a^*_{300} presented a decreasing trend along the experiment indicating a faster removal of CDOM compared to the bulk DOC, while CS presented uniform values.

9.3 Zooplankton Experiment

9.3.1 Experimental Procedure

Zooplankton (figure 9.2) was collected from the sea from the surface up to 10m (2.2g), rinsed with 0.22 μm filtered seawater, added immediately in translucent nalgene bottles filled with 2L of 0.22 μm filtered seawater and incubated for 24 hours at T=15˚C (sea temperature during the sampling) under a 12h/12h photo cycle.

Figure 9.3: Zooplankton (after filtration).

Upon the incubation, the water was filtered through 0.22 μm and the filtrate was added in a 10L nalgene bottle along with 3L of seawater filtered through 0.8μm in order to provide a bacterial inoculum and filled with 5L of 0.22 μm filtered seawater. A control sample was also prepared by mixing 3L of 0.8 μm filtered seawater and 7L of 0.22 μm filtered seawater. Then each sample (zooplankton and control) was split in seven bottles. The first bottle was filtered within the first hour and samples were taken for DOC and CDOM analysis. The rest of the bottles were incubated in the dark and were filtered and sampled in specific time intervals. In Table 9.2 are summarized the results of the measurements for the various sampling intervals.

Table 9.2: Sampling times and measured values of D.O., DOC and absorption indices in zooplankton samples (ZS) and control samples (CS).

Time	*Sample*	*DOC (μmol/L)*	α_{300} (m^{-1})	$S_{275-295}$ (nm^{-1})	α^*_{300} ($m^2\ g^{-1}$)
1h	ZS	96	1.29	0.0208	1.12
	CS	79	0.69	0.0229	1.09
6h	ZS	70	0.91	0.0229	1.09
	CS	65	0.67	0.0266	0.86
1day	ZS	66	0.77	0.0243	0.98
	CS	64	0.58	0.0269	0.75
2days	ZS	68	0.63	0.0253	0.77
	CS	66	0.52	0.0292	0.66
5days	ZS	63	0.64	0.0262	0.85
	CS	63	0.59	0.0263	0.75
7days	ZS	58	0.60	0.0270	0.86
	CS	60	0.59	0.0270	0.82
14days	ZS	62	0.69	0.0224	0.93
	CS	65	0.51	0.0298	0.65

9.3.2 Results

Figure 10.2 illustrates the distribution of DOC, a_{300}, $S_{275-295}$, and a^*_{300} during the experiment in both control samples (CS) and zooplankton samples (ZS). DOC in the ZS presented higher value (96 μmol/L) at the initial measurement

compared to CS (79 μmol/L) indicating the release of DOM from zooplankton during the incubation (17 μmol/L of excess DOC) which corresponds to approximately 8 μmol/L DOC per 1gr of zooplankton. A significant decrease in DOC concentrations was observed in the ZS within the first 6 hours while a more gradual decrease followed up to day 7. A parallel decrease was also observed in the CS so that DOC concentrations in the two samples were almost equal by day 1. This was not observed at the experiment with the macroalgae as higher DOC values persisted in the MS up to day 5. Absorption coefficient a_{300} in the ZS presented two times higher value (1.29 m^{-1}) at initial sampling compared to the CS (0.69 m^{-1}) indicating the direct release of CDOM during the incubation of zooplankton. A decreasing trend was also observed in a_{300} values but only up to day 2 preserving at the same time higher values than the CS. During days 5 and 7 a_{300} coefficients reached similar values in the two samples. Absorption slope $S_{275-295}$ during the first two days was lower in the ZS than the CS indicating freshly released CDOM. In both samples the lowest values were recorded at the beginning of the experiment gradually increasing towards the end of the experiment. During days 5 and 7 the two samples presented similar values as slope in the ZS kept increasing indicating the transformation processes, in a lower rate though, while in the CS the slope decreased.

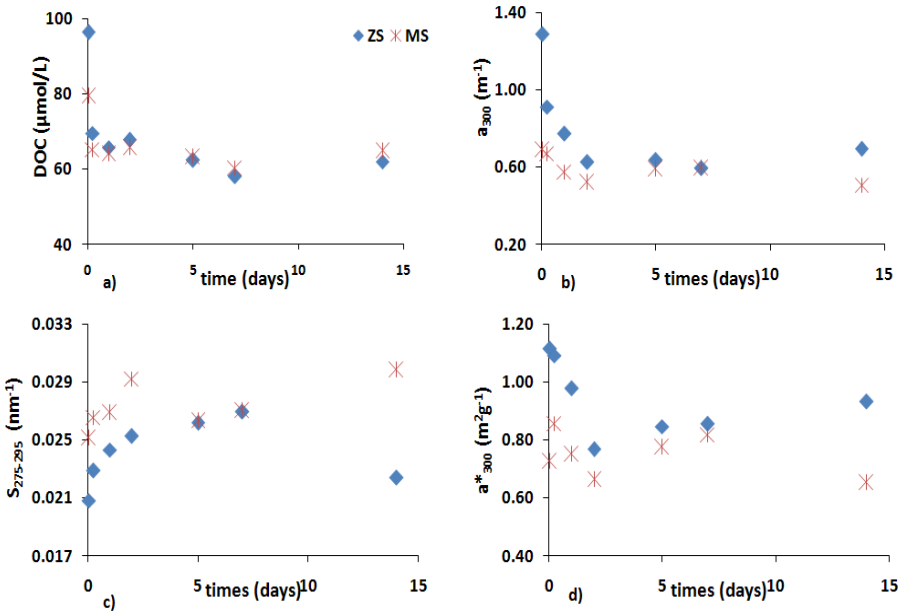

Figure 9.4 : a) D.O. (ml/L), b) DOC (μmol/L), c) a_{300} (m^{-1}), d) $S_{275-295}$ (nm^{-1}) and a^*_{300} (m^2g^{-1}) distribution during the experiment.

The absorption specific coefficient a^*_{300} presented higher values in the ZS throughout the experiment indicating a constant higher CDOM fraction in the bulk DOC in the ZS. In the ZS the highest value was observed at the beginning of the experiment decreasing up to day 2 while days 5 and 7 presented elevated values. The CS on the other hand presented more constant values. During the last day of the experiment, day 14, ZS presented somehow elevated values of both DOC and a_{300} compared to day 7 while the slope was significantly decreased. The CS presented also elevated DOC values but a_{300} was decreased while slope was increased. Due to the fact that there are no data available beyond day 14 we cannot conclude if there is indeed an increase in CDOM in ZS that could be linked to microbial activity.

9.4 Conclusions

These results indicate the direct release of DOC and CDOM from both macroalgae and zooplankton. Zooplankton appears to release more DOC (8 μmol/L DOC per 1gr) than the macroalgae (0.4 μmol/L DOC per 1gr) during incubation. The greater though decrease in DOC concentrations at the zooplankton experiment reaching the values of the control sample by day 1 may indicate that DOM released by zooplankton is more susceptible to microbial degradation than DOM from macroalgae. In the macroalgae experiment CDOM decreased along time with a concurrent increase of the slope while the carbon specific absorption coefficient showed that the CDOM content in the bulk DOC also decreased. Despite though these transformations, a_{300} in the MS retained higher values compared to the CS after the 5 days of incubation while the absorption slope also retained lower values and the a^*_{300} higher. This could indicate that CDOM released from macroalgae is comprised of substances of different lability. The abrupt decrease in a_{300} within the first hours indicates that a very biolabile fraction exists with turnover times of hours. This is in agreement with the characterization of the major fraction of DOM released by living organisms in the sea as very labile with turnover times of hours to days [15]. The persistence though of relatively high a_{300} values in the MS (two times higher than the CS) after the five days indicates either that a fraction of the released CDOM is more persistent to biodegradation or there is a concurrent

production of CDOM through the bacterial activity. Contrary CDOM released by zooplankton appeared to be consumed in total by day 5 indicating that is constituted by only very labile substances. The fact that CDOM contrary to DOC in ZS retained higher values than the control up to day 2 and moreover stopped decreasing after that day while DOC kept decreasing up to day 7 may suggest that CDOM released by zooplankton is either more resistant to microbial remineralization than the non absorbing released substances of DOC (e.g. the bio-labile carbohydrates) or that during the microbial activity there is also a release of CDOM parallel to consumption. Nevertheless, the results from the two experiments indicate that absorption could be a better tracer of the release and transformation of DOM than the DOC since the differences between the macroalgae/zooplankton and control sample were more evident in the absorption indices. CDOM indices can furthermore give quality information according the released CDOM and the transformation processes along the bacteria utilization.

CHAPTER 10

SYNOPSIS OF THE RESULTS AND CONCLUSION

Here we summarize the results of CDOM properties of all the regions examined in the present study. In figure 10.1 are given the relationships of specific absorption coefficients a^*_{300} and spectral slopes $S_{275-295}$ in the identified water masses.

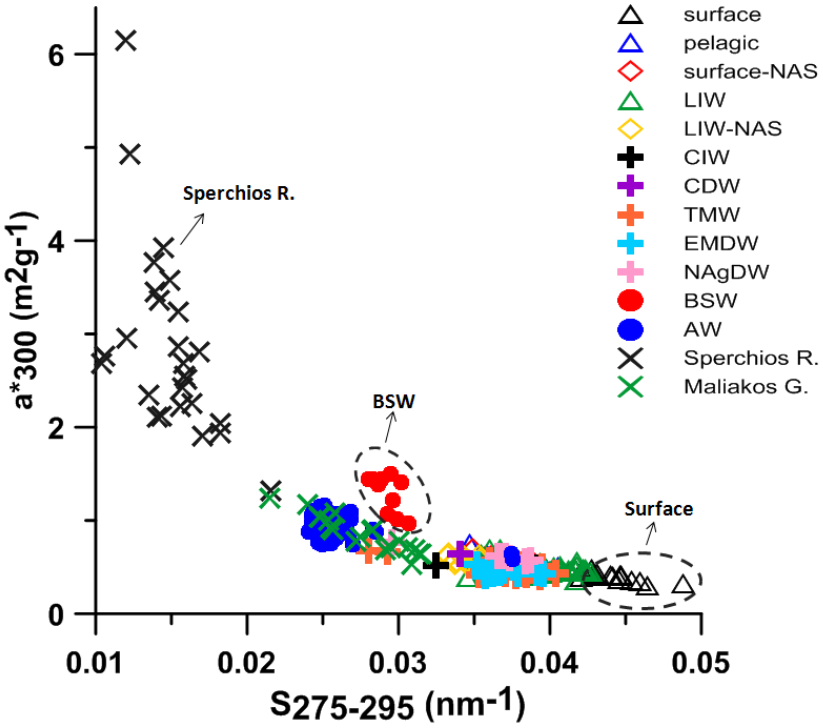

Figure 10.1: Relationships of a*300 and spectral slope in the examined aquatic environments.

Specific absorption coefficient a^*_{300} presents an exponential decreasing trend with increasing spectral slope from the riverine to to the surface samples of the Aegean Sea indicating a shift in the CDOM composition towards lower MW and less aromatic substances. Sperchios River reveals the highest a^*_{300} values and the lowest spectral slopes indicating that the overall higher MW and aromatic DOM among the studied aquatic environments is present in Sperchios River. Contrary the lowest a^*_{300} values and the highest spectral slopes are found in the surface (0- 30m) of the Aegean Sea indicating the impact of photodegradation. The samples of the Maliakos Gulf present as expected a^*_{300} values and spectral slopes between the riverine and marine

samples of the Aegean Sea indicating mixIing features between the fresh and the marine water and the degradation processes of CDOM in the gulf. The samples from the AW underlying water mass of the Marmara Sea and the surface, pelagic and LIW water of the Aegean Sea also fall well along the decreasing line between Sperchios River and the surface waters of the Aegean Sea. Contrary the samples of the BSW of the Marmara Sea clearly deviate positively from the general trend presenting elevated a^*_{300} values with a very narrow spectral slope range. This illustrates the different CDOM dynamics in the BSW that result in higher content of the bulk DOC in CDOM compared to the other studied marine environments. BSW also presented lower spectral slope values compared to the Aegean Sea. Both indices point to HMW aromatic CDOM which is representative of the more significant terrestrial content of BSW as discussed in Chapter 7. BSW is characterized however by higher spectral slope values compared to the underlying AW which illustrate the effect of photodegradation. In figure 10.1 is also obvious that the spectral slopes of the samples from BSW and AW are relatively constant presenting a very narrow range. Contrary Sperchios River and Maliakos Gulf reveal a wide range of spectral slopes. This indicates that CDOM in BSW and AW is more homogeneous compared to the river and the gulf. As discussed in Chapter 5 the production and transformation processes of CDOM through enhanced primary production and microbial activity seems to be a major factor in CDOM dynamics in the eutrophic BSW contributing to a more constant character of DOM. The optical characteristics of the AW mass (low and consistent slopes and elevated a^*_{300} values) differentiate from those of their source LIW waters of the NAS and result from the receiving POM from the overlying BSW as well as from the microbial induced humification processes (Chapter 5). Contrary in Sperchios River the great variability of CDOM sources and transformation processes along the river (Chapter 8) results in a wide range of spectral slopes while in the Maliakos Gulf the combined effects of the mixing and photodegradation seems also to result in variable spectral slopes.

Figure 10.2 presents only the samples from the Aegean Sea. A straight decreasing line can be distinguished connecting the samples from the LIW, pelagic (30-100m) and surface (0-30m) waters.

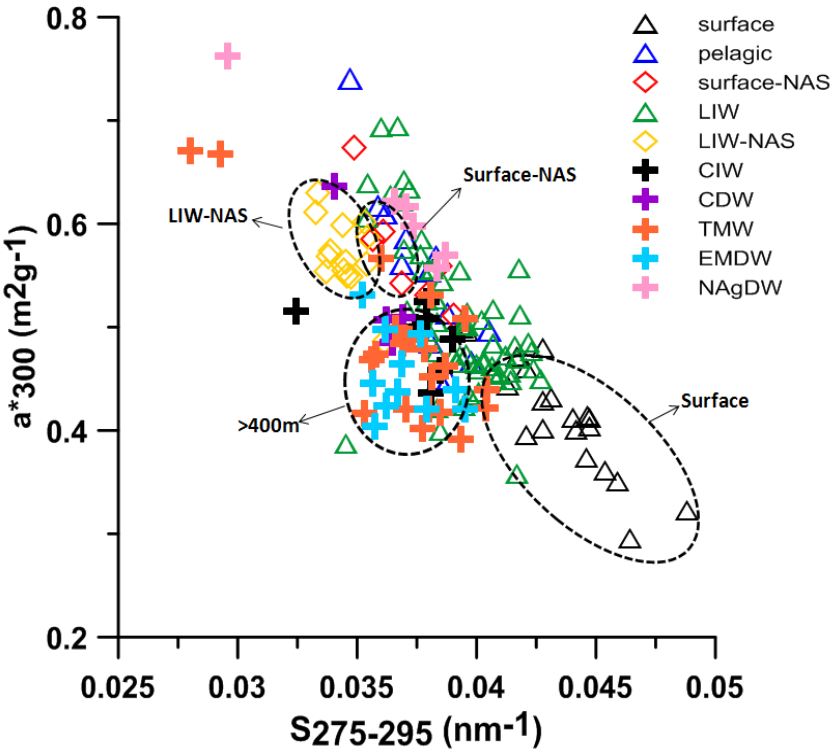

Figure 10.2: Relationships of a*300 and spectral slope in the Aegean Sea.

The surface samples of the North Aegean Sea that are influenced by the outflowing BSW (Chapter 6) clearly deviate from the bulk surface samples of the Aegean Sea presenting higher a^*_{300} and lower spectral slopes, representative of higher MW and aromatic CDOM. Also the samples of the LIW of these stations influenced by the BSW revealed lower slopes than the bulk LIW. This indicates the great influence of the rich in HMW CDOM BSW spreading in the optical properties of the NAS and CDOM composition that expands also to subsurface layers. The samples from the deeper waters, >400m, (CIW, TMW, CDW, EMDW, NAgDW) also deviate from the line presenting lower spectral slopes. The a^*_{300} values in these water masses retained higher values than the surface samples and were similar to the lower and intermediate values of the LIW. This indicates that in water masses unaffected from the solar radiation where the microbial activity is the main pathway of CDOM transformation and degradation, a higher CDOM background is maintained compared to the surface water. Photodegradation

appears to be the most efficient degradation process of CDOM while the increase of CDOM in deep waters indicates the existence of a refractory or semi-refractory fraction of CDOM that either is transferred there and/or is produced through microbial activity. This is of particular importance for the Eastern Mediterranean Sea where the deep vertical mixing and upwelling of deep waters is limited compared to the Western Mediterranean Sea, and therefore sequestration of CDOM in deep waters is expected.

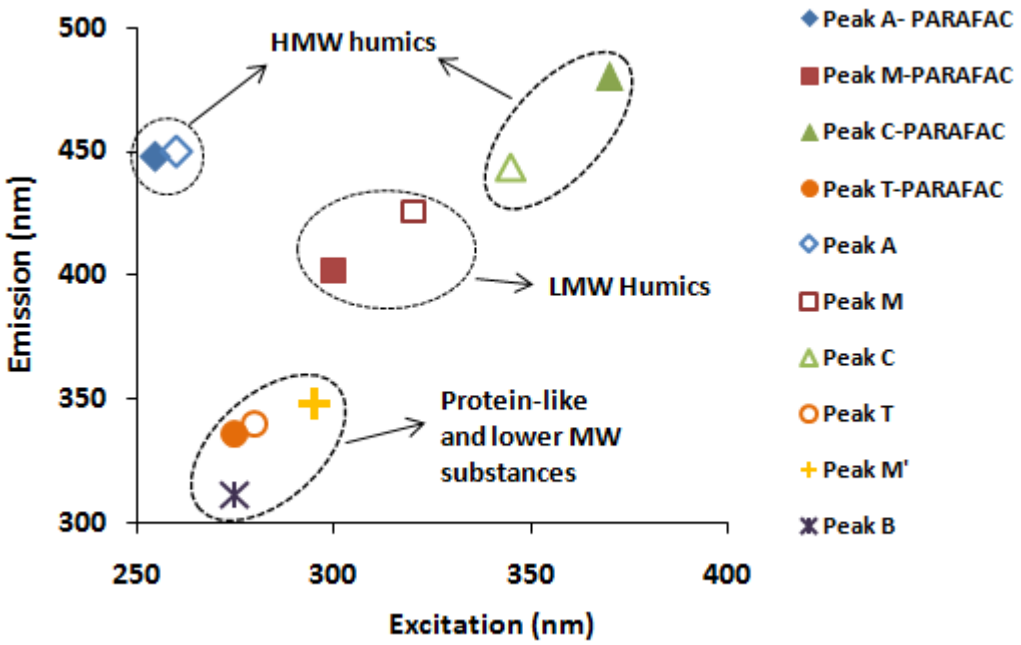

Figure 10.3: Fluorescent peaks identified in the examined aquatic environments.

Figure 10.3 summarizes the fluorescent peaks identified in the present study both through PARAFAC modelling (marine samples) as well as through 'peak-picking' method (Sperchios river and Maliakos Gulf). PARAFAC analysis identified the same components that represent common natural fluorescence peaks of the aquatic DOM, among the studied marine environments. A greater variability of components was observed in Sperchios River indicating shifts in DOM nature along the river. The primary terrestrial humic-like peak A and the protein-like peak T (tryptophan-like) found in the marine samples coincide almost completely with the respective peaks in the Sperchios River and Maliakos Gulf. This indicates the similarity of substances responsible for peak A and peak T in the marine and the riverine samples. Contrary peak C was

found to be red shifted in the marine samples compared to Sperchios River and Maliakos Gulf. A red shift generally appears with increasing MW, conjugation of aromatic compounds and oxidized forms. Peak C in the marine samples is the only peak that showed excitation wavelength longer than 350nm and emission wavelength longer than 450nm. At these long wavelengths absorption is due to the presence of oxidized forms of polyhydroxyl-aromatic substances (terrestrially derived such as lignin) that act as electron acceptors resulting to intramolecular charge-transfer interactions with electron donors (non oxidized forms of lignin or other terrestrial aromatic substances). Thus the absorption and emission of peak C at longer wavelength in the marine compared to the riverine samples is probably a result of the partial oxidation in the sea of the terrestrially derived substances. Contrary, in the river CDOM seems to be largely unaltered resulting to lower excitation and emission wavelengths. Peak M on the other hand was found to be red shifted in the Sperchios River and Maliakos Gulf compared to the marine samples. Peak M has been linked to biological activity and was considered to result from microbial processes as well as being directly released from marine phytoplankton. Peak M has been also widely reported in agricultural subcatchments and in wastewaters. The different excitation and emission wavelength of peak M between the riverine and marine samples indicates differences in the structure of the substances and possible different sources. The red shifted peak M in the riverine samples indicate higher MW and more aromatic substances that could be related to imports of agricultural and wastewater runoffs in the rivers basin. Contrary the marine samples indicate lower MW and less aromatic substances more related to microbial activity. The blue shifted peak M´ identified in the middle part of Sperchios River presents notable lower excitation wavelength than peak M identified in the river but almost the same excitation wavelength with peak M of the marine samples (λ=295nm for peak M´ and 300nm for marine peak M). The emission wavelength of peak M´ was significantly lower than both riverine and marine samples falling in the emission band of the protein-like peak T, it was however closer to marine rather than the riverine peak M. As discussed in Chapter 8 the blue shift in the emission of peak M could be due to the release of less complex compounds through biological activity and the interaction between

them. Peak B presenting the lower emission wavelength was identified only in Maliakos Gulf. Peak B representative of more degraded peptide material would be expected to be identified also in the sea. The fact that it was identified only in the Maliakos Gulf could indicate that these substances are better traced in estuarine and coastal environments under the freshwater influence. On the other hand, as discussed in Chapter 4 (section 4.4.3.2) the non identification of peak B in marine samples could resulted from the spectra handling in order to eliminate primary Rayleigh scatter.

A comparison among the intensities of the fluorescent components of Sperchios River and Maliakos Gulf and the intensities of the marine samples is not possible because the intensities of the marine samples are the outcome of the PARAFAC analysis. A comparison though among Marmaras Sea and Aegean Sea is valid. BSW presents notable higher intensities of all the identified components than the Aegean Sea which is probably associated with the significant terrestrial inputs and enhanced biological activity as already mentioned. Beside the very high intensities of all the components in the BSW, the humic-like fluorescence signal was higher than the protein-like. AW shows also higher humic-like intensities (peaks A,M,C) than the Aegean Sea resulting from the vertical transport of POC and DOM from the BSW as well as the microbial humification processes taking place in AW. Contrary AW presented very low protein-like intensities (peak T) reaching those of the deep layers of the Aegean Sea. In both Marmaras Sea and Aegean Sea these low intensities of the protein-like component are a result of microbial reminerilazation of DOM-CDOM evident by the high AOU values. In the Aegean Sea fluorescence analysis reveal the different fluorescence character of each water mass and gives qualitative information of the existing CDOM. A general trend of higher protein-like intensities at the surface decreasing towards the bottom was observed while the exact opposite was found for the humic-intensities. These trends evidence the bio-labile character of the protein-like substances and the photo-labile character of the humic-like components as well as the humification processes in deeper layers. Sperchios River and Maliakos presented a variety of fluorescent components. The humic signal was constantly elevated in both Sperchios River and Maliakos Gulf as

observed for the BSW, indicating the dominance of the terrestrial inputs and revealing a contrast of these aquatic environments and the surface of the Aegean Sea. However many peaks associated with biological activity were also observed in the Sperchios River and Maliakos Gulf.

10.1 Conclusion

This study provides information about the absorption and fluorescence properties of CDOM in various aquatic environments in Eastern Mediterranean Sea. It furthermore uses the results from these analyses in order to give insights regarding the composition and dynamics of CDOM. The continuum in the a^*_{300} *vs* spectral slope relationships between Sperchios River, Maliakos Gulf and the surface of the Aegean Sea indicates a gradual decrease in CDOM content and a shift to lower MW and aromatic character from the freshwater towards the coastal and marine environments. Contrary the deviation of BSW in the Marmaras Sea indicates different CDOM dynamics than the Aegean Sea that are probably a result of the eutrophic character of BSW and its higher terrestrial content. The North Aegean Sea has also the potential of showing distinct optical properties under the influence of the ouflowing BSW while in deep waters of the Aegean Sea the absence of the influence of solar radiation coupled with microbial transformations result to the preservation of semi-refractory CDOM. Fluorescence analysis revealed the dominance of commonly observed natural fluorescence peaks of aquatic DOM in all the studied aquatic environments. Sperchios River, Maliakos Gulf and BSW present higher humic-like fluorescence than protein-like indicating the impact of significant terrestrial inputs. Contrary, the surface of the Aegean Sea away from the direct terrestrial sources presented higher protein-like fluorescence. The deep waters of both Marmaras Sea and Aegean Sea are characterized by depletion of the labile protein-like substances but increased humic-like fluorescence. Fluorescence analysis also revealed the differences of peaks C and M among freshwater and marine environments that are due different sources and alteration processes.

ABBREVATIONS

DOM	Dissolved Organic Matter
DOC	Dissolved Organic Carbon
CDOM	Chromophoric Dissolved Organic Matter
FDOM	Fluorescence Dissolved Organic Matter
EEMs	Excitation Emission Matrices
PARAFAC	Parallel Factor Analysis
HIX	Humification Index
BIX	Biological Index
BSW	Black Sea Water
NAS	North Aegean Sea
LW/ LSW /LIW	Levantine Water/ Lev. Surface Wat., Lev. Intermediate Wat.
LDOC/ SLDOC	Labile DOC / Semi-labile DOC
SRDOC	Semi-refractory DOC
RDOC/ URDOC	Refractory DOC/ Ultra-refractory DOC
UV	Ultra violet radiation
MW/ LMW/ HMW	Molecular Weight/ Low MW / High MW
Chl-a	Chlorophyll a
AOU	Apparent Oxygen Utilization
C / I	Fluorescence Component / Intensity of fl. component
AgW	Aegean Water
CID/ CDW	Cretan intermediate Water/ Cretan Deep Water

TMW	Transitional Mediterranean Water
EMDW	Eatern Mediterranean Deep Water
NAgDW	North Aegean Deep Water
DON	Dissolved Organic Nitrogen
CS	Control Sample
MS	Macroalgae Sample
ZS	Zooplankton Sample
a_{300}	Absorption coefficient at 300nm
$S_{275-295}$	Spectral slope at region 275-295nm
a^*_{300}	Carbon specific absorption coefficient

REFERENCES

1. D.J. Repeta, Chemical Characterization and Cycling of Dissolved Organic Matter, *Biogeochemistry of Dissolved Organic Matter*, D.A. Hansell and C.A. Carlson, eds, 2nd ed. Elsevier, Burlington: Academic Press, 2015, pp. 22-58.

2. C.A. Carlson and D.A. Hansell, DOM sources, sinks, reactivity and budgets, *Biogeochemistry of Dissolved Organic Matter*, D.A. Hansell and C.A. Carlson, eds, 2nd ed. Elsevier, Burlington: Academic Press, 2015, pp. 66-109.

3. H. Ogawa and E. Tanoue, Dissolved organic matter in oceanic waters, *Journal of Oceanography*, 2003, vol. 59, pp. 129-147.

4. F. Azam, T. Frenchel, J.G. Field, J.S. Gray, L.A. Meyer-Reil and F. Thingstad, The ecological role of water-column microbes in the sea, *Marine Ecology Progress Series*, 1983, vol.10, pp. 257-263.

5. N. Jiao, G.J Herndl, D.A. Hansell, R. Benner, G. Kattner, S.W. Wilhelm, D.L. Kirchman, M.G. Weinbauer, T. Luo, F. Chen and F. Azam, Microbial production of recalcitrant dissolved organic matter: long-term carbon storage in the global ocean, *Nature*, 2010, vol.8, pp. 593-599.

6. H.W. Ducklow, D.A. Purdie, P.J.L Williams and J.M. Davies, Bacterioplankton: a sink for carbon in a coastal marine plankton community, *Science*, 1986, vol.232, pp. 865-867.

7. J.C. Goldman and M.R. Dennett, Growth of marine bacteria in batch and continuous culture under carbon and nitrogen limitation, *Limnology and Oceanography*, 2000, vol.45, pp. 789-800.

8. K. Mopper and D.J Kieber, Photochemistry and cycling of carbon, sulfur, nitrogen and phosphorus, *Biogeochemistry of Marine Dissolved Organic Matter*, D.A. Hansell, C.A., Carlson, eds., Academic Press, San Diego, 2002, pp. 455-507.

9. K., Mopper, X.L. Zhou, R.J Kieber, D.J Kieber, R.J. Sikorski, and R.D. Jones, Photochemical degradation of dissolved organic carbon and its impact on the oceanic carbon cycle, *Nature*, 1991, vol.353, pp. 60–62.

10. M.A. Moran and R.G. Zepp, Role of photoreactions in the formation of biologically labile compounds from dissolved organic matter, *Limnology and Oceanography*, 1997, vol.42, pp. 1307–1316.

11. A. Stubbins, G. Uher, C.S. Law, K. Mopper, C. Robinson and R.C. Upstill-Goddard, R.C., Open-ocean carbon monoxide photoproduction, *Deep-Sea Research II*, 2006, vol.53, pp. 1695–1705.

12. E.R.M. Druffel and P.M. Williams, Identification of deep marine source of particulate organic carbon using bomb 14C, *Nature*, 1990, vol.347, pp. 172–174.

13. E.R.M. Druffel, S. Griffin, J.E. Bauer, D.M. Wolgast, X.C. Wang, Distribution of particulate organic carbon and radiocarbon in the water column from the upper slope to the abyssal NE Pacific Ocean, *Deep-Sea Research II*, 1998, vol.45, pp. 667–687.

14. P. Verdugo, C. Carlson and S. Giovannoni, S., Marine microgels, *Annual Review of Marine Science*, 2012, vol.4, pp. 375–400.

15. D.A. Hansell, Recalcitrant dissolved organic carbon fractions, *Annual Review of Marine Science*, 2013, vol.5, pp. 421-445.

16. C.A. Carlson and H.W. Ducklow, Growth of bacterioplankton and consumption of dissolved organic carbon in the Sargasso Sea*, Aquatic Microbial Ecology*, 1996, vol.10, pp. 69–85.

17. H.W. Ducklow, The bacterial component of the oceanic euphotic zone, *FEMS Microbiology Ecology*, 1999, vol.30, pp. 1-10.

18. G.R. Harvey, D.A. Boran, L.A. Chesal, and J.M. Tokar, The structure of marine fulvic and humic acids, *Marine Chemistry*, 1983, vol.12, pp. 119-132.

19. D.J. Carlson, L.M. Mayer, M.L., Brann and T.H. Mague, Binding of monomeric organic compounds to macromolecular dissolced organic matter in seawater, *Marine Chemistry,* 1985, vol.16, pp.141-153.

20. D.L. Kirchman, D.L Henry, and D.C. Dexter, Adsorption of protein to surfaces in seawater, *Marine Chemistry*, 1989, vol.27, pp. 201–217.

21. T. Nagata and D.L. Kirchman, Bacterial degradation of protein adsorbed to model submicron particles in seawater, *Marine Ecology Progress Series*, 1996, vol.132, pp. 241–248.

22. R. Benner and B. Biddanda, Photochemical transformation of surface and deep marine dissolved organic matter: effects on bacterial growth, *Limnology and Oceanography*, 1998, vol.43, pp. 1373–1378.

23. L. Tranvik and S Kokalj, Decreased biodegradability of algal DOC due to interactive effects of UV radiation and humic matter, *Aquatic Microbial Ecology*, 1998, vol.14, pp. 301–307.

24. I. Obernosterer, B. Reitner and G.J Herndl, Contrasting effects of solar radiation on dissolved organic matter and its bioavailability to marine bacterioplankton, *Limnology and Oceanography*, 1991, vol.44, pp. 1645–1654.

25. R.M. Cory, K. McNeill, J.P Cotner, A. Amado, J. M. Purcell and A.G. Marshall, Singlet oxygen in the coupled photochemical and biochemical oxidation of dissolved organic matter, *Environmental Science and Technology*, 2010, vol.44, pp. 3683–3689.

26. T. Dittmar and J Paeng, 2009, A heat-induced molecular signature in marine dissolved organic matter, *Nature Geoscience*, 2009, vol.2, pp. 175–179.

27. L. Ziolkowski, E. Druffel, Aged black carbon identified in marine dissolved organic carbon, *Geophysical Research Letters*, 2010, vol.37, L16601.

28. A. Mannino and R.H. Harvey, Black carbon in estuarine and coastal ocean dissolved organic matter, *Limnology and Oceanography*, 2004, vol.49, pp. 735-740.

29. R. Jaffe, Y. Ding, J. Niggemann, A. V. Vahatalo, A. Stubbins, R.G.M. Spencer, J. Campbell and T. Dittmar, Global Charcoal Mobilization from Soils via Dissolution and Riverine Transport to the Oceans, *Science,* 2013, vol.340, pp. 345-347.

30. J.E. Brophy and D.J. Carlson, Production of biologically refractory dissolved organic carbon by natural seawater microbial populations, *Deep-Sea Research I*, 1989, vol.36, pp. 497–507.

31. L.J. Tranvik, E. Sherr and B.F Sherr, Uptake and utilization of 'colloidal DOM' by heterotrophic flagellates in seawater, *Marine Ecology Progress Series*, 1993, vol.92, pp. 301–309.

32. K. Stoderegger and G.J Herndl, Production and release of bacterial capsular material and its subsequent utilization by marine bacterioplankton, *Limnology and Oceanography*, 1998, vol. 43, pp. 877–884.

33. N. Jiao, G.J Herndl, D.A. Hansell, R. Benner, G. Kattner, S.W. Wilhelm, D.L. Kirchman, M.G. Weinbauer, T. Kuo, F. Chen and F. Azam, The microbial carbon pump and the oceanic recalcitrant dissolved organic matter pool, *Nature Reviews Microbiology*, 2011, vol.9, p.555.

34. J.J. Cole, S. Findlay and M.L. Pace, Bacterial production in fresh and saltwater ecosystems: a cross-system overview, *Marine Ecology Progress Series*, 1988, vol.43, pp. 1-10.

35. H.W. Ducklow and F. Shiah, Bacterial production in estuaries, *Aquatic Microbiology: An Ecological Approach*, T. Ford, ed., Blackwell Science, Cambridge,MA, 1993, pp. 261–288.

36. E. Tanoue, Detection of dissolved protein molecules in oceanic waters, *Marine Chemistry,* 1995, vol.51, pp. 239-252.

37. K. Kaiser, and R. Benner, Major bacterial contribution to the ocean reservoir of detrital organic carbon and nitrogen, *Limnology and Oceanography*, vol.53, pp. 99-112.

38. A. Heissenberber and G. J. Herndl, Formation of high molecular weight material be free-living marine bacteria, *Marine Ecology Progress Series*, 1994, vol. 111, pp.129-135.

39. H. Ogawa, Y. Amagai, I. Koike, K. Kaiser, and R. Benner, Production of refractory dissolved organic matter by bacteria, *Science*, 2001, vol.292, pp.917–920.

40. G.D. Kramer and G.J. Herndl., Photo- and bioreactivity of chromophoric dissolved organic matter produced by marine bacterioplankton, *Aquatic Microbial Ecology*, 2004, vol.36, pp. 239-246.

41. K. Shimotori, Y. Omori and T. Hama, Bacterial production of marine humic-like fluorescent dissolved organic matter and its biogeochemical importance, *Aquatic Microbial Ecology*, 2009, vol.58, pp. 55-66.

42. R. Benner and G. Herndl, Bacterially derived dissolved organic matter in the microbial carbon pump, *Microbial Carbon Pump in the Ocean*, N Jiao, F. Azam, S. Sanders, eds., Science/AAAS, Washington, DC, 2011, pp. 46–48.

43. J. Aristegui, S. Agusti and C.M. Duarte, Respiration in the dark ocean, *Geophysical Research Letter*, 2003, vol.30, 1041.

44. J.J Hung, S.M. Wang, Y.L. Chen, Biogeochemical controls on distributions and fluxes of dissolved and particulate organic carbon in the northern South China Sea, *Deep-Sea Research II*, 2007, vol. 54, pp. 1486–503.

45. C.A. Carlson, D.A. Hansell, N.B. Nelson, D.A. Siegel, W.M. Smethie, S. Khatiwala et al., 2010. Dissolved organic carbon export and subsequent remineralization in the mesopelagic and bathypelagic realms of the North Atlantic basin, *Deep-Sea Research II*, 2010, vol.57, pp. 1433–1445.

46. D.J. Kieber, J. McDaniel and K. Mopper, Photochemical source of biological substrates in sea water: implications for carbon cycling, *Nature*, 1989, vol.341, pp. 637–639.

47. P. Verdugo, P.H. Santschi, Polymer dynamics of DOC networks and gel formation in seawater, *Deep-Sea Research II*, 2010, vol. 57, pp.1486–93.

48. A. Engel, S. Thoms, U. Riabesell, E. Rochelle-Newall, and I. Zondervan, Polysaccharide aggregation as a potential sink of marine dissolved organic carbon, *Nature*, 2004, vol.428 pp.929–32.

49. P. Verdugo, A.L. Alldredge, F. Azam, D.L. Kirchman, U. Passow, and P.H. Santschi, The oceanic gel phase: a bridge in the DOM-POM continuum, *Marine Chemistry*, 2004, vol. 92, pp.67–85.

50. D.A. Hansell and C.A Carlson, Deep-ocean gradients in the concentration of dissolved organic carbon, *Nature,* 1998, vol.395, pp.263–66.

51. J. Aristegui, C.M. Duarte CM, S. Agusti S, M. Doval, X.A. Alvarez-Salgado and D.A. Hansell, Dissolved organic carbon support of respiration in the dark ocean, *Science*, 2002, vol.298 p. 1967.

52. Santinelli, L. Nannicini and A. Seritti, DOC dynamics in the meso and bathypelagic layers of the Mediterranean Sea, *Deep-Sea Research II*, 2010, vol.57, pp. 1446-1459.

53. P.A. Raymond and R.G.M. Spencer, Riverine DOM, *Biogeochemistry of Dissolved Organic Matter*, D.A. Hansell and C.A. Carlson, eds, 2nd ed. Elsevier, Burlington: Academic Press, 2015, pp. 509-525.

54. B.E. Longworth, S.T. Petsch, P.A. Raymond and J.E. Bauer, Linking lithology and land use to sources of dissolved and particulate organic matter in headwaters of a temperate, passive-margin river system, *Geochimica Cosmochimica Acta*, 2007, vol.71, pp. 4233–4250.

55. J.C. Neff, J.C. Finlay, S.A. Zimov, S.P. Davydov, J.J Carrasco, E.A.G. Schuur et al., Seasonal changes in the age and structure of dissolved organic carbon in Siberian rivers and streams, *Geophysical Research Letters*, 2006, vol. 33, L23401.

56. P.A. Raymond and N-h Oh, An empirical study of climatic controls on riverine c export from three major U.S. watersheds, *Global Biogeochemical Cycles*, 2007, vol.21, GB2022.

57. C.A. Masiello and E.R.M. Druffel, Carbon isotope geochemistry of the Santa Clara River, *Global Biogeochemical Cycles*, 2001, vol.15, pp.407–416.

58. X.A. Alvarez-Salgado and A.E.J. Miller, Dissolved organic carbon in a large macrotidal estuary (the Humber, UK): Behaviour during estuarine mixing, *Marine Pollution Bulletin*, 1998, vol.37, pp.216–224.

59. G. Abril, M. Nogueira, H. Etcheber, G. Cabeçadas, E. Lemaire, and M.J Brogueira, M.J, Behaviour of organic carbon in nine contrasting European estuaries, *Estuarine, Coastal and Shelf Science*, 2002, vol.54, pp. 241–262.

60. R. Benner and S. Opsahl, Molecular indicators of the sources and transformations of dissolved organic matter in the Mississippi River plume, *Organic Geochemistry*, 2001, vol.32, pp. 597–611.

61. P.J Hernes and R. Benner, Photochemical and microbial degradation of dissolved lignin phenols: implications for the fate of terrigenous dissolved organic matter in marine environments, *Journal of Geophysical Research Ocean*, 2003, vol.108, C9, 3291.

62. R.F. Chen and G.B Gardner, High-resolution measurements of chromophoric dissolved organic matter in the Mississippi and Atchafalaya River plume regions, *Marine Chemistry*, 2004, vol.89, pp. 103–125.

63. P.A. Raymond and C.S. Hopkinson, Ecosystem modulation of dissolved carbon age in a temperate marsh-dominated estuary, *Ecosystems,* 2003, vol.6, pp. 694–705.

64. R. Stepanauskas, L. Leonardson, and L.J. Tranvik, Bioavailability of wetland-derived DON to freshwater andmarine bacterioplankton, *Limnology and Oceanography*, 1999, vol,44, pp.1477–1485.

65. M, Sondergaard, C.A. Stedmon and N.H. Borch, Fate of terrigenous dissolved organic matter (DOM) in estuaries: aggregation and bioavailability, *Ophelia*, 2003, vol.57, pp.161–176.

66. J.B. Fellman, E. Hood and R.G.M. Spencer, Fluorescence spectroscopy opens new windows into dissolved organic matter dynamics in freshwater ecosystems: a review, *Limnology and Oceanography*, 2010, vol.55, pp.2452–2462.

67. K. Tockner, D. Pennetzdorfer, N. Reiner, F. Schiemer, and J.V. Ward, Hydrological connectivity, and the exchange of organic matter and nutrients in a dynamic river-floodplainsystem (Danube, Austria), *Freshwater Biology*, 1999, vol.41, pp. 521–535.

68. M. Tzortziou, P.J. Neale, J.P. Megonigal, C.L. Powa and M. Butterworth, Spatial gradients in dissolved carbon due to tidal marsh outwelling into a Chesapeake Bay estuary, *Marine Ecology Progress Series*, 2011, vol.426, pp.41–56.

69. C.J. Mann and R.G. Wetzel, Dissolved organic carbon and its utilization in a riverine wetland ecosystem, *Biogeochemistry*, 1995, vol.31, pp. 99–120.

70. M.A. Moran and R.E. Hodson, Dissolved humic substances of vascular plant-origin in a coastal marine-environment, *Limnology and Oceanography*, 1994, vol.39, pp. 762–771.

71. Franke, M.W. Hamilton and S.E. Ziegler, Variation in the photochemical lability of dissolved organic matter in a large boreal watershed, *Aquatic Science*, 2012, vol.74, pp.751–768.

72. M.F. Adame and C.E. Lovelock, Carbon and nutrient exchange of mangrove forests with the coastal ocean, *Hydrobiologia,* 2011, vol.663, pp. 23–50.

73. T. Dittmar, N. Hertkorn, G. Kattner and R.J Lara 2006. Mangroves, a major source of dissolved organic carbon to the oceans, *Global Biogeochemical Cycles*, vol.20, GB1012.

74. R. Lauerwald, J. Hartmann, W. Ludwig, and N. Moosdorf, Assessing the nonconservative fluvial fluxes of dissolved organic carbon in North America. *Journal of Geophysical Research*, 2012, vol.117, G01027.

75. R. Lauerwald, G.G. Laruelle, J. Hatmann, P Ciais et P.A.G. Regnier, Spatial patterns in CO2 evasion from the global river network, *Global Biogeochemical Cycles*, 2015, vol.29, pp. 534-554.

76. J.B. Fellman, E. Hood, E., R.T. Edwards, and D.V. D'Amore, Changes in the concentration, biodegradability, and fluorescent properties of dissolved organic matter during stormflows in coastal temperate watersheds, *Journal of Geophysical Research*, 2009, vol. 114, G01021.

77. E.M. White, D.J. Kieber, J. Sherrard, W.L. Miller and K. Mopper, Carbon dioxide and carbon monoxide photoproduction quantum yields in the Delaware estuary, *Marine Chemistry*, 2010, vol.118, pp.11–21.

78. Stubbins, C.S. Law, G. Uher and R.C Upstill-Goddard, Carbon monoxide apparent quantum yields and photoproduction in the Tyne estuary, *Biogeosciences*, 2011, vol.8, pp.703–713.

79. M.A. Moran, W.M. Sheldon and R.G. Zepp, Carbon loss and optical property changes during long-term photochemical and biological degradation of estuarine dissolved organic matter, *Limnology and Oceanography*, 2000, vol.45, pp.1254–1264.

80. S.P. Opsahl and R.G Zepp, Photochemically-induced alteration of stable carbon isotope ratios (delta C-13) in terrigenous dissolved organic carbon, *Geophysical Research Letters*, 2001, vol.28, pp. 2417–2420.

81. Stubbins, R.G.M. Spencer, H. Chen, PG. Hatcher, K. Mopper, P.J Herneset al., 2010, Illuminated darkness: molecular signatures of Congo river dissolved organic matter and its photochemical alteration as revealed by ultrahigh precision mass spectrometry, *Limnology and Oceanography*, 2010, vol.55, pp.1467–1477.

82. S. Kim, L.A. Kaplan, and P.G Hatcher, Biodegradable dissolved organic matter in a temperate and a tropical stream determined from ultra-high resolution mass spectrometry, *Limnology and Oceanography*, 2006, vol.51, pp.1054–1063.

83. K Kalle, Zum problem der meerwasserfarbe, Ann.Hydrol. Mar mitteilungen, 1938, vol.66, pp. 1–13.

84. R. W. P. M. Laane and L. Koole, The relation between fluorescence and dissolved organic carbon in the Ems-Dollert estuary and the western Wadden Sea, *Netherlands Journal of Sea Research*, 1982, vol.15, pp. 217-227.

85. P.G Coble, Marine optical biogeochemistry: the chemistry of ocean color, *Chemical Reviews*, 2007, vol. 107, pp. 402-418.

86. J.T.O Kirk, *Light and Photosynthesis in Aquatic Ecosystems*, Second Edition, Cambridge Univ. Press, 1994.

87. D.A. Siegel and A.F. Michaels, Quantification of non-algal light attenuation in the Sargasso Sea: Implications for biogeochemistry and remote sensing, *Deep Sea Research II*, 1996, vol.43, pp. 321 – 345.

88. N.B. Nelson, D.A. Siegel and A.F. Michaels, Seasonal dynamics of colored dissolved material in the Sargasso Sea, *Deep Sea Research I*, 1998, vol.45, pp. 931 – 957.

89. K. Arrigo, and C. Brown, Impact of chromophoric dissolved organic matter on UV inhibition of primary productivity in the sea, *Marine Ecology Progress Series*, 1996, vol.140, pp. 207–216.

90. W.L Miller and R.G. Zepp, Photochemical production of dissolved inorganic carbon from terrestrial organic matter: significance to the oceanic organic carbon cycle, *Geophysical Research Letters*, 1995, vol.22, pp. 417–420.

91. M.A. Moran and R. G. Zepp, UV radiation effects on microbes and microbial processes, *Microbial ecology of the oceans*, D.L. Kirchman and R. Mitchell, eds, Wiley, 2000, pp. 201–228.

92. R.G. Zepp, Environmental photoprocesses involving natural organic matter, *Humic substances and their role in the environment*, F.H. Frimmel and R.F. Christman, eds, Wiley, 1998, pp. 193–214.

93. S. Tassan, The effect of dissolved “yellow substance” on the quantitative retrieval ofchlorophyll and total suspended sediment concentrations from remote measurements of water colour, *Remote Sensing*, 1988, vol.9, pp. 787–797.

94. F.E. Hoge, M.E. Williams, R.N. Swift, J.K. Yungel and A. Vodacek, Satellite retrieval of the absorption coefficient of chromophoric dissolved organic matter in continental margins, *Journal of Geophysical Research*, 1995, vol.100, issue24, pp. 847–854.

95. D.A. Siegel, S. Maritorena, N.B. Nelson, M.J. Behrenfeld and C.R. McClain, Colored dissolved organic matter and its influence on the satellite-based characterization of the ocean biosphere, *Geophysical Research Letters*, 2005, vol.32, L20605.

96. R.W.P.M. Laane and K.J.M Kramer, Natural fluorescence in the North Sea and its major estuaries, *Netherlands Journal of Sea Research*, 1990, vol.26, pp. 1–9.

97. M.M De Souza-Sierra, O.F.X. Donard and Lamotte, Spectral identification and behaviour of dissolved organic fluorescent material during estuarine mixing processes, *Marine Chemistry*, 1997, vol.58, pp. 51-58.

98. K., Mopper, and C. A. Schultz, Fluorescence as a possible tool for studying the nature and water column distribution of DOC components, *Marine Chemistry*, 1993, vol.41, pp.229 – 238.

99. P.G. Coble, Characterization of marine and terrestrial DOM in seawater using excitation-emission matrix spectroscopy, *Marine Chemistry*, 1996, vol.51, pp. 325–346.

100. Baker and R.G.M. Spencer, Characterization of dissolved organic matter from source to sea using fluorescence and absorbance spectroscopy, *Science of the Total Environment*, 2004, vol.333, pp. 217-232.

101. F.E. Hoge and P.E. Lyon, New tools for the study of oceanic eddies: satellite derived inherent optical properties, *Remote Sensing of Environment*, 2005, vol.95, pp. 444–452.

102. N.B Nelson, D.A. Siegel, C.A. Carlson, C. Swan, C., W.M. Jr. Smethie, S. Khatiwala, Hydrography of chromophoric dissolved organic matter in the North Atlantic, *Deep-Sea Research I*, 2007, vol.54, pp. 710–731.

103. C. Swan, D. Siegel, N. Nelson, C. Carlson, and E. Nasir, Biogeochemical and hydrographic controls on chromophoric dissolved organic matter distribution in the Pacific Ocean, *Deep-Sea Research I*, 2009, vol.56, pp. 2175–2192.

104. A. Morel and L. Prieur, Analysis of variations in ocean color, *Limnology and Oceanography*, 1971, vol.22, pp. 709-722.

105. B Wozniak and J Dera, The interaction of light with organic molecules present in sea water: physical principles, *Light Absorption in Sea Water*, L.A. Mysak and K. Hamilton, eds, Springer Science+Business Media, LLC, New York, 2007, pp.82-110.

106. D.A. Skoog, D.M. West, F.J Holler and S.R. Crouch, Molecular Absoprion Spectrometry, *Fundamentals of Analytical Chemisrty*,Brools/Cole, Cengage Learning, 9th edition, 2014, pp. 722-760.

107. R. Del Vecchio and N. V Blough, On the origin of the optical properties of humic substances, Environment Science and technology, 2004, vol.38, pp. 3885-3891.

108. E.S. Boyle, N. Gueriero, A. Thiallet, R. Del Vecchio and N.V Blough, Optical properties of humic substances and CDOM: Relation to structure, *Environment Science and Technology*, 2009, vol.43, pp. 2262-2268.

109. A.A. Andrew, R. Del Vecchio, A. Subramaniam, N.V Blough, Chromophoric dissolved organic matter (CDOM) in the Equatorial Atlantic Ocean: Optical properties and their relation to CDOM structure and source*, Marine Chemistry*, 2013, vol. 148, pp.33-43.

110. A. Bricaud, A. Morel and L.Prieur, Absorption by dissolved organic matter of the sea (yellow substances) in the UV and visible domains, *Limnology and Oceanography*, 1981, vol.26, pp.43-53.

111. C.A. Stedmon and N.B. Nelson, The optical properties of DOM in the Ocean, *Biogeochemistry of Dissolved Organic Matter*, D.A. Hansell and C.A. Carlson, eds, 2nd ed. Elsevier, Burlington: Academic Press, 2015, pp. 481-503.

112. N.L Blough and R. Del Vecchio, Chromophoric DOM in coastal environment, *Biogeochemistry of marine dissolved organic matter*, D.A. Hansell, C.A Carlson, eds. Academic., 2002, pp. 509-546.

113. A. Vodacek, N.V Blough, M.D DeGrandpre, E.T Peltzer and R.K Nelson, Seasonal variation of CDOM and DOC in the Middle Atlantic Bight: Terrestrial inputs and photooxidation, *Limnology and Oceanography*, 1997, vol.42, pp.674-686.

114. S.A. Green and N.V. Blough, N.V., Optical absorption and fluorescence properties of chromophoric dissolved organic matter in natural waters*, Limnology and Oceanography*, 1994, vol.39, pp.1903–1916.

115. S.A Floge, M.L Wells, Variation in colloidal chromophoric dissolved organic matter in the Damariscotta Estuary, *Limnology and Oceanography*, 2007, vol.52, pp. 32–45.

116. C. Ortega-Retuerta, T.K. Frazer, C.M Duarte, S. Ruiz-halpern, A. Tovar-sa, J.M Arrieta et al., Biogeneration of chromophoric dissolved organic matter by bacteria and krill in the Southern Ocean, *Limnology and Oceanography*, 2009, vol.54, pp. 1941–1950.

117. Y. Yamashita, J.N Boyer and R. Jaffe, Evaluating the distribution of terrestrial dissolved organic matter in a complex coastal ecosystem using fluorescence spectroscopy*, Continental Shelf Research*, 2013, vol.66, pp.136-144.

118. J.R. Helms, A. Stubbins, J.D. Ritchie, E.C. Minor, D.J Kieber and K Mopper, Absorption spectral slopes and slope ratios as indicators of molecular weight, source, and photobleaching of chromophoric dissolved organic matter, *Limnology and Oceanography*, 2008, vol.53, pp. 955–969.

119. C. Guéguen and C.W. Cuss, Characterization of aquatic dissolved organic matter by asymmetrical flow fieldflow fractionation coupled to UV-visible diode array and excitation emission matrix fluorescence, *Journal of Chromatography A*, 2011, vol.1218, pp.4188–4198.

120. Y-P. Chin, G. Alken and E. O'Loughlin, Molecular Weigh, Polydispersity and Spectroscopic Properties of Aquatic Humic Substances, *Environment, Science and Technology*, 1994, vol.28, pp. 1853-1858.

121. C.L. Gueguen, G.D. Wang, N. Tanaka and C.C. Hung, Chemical characteristics and origin of dissolved organic matter in the Yukon River, *Biogeochemistry*, 2006, vol.77, pp. 139-155.

123. Kalle, Fluoreszenz und Gelbstoff im Bottnischen und Finnischen Meerbusen, Dtsch. Hydrogr. Z., 1949, vol.2, pp. 117-124.

124. P.G. Coble, S.A. Green, N.V. Blough and R.B. Gagosian, Characterisation of dissolved organic matter in the Black Sea by fluorescence spectroscopy, *Nature*, 1990, vol.348, pp. 432-435.

125. P.G. Coble, C.E. Del Castillo and B. Avril, Distribution and optical of CDOM in the Arabian Sea during the 1995 Southwest Monsoon, *Deep-Sea Research II*, 1998, vol.45, pp. 2195–2223.

126. Huguet, L. Vacher, S. Relexans, S. Saubusse, J.M. Froidefond and E. Perlanti, Properties of fluorescent dissolved organic matter in the Gironde Estuary, *Organic Geochemistry*, 2009, vol.40, pp. 706-719.

127. J. E. Birdwell and A.S. Engel, Characterization of dissolved organic matter in cave and spring waters using UV–Vis absorbance and fluorescence spectroscopy, *Organic Geochemistr*y, 2010, vol. 41, pp. 270-280.

128. P. Kowalczuk, G.H. Tilstone, M. Zabłocka, R. Röttgers, and R. Thomas, Composition of dissolved organic matter along an Atlantic Meridional Transect from fluorescence spectroscopy and Parallel Factor Analysis, *Marine Chemistry*, 2013, vol.157, pp. 170–184.

129. M.Tzortziou, C. Zeri, E. Dimitriou, Y. Ding, R. Jaffe, E. Anagnostou, E.Pitta and A. Mentzafou, Colored dissolved organic matter dynamics and anthropogenic influences in a major transboundary river and its coastal wetland, *Limnology and Oceanography*, 2015, vol. 60, issue 4, pp. 1222-1240.

130. Y. Yamashita and E.Tanoue, Chemical characterization of protein-like fluorophores in DOM in relation to aromatic amino acids, *Marine Chemistry*, 2003, vol.82, pp. 255–271.

131. R.M. Cory and D. M. McKnight, Fluorescence spectroscopy reveals ubiquitous presence of oxidized and reduced quinines in dissolved organic matter, *Environment Science and Technology*, 2005, vol.39, pp.5142–8149.

132. Maie, N.M., Scully, O. Pisani, R. Jaffé, Composition of a protein-like fluorophore of dissolved organic matter in coastal wetland and estuarine ecosystems, *Water Research*, 2007, vol.41, pp.563–570.

133. Y. Yamashita and E. Tanoue, Chemical characteristics of amino acid-containing dissolved organic matter in seawater, *Organic Geochemistry*, 2004, vol.35, pp. 679-692.

134. O.S. Wolfbeis, Fluorescence optical sensors in analytical chemistry, *Trends in Analytical Chemistry*, 1985, vol.4, issue, 7, pp. 184–188.

135. J.R. Lakowicz, *Principles of Fluorescence Spectroscopy*, 3rd ed. Springer, New York, 2006.

136. J.R. Ertel, and J.I. Hedges, Bulk chemical and spectroscopic properties of marine and terrestrial humic acids, melanoidins and catecholbased synthetic polymers, *Aquatic and Terrestrial Humic Materials*, R.F. Christman and E.T. Gjessing eds, Ann Arbor Sci., Ann Arbor, Mich, 1983, pp. 143-163.

137. J.I. Hedges, P.G. Hathcer, J. R. Ertel and K.J. Meyers-Schulte, A comparison of dissolved humic substances from seawater with Amazon River counterparts by ^{13}C-NMR spectrometry, *Geochimica et Cosmochimica Acta*, 1992, vol. 56, pp. 1753-1757.

138. C.A. Stedmon and S. Markager, Resolving the variability in dissolved organic matter fluorescence in a temperate estuary and its catchment using PARAFAC analysis. *Limnology and Oceanography*, 2005, vol.50(2), pp. 686-697.

139. K.R. Murphy, C.A. Stedmon, T.D. Waite and G.M. Ruiz, Distinguishing between terrestrial and autochthonous organic matter sources in marine environments using fluorescence spectroscopy, *Marine Chemistry*, 2008, vol. 108, pp. 40–58.

140. T. S. Catala, I. Reche, A. Fuentes-Lema, C. Romera-Castillo, M. Nieto-Cid, E. Ortega-Retuerta, E. Calvo, M. Alvarez, C. Marrase, C. A. Stedmon and X. A. Alvarez-Salgado, Turnover time of fluorescent dissolved organic matter in the dark global ocean, *Nature Communications*, 2015, 6, 5986.

141. D.A. Hansell, C.A. Carlson, D.J. Repeta, and R. Schlitzer, Dissolved organic matter in the ocean: new insights stimulated by a controversy, *Oceanography,* 2009, vol.22, pp. 52–61.

142. Y. Yamashita, R. Jaffe, N. Maie, and E. Tanoue, Assessing the dynamics of dissolved organic matter (DOM) in coastal environments by excitation and emission matrix fluorescence and parallel factor analysis (EEM-PARAFAC), *Limnology and Oceanography*, 2008, vol.53, pp. 1900–1908.

143. N.B. Nelson and D.A. Siegel, The global distribution and dynamics of Chromophoric Dissolved Organic Matter, *Annual Review of Marine Science*, 2013, vol.5, 447-476.

144. S. Opsahl and R. Benner, Distribution and cycling of terrigenous dissolved organic matter in the ocean, *Nature,* 1997, vol.386, pp. 480-482.

145. M.S. Twardowsky and P.L Donaghay, Separating in situ and terrigenous sources of absorption by dissolved materials in coastal waters, *Journal of Geophysical Research*, vol.106, pp. 2545-2560.

146. V. Kitidis, A.P. Stubbins, G. Uher, R.C Upstill Goddard, C.S. Law, and E.M.S. Woodward, Variability of chromophoric organic matter in surface waters of the Atlantic Ocean, *Deep Sea Research Part II*, 2006, vol.53, pp. 1666–1684.

147. C. Romera-Castillo, H. Sarmento, X.A. Álvarez-Salgado, J.M. Gasol and C. Marrase, Production of chromophoric dissolved organic matter by marine phytoplankton, *Limnology and Oceanography*, 2010, vol.55, pp. 446–454.

148. E.J. Rochelle-Newall and T.R. Fisher, Production of chromophoric dissolved organic matter fluorescence in marine and estuarine environments: an investigation into the role of phytoplankton, *Marine Chemistry*, 2002, vol.77, pp. 7–21.

149. N.B Nelson, C.A. Carlson and D.K. Steinberg, Production of chromophoric dissolved organic matter by Sargasso Sea microbes, *Marine Chemistry*, 2004, vol.89, 273–287.

150. C. Lonborg, K. Davidson, X.A. Alvarez-Salgado, Bioavailability and bacterial degradation rates of dissolved organic matter in a temperate coastal area during an annual cycle, *Marine Chemistry*, 2009, vol.113, pp. 219–226.

151. D. Organelli, A. Bricaud, D. Antoine and A. Matsuoka A., Seasonal dynamics of light absorption by chromophoric dissolved organic matter (CDOM) in the NW Mediterranean Sea (BOUSSOLE site), *Deep-Sea Research I*, 2014, vol.91, pp. 72-85.

152. X. Xing, H. Claustre, H. Wang, A. Poteau, F. D'Ortenzio, Seasonal dynamics of collared dissolved organic matter in the Mediterranean Sea: Patterns and drivers, *Deep-Sea Research I*, 2014, vol.83, pp.93-101.

153. F.G. Prahl and P.G. Coble, Input and behaviour of dissolved organic carbon in the Columbia River Estur., *Changes in Fluxes in Estuaries: Implications from sciences to management*, Olsen and Olsen, Fredensberg, 1994, pp. 451-458.

154. B. Reitner, A. Herzig and G.J. Herndl, Photoreactivity and bacterioplankton availability of aliphatic versus aromatic amino acids and a protein, 2002, *Aquatic Microbial Ecology*, vol.26, pp. 305–311.

155. E. J Biers, R.G. Zepp and M.A. Moran, The role of nitrogen in chromophoric and fluorescent dissolved organic matter formation, *Marine Chemistry*, 2007, vol. 103, pp. 46–60.

156. Skoog, P.O.J. Hall, S. Hulth, N. Paxéus, M. Rutgers van der Loeff and S. Westerlund, Early diagenetic production and sediment-water exchange of fluorescent dissolved organic matter in the coastal environment, *Geochimica et Cosmochimica Acta*, 1996, vol.60, pp.3619–3629.

157. C.L. Osburn, L.T. Handsel, M.P. Mikan , H.W. Paerl, and M.T. Montgomery, Fluorescence tracking of dissolved and particulate organic matter quality in a river-dominated estuary, *Environmental and Science Technology*, 2012, vol.46, pp.8628–8636.

158. R.F. Chen and J.L. Bada, The fluorescence of dissolved organic matter in porewaters of marine sediments, 1994, *Marine Chemistry*, vol.45, pp. 31–42.

159. D.J. Burdige, S.W. Kline, and W. Chen, Fluorescent dissolved organic matter in marine sediment pore waters, *Marine Chemistry*, 2004, vol.89, pp.289–311.

160. N.V.H.K. Chari, S. Keerthi, N. S., Sarma, S.R., Pandi, G. Chiranjeevulu, R. Kiran, et al., Fluorescence and absorption characteristics of dissolved organic matter excreted by phytoplankton species of western Bay of Bengal under axenic laboratory condition, *Journal of Experimental Marine Biology and Ecology*, 2013, vol.445, pp. 148–155.

161. K. Fukuzaki, I. Imai, K. Fukushima, K-I. Ishi, S. Sawayama and T. Yoshioka, Fluorescent characteristics of dissolved organic matter produced by bloom forming coastal phytoplankton, *Journal of Plankton Research*, 2014, vol.0, no 0, pp. 1-10.

162. Nieto-Cid, X.A. Álvarez-Salgado, J. Gago and F.F Pérez, DOM fluorescence, a tracer for biogeochemical processes in a coastal upwelling system (NW Iberian Peninsula), *Marine Ecology Progress Series*, 2005, vol.297, pp. 33–50.

163. C. Romera-Castillo, H. Sarmento, X.A. Alvarez-Salgado, J. M. Gasol and C. Marrase, Net production and consumption of fluorescent colored dissolved organic matter by natural bacterial assemblages growing on marine phytoplankton exudates, *Applied and Environmental Microbiology*, 2011, vol.77, pp. 7490–7498.

164. C.A. Stedmon and S. Markager, Tracing the production and degradation of autochthonous fractions of dissolved organic matter by fluorescence analysis, *Limnology and Oceanography*, 2005, vol.50, pp. 1415–1426.

165. M. Nieto-Cid, X. Álvarez-Salgado and F. Pérez, Microbial and photochemical reactivity of fluorescent dissolved organic matter in a coastal upwelling system, *Limnology and Oceanography*, 2006,5vol.1, pp.1391–1400.

166. C. Lonborg, X.A. Álvarez-Salgado, K. Davidson, S. Martínez-García and E. Teira, Assessing the microbial bioavailability and degradation rate constants of dissolved organic matter by fluorescence spectroscopy in the coastal upwelling system of the Ría de Vigo, *Marine Chemistry*, 2010, vol.119, pp. 121–129.

167. T. S. Catala, X. A. Alvarez-Salgado, J. Otero, F. Iuculano, B. Companys, B. Horstkotte, C. Romera-Castillo, M. Nieto-Cid, M. Latasa, X. A. G. Moran, J. M. Gasol,4 C. Marrase, C. A. Stedmon and I. Reche, Drivers of fluorescent dissolved organic matter in the global epipelagic ocean, *Limnology and Oceanography*, 2016, vol.61, issue 3, pp. 1101-1119.

168. G.R. Harvey, D.A. Boran, L.A., Chesal and J.M Tokar, The structure of marine fulvic and humic acids, *Marine Chemistry*, 1983, vol. 12, pp. 119–132.

169. E. M. Thurman, Organic Geochemistry of natural Waters, *Developments in Biogeochemistry*, vol.2, 1985.

170. P.J. Hernes and R. Benner, Terrigenous organic matter sources and reactivity in the North Atlantic Ocean and a comparison to the Arctic and Pacific oceans, Marine *Chemistry*, 2006, 100, pp. 66 – 79.

171. A. Andrew, R. Del Vecchio , A. Subramaniam, N. V. Blough, Chromophoric dissolved organic matter (CDOM) in the Equatorial Atlantic Ocean: Optical properties and their relation to CDOM structure and source, *Marine Chemistry*, 2013, vo.148, pp. 33-43.

172. L. Jorgensen, C.A. Stedmon, M. Granskog, M., Middelboe, Tracing the long-term microbial production of recalcitrant fluorescent dissolved organic matter in seawater, *Geophysical Research Letters*, 2014, vol.41, pp. 2481-2488.

173. C. Lonborg, T. Yokokawa, G.J. Herndl and X.A. Alvarez-Salgado, Production and degradation of fluorescent dissolved organic matter in surface waters of the eastern north Atlantic ocean, *Deep-Sea Research I*, 2015, vol. 96, pp. 28-37.

174. C.E. Del Castillo, P.G. Coble, J.M. Morel, J.M. Lopez and J.E. Corredor, Analysis of the optical properties of the Orinoco River Plume by absorption and fluorescence spectroscopy, *Marine Chemistry*,1999, vol.66, pp. 35-51.

175. S.C. Johannessen and W.L. Miller, Quantum yield for the photochemical production of dissolved inorganic carbon in seawater, *Marine Chemistry*, 2001, vol.76, pp. 271–283.

176. R. Del Vecchio and N.V. Blough, Photobleaching of chromophoric dissolved organic matter in natural waters: kinetics and modelling, 2002, *Marine Chemistry*, vol.78, pp. 231-253.

177. A.V. Vahatalo and R.G. Wetzel, Photochemical and microbial decomposition of chromophoric dissolved organic matter during long (months–years) exposures*, Marine Chemistry*, 2004, vol.89, pp.313–326.

178. C.M. Swan, N.B. Nelson, D.A. Siegel and T.S. Kostadinov, The effect of surface irradiance on the absorption spectrum of chromophoric dissolved organic matter in the global ocean, *Deep Sea Research Part I: Oceanographic Research Papers*, vol.63, pp. 52–64.

179. J.R. Helms, A. Stubbins, E.M. Perdue, N.W. Green, H. Chen, and K. Mopper, Photochemical bleaching of oceanic dissolved organic matter and its effect on absorption spectral slope and fluorescence, 2013, *Marine Chemistry*, vol.155, pp.81–91.

180. T.J. Boyd and C. L. Osburn, Changes in CDOM fluorescence from allochthonous and autochthonous sources during tidal mixing and bacterial degradation in two coastal estuaries, *Marine Chemistry*, 2004, vol.89, pp. 189–210.

181. Obernosterer and R. Benner, Competition between biological and photochemical processes in the mineralization of dissolved organic carbon, *Limnology and Oceanography*, 2004, vol.49, pp. 117–124.

182. Y. Yamashita, and E. Tanoue, Basin scale distribution of chromophoric dissolved organic matter in the Pacific Ocean, *Limnology and Oceanography*, 2009, vol.54, pp. 598–609.

183. N.B. Nelson, D.A. Siegel, C.A., Carlson, C.M. Swan, C.M., Tracing global biogeochemical cycles and meridional overturning circulation using chromophoric dissolved organic matter, *Geophysical Research Letters*, 2010, vol.37, pp. L03610.

184. L. Jorgensen, C. A. Stedmon, T. Kragh, S. Markager, M. Middelboe, and M. Sondergaard, Global trends in the fluorescence characteristics and distribution of marine dissolved organic matter, *Marine Chemistry*, 2011, vol. 126, pp. 139–148.

185. D.A. Siegel, S. Maritorena, N.B. Nelson, D.A. Hansell, and M. Lorenzi-Kayser, Global distribution and dynamics of colored dissolved and detrital organic materials, 2002, *Journal of Geophysical Research*, vol.107, pp. 3228.

186. C.A. Stedmon and S. Markager, The optics of chromophoric dissolved organic matter (CDOM) in the Greenland Sea: an algorithm for differentiation between marine and terrestrially derived organic matter, *Limnology and Oceanography*, 2001, vol. 46, pp. 2087–2093.

187. R.F. Chen and J.L. Bada, The fuorescence of dissolved organic matter in seawater, *Marine Chemistry*, 1992, vol.37, pp. 191-221.

188. Hayase and N. Shinozuka, Vertical distribution of fluorescent organic matter along with AOU and nutrients in the equatorial Central Pacific, *Marine Chemistry*, 1995, vol.48, pp. 283 – 290.

189. Y. Yamashita and E. Tanoue, Production of bio-refractory fluorescent dissolved organic matter in the ocean interior, *Nature Geoscience*, 2008, vol.1, pp. 579-582.

190. Y. Yamashita, N. Maie, H. Briceno and R. Jaffe, Optical characterization of dissolved organic matter in tropical rivers of the Guayana Shield, Venezuela, *Journal of Geophysical Research*, 2010, vol. 115, G00F10.

191. T. Komada, O.M.E. Schofield and C.E Reimers, Fluorescence characteristics of organic matter released from coastal sediments during resuspension, *Marine Chemistry*, 2002, vol.79, pp. 81-77.

192. Vodacek, F.E. Hoge, R.N. Swift, J.K. Yungel, E.T. Peltzer and N.V. Blough, The use of in situ and airborne fluorescence measurements to determine UV absorption coefficients and DOC concentrations in surface waters, *Limnology and Oceanography*, 1995, vol.40, pp. 411–415.

193. G.M. Ferrari, M.D. Dowel, S. Grossi and C. Targa, C., Relationship between the optical properties of chromophoric dissolved organic matter and total concentration of dissolved organic carbon in the southern Baltic Sea region, *Marine Chemistry*, 1996, vol.55, pp. 299–316.

194. C.A. Stedmon, S. Markager and H. Kaas, Optical properties and signatures of chromophoric dissolved organic matter (CDOM) in Danish coastal waters, *Estuarine Coastal and Shelf Science*, 2000, vol. 51, pp. 267–278.

195. A.R. Robinson and M. Golnaraghi, The physical and dynamical oceanography of the Mediterranean Sea, *Ocean Processes in Climate Dynamics: Global and Mediterranean Examples*, P. Malanotte-Rizzoli and A.R. Robinson (eds), NATO ASI Series, Kluwer Academic Publishers, 1994, pp. 255-306.

196. Cruzado, Chemistry of Mediterranean Waters, *Western Mediterranean*, R. Margalef (ed), Pergamon Press, 1985, pp. 126-147.

197. W. Ludwig, E. Dumont, M. Meybeck and S. Heussner, River discharges of water and nutrients to the Mediterranean and Black Sea: major drivers for ecosystem changes during past and future decades?, *Progress in Oceanography*, 2009, vol.80, pp.199–217.

198. T.S. Hopkins, Physics of the sea, *Key environment: Western Mediterranean*, R. Margalef, ed, Pergamon Press, New York, 1985, pp. 100-125.

199. E. Bosc, A. Bricaud, and D. Antoine, Seasonal and interannual variability in algal biomass and primary production in the Mediterranean Sea, as derived from 4 years of SeaWiFS observations, *Global Biogeochemical Cycles*, 2004, vol.18, GB1005.

200. C. Santinelli, DOC in the Mediterranean Sea, *Biogeochemistry of Dissolved Organic Matter*, D.A. Hansell and C.A. Carlson, eds, 2nd ed. Elsevier, Burlington: Academic Press, 2015, pp. 579-605.

201. C. Polat and S. Tugrul, Chemical exchange between the Mediterranean and the Black Sea via the Turkish Straits, *Bull. Inst. Oceanogr*., 1996, vol.17, pp. 167–186.

202. M. Pujo-Pay, P. Conan, L. Oriol, V. Cornet-Barthaux, C. Falco, J-F. Ghiglione, et al., Integrated survey of elemental stoichiometry (C, N, P) from the Western to Eastern Mediterranean Sea, *Biogeosciences*, 2011, vol.8, pp. 883–899.

203. C. Santinelli, G.P. Gasparini, L. Nannicini, and A. Seritti, Vertical distribution of dissolved organic carbon (DOC) in the western Mediterranean Sea in relation to the hydrological characteristics, *Deep-Sea Research I*, 2012, vol.49, pp. 2203–2219.

204. B. Avril, DOC dynamics in the northwestern Mediterranean Sea (DYFAMED site), *Deep-Sea Research II*, 2002, vol.49, pp. 2163–2182.

205. C. Santinelli, D.A. Hansell, M. Ribera d'Alcalà, M.,Influence of stratification on marine dissolved organic carbon (DOC) dynamics: the Mediterranean Sea case, *Progress in Oceanography*,2013, vol. 119, pp. 68-77.

206. D.A Hansell and C.A. Carlson, Localized refractory dissolved organic carbon sinks in the deep ocean, Global Biogeochemical Cycles, 2013, vol.27, pp. 705–710.

207. A. Morel and B. Gentili, The dissolved yellow substance and the shades of blue in the Mediterranean Sea, *Biogeosciences*, 2009, vol.6, pp. 2625-2636.

208. L. Bracchini, A. Tognazzi, A.M. Dattilo, et al., Sensitivity analysis of CDOM spectral slope in artificial and natural samples: an application in the central eastern Mediterranean Basin, *Aquatic Sciences*, 2010, DOI 10.1007/s00027-010-0150-y.

209. Z. Lee and C. Hu, Global distribution of Case-1 waters: An analysis from Swe WiFSF measurements, *Remote Sensing of Environment*, 2006, vol.101, pp.270-276.

210. M. Abboudi, W. H. Jeffrey, J.-F. Ghiglione, M. Pujo-Pay, L. Oriol, R. Sempéré B. Charrière and F. Joux, Effects of Photochemical Transformations of Dissolved Organic Matter on Bacterial Metabolism and Diversity in Three Contrasting Coastal Sites in the Northwestern Mediterranean Sea during Summer, *Microbial Ecology*, 2008, vol.55, pp. 344-357.

211. J. Para, P. G. Coble, B. Charriere, M. Tedetti, C. Fontana, and R. Sempere, Fluorescence and absorption properties of chromophoric dissolved organic matter (CDOM) in coastal surface waters of the northwestern Mediterranean Sea, influence of the Rhone River, *Biogeosciences*, 2010, vol.7, pp. 4083-4103.

212. M. Babin, D. Stramski, G. M. Ferrari, H. Claustre, A. Bricaud, G. Obolensky, and Nicolas Hoepffner, Variations in the light absorption coefficients of phytoplankton, nonalgal particles, and dissolved organic matter in coastal waters around Europe, *Journal of Geophysical Research*, 2003, vol. 108, no C7, 3211.

213. G.M. Ferrari, The relationship between chromophoric dissolved organic matter and dissolved organic carbon in the European Atlantic coastal area and in the West Mediterranean Sea (Gulf of Lions), *Marine Chemistry*, 2000, vol.70, pp. 339-357.

214. Serriti, D. Russo, L. Nannicini and R. Del Vecchio, DOC, absorption and fluorescence properties of estuarine and coastal waters of the Northern Tyrrhenian Sea, *Chemical Speciation and Bioavailability*, 1998, vol.10, pp. 95-106.

215. S. Retelleti Brogi, M. Conelli, S. Vestrri and C. Santinelli, Biophysical processes affecting DOM dynamics at the Arno river mouth (Tyrrhenian Sea), *Biophysical Chemistry*, 2015, vol.197, pp. 1-9.

216. C. Romera-Castillo, X.A. Alvarez-Salgado, M. Gali, J.M. Gasol and C. Marrase, Combined effect of light exposure and microbial activity on distinct dissolved organic matter pools. A seasonal field study in an oligotrophic coastal system (Blanes Bay, NW Mediterranean), *Marine Chemistry*, 2013, vol.148, pp. 44-51.

217. D. Berto, M. Giani, F. Savelli , E. Centanni , C.R. Ferrari and B. Pavoni, Winter to spring variations of chromophoric dissolved organic matter in a temperate estuary (Po river, northern Adriatic Sea), *Marine Environmental Research*, 2010, vol.70, pp.73-81.

218. Obernosterer and G. Herndl, Differences in the optical and biological reactivity of the humic and nonhumic dissolved organic carbon component in two contrasting coastal marine environments, *Limnology and Oceanography*, 2000, vol.45, pp. 1120-1129.

219. V. Kitidis, G. Uher, R. C. Upstill-Goddard, R.F.C. Mantoura, G. Spyres, and E. M.S. Woodward, Photochemical production of ammonium in the oligotrophic CyprusGyre (Eastern Mediterranean), *Biogeosciences,* vol.3, pp. 439-449.

220. Zeri, S. Besiktepe, A. Giannakourou, E. Krasakopoulou, M. Tzortziou, D. Tsoliakos et al., Chemical properties and fluorescence of DOM in relation to biodegradation in the interconnected Marmara-North Aegean Seas during August, Journal of Marine Systems, 2008, *Journal of Marine Systems*,2014, vol. 135, pp. 124-136.

221. Y. Sugimura and Y. Suzuki, A high-temperature catalytic oxidation method for the determination of non-volatile dissolved organic carbon in seawater by direct injection of a liquid sample, *Marine Chemistry*, 1998, vol.4, pp.105–131.

222. G. Cauwet, HTCO method for dissolved organic carbon analysis in seawater: Influence of catalyst on blank estimation, *Marine Chemistry* , 1994, vol.47, pp. 55-64.

223. A.J. Lawaetz and C.A. Stedmon, Fluorescence intensity calibration using the Raman scatter peak of water, *Applied Spectroscopy*, 2009, vol. 63, pp. 936-940.

224. R. Bro, PARAFAC. Tutorial and applications, *Chemometrics Intelligent Laboratory Systems*, 1997, vol.38, pp. 149-171.

225. C.A Stedmon and R. Bro, Characterizing dissolved organic matter fluorescence with parallel factor analysis: a tutorial, *Limnology and Oceanography*: Methods, 2008, vol.6, pp. 572-579.

226. C.A. Andersson and R. Bro, The N-way Toolbox for MATLAB, *Chemometrics and Intelligent Laboratory Systems*, 2000, vol.52 (1), pp. 1-4.

227. C.A. Stedmon, S. Markager and R. Bro, Tracing dissolved organic matter in aquatic environments using a new approach to fluorescence spectroscopy, *Marine Chemistry*, 2003, vol.82, pp. 239–254.

228. D.M. McKnight, E.W. Boyer, P.K., Westerhoff, P.T. Doran, T. Kulbe, and D.T. Andersen, D.T., Spectrofluorometric characterization of dissolved organic matter for indication of precursor organic material and aromaticity, *Limnology and Oceanography*, 2001, vol.46(1), pp. 38-48.

229. Kowalczuk, M.J. Durako, H. Young, A.E. Kahn, W.J. Cooper and M. Gonsior, Characterization of dissolved organic matter fluorescence in the South Atlantic Bight with use of PARAFAC model: Interannual variability, *Marine Chemistry*, 2009, vol.113, pp. 182-196.

230. B. Coste, P. Le Corre and H.J Minas, Re-evaluation of the nutrient exchanges in the Strait of Gibraltar, *Deep-Sea Research Part A*, 1988, vol.35, pp. 767–775.

231. J. P.Bethoux, P. Morin, C. Chaumery, O. Connan, B. Gentili, and D. Ruiz-Pino. 1998. Nutrients in the Mediterranean Sea, mass balance and statistical analysis of concentrations with respect to environmental change, *Marine Chemistry*, 2002, vol.63, pp. 155-169.

232. S. Besiktepe, E. Ozsoy and U. Unluata, Filling of the Sea of Marmara by the Dardanelles Lower Layer inflow, *Deep Sea Research*, 1993, vol., 40, pp. 1815-1838.

233. U. Unluata, T. Oguz, M.A. Latif and E. Ozsoy, On the physical oceanography of the Turkish Straits, *The Physical Oceanography of Sea Straits*, L.J. Pratt, ed, NATO/ASI series, Kluwer, 1990, pp. 25-60.

234. W. Ludwig, M. Meybeck and F. Abousamra, Riverine transport of water, sediments, and pollutants to the Mediterranean Sea, *UNEP MAP Technical report Series* 141, UNEP/MAP Athens, 2003, pp. 111.

235. Basturk, C. SAydam, I. Salihoglu and A. Yilmaz, , Health of the Turkish Straits: Chemical and Environmental Aspects of the Sea of Marmara, Oceanography of the Turkish Straits - *First Annual Report, Vol.II , Institute of Marine Sciences, METU*, Erdemli, Iqel, pp.69.

236. D. Ohron, Evaluation of the impact from the Black Sea on the pollution of the Marmara Sea, *Water Science and Technology*, 1995, vol.32, pp. 191-198.

237. E. T. Ozsoy, M.A. Oguz, M.A. Latif and U. Unluata, Oceanography of the Turkish Straits, *First Annual Report, Institute of Marine Sciences, METU*, 1986, vol.1, pp.269.

238. S.T. Besiktepe, H.I. Sur, E. Ozsoy, M.A. Latif, T. Oguz and U. Unluata, The circulation and hydrography of the Marmara Sea, *Progress in Oceanography*, 1994, vol.34, pp. 285-334.

239. H.W. Ducklow, D.A. Hansell, and J.A. Morgan, Dissolved organic carbon and nitrogen in the Western Black Sea, *Marine Chemistry*, 2007, vol.105, pp. 140–150.

240. C.A. Stedmon and S. Markager, Behaviour of the optical properties of coloured dissolved organic matter under conservative mixing, *Estuarine, Coastal and Shelf Science*, 2003, 57, pp. 973-979.

241. Lagaria, S. Psarra, A. Gogou, S. Tuğrul, and U. Christaki, Particulate and dissolved primary production along a pronounced hydrographic and trophic gradient (Turkish Straits System–NE Aegean Sea), *Journal of Marine Systems*, 2013, vol.119-120, pp. 1-10.

242. S.C. Polat and S. Tugrul, Nutrient and organic carbon exchanges between the Black and Marmara Seas through the Bosphorus Strait, *Continental Shelf Research*, 1995, vol.15, pp. 1115-1132.

243. M. Ergin, M.N. Bodur, D. Ediger, V. Ediger and A. Yilmaz, Organic carbon distribution in the surface sediments of the Sea of Marmara and its control by the inflows from adjacent water masses, *Marine Chemistry*, 1993, vol. 41, pp. 311-326.

244. Siokou-Frangou, S. Zervoudaki, E.D. Christou, V. Zervakis, and D. Georgopoulos Variability of mesozooplankton spatial distribution in the North Aegean Sea, as influenced by the Black Sea waters outflow, *Journal of Marine Systems*, 2009, vol.78, pp.557-575.

245. E. Krasakopoulou, V. Zervakis, E. Souvermezoglou and D. Georgopoulos, North-eastern Aegean sea: an effort to estimate steady-state N & P budgets during September 1998, *Mediterranean Marine Science*, 2002, vol.3, pp.43-53.

246. E. Souvermezoglou, E. Krasakopoulou, A. Pavlidou, Temporal and spatial variability of nutrients and oxygen in the North Aegean Sea during the last thirty years, *Mediterranean Marine Science*, 2014, vol.15, pp. 805-822.

247. Z. Kokkini, M. Potiris, A. Kalampokis, V. Zervakis, HF Radar observations of the Dardanelles outflow current in the North Eastern Aegean using validated WERA HF radar data, *Mediterranean Marine Science*, 2014, Special Issue, pp753-768.

248. T. Oguz and I.H. Sur, A two-layer model of water exchange through the Dardanelles Strait, *Oceanologica Acta*, 1989, vol.12, pp. 23-31.

249. S.E Poulos, P.G. Drakopoulos and M.B. Collins, Seasonal variability in sea surface oceanographic conditions in the Aegean Sea (Eastern Mediterranean): an overview, *Journal of Marine Systems*, 1997, vol.13, pp.225-244.

250. V. Zervakis and D. Georgopoulos, Hydrology and circulation in the North Aegean (eastern Mediterranean) throughout 1997 and 1998, *Mediterranean Marine Science*, 2002, vol.3, pp. 5-19.

251. D.B. Olson, V.H. Kourafalou, W.H. Johns, G. Samuels and M. Veneziani Aegean surface circulation from a satellite – tracked drifter array, *Journal of Physical Oceanograph*y, 2007, vol.37, pp. 1898-1917.

252. P.J.L.B Williams, Heterotrophic bacteria and the dynamics of dissolved organic material, *Microbial Ecology of the Oceans*, D.L. Kirchman, ed, New York: Wiley-Liss. 1st ed., 2000, pp. 153–200.

253. M. Tzortziou, C.L Osburn and P.J Neale, Photobleaching of dissolved organic material from a tidal march-estuarine system of the Chesapeake Bay*, Photochemistry and photobiology,* 2007, vol.83, pp. 782-792.

254. Giannakourou, P. Pitta P. et al., Microbial distribution and activity across a frontal zone in the N. Aegean-Black Sea interface, *Continental Shelf Research*, Special Issue, in press, 2016.

255. Y. Omori, T. Hama, M. Ishii, S. Saito, Vertical change in the composition of marine humic-like fluorescent dissolved organic matter in the subtropical western North Pacific and its relation to photoreactivity, *Marine Chemistry*, 2011, vol.124, pp. 38-47.

256. R.M. Cory, D.M. McKnight, Y. Chin, P. Miller, and C.L. Jaros, Chemical characteristics of fulvic acids from Arctic surface waters: Microbial contributions and photochemical transformations, *Journal of Geophysical Research*, 2007, vol.112, G04S51.

257. A. Karageorgis et al., Using inherent optical properties to investigate particle distribution and composition in the NE Aegean Sea, *Continental Shelf Research*, Special Issue, in press, 2016.

258. E. Souvermezoglou, Distribution of nutrients and oxygen in the Eastern Mediterranean Sea. *Proceedings of the UNESCO/ IOC Second Scientific Workshop*, Trieste, Italy, POEM Sci. Repts. 3, Cambridge, Massachusetts, USA, 1989, pp. 85-102.

259. D. Velaoras, G. Krokos, K. Nittis and A. Theocharis, Dense intermediate water outflow from the Cretan Sea: A salinity driven, recurrent phenomenon, connected to thermohaline circulation changes, *Journal of Geophysical Research: Oceans*, 2014, pp. 4797-4820.

260. E. Ozturgut, The source and spreading of the Levantine intermediate water in the Eastern Mediterranean*, Saclant Antisubmarine Warfare* Res. Cen. Memor. SM-92, La Spezia, Italy, 1976, pp.45.

261. A. Theocharis and D. Georgopoulos, Dense water formation over the Samothraki and Limnos Plateaux in the north Aegean Sea (Eastern Mediterranean Sea), *Continental Shelf Research*, 1993, vol.13, pp. 919-939.

262. Theocharis, E. Balopoulos, S. Kioroglou, H. Kontoyiannis and A. Iona, A synthesis of the circulation and hydrography of the South Aegean Sea and the Straits of the Cretan Arc (March 1994–January 1995), *Progress in Oceanography*, 1999, vol.44, pp. 469-509.

263. M. I. Pollak, The sources of the Deep Water in the Eastern Mediterranean Sea, *Journal of Marine Research*, 1951, vol.10, pp. 128–152.

264. E. Souvermezoglou and E. Krasakopoulou, Evolution of oxygen and nutrient concentrations in the deep basins of the northern Aegean Sea. *4th MTP Workshop*, 28-30 October 1999, Perpignan, France, 1999, pp. 150-151.

265. W. Roether and R. Schlitzer, Eastern Mediterranean deep water renewal on the basis of CFM and tritium data, *Dynamics of Atmosphere and Oceans*, 1991, vol.15, pp.333-354.

266. V.Zervakis, D. Georgopoulos, PG, Drakopoulos, The role of the north Aegean in triggering the recent eastern Mediterranean climatic changes, *Journal of Geophysical Research*, 2000, vol.105, pp. 26 103–26 116.

267. Y.S. Androulidakis, V.H Kourafalou, Y.N. Krestenitis and V. Zervakis, Variability of deep water mass characteristics in the North Aegean Sea: The role of lateral inputs and atmospheric conditions, *Deep-Sea Research I*, 2012, vol. 67, pp. 55-72.

268. V.D. Vervatis, S. Sofianos and A.Theocharis, Distribution of the thermohaline characteristics in the Aegean Sea related to water mass formation processes (2005-2006 winter surveys), *Journal of Geophysical Research*, 2011, vol. 116, C09034.

269. Theocharis, K. Nittis, H. Kontoyiannis, E. Papageorgiou and E. Balopoulos, Climatic changes in the Aegean Sea influence the Eastern Mediterranean thermohaline circulation (1986-1997), *Geophysical Research Letters*, 1999, vol.26, no.11, pp. 1617-1620.

270. Theocharis, D. Georgopoulos, P. Karagevrekis, A. Iona, L. Perivoliotis and N. Charalambidis, Aegean influence in the deep layers of the Eastern Ionian Sea (October 1991), *Rapports de Commission International de la Mer Mediterranee*, 2002, vol.33, p.235.

271. The POEM Group, General Circulation of the Eastern Mediterranean, *Earth Science Reviews*, 1992, vol.32, pp. 285–309.

272. S.A. Josey Changes in the heat and freshwater forcing of the eastern Mediterranean and their influence on deep water formation, *Journal of Geophysical Research*, 2003, vol.108, issue C7,3237.

273. G. Krokos, D. Velaoras, G. Korres, L. Perivoliotis and A. Theocharis, On the continuous functioning of an internal mechanism that drives the Eastern Mediterranean thermohaline circulation: The recent activation of the Aegean Sea as a dense water source area, *Journal of Marine Systems*, 2014, vol. 129, pp. 484-489.

274. S. Marullo, E. Napolitano, R. Santoleri, B. Manca and R. Evans, Variability of Rhodes and Ierapetra Gyres during Levantine Intermediate Water Experiment: Observations and model results, *Journal and Geophysical Research*, 2003, vol.108, no. C9, 8119.

275. S. Psarra, A. Tselepides and L. Ignatiades, Primary productivity in the oligotrophic Cretan Sea (NE Mediterranean): seasonal and interannual variability, *Progress in Oceanography*, 2000, vol.46, pp.187–204.

276. A.P. Karageorgis, D. Georgopoulos, T.D. Kanellopoulos, O.A. Mikkelsen, et al., Spatial and seasonal variability of particulate matter optical and size properties in the Eastern Mediterranean Sea, *Journal of Marine Systems*, 2007, vol.105–108, pp.123-134.

277. M.D Krom, S. Brenner, N. Kress, A. Neori and L.I. Gordon, Nutrient dynamics and new production in a warm-core eddy from the E. Mediterranean, 1992, *Deep-Sea Research*, 1992, vol.39, pp. 467–480.

278. T.F.Thingstad and F. Rassolzadegan, Nutrient limitation, microbial food webs and biological C-pumps: Suggested in a P-limited Medirerranean, *Marine Ecology Progress Serie*s, 1995, vol.117, pp. 299-306.

279. Lascaratos, R. Williams and E. Tragou, A Mixed Layer Study of the formation of Levantine Intermediate Water, *Journal of Geophysical Research*, 1993, vol.98, C9, pp.739-749.

280. E. Napolitano, T. Oguz, P. Malanotte-Rizzoli, A. Yilmatz, and E. Sansone, Simulations of biological production in the Rhodes and Ionian basins of the eastern Mediterranean, *Journal of Marine Systems*, 2000, vol.24, pp.277 – 298.

281. F. Vidussi, H. Claustre, B.B. Manca, A. Luchetta and J.C Marty, Phytoplankton pigment distribution in relation to upper thermohaline circulation in the eastern Mediterranean during winter, *Journal of Geophysical Research-Oceans*, 2001, vol.106, pp. 19939-19956.

282. X. Xing, A. Morel, H. Claustre,F. D'Ortenzio, and A. Poteau, Combined processing and mutual interpretation of radiometr and fluorometry from autonomous profiling Bio-Argo floats: 2. Colored dissolved organic matter absorption retrieval, *Journal of Geophysical Research*, 2012, vol. 117, C04022.

283. G. Kattner, J.M. Lobbes, H.P. Fitznar, R. Engbrodt, E-M. Nothig and R.J. Lara, Tracing dissolved organic substances and nutrients of Lena River through Laptev Sea (Arctic), *Marine Chemistry*, 1999, vol.65, pp. 25–39.

284. J.B. Fellman, K.C., Petrone, and F. Grierson, Source, biogeochemical cycling, and fluorescence characteristics of dissolved organic matter in an agro-urban estuary, *Limnology and Oceanography*, 2011, vol.56, pp.243–256.

285. T. Mattson, P. Kortelainen, A. Laubel, D. Evans, M. Pujo-Pay, M. A. Raike and P. Conan, Export of dissolved organic matter in relation to land use along a European climatic gradient, *Science of Total Environment*, 2009, vol.407, pp. 1967–1976.

286. P.J. Hernes, R. Benner, G.L. Cowie, M. Goni, B.A. Bergamaschi and J. Hedges, Tannin diagenesis in mangrove leaces from a tropical estuary: a novel molecular approach, *Geochimica et Cosmochimica Acta*, 2001, vol.64, pp. 3109-3122.

287. C.J. Williams, Y. Yamashita, H.F. Wilson, R. Jaffe and M.A. Xenopoulos, Unraveling the role of land use and microbial activity in shaping dissolved organic matter characteristics in stream ecosystems, *Limnology and Oceanography*, 2010, vol.55, pp. 1159–1171.

288. P.A. Raymond, J.W. McClelland, R.M. Holmes, A.V. Zhulidov, K. Mull, B.J Peterson, B.J., Flux and age of dissolved organic carbon exported to the arctic ocean: a carbon isotopic study of the five largest arctic rivers, *Global Biogeochemical Cycles*, 2007, vol.21, GB4011.

289. H.F. Wilson and M.A. Xenopoulos, Effects of agricultural land use on the composition of fluvial dissolved organic matter, *Nature Geoscience*, 2009, vol.2, pp.37-41.

290. P.A. Raymond and J. E. Bauer, Bacterial utilization and transport of DOC in a temperate estuary, *Aquatic Microbial Ecology*, 2000, vol.22, pp. 1–12.

291. R.M.W Amon and B. Meon, The biogeochemistry of dissolved organic matter and nutrients in two large Arctic estuaries and potential implications for our understanding of the Arctic Ocean system, *Marine Chemistry*, 2004, 92, pp. 311 – 330.

292. E.D. Christou, K. Pagou, S. Christianidis and E. Papathanassiou, Temporal and spatial variability of plankton communities in a shallow embayment of the eastern Mediterranean, : *Biology and ecology of shallow coastal waters*, A. Eleftheriou, A. D. Ansell and C. J. Smith, Fredensborg, Olsen & Olsen, 1995, pp. 3-10.

293. K. A. Kormas, A. Nikolaidou and M. Thessalou-Lagaki, Variability of environmental factors of an eastern Mediterranean Sea river influenced coastal system, *Mediterranean Marine Science*, 2003, vol.4, pp. 67-77.

294. A.D. Therianos, The geographic distribution of river water supply in Hellas, *Bulletin of the Hellenic Geological Society*, 1974, vol.11, pp. 28-58 (in Greek).

295. G. Efthimiou, A. Mertzanis, M. Sapountzis and G. Zakynthinos, Anthropogenic effects at the Sperchios river delta – Protection measures for the depiction and management of the natural ecosystems. Minutes *5th International Conference for the Environmental Technology -«Heleco' 05*», CD-ROM, 3-6 February 2005, Athens (in Greek).

296. HCMR, Τεχνική έκθεση με τα αποτελέσματα της ετήσιας αξιολόγησης της οικολογικής ποιότητας για κάθε υδάτινο σώμα, ΚΡΗΠΙΣ-ΙΘΑΒΙΠΕΥ, 2015.

297. N. Th. Skoulikidis, The environmental state of rivers in the Balkans—A reviewwithin the DPSIR framework, *Science of the Total Environment*, 2009, vol.407, pp. 2501-2516.

298. K. Vouvalidis, G. Syrides, K. Pavlopoulos , M. Papakonstantinou and P. Tsourlos, Holocene palaeoenvironmental changes in Agia Paraskevi prehistoric settlement, Lamia, Central Greece, *Quaternary International*, 2009, pp.1-11.

299. Ε. Πίττα, Ανόργανα θρεπτικά συστατικά και διαλυμένη οργανική ύλη σε δύο ποτάμια της Ανατολικής Μεσογείου: Έβρος και Σπερχειός, *Διπλωματική Εργασία*, Τμήμα Χημείας, ΕΚΠΑ-ΕΛΚΕΘΕ, 2010.

300. E. Parlanti, K. Worz, L. Geoffroy and M. Lamotte, Dissolved organic matter fuorescence spectroscopy as a tool to estimate biological activity in a coastal zone submitted to anthropogenic inputs, *Organic Geochemistry*, vol.31, pp. 1765-1781.

301. M. Tzortziou et al., Dynamics and properties of colored dissolved organic matter, CDOM, in wetland ecosystems and coastal waters of the Eastern Mediterranean, *Aquatic Science Meeting*, Poster, 2010.

302. E. Dimitriou, A. Mentzafou, M. Tzortziou and C. Zeri, Environmental monitoring and pollution pressures identification in Sperchios river catchment, Conference Paper, 3rd *International CEMEPE & SECOTOX Conference*, Skiathos, 2011.

303. N. Hudson, A. Baker, D. Ward, D. M. Reynolds, C. Brunsdon, C. Carliell-Marquet, and S. Browning, Can fluorescence spectrometry be used as a surrogate for the Biochemical Oxygen Demand (BOD) test in water quality assessment? An example from South West England, *Science of the Total Environment*, 2008, vol.391, pp. 149–158.

304. N.M Scully, N. Maie, S.K. Dailey, J.N. Boyer, R.D Jones and R. Jaffe, Early diagenesis of plant-derived dissolved organic matter along a wetland, mangrove, estuary ecotone, *Limnology and Oceanography*, 2004, vol. 49, pp. 1667-1678.

305. S. Vignudelli, C. Santinelli, E. Murru, L. Nannicina and A. Seritti, Distributions of dissolved organic carbon (DOC) and chromophoric dissolved organic matter (CDOM) in coastal waters of the northern Tyrrhenian Sea (Italy), *Estuarine, Coastal and Shelf Science*, 2004, vol. 60, 133-149.

306. L.W. Winkler, Die Bestimmung des im Wasser gelosten Sauerstoffes, *Chemische Berichte*, 1888, vol.21, pp. 2843-2855.